Design and development of a hominid robot with local control in its adaptable feet to enhance locomotion capabilities

von

Daniel Kühn

Dissertation
zur Erlangung des akademischen Grades eines
Doktors der Ingenieurwissenschaften
- Dr. Ing. -

Vorgelegt im Fachbereich 3
Informatik und Mathematik
der Universität Bremen

Bremen, December 12, 2016

Datum des Promotionskolloquiums: 05.12.2016

Gutachter:
Prof. Dr. Frank Kirchner
Prof. Dr. Udo Frese

Abstract

With increasing mechanization of our daily lives, the expectations and demands in robotic systems increase in the general public and in scientists alike. In recent events such as the "Deepwater Horizon"-accident or the nuclear disaster at Fukushima, mobile robotic systems were used, e.g., to support local task forces by gaining visual material to allow an analysis of the situation. Especially the Fukushima example shows that the robotic systems not only have to face a variety of different tasks during operation but also have to deal with different demands regarding the robot's mobility characteristics.

To be able to cope with future requirements, it seems necessary to develop kinematically complex systems that feature several different operating modes. That is where this thesis comes in: A robotic system is developed, whose morphology is oriented on chimpanzees and which has the possibility due to its electro-mechanical structure and the degrees of freedom in its arms and legs to walk with different gaits in different postures. For the proposed robot, the chimpanzee was chosen as a model, since these animals show a multitude of different gaits in nature. A quadrupedal gait like crawl allows the robot to traverse safely and stable over rough terrain. A change into the humanoid, bipedal posture enables the robot to move in man-made environments.

The structures, which are necessary to ensure an effective and stable locomotion in these two poses, e.g., the feet, are presented in more detail within the thesis. This includes the biological model and an abstraction to allow a technical implementation. In addition, biological spines are analyzed and the development of an active, artificial spine for the robotic system is described. These additional degrees of freedom can increase the robot's locomotion and manipulation capabilities and even allow to show movements, which are not possible without a spine. Unfortunately, the benefits of using an artificial spine in robotic systems are nowadays still neglected, due to the increased complexity of system design and control.

To be able to control such a kinematically complex system, a multitude of sensors is installed within the robot's structures. By placing evaluation electronics close by, a local and decentralized preprocessing is realized. Due to this preprocessing is it possible to realize behaviors on the lowest level of robot control: in this thesis it is exemplarily demonstrated by a local controller in the robot's lower leg. In addition to the development and evaluation of robot's structures, the functionality of the overall system is analyzed in different environments. This includes the presentation of detailed data to show the advantages and disadvantages of the local controller. The robot can change its posture independently from a quadrupedal into a bipedal stance and the other way around without external assistance. Once the robot stands upright, it is to investigate to what extent the quadrupedal walking pattern and control structures (like the local controller) have to be modified to contribute to the bipedal walking as well.

Zusammenfassung

Mit steigender Technisierung des alltäglichen Lebens steigen auch die Erwartungen und Anforderungen in der Bevölkerung und von Wissenschaftlern gleichermaßen, die an robotische Systeme gestellt werden. Bei jüngsten Ereignissen wie dem "Deepwater Horizon"-Unglück oder der Nuklearkatastrophe von Fukushima kamen jeweils mobile robotische Systeme in unterstützender Funktion zum Einsatz, beispielsweise um Aufklärung zu betreiben. Gerade am Fukushima-Beispiel hat sich gezeigt, dass die robotischen Systeme bei einem solchen Einsatz nicht nur mit einer Vielzahl von verschiedenen Aufgaben sondern auch mit unterschiedlichen Anforderungen an dessen Mobilitätseigenschaften konfrontiert sind.

Um zukünftigen Anforderungen gewachsen zu sein, empfiehlt es sich, kinematisch komplexe Systeme zu entwickeln, die zudem über mehrere Operationsmodi verfügen. An dieser Stelle setzt die vorliegende Arbeit an: Es wird ein Roboter entwickelt, dessen Morphologie am Schimpansen orientiert ist. Aufgrund seines elektromechanischen Aufbaus und den Bewegungsfreiheiten in den Armen und Beinen hat das System die Möglichkeit, sich mit verschiedenen Lokomotionsarten fortzubewegen. Der Schimpanse wurde als Vorbild gewählt, da dieser in der Natur verschiedene Lokomotionsarten zeigt. Eine quadrupedale Lokomotion bietet dem Roboter die Möglichkeit, sich sicher und stabil über unebenes Gelände zu bewegen, während ein Wechsel in die humanoide, bipedale Pose es ermöglicht, sich in für Menschen gemachten Umgebungen aufzuhalten.

Die Strukturen, die nötig sind, um eine effektive und stabile Lokomotion in beiden Posen zu gewährleisten, wie beispielsweise die Füße, werden im Verlauf der Arbeit anhand des biologischen Vorbild betrachtet und für eine technische Umsetzung abstrahiert. Dazu gehört auch die Entwicklung und Integration einer künstlichen, aktiven Wirbelsäule. Diese zusätzlichen Freiheiten können die Lokomotions- und Manipulationsfähigkeiten des mobilen Roboters erhöhen, indem neuartige Bewegungen erlaubt werden. Die Vorteile, die eine künstliche Wirbelsäule robotischen Systemen eröffnen könnte, werden heutzutage aufgrund der erhöhten Komplexität im Systemdesign und in der Kontrolle noch vernachlässigt.

Zur Regelung des kinematisch komplexen Systems wird eine Vielzahl von Sensoren in die einzelnen Strukturen integriert und selbige lokal und dezentral vorverarbeitet. Durch den Einsatz von lokalen Vorverarbeitungseinheiten lassen sich bereits auf den untersten Level der Roboterkontrolle Verhalten implementieren, die innerhalb der Arbeit am Beispiel eines lokalen Reglers im Unterschenkel aufgezeigt werden. Neben der Entwicklung und Evaluation der Strukturen, wird ebenfalls das Gesamtsystem betrachtet und dessen Funktionalität in verschiedenen Umgebungen analysiert. Ebenfalls werden die Vor- und Nachteile der lokalen Regelung in den jeweiligen Umgebungen dargestellt. Nach einer Änderung der Grundhaltung, die der Roboter eigenständig ohne externe Hilfestellung vornehmen kann, wird untersucht, inwiefern sich die Kontrollansätze und Laufmuster des quadrupedalen Gangs auf den bipedalen übertragen lassen.

Danksagung

An dieser Stelle möchte ich verschiedenen Personen meinen Dank aussprechen, ohne deren Unterstützung es nicht möglich gewesen wäre, diese Doktorarbeit fertig zu stellen.

Ganz besonders möchte ich meinem Doktorvater Prof. Dr. Frank Kirchner danken, für seine Unterstützung und die inhaltlichen Diskussionen in den vergangenen Jahren. Er hat mir die Möglichkeit gegeben, mich unter idealen Bedingungen am Deutschen Forschungszentrum für künstliche Intelligenz (DFKI) zu entwickeln und hier zu forschen. Für die Möglichkeit und sein Vertrauen, mir früh zu Beginn meines Berufslebens die Leitung von Projekten zu übertragen, danke ich Prof. Kirchner besonders.

Die technische Voraussetzung für diese Doktorarbeit ist am DFKI innerhalb des iStruct Projekts entstanden. Hierfür möchte ich mich ganz herzlich bei meinem alten Team, Frank Beinersdorf, Felix Bernhard, Armin Burchard, Kristin Fondahl, Lan Yu Ji, Patrick Schöberl, Dr. Marc Simnofske, Tobias Stark, Moritz Schilling und Martin Zenzes, bedanken, die geholfen haben, den Roboter Charlie zu entwickeln.

Hervorheben möchte ich an dieser Stelle Felix Grimminger, für die ganzen anregenden Diskussionen bezüglich der Hardware und des Designs von Charlie, der bei dem einen oder anderen Kneipenbesuch immer ein offenes Ohr und viele gute Ratschläge hatte.

Neben dem wissenschaftlich-technischen Kollegen gilt mein Dank gerade den Kollegen der administrativen Ebene für die problemlose und immer freundliche Zusammenarbeit.

Meinen Freunden und Kollegen, Ajish Babu, Alexander Dettmann, Dr. Peter Kampmann, Malte Langosz, Thomas Röhr, Dr. Sebastian Bartsch und besonders Florian Cordes, die mir beim Verfassen dieser Arbeit immer wieder mit Anregungen und Verbesserungsvorschlägen zur Seite standen, möchte ich herzlich danken.

Meinen Freunden, meiner Familie und besonderer meiner Frau Stina gilt ein spezieller Dank für ihre Liebe, unendliche Unterstützung und das entgegengebrachte Verständnis, welches sich eigentlich kaum in Worte fassen lässt. Besonders in schwierigen, arbeitsintensiven Zeiten hatten sie immer ein offenes Ohr und die richtigen Worte parat. Vielen Dank dafür.

Contents

Abbreviations

ADC	Analog-to-Digital Converter
AEP	Anterior Extreme Position
BLDC	Brushless Direct Current
CoM	Center of Mass
CoSP	Center of Support Polygon
CPG	Central Pattern Generator
CS	Coordinate Systems
DoF	Degree of Freedom
DRC	DARPA Robotics Challenge
EEPROM	Electrically Erasable Programmable Read-Only Memory
FEM	Finite Element Method
FSR	Force Sensing Resistor
FPGA	Field Programmable Gate Array
GPIO	General Purpose Inputs and Output
IMU	Inertia Measurement Unit
IR	Infrared
LVDS	Low Voltage Differential Signaling
MCS	Motion Control System
MCU	Motion Control Unit
MPCF	Multi-Point-Contact Feet
NDLCom	Node-level Data Link Communication
PCB	Printed Circuit Board

PEP	Posterior Extreme Position
PID	Proportional-Integral-Derivative
PI	Proportional-Integral
PWM	Pulse-Width Modulation
RoM	Range of Motion
SPCF	Single-Point-Contact Feet
UART	Universal Asynchronous Receiver Transmitter
wcp	walking cycle progress
ZMP	Zero Moment Point

Part I

Thesis

Chapter 1

Introduction

In this chapter, the motivation and goals behind this thesis are introduced and the structure of the document is shown.

1.1 Motivation

The idea to design and built tools or machines able to reduce the human workload or to increase the efficiency at constant effort goes back thousands of years. The Greek polymath Archimedes of Syracuse (287 BC to 212 BC) invented a machine allowing to transfer water from a lower surface level to a higher region. Dalley found evidence indicating that even 350 to 400 years before Archimedes was born the assyrian (nowadays Iraq) king Sennacherib made use of a comparable device for one of his gardens, later on known as the Hanging Gardens of Babylon [DO03].

Besides tools, examples can be found in history where man designed and built human and animal like machines for technical and scientific studies, entertainment, or religious purposes, e.g., in 1495 Leonardo DaVinci designed a cable driven, armored knight: "Last Supper"; according to the Museo Galileo [1] this is possibly the first humanoid robot built in western civilization.

At that time, the design of both, tools and machines, was purely mechanical. With increasing technology level (mechanical, electronic and chemical), more possible areas of application for machines arose, as it is shown by the industrial revolutions, where the production processes have been increased in both, quantity and quality, compared to human workers using manual tools.

Nowadays, besides stationary robots, a wide range of possible areas of application

---

[1] http://www.museogalileo.it/

for mobile robotic systems exists, like search and rescue, human assistance, security, or (planetary) exploration. In particular in hazardous and dangerous environments, the usage of mobile robots is a viable alternative compared to endangering human life. In contrast to robots in industrial workplaces, mobile robots have to be able to operate in environments, which are not specially designed for them. This means that the robots today are and in the future will be confronted with a multitude of different environments as well as with increasingly challenging tasks.

Compared to driving, legged locomotion seems to be a promising approach, although wheeled or tracked vehicles have advantages in covering a greater distance regarding their energy-efficiency and are in general more easy to control. However, legged robots are able to cover rugged terrain including slopes, can overcome obstacles and can cope with fine-grained surfaces and thus have access to a wider range of terrains. This is because they are capable of applying forces in noncontinuous ways to the environment and need only small areas of support for their feet.

These days most robotic systems focus on a single motion mode. A mobile robot is selected to participate in a given scenario when the mission requirements correspond to the robot's abilities, like motion skills, locomotion speed and stability, manipulation capabilities as well as sensor equipment. A robot, combining different capabilities into one multi-locomotion robot, can be especially useful in scenarios, in which the robot has to deal with a yet unknown environmental state, like in space exploration or on-site evaluation in disaster areas. In addition to the mentioned scenarios, the closer the robot's outer appearance resembles the human form, the more likely it can handle man-made structures like doors, use tools, and move in workspaces designed for human's.

A possible approach for such a multi-locomotion robot can be a system that is able to perform a stable and robust quadrupedal gait in rugged terrain, but has also the potential to stand up and change into a bipedal posture. A change of posture into bipedal opens up the opportunity to use certain limbs differently, e.g., for manipulation since they are no longer required to participate in maintaining the robot's stability or in locomotion and thus can be assigned to other tasks. In addition, due to the posture change the field of view of an applied imaging system on the robot will be increased, which helps to reduce blind spots during the generation of maps and can increase the precision of self-localization.

From a scientific point of view, such a multi-locomotion system is highly interesting since it provides the possibility to evaluate the transfer of control mechanisms and motion patterns between different postures. Such a system can be used to answer questions regarding how the activation patterns of single joints have to be modified to generate a stable locomotion in both postures or if they are purely gait specific; thus it could give clues for a better understanding of the evolutionary process of bipedal walking.

To gain higher mobility, it seems necessary to revise the common design patterns of a robot's body. In most robots, the wheels or legs are attached to a body, which is one rigid unit to reduce design and control complexity. Consequently, the locomotion often appears constrained. Nature shows a different approach. In vertebrates, the spine is a central element and offers a variety of benefits, including the support of limb motions. In robotics, however, the implementation of an artificial spine to a robotic system is ongoing research. Current robots with a biologically inspired spine are able to demonstrate limited motions while sitting but are not able to walk yet.

By increasing the kinematic complexity of a robot, not only by introducing an artificial spine but also because of added Degree of Freedoms (DoFs) in the limbs, the number of applied sensors should be increased too. Otherwise, there is a risk that the robot's state is undefined and therefore controlling the robot will be difficult - if not impossible. Brooks stated that "a robot should be able to react to its environment within a human-like time-frame" [Bro91], which stands in contrast to generating a complete world model and start acting afterwards. Basically this means that, due to interaction with the world, a certain stimulus can be used to generate a respective response. To allow a mobile robot to deal with the above mentioned increased demands and to be able to perceive the environment, it is necessary to increase the robot's sensor density accordingly.

This, however, presupposes that the robot's control electronics is able to handle the high sensor density, i.e. to provide sufficient electrical connectors as well as computation power to process the data. One possibility is to preprocess the data locally with respect to each sensor and with the effect that the computational load is effectively distributed in the robotic system relieving the main computer. In addition, in such a scenario the sensor signals are less prone to error compared to an analog signal which has to be transmitted to a central processing unit, due to a reduced cabling throughout the robot's limbs and body. A further advantage of local data processing is that within a sub-structure, e.g., a leg, the actuators, and sensor system could be combined to a logical unit, which could react to external influences all by themselves with minor latency. This can be compared to the impedance control in a robotic manipulator, where the trajectory can be influenced, e.g., by applying forces and torques to the actuators or to an installed force/torque sensor.

The measured stimulus is sent to the main controller and the motion trajectory is altered accordingly. The difference in this thesis is that the position offsets are not set by the main controller, but locally. Advantages and disadvantages of using a controller, which can alter the desired foot trajectories independently, have so far not been analyzed in a robotic system, to the best of the authors knowledge.

1.2 Objective

The main goal of this thesis is the development and evaluation of a biologically inspired, hominid robot which is able to operate in unstructured environments, provides the possibility to change its posture from quadrupedal to bipedal and is able to demonstrate different gaits. Through an experimental validation, the stability of locomotion in a quadrupedal posture in indoor and outdoor environment as well as the bipedal locomotion in man-made environment shall be proven.

To realize a robot capable of both, bi- and quadrupedal patterns, its morphology must be accordingly designed and the defining features of both motion modes have to be considered. In multi-legged robots, often spherically shaped feet or feet with a small supporting surface are used. For bipedal walking, these feet are inadequate. Besides the structures, the availability of a high sensor density is desired and has to be chosen to be suitable for both locomotion modes. To deal with the expected variety of data, in this thesis an exemplary local data preprocessing and data evaluation has to be implemented within the structures, to limit data traffic in the robot. This means that instead of sending a large volume of raw data, the envisioned structures use the sensor information to create a certain, yet local, knowledge, which is transferred to the central controller.

It is intended to form logical units, for example the lower leg and the desired sensor foot can be combined. This, for example, would allow an central CPU independent alteration of the given foot trajectories to realize a ground adaption behaviour at the lowest control level, since the sensory and actuator system are interconnected. A analysis of local control loops lies in the scope of the thesis as well. On the example of a local control loop in each foot it is investigated, whether or not this control loop is context independent and if not, how much context information is needed for proper functionality.

The transferability of control mechanisms and motion patterns from quadrupeds to bipeds - or vice versa is an highly interesting scientific question. With the indented robot, a transfer of these joint trajectories from quadrupedal walking to bipedal walking and a comparison of these two motion patterns is envisaged. This would be the first time that a real-world robotic system (as opposed to a simulation model) allows such a comparison without manually changing the robot's morphology in-between. In a final step, besides joint trajectories, the possibility to transfer the local control mechanism to bipedal walking will be analyzed as well.

1.3 Multi-Legged and Multi-Locomotion

To avoid confusion, the terms multi-legged and multi-locomotion are defined in the following. A robot is considered as multi-legged, when the number of limbs participating in locomotion is $\geqq 3$. Bipedal systems are categorized as humanoid robots and not as multi-legged, even when their arms are equipped with walking aids like a cane and are actively used to support the bipedal gait.

In this thesis, a robot that is said to be a multi-locomotion robot is defined as a system that

- is capable to show gaits in significant different postures and
- is able to use different numbers of limbs for locomotion
  or
- shows types of motion that are significantly different compared to walking, e.g., climbing, brachiating or swimming motions, even though the posture or number of legs involved may be equal to the ones used for walking.

If a six-legged robot loses two of its legs and continues its locomotion on four legs, the robot shows a multi-locomotion ability. A robot does not show multi-locomotion modes, when simply the order of leg movements or the phase offset between the legs is changed. The ability to manipulate objects is not a locomotion mode, otherwise this definition would include all humanoids robots.

1.4 Frame of the Thesis

The initial research activities were conducted within the LittleApe project, an internal project sponsored by the German Research Center for Artificial Intelligence GmbH at the Robotics Innovation Center, whereas the research activities performed within the iStruct project (Grant no. 50RA1013 and 50RA1014) led to the electro-mechanical system design of hominid robot Charlie. The empirical system evaluation of the hominid robot as well as the transferability analyzes were performed following the iStruct project.

1.5 Document Structure

This document is structured in seven chapters. Fig. 1.1 shows the structure of the thesis and the peer-reviewed publications, which support the respective chapter. In the first chapter, the motivation and objectives of the thesis are introduced. A research regarding the state of the art in mobile robots and robot control is given in chapter two. Chapter three introduces the developed hominid robot Charlie. This includes the biological background, the mechanical and electrical system design of the overall robotic system as well as its subsystems: the sensor feet and its active artificial spine. The biologically inspired robot control concept is presented in chapter four. The experimental evaluation of Charlie is divided into two chapters. Chapter five presents the experimental environment, lists the performed experiments, describes the evaluation criteria, and discusses the gained results from investigating the robot's performance in a quadrupedal posture, whereas the transformation to the bipedal locomotion mode and the bipedal experiments are shown in the sixth chapter. Finally, the presented thesis closes with chapter seven by reflecting upon the achieved results and gives an outlook regarding possible future work.

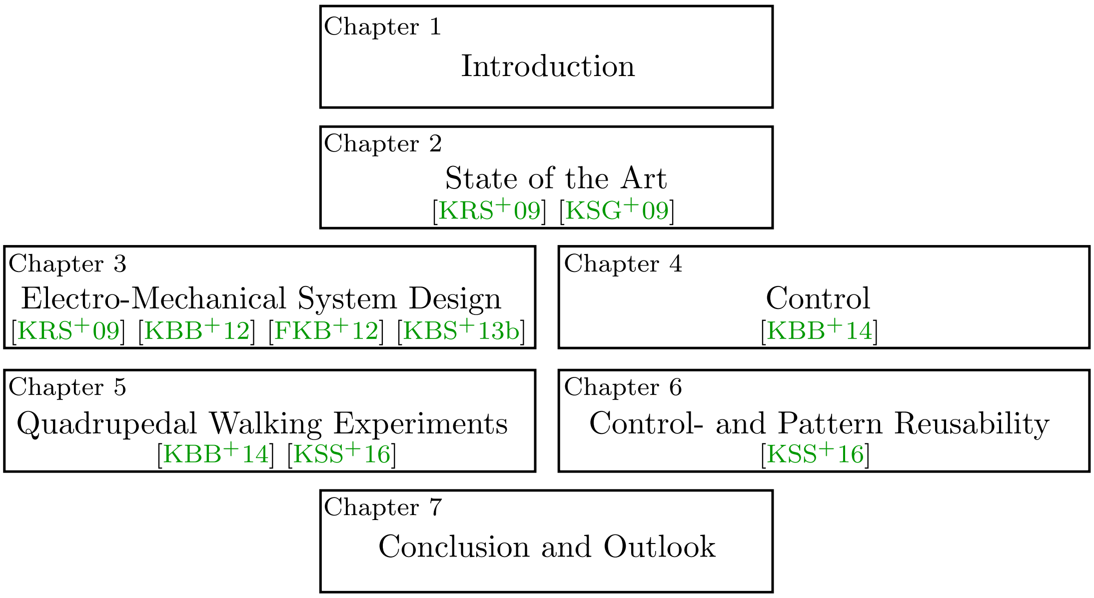

Figure 1.1: Structure of this thesis.

Chapter 2

Mobile Robots and Classical Control Methods

Robots equipped with wheels like the vacuum cleaner Roomba or equipped with tracks like Lego Mindstorm robots become more and more popular products for consumers. Especially for Lego, this popularity can be explained by the simplicity to design and build, program and control robots as well as comparatively low acquisition costs. In robotic research wheeled or tracked vehicles are appreciated as well, since they are - even in the absence of a building block system like the one Lego provides - in general more easier to design and to control than legged robots. As long as the field of application is undemanding, e.g., a flat surface without obstacles or terrain with minor slopes and sufficient grip, wheeled or tracked systems have the advantage of low energy costs to cover a certain distance compared to walking machines. If, however, the application area becomes more demanding, e.g., outdoor use-cases on unstructured terrain in exploration, agriculture, or search and rescue sites, inside a building with several floors, or on grounds with low friction, these systems quickly reach their mobility limit.

Legged robots, on the other hand, offer the possibility to select their points of interaction with the environment, which is why these kinds of robots are able to cope with a variety of different environments. This flexibility comes of course at the expense of simplicity in design, control, energy consumption, and motion speed. For legged locomotion, worldwide only a few systems are able to show such the intended multi-locomotion functionality.

By combining wheeled and legged locomotion, another category of ground-based vehicles is introduced, which can maintain the advantage of energy-efficient motion which wheeled systems generally provide. Basically, two different versions of these hybrid robots exist. In the first approach, the hand or foot serving as end-effector of a legged robot is replaced by a wheel (wheel-on-leg system). The second approach replaces wheels by well arranged legs (the point of intersection is on the axis of the driving motor), so that the end-effector(s) run on a circular path (legged wheel).

This chapter describes the current state of the art of mobile robots and gives a brief review on most commonly used control methods in mobile robots. Changing the robot's operating mode can often be seen in rovers with an active suspension system. Because of this multi-locomotion ability, at first wheeled rovers with an active suspension system are described, followed by a section regarding legged-locomotion in which a distinction between Single-Point-Contact Feet (SPCF) and Multi-Point-Contact Feet (MPCF) is made and their advantages and disadvantages are discussed. Because of this multi-locomotion ability, at first wheeled rovers with an active suspension system are described, followed by a section regarding legged-locomotion. For the legged-locomotion, a distinction between SPCF and MPCF is made. Since many multi-legged robots have the intrinsic ability to generate a statically stable gait, a point contact to the ground is sufficient and therefore a complex foot structure seems unnecessary. For the intended multi-locomotion robot, the realization of a bipedal gait is desired, which is more difficult to control the smaller the feet are.

In biological systems, a spine allows the body to move, rotate, and bend independently from the legs. In addition, the Range of Motion (RoM) of the limbs becomes increased due to the spine. Consequently, to increase the abilities of a mobile robotic system, an artificial spine can be beneficial. Hence, this chapter aims at introducing the concepts of passive and active artificial spines and closes with a brief overview of control approaches for complex walking machines.

2.1 Wheel-on-Leg Systems

This section presents multi-locomotion systems based on a hybrid design, where the robot's hand or foot is replaced by a wheel. In contrast to Mars rovers, which use a rocker-bogie suspension system [Bic88], [MIT12], rovers with an active suspension system allow a variety of locomotion modes. An active suspension system provides the possibility to select the contact point between wheel and ground in relation to the rover's body, thus enabling the robot to change its wheelbase, e.g., to drive through narrow passages. Furthermore, the rover can use the energy-efficient driving behavior for flat terrain and start walking over rugged terrain or terrain with low friction, where driving is not an option. These wheel-on-leg rovers allow a multitude of motion modes and eliminate one of the major drawbacks of the rocker-bogie or other passive suspension systems: the possibility of getting stuck, e.g., in sandy soil. Besides walking, the active suspension system can be used to change the rover's posture and thus improve the traction on the ground.

The most popular wheel-on-leg rover is the six-limbed lunar rover ATHLETE [Hev08] (shown in Fig. 2.1(a)) from the Jet Propulsion Laboratory (JPL). The rover is 2 m tall and has a weight of 850 kg. During field tests, the rover's capabilities using its six DoFs legs are shown such as overcoming soft terrain, walking, or its manipulation abilities. ATHLETE's successor is called Tri-ATHLETE and is JPLs second generation of a wheel-on-limb vehicle (cf. Fig. 2.1(b)). The requirement to use the rover for exploration as well as a cargo transporter led to the design of two identical, three legged units with seven DoFs per leg. By docking to a cargo unit, a six-legged system is formed. Each Tri-ATHLETE unit weights 720 kg. Combined to one rover, it has a height of 4 m and can carry a payload of 500 kg [HMFMQ10]. Up to now, the rover demonstrated a variety of different behaviors including docking to a cargo unit located in 3.2 m height below the body and walking over obstacles over 25 % of the rover's body height.

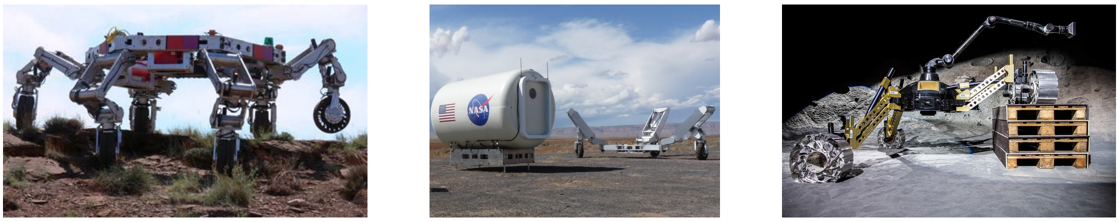

(a) The ATHLETE rover. Source: [Hev08].

(b) One Tri-ATHLETE unit before docking a cargo-unit. Adapted from: [HMFMQ10].

(c) The quadruped rover Sherpa stepping on an obstacle. Source: [COB+14].

Figure 2.1: Wheel-on-leg rover

The DFKI's four-legged Sherpa rover (see Fig. 2.1(c)) is smaller and has considerably less weight, compared to the ATHLETE-family, but shows multi-locomotion abilities, too. The robot has a square shaped footprint with a radius of 2.5 m in low body cross stance [RCK14]. The weight of 160 kg includes Sherpa's additional limb, a manipulator arm installed on top of the rover's main body. The manipulator allows the rover to use this fifth limb as a leg. Able to support the weight of the robot, so that two legs can be lifted off the ground, e.g., for climbing movements. The legs of Sherpa can reach a negative ground clearance, which means that the wheels can be lifted above the body. This gives the rover the opportunity to step onto high obstacles (see Fig. 2.1(c)). In a second version of Sherpa, a rearrangement of the DoFs introduces a knee joint in the rover's limb kinematics. This joint enables the rover to move the wheel independently in x-y plane, which was not possible in the first version of Sherpa's suspension [COB+14].

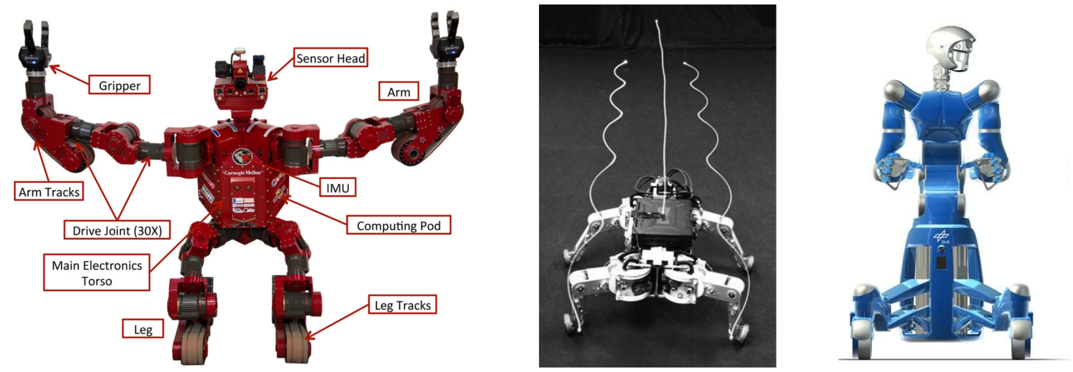

(a) The Chimp robot. Source: [SHK+15].

(b) The RollerWalker. Source: [EH12].

(c) The humanoid body of Justin on a four wheeled driving plattform. Adapted from [GFASH09].

Figure 2.2: Wheels and tracks as feet.

A different kind of driving unit is presented in the Chimp robot [SHK+15] (shown in Fig. 2.2(a)) developed by the Carnegie Mellon University. Motorized tracks are located on the end of each leg. With a total weight of 182 kg and a size of 1.6 m the Chimp robot enqueues itself in the dimensions of wheel-on-leg rovers. Due to the dimensions of 40 cm in length and 10 cm in width of each track, these support areas provide a stable stand for the anthropoid robot and thus lays the foundation to enable the robot to perform a wide range of tasks, including driving on two and on four legs. A folding of the tracks on the front arms allows the usage of dexterous hands for manipulation.

The clear differentiation between walking and driving was dissolved by the RollerWalker, developed by the Tokyo Institute of Technology. Passive wheels are installed on the end of each leg, as shown in Fig. 2.2(b). This rover uses skating motions to generate a forward motion in its drive-mode [EH08]. For rough terrain, the rover can be switched into a walking mode. For walking the wheel suspensions are flipped 90°

by an active ankle roll joint, since the passive wheels have no brakes installed, such that the rotation axis is oriented towards the ground to provide a stable and immobile structure. The rover is able to use different motion modes and Endo [EH12] states that the skating motion is eight times more efficient compared to the crawling gait of RollerWalker. However, due to the limitation of using leg motions to create a driving behavior, the energy-efficiency is lower compared to robots which use conventional active wheels for driving [EH12].

As shown above, rovers with an active suspension system and high ground clearance are able to perform a variety of different motion modes and therefore qualify as multi-locomotion systems. Unfortunately, the average weight of these rovers is mostly above 100 kg and thus very high. They are most likely too heavy for reconnaissance mission in degraded human environments, which are in danger of collapsing. Besides, the dimensions of these systems make an usage in indoor applications, where opening, closing, and passing of doors is required, very difficult, if not impossible.

Dealing with this size issue, the latest mobile platform for the two arm humanoid Justin (shown in Fig. 2.2(c)) is equipped with an active suspension system and can now change the footprint. Four wheeled limbs are connected to the platform and can extend and retract in horizontal direction without changing the robot's height [GFASH09]. This allows the robot to enlarge its support polygon resulting in a higher stability and the possibility to perform a manipulation of heavy objects or to decrease the footprint to be able to drive through narrow passages. Yet, the RoM of the limbs is restricted to the horizontal direction with about 15 cm per wheel. Even though the dimensions of Justin are suitable for the above mentioned applications, due to the size of its active suspension system the RoM is limited and the robot is unable to perform multiple motion modes like a walking behavior or climbing motions to overcome various obstacles. As stated in the definition of a multi-locomotion robot, manipulation abilities are excepted as motion mode.

2.2 Legged Robots

In general, wheeled robots are basically quipped with a maximum of four or six wheels. In the area of legged robots research, however, such a focus regarding the number of legs cannot be seen. A magnitude of different morphologies (biologically inspired as well as purely fictional), ranging from an one leg hopper to an artificial centipede, exists and are described in literature. Most of these legged robots show high mobility skills in their designated application areas; however, they are mainly designed to perform one single type of locomotion. Since robotic systems able to perform both, bipedal and quadrupedal locomotion are rare, this section discusses the technical details of robotic systems which are state of the art and able to perform one of the desired motion modes.

2.2.1 Single-Point Contact Feet

In legged locomotion, the contact between ground and the walking system is established through feet. Spherical feet (or feet close to spherical) generate a point contact with the environment (SPCF) and have the intrinsic advantage of providing traction between feet and ground at any contact angle. On one hand, feet that have multiple contact points to the ground lead to a better traction as well as a larger support polygon. On the other hand, they are more expensive, complex in design, heavier, and even more difficult to control. As a result, most robotic systems with four or more legs feature spherical formed feet.

Multi-legged robots like the eight-legged Scorpion [KSL02] have the intrinsic ability to create a stable stance at all times. All feet with ground contact are forming the corners of a ground projected 2D convex hull. As long the robot's, along the gravity vector projected, Center of Mass (CoM) is inside the convex hull, the system is statically stable.

One of the first quadruped robots showing multi-locomotion abilities, in particular the gaits trot, pace, or bound is shown in Fig. 2.3(a) and was developed by MIT Leg Laboratory in the mid-eighties [Rai86]. Even nowadays, this kind of spherical feet can be seen in many actual robots. Fig. 2.3(b) shows the quadruped robots developed by the U.S. company Boston Dynamics including LittleDog [MSM+11], the Spot robot, two BigDog [WMB+10] versions, and the military application LSIII (Legged Squad Support System).

The goal behind the BigDog family is to achieve a stable and reliable locomotion on rough and rugged terrain [RBN+08]. The robot BigDog (see Fig. 2.3(b) d)) is about 91 cm long, 76 cm tall, and weighs 110 kg. An engine is used to drive the robot's hydraulic actuation system. Designed to support military ground operations, the robot can walk with different gaits, e.g., a cross gait or gallop, reaches a maximum speed of 6.4 $\frac{\mathrm{km}}{\mathrm{h}}$, and carry a payload of up to 150 kg [BD216]. Due to the former military affiliation, information regarding sensory equipment and robot

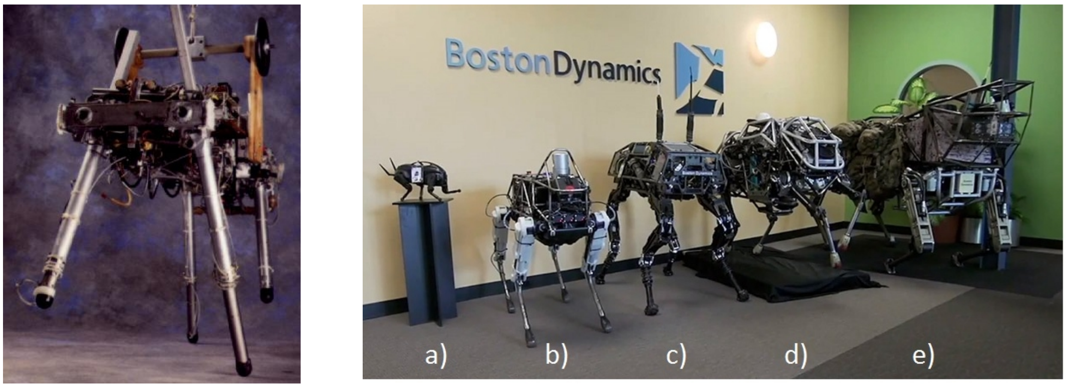

(a) Four-legged walking machine “Quadruped” from MIT. Source: [MIT].

(b) The Boston Dynamics four-legged robot family. a) LittleDog, b) Spot, c) + d) two versions of BigDog, and e) LSIII. Copyright: Boston Dynamics. Source: [hcdsrd].

Figure 2.3: Quadrupedal robots with single-point contact feet.

control are limited. A later version of BigDog features an arm, installed like an elephant trunk at the front of the robot. Because of this additional limb, the robot is able to perform additional behaviors besides locomotion, e.g., the manipulation of objects.

The quadruped robot HyQ [STG+11], shown in Fig. 2.4(a), was developed by the Istituto Italiano di Tecnologia (IIT) and uses an actuation principle similar to BigDog and is torque-controlled as well. The idea behind HyQ is to be able to study different aspects of quadrupedal locomotion, independent of the surrounding terrain, which is also desired for the in this thesis envisaged robot. HyQ has twelve active DoFs, two close to the torso to realize a forward/backward as well as a lateral motion and one as knee joint. Four passive, prismatic DoFs are installed in the ankle. In the beginning, research on HyQ had focused on reactive behaviors to allow the robot, which has a mass of 91 kg, to overcome obstacles or to recover from stumbles [STG+11]. Recent work focuses on making the robot more autonomous by integrating a planner, which processes terrain information gained by vision systems onboard and generates a suitable movement online [MWH+15]. Tactile sensors, however, which could give additional information regarding soil conditions, are neglected. Unfortunately, the robot’s abilities are shown only when wired to an external power supply and so far it is unknown if the robot can be operated with an on-board power supply.

Walking systems with a hydraulic drive principle are a minority within the mobile robots research area, compared to robots driven by electro-motors, because

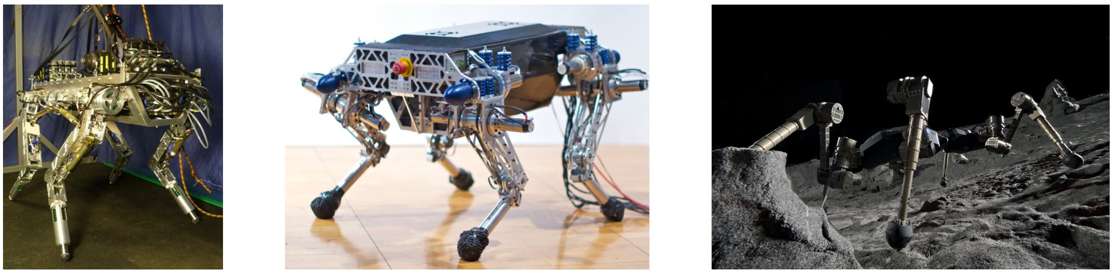

(a) The hydraulically actuated quadruped robot HyQ. Source: [STG+11].

(b) The quadruped robot StarlETH. Source: [HGB+12].

(c) The six-legged walking robot SpaceClimber. Source: DFKI GmbH RIC.

Figure 2.4: Multi-legged robots with single-point contact feet.

components like valves are expensive and the drives are mostly heavy and noisy. The LittleDog robot (shown in a) in Fig. 2.3(b)) is a small-size, 2 kg light-weight four-legged system intended as common robot platform for different research groups focussing on legged locomotion research [MSM+11]. The robot successfully showed its mobility on very rough, yet miniaturized terrain. To be able to walk in this terrain, LittleDog requires a high resolution terrain map, which is created by using external imaging equipment. Due to the knowledge of the environment, its leg motions are a sequence of discrete movements, generating a stable stance and posture at all times [GSVI13]. In addition, because of the robot's dimension and its control approach, the probability to use this robot in real world application is low.

In terms of weight and size, the quadruped robot StarlETH [HGB+12] (see Fig. 2.4(b)) from the ETH Zurich is in-between BigDog and LittleDog. The robot has a dimension of 71 cm x 64 cm x 58 cm and weight of 25 kg. Having altogether twelve DoFs, it is developed to show robust, energy-efficient, and versatile locomotion on four legs, according to the authors [HGB+12]. In contrast to LittleDog, StarlETH uses a reactive control approach and does not need external information for slow locomotion. Its multi-locomotion abilities include a cross gait and a gallop. The robot currently shows a stable gait, even when minor obstacles are placed in front of the robot. The lasted research on this walking machine focusses on increasing the robot's autonomy level. However, while generating a map of the surrounding environment, the robot field of view is limited to its quadrupedal pose. In addition, to be able to tackle bigger obstacles, a posture change can be beneficial as well.

For the sake of completeness, it should be noted that in addition to quadrupedal robots, robots with six or more legs also show multi-locomotion abilities. A leg design similar to the quadruped robot StarlETH can be seen in multi-legged robots like the six-legged robot SpaceClimber [BBR+12] (shown in Fig. 2.4(c)) or the eight-legged robot Scorpion [SK00], but with the extension that in these two robots one leg is equipped with a small gripping device to collect loose soil samples. Both multi-legged robots feature a lower leg with a compliant passive DoF. In each case, a spherical foot is located on the robot's end-effector. With these structures, the robots have shown their cross-country mobility, e.g., the robot SpaceClimber, which is able to walk in unstructured environment and can overcome slopes of up to 35° [Bar14]. The robot Scorpion showed its multi-locomotion skills in various terrains including a brachiating-like motion [SK07]. Even more, it demonstrated how multi-legged systems can fixate an object with a leg on their body and continue to walk, or deal with missing or non-functional limbs [SMK04]. Like StarlETH, both robots have a limited field of view since they operate only in one posture.

The six-limbed robot SmalBoSSE [Vol14] was developed for the exploration of small space bodies like asteroids. The robot has a mass of 15 kg and its legs are attached in a hexagonal pattern. Besides robust and stable walking, a hopping behavior was implemented [HDB14], which was tested while simulating micro-gravity. This also implies that the robot's multi-locomotion ability outside the testbed, where gravity is not absent, is limited.

The four-legged and six-legged Lemur [KAC+01] robots show a different way of dealing with varying terrain conditions. Their legs provide an interface to allow an operator to rapidly change any of its end-effectors, enabling the robots to climb on slopes including overhangs and performing tasks like sample acquisition or instrument placement. Yet, certain application areas do not allow a direct interaction with the robot to change its end-effectors depending on the task and a multi-locomotion robot should have the intrinsic ability to perform diverse locomotion.

In summary, as pointed out above, robotic systems with SPCF have a very high mobility and the advantage of a stable static locomotion at any time. Some of the presented systems are able to perform multiple locomotion modes, not least because of their number of limbs or additional devices. A change of the robots posture cannot be seen in any of the presented robots, which is mainly because of the design of the feet or missing DoFs in the robot's body structure. When a deployment scenario requires diversified solutions it is shown that these systems have their limitations, such that overcoming obstacles which are higher than the robot in its primary posture or the restricted field of view.

2.2.2 Multi-Point Contact Feet

MPCF describe all feet producing a surface contact with the ground. This type of foot can be divided into two categories: active and passive MPCF. Passive MPCF have adapting mechanical mechanisms, e.g., spring damper systems, allowing the foot to adjust itself to the ground conditions accordingly.

Depending on the dimensions of MPCF, additional sensors can be located within the structure. Recent developments in sensor technology led to a significant reduction of sensor size while maintaining the quality of information. Yet, it can be stated that the sensor density in robotic structures is very low compared to biological systems, which receive sensory feedback not only from receptors embedded in the skin but also from receptors within the muscles. The more sensors are integrated, the more information about the surroundings can be obtained and improve the overall robot control, including a context-based adaption of the locomotion behavior. Besides visual approaches, proprioceptive information is often used to classify the current terrain [GD09], [HRH+10], [OSJ+13], which allows to adapt the walking pattern accordingly.

Another aspect of MPCF is to improve the robot's traction to prevent the system from skidding, since a more sophisticated ground adaptation leads to an increased traction. In contrast to SPCF, MPCF allow the generation of a local support polygon, resulting in a more stable stance and thus a larger shift of the CoM in the desired direction, if necessary.

When considering extended use cases for mobile robots, an aspect which must not be neglected is that entirely different motion patterns or behaviors can be realized using MPCF which otherwise (with SPCF) would be difficult or impossible to implement.

A large number of research institutes are performing research on this topic to exploit the benefits, MPCF have to offer, regardless of the number of legs attached to the robotic system. Multi-legged robots have the intrinsic ability to walk with a statically stable gait, therefore a foot structure can be small, light-weight, and is easy to design compared to the ones used in humanoid robots. However, recent demands on robots in various areas and application scenarios require an improved skill set of the robot, which also includes an ideal handling of the interaction between foot and ground. Basically, the smaller the structure, the less sensors or printed circuit boards can be installed in the structure, which is a typical shortcoming of spherical shaped feet. In addition, a bipedal walking is more difficult to control the smaller the contact area that touches the ground. In this section, MPCF within multi-legged robots are discussed. Humanoid robots are addressed in the following.

Multi-Legged Robots

The Titan VII [HYT97] robot, shown in Fig. 2.5(a), was designed to support work at construction fields with steep inclines. Secured by wires, the robot was designed to be able to operate in slopes of up to 70°. To compensate unevenness within the terrain, its feet rely on a rocker-bogie mechanism at the sole to ensure the terrain adaption of the foot [HYT97]. No sensors or computational power are needed to adapt the foot to the ground, this means a reaction without latency is possible. A further advantage of passive MPCF is that no energy is required to archive the desired motion. If, however, a certain force has to be applied to achieve an objective, those passive systems are unfavorable. Unfortunately, this is the case in bipedal walking, therefore a MPCF with a passive ankle joint cannot be used for the envisaged robot.

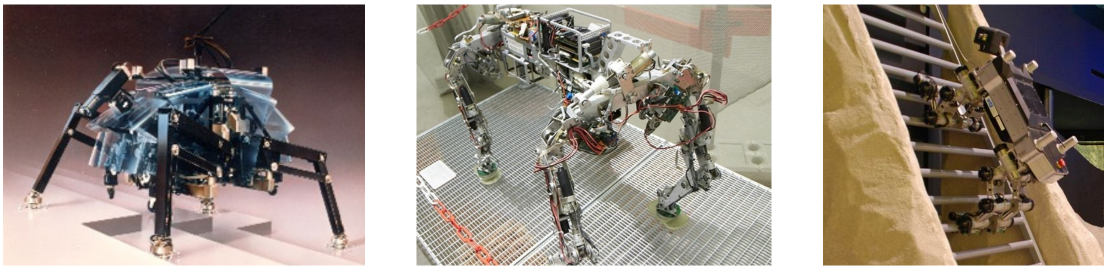

(a) The Titan robot. Source: [htt].

(b) The robot BISAM. Adapted from: [hBDC].

(c) The robot Aramies features actuated claws. Source: DFKI GmbH RIC.

Figure 2.5: Quadruped robots with MPCF.

The first version of the quadruped BISAM [PC05] robot was equipped with SPCF. Later on, a bigger support area, an increased sensor density and a higher friction was desired, which resulted in the installation of a MPCF including a six DoF force/torque sensor and an active ankle joint [ADH05] (see Fig. 2.5(b)). BISAM showed its multi-locomotion abilities by using the statically stable crawl gait in unstructured environment and a cross gait in flat terrain. Unfortunately, the robot is not able to change its posture, to gain the above mentioned advantages.

The quadruped robot Aramies [HSK05] (shown in Fig. 2.5(c)) was mainly designed for difficult environments like rugged terrain. The robot has four identical feet, each with actuated claws, which can be used to get better grip in steep inclinations. Aramies claws feature five pressure sensors and an Infrared (IR)-distance sensor to allow ground contact detection. Besides walking, Aramies makes use of its toes for a climbing behavior on a scaffold-like structure, as seen in Fig. 2.5(c). A change of posture without the climbing frame, is yet not possible in Aramies.

The robot Mantis [MBK13] is a six-limbed robot inspired by the praying mantis, see Fig. 2.6(a). The four rear legs are modeled different than the two front legs, which have an actuated hand installed. The locomotor system is flexible and offers the possibility to walk on six as well as on four legs. Four legs are sufficient for locomotion or to generate a stabile stance, therefore the front arms can be used for manipulation. Mantis is able to make extensive use of its tactile and visual perception of the environment. The information gathered about the substrate and context the robot is situated in allows it to choose the ideal locomotion behavior out of a database were a set of locomotion behaviors is stored [DBBK15].

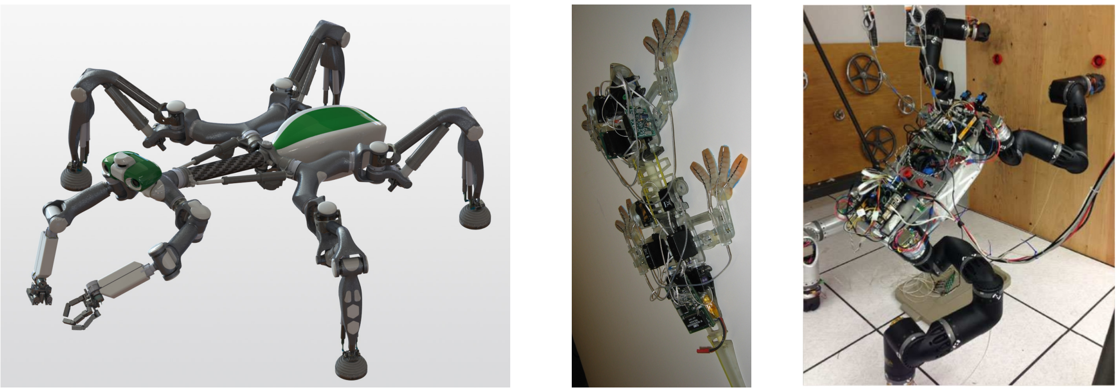

(a) The robot Mantis with its front limbs, which can either be used for manipulation or locomotion tasks. Source: DFKI GmbH RIC.

(b) The StickyBot robot. Source: [SHK$^+$08].

(c) The robot RoboSimian. Source: [HBM$^+$15].

Figure 2.6: Multi-talented quadruped robots.

The robot StickyBot [HUEC11] (see Fig. 2.6(b)) shows, how important the design of the robot's structures and subsystems is. An enhancement of the robot's locomotion behavior is realized by using MPCF. StickyBot is able to climb by employing several principles adapted from the gecko like dry adhesion in a flat foot [KST$^+$08]. The adhesive pads on the four toes per foot allow the robot to climb vertically on different surfaces like wood, metal or even glass. As for the above mentioned robots, a posture chance is also not foreseen.

Figure 2.6(c) shows RoboSimian [HBM$^+$15], a four limbed robot which participated at the DARPA Robotics Challenge (DRC) in 2015. The robot's general-purpose limbs are arranged in an axis-symmetric fashion and feature seven DoFs per limb [SLBB14]. In addition, each limb is equipped with two passive caster wheels, allowing the robot to adopt passively stable postures. Its limbs are capable of both, mobility and manipulation, allowing the robot to traverse rugged terrain to manipulate certain objects, e.g., valves. The limb's end-effector is shaped like a food can and has, like SpaceClimber, a gripping module installed which can become extended, when required. It is stated that the robot can perform basic behaviors autonomously, such as walking, yet high level tasks are assigned by an operator, which also has to review and approve the robot's calculated motion plan [HBM+15]. The sensor density in the limbs is relatively modest, since only one force/torque sensor is integrated and the robot control relies heavily on imaging sensors. A context-based change of the robot's motion with respect to the soil properties or an enrichment of the generated maps by tactile information are not foreseen.

Humanoid Robots

To show different motion modes and to study the transferability of motion patterns or joint trajectories of a quadrupedal walking pattern to a bipedal gait, the robot Charlie, introduced in this thesis, has to have the technical and mechanical requirements to achieve these objectives. Therefore, the design of humanoid robots and their MPCF is an important factor, as can be deduced from literature on research on humanoid robots.

One of the most advanced humanoid robots worldwide is Hondas Asimo [SWA+02]. The development of the first Asimo predecessor started in the 1980s. Figure 2.7 shows the robots from the early beginnings to the actual Asimo model. With a height of 130 cm, a weight of 50 kg and altogether 57 DoFs, Asimo is able to run with a speed of 7 $\frac{\mathrm{km}}{\mathrm{h}}$ [Spe16] or to hop on one leg and is one of the few robots able to show multi-locomotion. Recently, Hondas research and development department increased Asimo's multi-locomotion abilities even more and proposed a control algorithm which allows a modified version to make a dynamic transition between quadrupedal and bipedal locomotion [KWK+15]. The robot's quadrupedal motion, however, appears restricted and somewhat surreal due to to humanoid design of the robot.

A recently developed robot designed for usage in disaster scenarios is Atlas (see Fig. 2.8(a)). Atlas is a hydraulically-actuated humanoid robot with six DoFs in each leg. Its sensory equipment includes an array of strain gauges which allows a three-

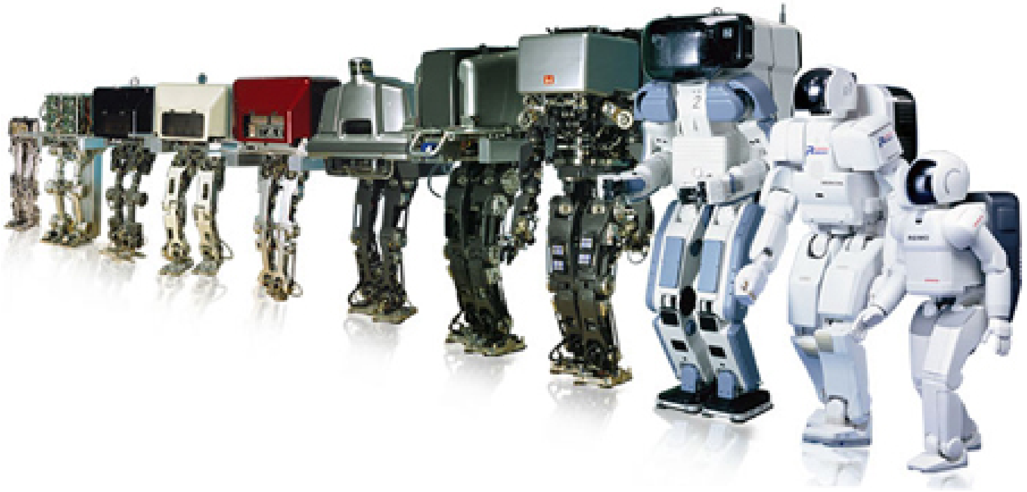

Figure 2.7: Honda research in bipedal locomotion started in 1986 and continues until present. Source: [hrj].

axis force-torque sensing in the foot [FKK+14]. Due to its mechatronic state-of-the-art design, this robot was chosen to be provided to those teams participating in the DRC, which were focussing more on software rather than on hardware development. Up to now, Atlas does not show any multi-locomotion abilities.

The DRC-Hubo robot (see Fig. 2.8(b)), also developed to participate in the DRC, has a three axis force/torque sensor integrated in each ankle, where the roll and pitch axis can be actively actuated [LZH+14]. The sensory equipment is completed by accelerometers and gyros, which are utilized to control the robot. Like Asimo, its feet are designed without any toe joints. The leg actuator provides sufficient torque to allow the robot to lift itself up on one leg.

The Gorilla Robot III [KAS+13b] (shown in Fig. 2.8(c)) is in between the two categories, since it is neither a humanoid nor a quadruped robot. The robot weights 24 kg and has 26 DoFs. Inspired by gorillas, the robot has three motion modes such as bipedal (see Fig. 2.8(c)) and quadrupedal locomotion and is able to brachiate [ASHF09] [FKSH07]. The transition between bipedal and quadrupedal pose is realized with a statically stable joint angle sequence [SSK+08]. The robot is not autonomous in terms of energy supply but connected to an wiring harness and is powered externally. Unfortunately, the influence of this cable loom on the stabilization is not further discussed in literature.

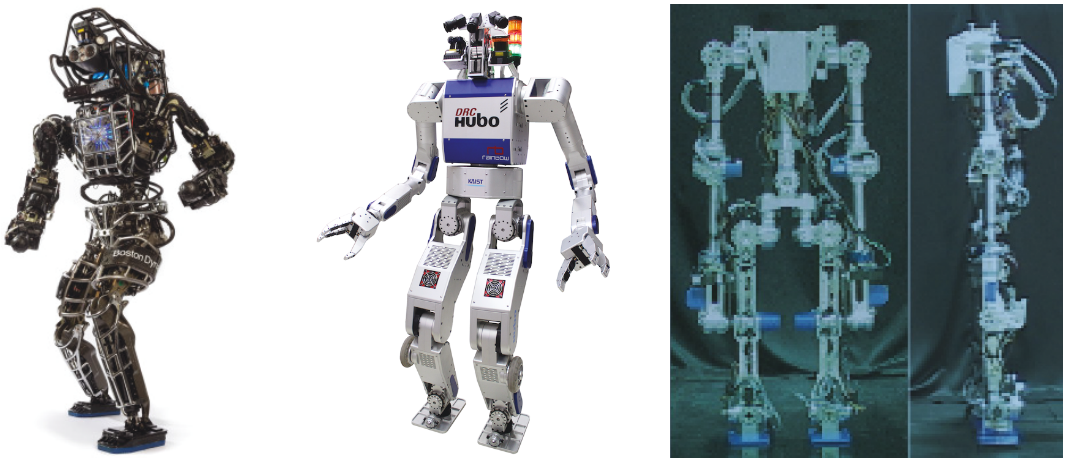

(a) The humanoid robot Atlas. Source: [Atl16].

(b) Darpa Robotics Challenge participant Hubo2. Source: [hcfD].

(c) Gorilla Robot III. Source: [KAS$^+$13b].

Figure 2.8: Robots able to perform bipedal locomotion.

2.3 Artificial Spines

In nature, the spine is a central element in vertebrates bodies. Due to the spine, the area between head and pelvis remains mobile and flexible. The specific role of the spine depends on the respective vertebrate species including body posture and favoured type of locomotion. In general, the structure of the spinal column allows to absorb shocks, store and release energy to allow an energy efficient walking and the enhancement of locomotion capabilities [Kap99b].

An extreme example of the spine's movement can be observed in a cheetah while sprinting. The spine's bending and stretching is an essential part of this gait. But locomotion is only one instance to point out why having a spine is beneficial. In day-to-day activities like cooking, the body is bend and stretched, e.g., to pick up pans and pots and the torso can be twisted to reach for spices while the feet remain stationary. Based on these examples one can imagine how an active spine could improve the locomotion and manipulation capabilities of a robot, if properly built and controlled.

Robotic research groups, working on different kinds of locomotion from bipedal to multi-legged walking, are using biologically inspired designs and control approaches, but neglect the DoFs introduced by the spine in nature. Robots or simulation models of robots are often simplified by implementing a rigid body between head and pelvis, which is a valid approach to simplify the research problem on legged locomotion. On the other hand it limits the transferability of, e.g., natural walking patterns to robotic systems, since humans and animals use all of their given DoFs during locomotion.

Although the majority of mobile, biologically inspired walking robots have a rigid body, research activities increasingly intend to replace the rigid structural bodies with additional DoFs. The benefits of a spine come at the expense of increasingly complex mechatronics and control algorithms. Nevertheless, for future tasks it will not be possible to simply dismiss the benefits of a spine.

The artificial spine developments can be categorized into passive and active artificial spines. Using passive spines with elastic elements has the advantage that vibrations and abrupt movements can be absorbed without passing through the robot. Besides, it can also help to prevent a possible loss of ground contact after a hard impact from the foot to the ground. One disadvantage is that the flexibility cannot be switched off. By installing an spine with active DoFs, additional mobility possibilities can be introduced to the robot. This means not only that existing walking patterns can be improved, but more importantly that some kinds of locomotion behaviors can be realized, which are not possible if these extra DoFs are missing.

Passive Artificial Spines

Passive artificial spines can mostly be seen in small and lightweight robots. Most of the existing passive spines are made of multiple parts. Researchers from the Beijing Jiaotong University state that this design makes the spines difficult to manufacture, because the adjustment of the spine's stiffness is more complex [ZYLG13]. Therefore, they present the simplest design of a passive spine, which can be seen in Light-Dog [ZYLG13] in Fig. 2.9(a). The front and rear bodies are connected by one piece of elastic material. However, compliance in various segments of the passive spine allows to introduce axial or torsional elasticity where it is desired.

The robot Fanari [KDBA11] has three different customized spines, whereas two versions are close to flexible bars and only the third one is more complex in its design. It consists of equal parts and can be bent in two directions: up/down and left/right. Flexibility is gained by inserting three pairs of springs between these elements. The robot shows, like a passive dynamic walker, a bounding gait down a slope, whereas its stability completely depends on the spine. Without the spine, the authors state that the robot becomes unstable [KDBA11]. Its rear body rotates around the front legs and the robot overturns.

Another approach is implemented in the robot Tiger [KBS+13a], see Fig. 2.9(b).

For this robot, different spine designs are installed and tested, which differs+ in their flexibility. A linear spring is located on a soft metal sheet which connects the front with the rear body. The metal sheet has horizontal gaps, to allow a downward bending. The RoM can be adjusted by the depth of the gaps. By utilizing the artificial spine, the authors claim to be able to increase the velocity to a minor extent, while reducing the energy consumption and increasing the stability [BVSA10].

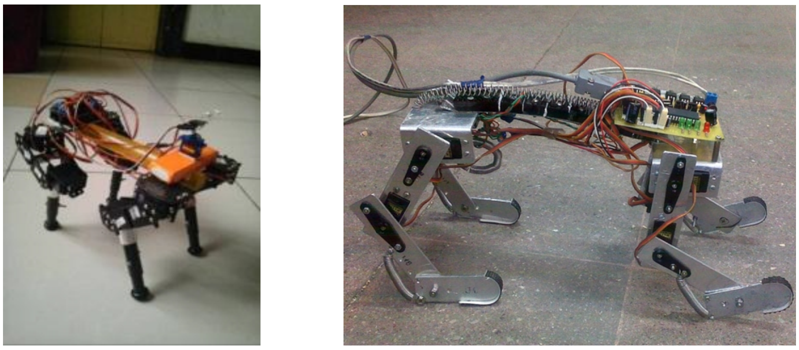

(a) The robot LightDog. Source: [ZYLG13].

(b) The robot Tiger. Source: [KBS+13a].

Figure 2.9: Robots with a passive spine.

The LittleApe [KRS+09] robot uses hook shaped front feet, to climb a vertical surface. Its passive spine adds additional flexibility and damping capabilities to the robot. The spine configuration like RoM and torsion ratio can be directly adjusted. It was shown experimentally that the spine in LittleApe reduces the shocks while walking [KBG+10].

With the implementation of a passive spine, the conventionally used rigid torso can be replaced. The functionality of a passive spine is limited to adding extra damping capabilities to the robot. The serious disadvantage is that it can introduce uncoordinated motions to the robot's body, which can be counterproductive for the desired leg motion or the walking behavior, due to early leg touchdowns or possible changes of direction or the like. To increase the robot's functionality and its RoM an active artificial spine is needed.

Active Artificial Spines

To show the advantages of an active artificial spine, investigations are performed in simulation and on real-world robots. With a simulation model of the robot Wabian-2, it has been investigated by Or how a spine affects the overall current consumption of humanoid robots in simulation [Or13]. The simulation model is based on the design and arrangement of the DoFs from the robot Wabian-2, including three DoF segments in its torso, which is not installed in the real robot. Or experimented with different kinds of spinal movements and compared the power consumption needed for walking. He showed that using the spine improperly is counterproductive, but with the right motion, up to 26.5 % less energy was required while walking, compared to walking with a rigid body.

The quadruped robot Cheetah from Boston Dynamics is a real-world robot with one active DoF between front and rear body. This allows to flex and stretch the robot's back in each step of the implemented gallop gait. With this gait, the robot reaches a top speed of 46.6 $\frac{\mathrm{km}}{\mathrm{h}}$ while running on a treadmill [Che16]. Like in natural cheetahs, the articulated back actively increases the robot's stride length and its running speed. Unfortunately, at present no scientific data is available on it. Currently, Cheetah is not able to walk without external assistance; its power supply (a hydraulic pump) is located off-board and the robot needs a stabilising device (a rigid rod which connects the robot laterally to the test bed) to stay onto the treadmill.

The quadruped robot Bobcat [KST+13] makes use of two DoFs per leg, has one DoF in its spine and is able to walk without external support. It is a small-size and lightweight robot with a mass of 1 kg. The spine actuator allows a rotation in the sagittal plane [SBK+13]. In [KBS+13a], the authors present experimental results to show how an active spine can increase the robot's walking velocity and furthermore a positive effect on its stability margin can be observed. The single DoF, however, allows only a limited RoM. To support different gaits in various ways, a technically more sophisticated solution is required.

Besides multi-legged locomotion, tendon-based approaches to drive artificial spines can be seen in humanoid robots as well. Kenta, a man-size humanoid shown in Fig. 2.10(a), was introduced by Mizuuchi *et al.* [MTY+02]. Inspired by the spine of humans and their muscle driven system, Kenta's whole body is designed as a tendon-driven system. In sitting position, the robot's back can stabilize itself and can track objects by moving the spine. Continuing this development, the successor Kojiro was able to stand by itself [MNS+07], see Fig. 2.10(b). Holland *et al.* introduced the ECCE robot, shown in Fig. 2.10(c), which has resemblance to Kojiro [HK06]. Due to the tensions within the robotic skeleton, the "multi-degree-of-freedom structure" [HK06], with its elastic elements reacting with its whole body to allow a more human-like and fluid motion.

The installation of one or two additional rotational DoFs in the trunk in quadrupeds as well as in humanoid robots like in Atlas or Hubo2 (see Fig. 2.8

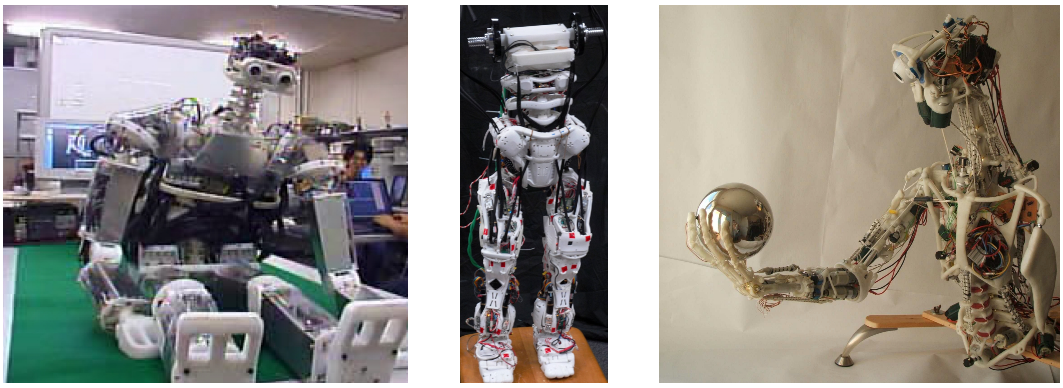

(a) An active spine in the robot Kenta. Source: [MTY+02].

(b) Torso and lower body of Kojiro. Source: [MNS+07].

(c) Torso of the ECCE robot. Source: [HK06].

Figure 2.10: Robots with an active artificial spine.

on page 25), is a first step but since the RoM is limited, it is less realistic compared to nature and simplifies the research problem. The tendon-based approaches to implement an artificial spine in humanoids are highly complex structures with a design close to the natural counterpart. Unfortunately, due to their weight and the complexity of their design, these humanoid robots are not able to stand up or walk yet [Or13]. Therefore, an abstraction of the natural spine would make sense, without simplifying the research problem.

2.4 Control Approaches for Complex Walking Machines

Generally, control in the context of mobile robots means the motion planning and execution for several DoFs to gain an uniform, coherent, continuous, stable, and energy-efficient motion. The control of a kinematically complex robotic system is a demanding task where in recent years intensive research has taken place and is indeed still taking place.

The first robots used in real world applications were “classical” industrial robots, basically machines which perform a certain task over and over again without the need of human assistance or interaction. Besides the monotonous task, even nowadays the workspace, e.g., in production facilities and the production processes are specially designed for these kinds of robots. Consequently, the control of these machines seems relatively straightforward.

With the development of the first mobile robots, due to the complexity regarding the surrounding workspace and tasks, an increased need for robot control arose. In literature, different control paradigms can be found. This section focuses on the control of mobile robots and introduces the most commonly used control architectures today. In the following, the ideas behind reactive and deliberative control are briefly described, including strengths and weaknesses of each method, see also Fig. 2.11. By discussing the hybrid control approach, an architecture designed to diminish the limitations of both presented methods is introduced.

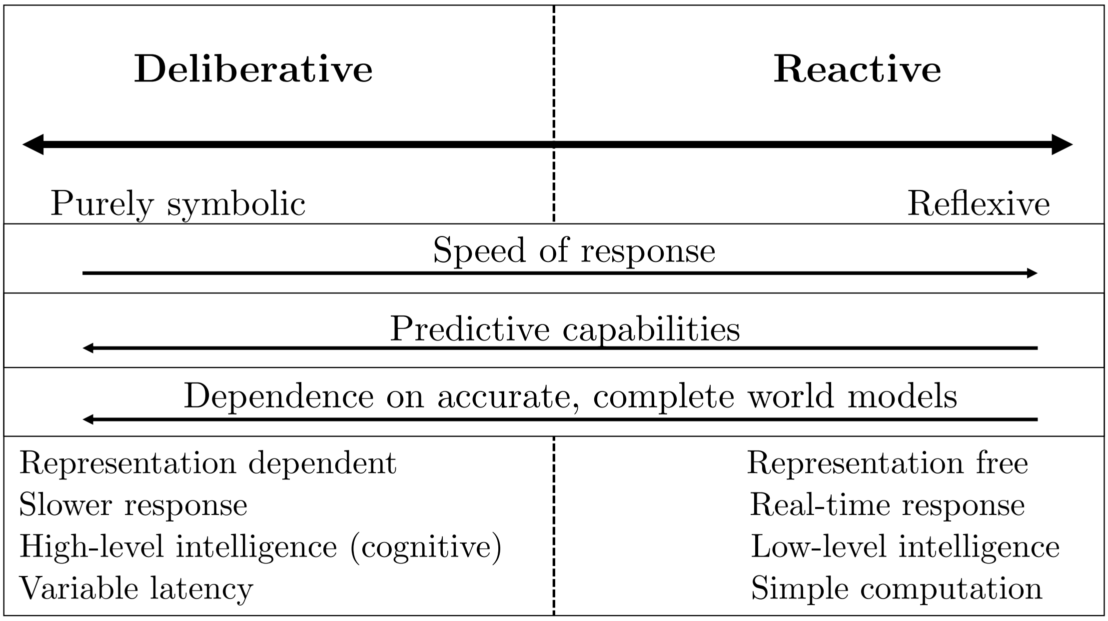

Figure 2.11: Comparison of control paradigm by Arkin [Ark98].

2.4.1 Model-Based or Deliberative Control

Deliberative control architectures are goal oriented and are planning ahead before starting to act. Robots using this control paradigm fulfill continuously a strict order of three states: sensing, planning, and acting. When a task is assigned to the robot, it relies on a given model of its environment or creates one using its sensory information. The more knowledge the robot has about its environment the better the world model, the robot has. After planning and selecting an appropriate solution, the robot executes its plan using its actuators.

When the overall mission consists of several tasks, the robot can update its model and repeat this process after each successfully finished task until the goal is reached.

As long as the model is nearly perfect and the environment is predictable, ie. no uncertainties are present and the environment does not change, this kind of robot control is working very well, e.g., for space exploration. If the plan emerges as non-executable a replanning has to take place. Within slowly changing environments or when the model is not entirely consistent, this approach can still work. This, however, is one of the major drawbacks of this control paradigm. The more the robot's surrounding differs at the execution phase compared to the world model used for planning, the more likely the plan will fail, which may require a permanent replanning without any movement of the robot.

2.4.2 Reactive Control

A reactive control system can make use of different behaviors and generate an emergent behavior of the whole robot by coordinating the individual behaviors. The first robots that were able to show complex behaviors (built with analog electronics), were invented in 1949 by the neurophysiologist William Grey Walter [Wal50]. Walter's robots had different names, but are generally known as tortoise robots or Walter's turtles, most likely due to their appearance and their slow movements. Walter himself preferred the term *Machina speculatrix*. By using these three-wheeled robots, Walter was able to show a behavior, where the robots, when low on power, were able to find a recharging station which was indicated by a bright light.

Basically, a reactive control implies a designated and direct response on a certain stimulus. Like in Walter's turtles, the behavior of searching the recharging station can be seen as a mapping of sensor input to actuator output. In this case, a behavior becomes active when the "low on power" stimulus triggers the search behavior. The robot senses the light source and reacts by using its actuators to drive towards the light.

One advantage of the reactive or behavior based control is the fast response time. For example, if the recharging station ahead of the robot is switched off and another, e.g., to its left is switched on, the robot would immediately change its course and drive towards the new light source (when the light is within the sensors field of view, otherwise a light search behavior will be activated). With a model-based approach, however, the robot would have to stop and update its plan to reach the goal. This reactive control paradigm is very suitable for real-world applications and scenarios, where the robot is acting in a dynamic environment. The use of internal representations or world-models is not foreseen, since the generation of an accurate model is as difficult as it is time consuming. On the other hand, its weakness can be seen in tasks, where predictive planning is required to generate a certain outcome. No world knowledge is available, which means that a context-based adaption (which may have a positive influence on duration and longevity) is more challenging to achieve.

The behavior of reactive systems is only as good as the quality of their sensory perception, on which they heavily rely. Local failures in the sensory system can lead to serious consequences, but this is also true in the model-based approach, in cases where model updates are required.

The idea of this architecture is the basis for many different approaches put into practice, including the subsumption architecture of Brooks [Bro86]. Above descriptions represent only a brief summary to illustrate the principle of reactive control. A comprehensive listing of different approaches can be found, e.g., in [Ark98], [Alb07], or [LWT09].

2.4.3 Hybrid / Behavior-Based Control Architecture

As discussed above, the reactive as well as the deliberative control paradigm have their strengths and weaknesses. By combining both control paradigms, the mentioned shortcomings can be overcome.

Typically, a hybrid control architecture consists of three different layers [RN04]. Formulating a plan and maintaining the world model is still located in the deliberative layer, whereas the plan execution is controlled by the reactive layer. An intermediate level is responsible for the communication between both layers, e.g., as interpreter between the different scales. In [NTNM11] a review of various control architectures for mobile robots can be found.

The behavior based control is a biologically inspired alternative to the hybrid control paradigm, with the difference that the intermediate layer between reactive and deliberative control is omitted. Arkin, a proponent of the Behavior-Based control approach states in [Ark98] that roboticists can gain a lot of knowledge by studying biological systems including subject areas like neuroscience or psychology. To exploit the advantages of both approaches, he proposed the hybrid control architecture called Autonomous Robot Architecture (AuRA) [ARH88]. The world knowledge and context-based planning capabilities of the model-based control combined with the robust reactive approach including its ability to deal with a continuous sensor data stream results in a beneficial control architecture. The planner assumes that the robot itself is in an optimal condition. The robot's state is kept under surveillance by the lower level, which is monitoring the internal sensor data. If the condition of the robot's subsystems change negatively for the robot's overall functionality (e.g. the actuator temperature is increasing dramatically and a risk of failure is most likely) or safety, the deliberative layer is affected as well, since the plan cannot be executed as anticipated. Consequently, the higher level has to consider the new conditions, adapt its overall planning and perform behavioral changes.

2.4.4 Transfer of Biologically Inspired Control Methods

In nature, the control of complex systems (animal and man) is done by segmenting the control problem into a set of subproblems, which can be solved using a distributed control architecture. The brain for example is divided into several sections, each responsible for different tasks like speech, emotions, or to control the body's balance. Coordinated muscle function to generate rhythmic behaviors for locomotion, however, are realized regardless of the respective cognitive abilities.

At the beginning of the 20th century researchers tried to explain the principles which underlie rhythmic motion, nowadays known as Central Pattern Generator (CPG). Basically, Sherrington and Brown proposed two different explanations. Arguing with the rhythmic motion seen within the scratch-reflex in animals, Sherrington proposed that a chain of reflexes can result in the creation of rhythms and thus can also be used for locomotion [She06]. This means that locomotion is basically only a stringing together of reflexes. Brown included Sherrington's approach in [Bro11], where he laid the foundation for his proposed model. However, his idea is in contrast to Sherrington's reflexes theory. Brown suggested that the rhythms are generated centrally [Bro14], e.g., for locomotion, neural networks are located within the spinal cord. Brown called his concept the half-center model and explained the rhythmic motion by two coupled sets of neurons, which can mutually inhibit each other.

Ijspeert gives a detailed review about central pattern generators used for locomotion control in both, animals and robots. He argues that due to experiments on lampreys, salamander, frog embryos, or Brown's experiments with cats specific evidence exists "that rhythms are generated centrally without requiring sensory information" [Ijs08]. Although a feedback is not needed, it is still useful in order to shape the executed motion. In animal testing, cats were placed on a treadmill and despite their transected spinal cord, the steps of the rear legs adjusted themselves accordingly to the varying belt speed [FGHR80]. By changing the speed of the belt, gait transitions to trot and gallop could be observed, which shows the correlation between CPG and sensory feedback. Whereas the generation of rhythmic patterns for locomotion is localized on a lower level like networks located in the spine, deliberate actions like change of direction or posture control are located in higher-levels within the brain (e.g. motor cortex). In addition to animal experiments, in [CNSJ+94] it is stated, that evidence exists which suggests that the first example of a central pattern generator in an adult human was observed. A 37-year-old male, which injured cervical spinal cord resulted in a loss of movement and perception below the neck, showed rhythmic movements in the lower legs.

Biologically Inspired Distributed Control

By studying biological systems, a distributed control hierarchy is indicated which can be used for the control of mobile robots. Despite the different robots' scales and principles of locomotion, the distributed control approach has proven to be useful in a multitude of robotic systems; to control the six-legged robot Hannibal, the robot was segmented into single logical units, whereas each leg and the body represent a subsystem featuring sensors, actuators and a processing unit. The robot was able to demonstrate stable locomotion over rough terrain [Fer95].

Espenschied et al. introduced an insect-like hexapod [EQBC96] with a stick-insect inspired distributed control strategy. Designed for rough terrain as well, the robot was able to maintain its posture by responding to ground irregularities with passive and active compliance. The implementation of a human inspired distributed controller for an anthropomimetic robot ECCE is shown in [JWK10]. The authors state that the approach is feasible, even though the robot has a very high complexity regarding control due to its 80 artificial muscles with three sensors in each muscle.

Central Pattern Generator

In multi-legged robots the CPG approach can be seen in numerous robots. In humanoid robotics, however, the CPG approach has still not become widespread. Generally, for most humanoid robots a model-based control is chosen, which bases on the Zero Moment Point (ZMP). The ZMP concept was introduced in 1968 by Vukobratovic [VB04] although the actual term ZMP was introduced years later. The ZMP is a point P on the sole of a foot, where the moments $Mx = My = 0$. Only the reaction force R (the foot is resting on the ground) and the moment Mz are acting on P. If the support polygon of the foot is too small to contain an appropriate position for point P, the moments will become uncompensated and start acting on the foot, introducing a moment which results in an undesirable rotation around the foot and thus can cause the robot to tumble over. By planning the motion in a way that the ZMP stays inside the support polygon, a stable walk is ensured. Planning the motion can be done off-line, e.g., [TLTK90], [YTK93], or more recently due to increasing computation power available on the robot even in real-time [HHK+04], [SN05] or [HHC07].

As mentioned, current research showed the real-time capabilities of the ZMP approach, but the CPG concept still requires less computational power. In an ideal environment like in simulation, walking humanoid robots based on CPGs can be seen in [TNMY05], [HLWI07] or [LWF14]. A hybrid CPG ZMP control system is presented in [Or10], showing a humanoid robot in a simulated environment, able to walk and supported by the motion of a flexible spine. Nevertheless, the ECCE robot shows the drawback of the CPG approach. It can become difficult to find a good parameter set, e.g., for a neural network, to coordinate the magnitude of DoFs to generate a stable locomotion.

Robots which are mechanically less complex compared to ECCE like HOAP 1 [SN02] or Kondo [BK06], however, are able to walk in real world environments with the CPG approach. The robot presented in [RI06] has one CPG for each used DoF. By coupling these CPGs, the speed of locomotion can be modulated, including a reversal of direction allowing the robot to walk backwards. In the controller, a sensor feedback is integrated and according to the authors, the possibility to modulate the trajectories in real time increases the stability of the performed gaits. Utilizing learning frameworks, the parameter search can become automated (e.g. [MMN+05]). A learning framework for a CPG is presented in [EMM+08] and the results are used for the motion in a bipedal robot.

The range of functionality of the CPG approach is not limited to walking on flat and even terrain. In [Nag03] a humanoid robot shows a rhythmic motion to climb stairs and in [NHBC14], a neural model is described that can generate different motion patterns, rhythmic as well as non-rhythmic and demonstrates the functionality on a NAO robot.

2.5 Conclusion

This chapter reviewed the current developments in mobile robotics as well as the most common robot control methods. Focusing on systems with the ability to perform multiple locomotion modes as well as for the presented thesis important subcomponents - bipedal and quadrupedal locomotion - the chapter disclosed several robotic systems and their specific characteristics. These include, besides the electro-mechanical design, the robot's capabilities and limitations.

Two approaches are discussed, the wheel-on-leg systems as well as legged robots. Due to the size and weight of current wheel-on-leg multi-locomotion robots, their field of application ideally lies more in open field missions like space exploration and less in the area of search-and-rescue scenarios, man-machine-interaction, or human assistance in indoor environments with little space.

Animals, commonly used as inspiration for legged robots, regularly display a variety of precise and agile locomotion, independent of the given surrounding. Because of these capabilities, biologically inspired robots appear to be suitable for application in native or man-made environments. However, most of the above discussed multi-legged robots currently show no multi-locomotion abilities. The same is true for humanoid systems, where the robot ASIMO is the exception, because of its latest ability to walk on all four limbs. ASIMO's skill set was enhanced, since the stability of locomotion in unstructured environments is a weakness of humanoid robots in contrast to multi-legged robots.

In addition, an interesting scientific subject is the study of a possible reusability of joint trajectories for different walking patterns, e.g., quadrupedal and bipedal which may give clues about the evolution from quadrupedal to bipedal walking, which has yet not been conducted on one (mechanical) system as well due to the multi-functionality issue. These mentioned shortcomings and pending issues lead to the design and development of a biologically inspired, ape-like robotic system since chimpanzees and their conspecific are multi-talented animals which regularly display motion patterns involving two, three or four limbs and are capable of performing a variety of additional behaviors like climbing or dexterous manipulation [Bou69].

The introduction of additional DoFs in the robot's body lays the foundations for movements or motion sequences, which either cannot be realized without this newly gained flexibility or would require great effort of the electro-mechanical system. For the development of an artificial spine, the use of both alternatives (a passive and an active one) is discussed as well as the kinematic structure. It is shown that the functionality of a passive spine is limited to add damping capabilities to the robot and can introduce undesired motions to the robot's body. Therefore, for the intended robot the realization of an active artificial spine is pursued.

The control of such a kinematically complex mobile robot is still a demanding task. Due to the increased importance to percept the environmental conditions, special attention is given to the integration of sensor systems and electronics within the robot. For a robot without exteroceptive sensors like cameras or laser scanners, a contact-free perception of the environment is not possible. Thus, the reactive or behavior based control approach including a decentralization is most suitable. A high sensor density provides additional flexibility in controlling a robot and its stability, and create the basis for the implementation of local control loops.

Chapter 3

Electro-Mechanical System Design

Nature found a way to populate nearly all natural habitats, regardless of the partially extreme living conditions, e.g., fishes live up to 4000 m deep under the sea surface despite the high ambient pressure; animals like insects, lizards, or camels populate deserts; arctic animals survive the extreme cold of polar regions. By looking into wildlife, useful examples are provided of how a robot can complete a given task in a certain environment.

Multi-talented animals like apes are known for using tools to gain access to food or to process food like fruits, nuts and seeds, or vegetables. Apes also show different walking gaits (quadrupedal, bipedal, or on three legs) and have advanced climbing and manipulation abilities [TC06]. Lately, wild chimpanzees (Pan troglodytes) have been observed making tools: they sharpened sticks with their teeth to use it as a spear-like weapon for hunting bush babies [PB07]. The latest observation shows an extra set of behaviors these animals are capable of on both, a kinematic level as well as on a cognitive level. Because of these kinematic skills, chimpanzees are a suitable archetype for the design of a multi-talented robot.

Therefore, this chapter introduces the morphology of chimpanzees as biological foundation for the electro-mechanical system design of the hominid robot Charlie and its subcomponents. Charlie can be seen in Fig. 3.1 in a quadrupedal and in a bipedal pose. The first section describes the overall system and indicates the close connection between the morphology of Charlie and its natural model, followed by a description of the development of its legs, i.e., the actuation modules, the multi-point contact feet, and of the active, artificial spine including analogies to anatomical structures seen in nature. In addition, a division between a passive and an active spine concept is made. This chapter is supported by the following peer-reviewed

(a) Charlie in a quadrupedal posture. (b) Charlie in a bipedal posture.

Figure 3.1: The hominid robot Charlie.

publications:

- D. Kuehn, M. Rommermann, N. Sauthoff, F. Grimminger, and F. Kirchner. *Concept Evaluation of a new Biologically Inspired Robot LittleApe.* In Proceedings of IEEE/RSJ International Conference on Intelligent Robots and Systems (IROS-09), St. Louis, USA, 2009.
  Paper nominated for award.

- K. Fondahl, D. Kuehn, F. Beinersdorf, F. Bernhard, F. Grimminger, M. Schilling, T. Stark, and F. Kirchner. *An adaptive sensor foot for a bipedal and quadrupedal robot.* In Proceedings of IEEE International Conference on Biomedical Robotics and Biomechatronics, Rome, Italy, 2012.

- D. Kuehn, F. Beinersdorf, F. Bernhard, K. Fondahl, M. Schilling, M. Simnofske, T. Stark, and F. Kirchner. *Active spine and feet with increased sensing capabilities for walking robots.* In International Symposium on Artificial Intelligence, Robotics and Automation in Space (iSAIRAS-12), Turin, Italy, 2012.

- D. Kuehn, F. Beinersdorf, M. Simnofske, F. Bernhard, and F. Kirchner. *Towards an active spine for mobile robots.* In 3rd IFToMM International Symposium on Robotics and Mechatronics (ISRM-2013), Singapore, Singapore, 2013.
  Paper received conference award.

3.1 Overall System

The anatomy of bonobos (*Pan paniscus*) and chimpanzees (*Pan troglodytes*) is well documented in literature, e.g., [Bou69] or [Cro96]. Table 3.1 and Fig. 3.2 show the relation of chimpanzees body length compared to their limbs. Besides the limbs, the DoFs and the ranges of motion of chimpanzees are serving as a general guideline for the design and development of the hominid robot Charlie. In chimpanzees, the front limbs are longer than the rear legs. Therefore, Charlie's front limbs are 40 mm longer than a rear one. The difference in length gained due to the dimensions of the front foot. Apart from that is the design of the robot's lower leg and thigh identical for the front and rear legs.

Table 3.1: Ratio of a chimpanzee (from [Cro96]) and the limb lengths in Charlie.

No.	part	ratio chimp	ratio Charlie	Charlie's limb lenght in mm
1	Body	1	1	500
2	Upper arm	0.5	0.5	250
3	Lower arm	0.5	0.5	250
4	Hand	0.3	0.3	150
5	Thigh	0.5	0.5	250
6	Lower leg	0.5	0.5	250
7	Foot	0.4	0.4	195

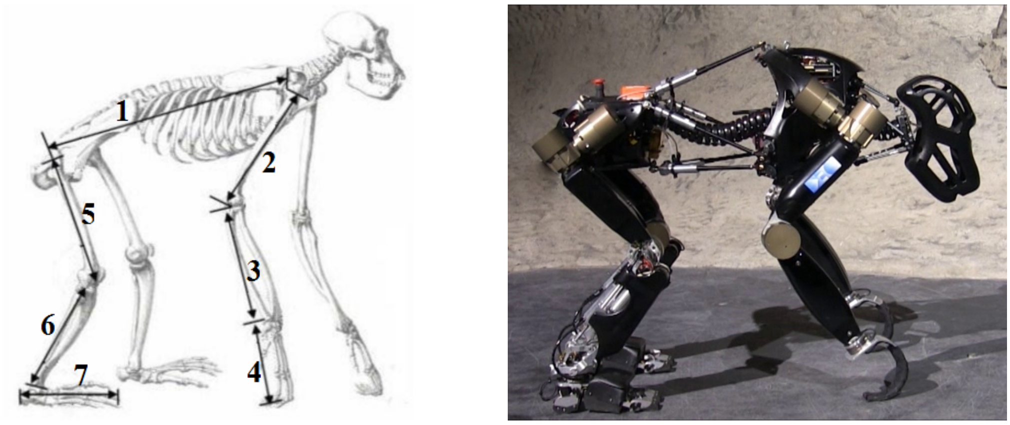

(a) Skeleton of a chimpanzee (adapted from [Bou69]).

(b) Photograph of the ape-like robot Charlie.

Figure 3.2: The biological archetype (a) and the Charlie robot (b) in a quadrupedal pose.

With these limb lengths the robot's height from shoulder to ground is 750 mm in a quadrupedal posture and 1300 mm in a bipedal pose, measured from head to ground. A summary of Charlie's key properties can be seen in Tab. 3.2. Charlie has currently 36 active and six passive DoFs, see Fig. 3.3(a). Without the motor housings, Charlie's shoulder is 440 mm and the hip 350 mm wide. Depending on the pose of the artificial spine, the distance from the first shoulder joint to the first hip joint varies between 500 mm and 544 mm. The actual weight of a fully equipped Charlie robot is 21.5 kg. The robot can either be powered externally or internally via rechargeable lithium polymer batteries of 44.4 V with 2.4 A h. The run time without motion is about 2 h.

The power consumption for the installed electronics is measured, while the robot is suspensed, i.e. no torques are needed for standing. Charlie's central electronics operates with 48 V and consumes about 10.5 W, the spine electronic consumes 7 W, all joint and foot electronics of the front legs about 6 W and the rear legs 9 W. Because the rear legs are equipped with more sensors and actuators, more electronics have been installed, which results in a higher current consumption. In a load free case the overall consumption is about 48 W. Less than 10 % (3.4 W) are additionally needed to support the robot's weight while standing on the ground.

The legs are attached to the shoulder and hip compartment, see Fig. 3.3(b). These two compartments are designed to be small in size and as light-weight and at the same time as robust as possible, like all subsystems in Charlie. The selective integration of supporting struts in these two bodies allows a thin wall thickness and thus supports the light-weight design. These supporting struts are necessary to maintain the structural integrity of these two compartments, because of the forces and torques introduced by the legs during locomotion.

Still, each body has to provide space for the integration of sensors (like the installation of an Inertia Measurement Unit (IMU) on each compartment), electronics, and cabling. To minimize possible electrical interferences introduced by the power electronics on the control units, these two are spatially separated. As shown in Fig. 3.3(b), the shoulder housing contains all electronics needed to communicate with the robot and the main control. In the hip compartment, all power electronics, the voltage transformer, and the rechargeable batteries are located.

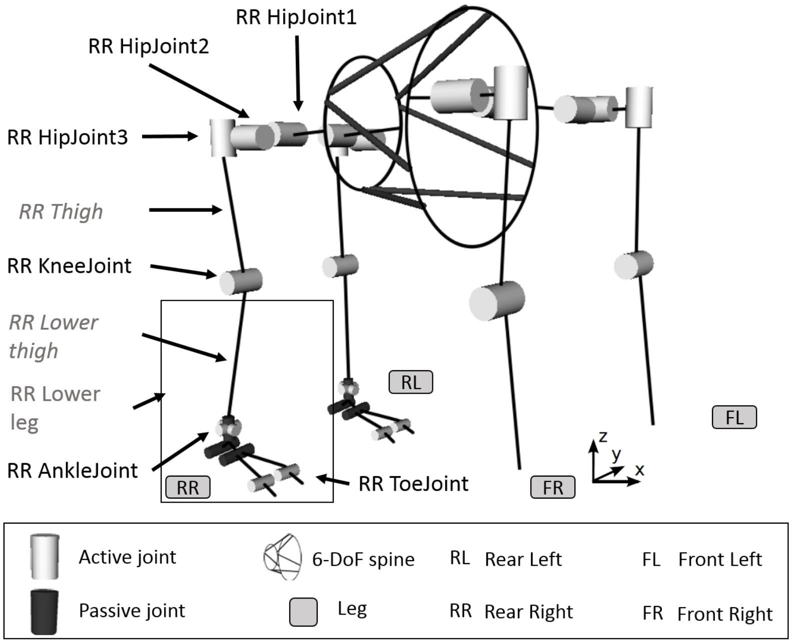

(a) DoFs in Charlie

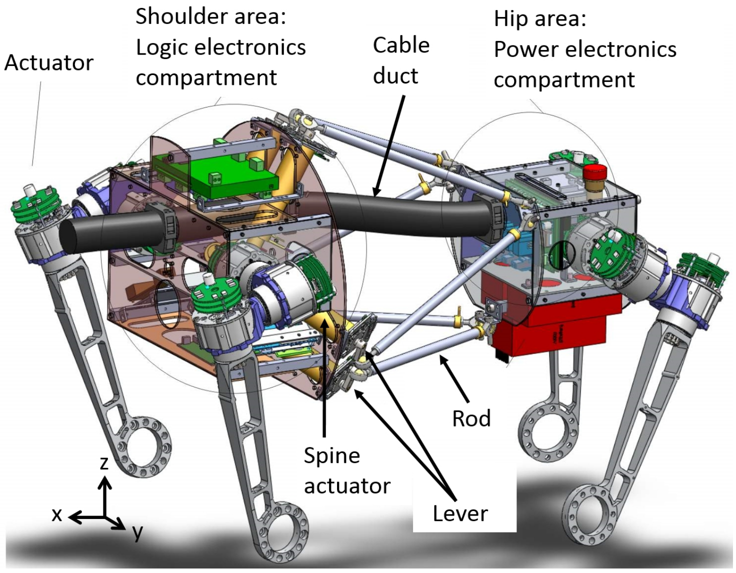

(b) CAD sketch of Charlie's front and rear body.

Figure 3.3: Labeling of Charlie's components [KSS$^+$16].

3.1.1 Electronics and Sensors

A simplified overview of the electronics and sensors installed in Charlie is given in Fig. 3.4. Each Printed Circuit Board (PCB) is a node in Charlie. The Motion Control Unit (MCU), located in the upper body is the central node. In this unit the desired joint positions are generated and sent to the respective joints. In addition,

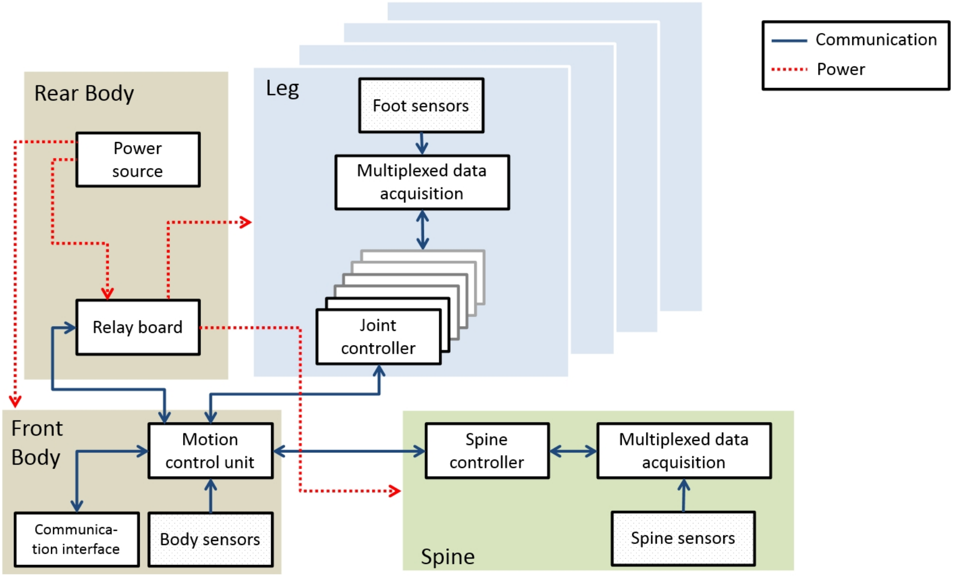

Figure 3.4: Block diagram of the electronic components and sensors within the system.

this node collects all information available. The MCU comes with an Overo Gumstix board with an OMAP3530 using a 720 MHz ARM Cortex A8 core and is equipped with 512 MByte NAND-Flash, 512 MByte DDR memory, a microSD card slot, and a WiFi module. A Linux kernel is running on this PCB, as well as Charlie's multi-threaded control program. The overall robot control is described in detail in chapter 4.4.

The MCU is a stack consisting of two additional PCBs, besides the Gumstix board. A Xilinx Spartan6 Field Programmable Gate Array (FPGA) is installed on one PCB, acting as a bridge between the Gumstix board and necessary peripheral components like Ethernet or Universal Asynchronous Receiver Transmitters (UARTs). In addition, the FPGA provides an interface to communicate with one extension board, which is essential to connect all of Charlie's nodes. For the communication with each node in the legs or spine, it provides Low Voltage Differential Signaling (LVDS) interfaces. Nodes like the IMU or the relay board located in the hip require an alternative communication channel, therefore additional communication possibilities like RS232, RS485 and several General Purpose Inputs and Outputs (GPIOs) are used to connect these peripherals to the MCU. The relay board measures the incoming voltage and powers legs, spine, and head each on a separate, fuse-protected channel.

Table 3.2: Key properties of the robot [KSS+16].

Dimension (quadruped posture) [LxWxH]	800 mm x 440 mm x 540 mm
Front body dimension (incl. head) [LxWxH]	400 mm x 300 mm x 250 mm
Rear body dimension [LxWxH]	180 mm x 160 mm x 150 mm
Maximum leg length front	680 mm
Maximum leg length rear	640 mm
Degrees of freedom	36 DoFs (body: 6, head: 6, front legs: 4, rear legs: 8)
Sensors	34 x motors: position, speed, current, temperature. Feet: acceleration (three axes), temperature, pressure-sensing array (49 elements), 4 x 6 DoFs force/torque sensors (one per limb), 8 x absolute encoder (one per toe, one per passive DoF) Spine: 6 x 1 DoF force sensor Body: orientation (three axes), supply voltage
Overall mass	21.5 kg
Single front leg mass	3.4 kg
Single rear leg mass	4.1 kg
Power supply	44.4 V to 50.2 V at 2.4 A h (Lithium Polymer)
Power consumption (at 48 V)	
Idle (legs switched off)	10.5 W
Load free (legs switched on)	47.5 W
Standing (in four-walking position)	52 W
Standing (in two-walking position)	50 W
Walking (average in 0°)	65 W
Posture modification:	
Min. / max. body height 2 legged	1060 mm / 1360 mm
Min. / max. body height 4 legged	505 mm / 750 mm
Min. / max. ground clearance 4 legged	225 mm / 470 mm
Min. / max. longitudinal body shift (x-axis) in body coordinates with respect to the initial quadrupedal walking pose	−320 mm / 210 mm
Min. / max. lateral body shift (y-axis) in body coordinates with respect to the initial quadrupedal walking pose	−220 mm / 220 mm
Maximum speed (up to now)	
Forward four-legged	$270 \frac{\text{mm}}{\text{s}}$
Forward two-legged	$100 \frac{\text{mm}}{\text{s}}$
Maximum turning angle per gait cycle (four-legged)	45°

3.2 Multi-point Contact Feet

The following section introduces the principles and design of feet in nature, followed by an abstraction of these designs and the description of an electro-mechanical solution. In addition, the individual sensors as well as the sensor concept are presented. The section closes with a first validation of the artificial foot.

3.2.1 Principles and Design in Nature

In nature, feet provide different functionalities, i.e., supporting functions, stabilising the body, absorbing shocks with their incorporated elasticities as well as generating and maintaining traction. The feet must be able to bear the body weight. Natural feet achieve this through a combination of ligaments, bones, and muscles. To minimize the moments of inertia of the leg, the feet have to be as lightweight as possible.

Feet must provide a reliable grip on all different types of soils and on inclinations, therefore a foot should be able to adapt to the ground to produce a good grip. In nature, this adaption is realized by i) allowing the foot to deform up to a certain level and ii) the DoFs introduced by the ankle joint. The contact area between foot and ground becomes maximized by adapting the foot pose accordingly [Kap99a] (see Fig. 3.5). In literature, the design of human foot is documented in detail. In [EM35] it is stated that the human foot and the one of apes show fundamental similarities in design. Therefore, when limited data is available on the feet of chimpanzees, the human foot will serve as a model instead, to show the design of a natural foot and its function principles.

Comparisons regarding the different dimensions of human and chimpanzee feet have been made [WC04]. These dimensions are shown in Tab. 3.3.

Table 3.3: Dimensions of human and chimpanzee feet (adapted from [WC04]).

	STATURE in m	FOOT LENGTH in m	FOOT HEIGHT in m
Human	1.75	0.25	0.072
Chimpanzee	1.19	0.20	0.042

A foot in chimpanzees and human has three active DoFs, shown in Fig. 3.5(a). According to [AE93], the RoM of a human foot is between 10° to $-20°$ in the frontal plane (eversion/inversion hereafter referred to as roll motion) and between 20° to $-30°$ in the sagittal plane (dorsiflexion/plantarflexion hereafter referred to as pitch motion). A rotation in the transverse plane (abduction/aduction hereafter referred to as yaw motion), of 10° to −10° can be observed, which is gained by the structure of the leg. This means that for a technical abstraction mainly two DoFs are necessary to drive an artificial foot, as shown in Fig. 3.5(b). Comparing the human ankle joint to the one of chimpanzees, it is reported in [DeS09] that the ankle joint in apes allows a slightly larger RoM.

For the toes basically one DoF is observed. The active RoM in humans is about 80° to 100°, divided in flexion (30° to 40°) and extension (50° to 60°) [Kap99a]. The passive RoM is increased, due to to rolling motion of the foot, where a passive extension of up to 90° can be seen [Kap99a]. Lateral movements of the toes are rather minimal. During locomotion, the toes are used to increase the time the foot has a contact to the ground. To the end of the leg's stance phase, the heel is already lifted and the main load is applied to the first three toes [Kap99a]. In addition, the toes can be used increase grip or get hold while walking or climbing in unstructured environments.

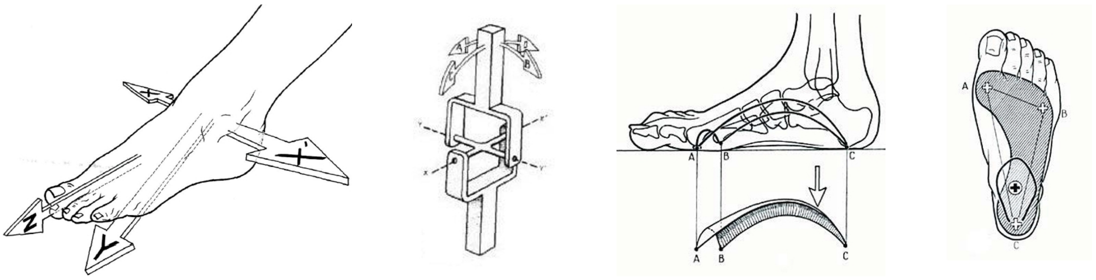

(a) Axes in the human foot.

(b) A cardan joint can be used to abstract the human ankle joint into a technical design.

(c) The arches of the foot in a lateral view. It has three main contact points, two in the ball of the foot and one in the heel.

(d) Points of support in the human foot as top view.

Figure 3.5: The figure shows the movement abilities of the human foot, the three main points of support as well as the foot arch (the illustrations are adapted from [Kap99a]).

A statically stable locomotion requires at least three contact points between the foot and the ground. In a human foot, these three points of contact can be seen in Fig. 3.5(c) and Fig. 3.5(d). The resulting support triangle spans between the heel and the medial and lateral ball area. The rounded form of the heel allows a rolling movement of the foot and simplifies a stable motion. The arch between heel and toe is maintained by ligaments and preloaded by muscles and tendons. The stiffness of the arch can be adjusted, depending on the properties of the ground the subject is walking on. While walking on flat and rigid surfaces, this adaptability is rarely needed, in contrast to standing or walking on a slope or in soft and compliant soils like sand. Damping is realized through the interaction of fat pads, the elastic and flexible connection of the bones by ligaments, muscles, and tendons. Especially ligaments and tendons act as natural spring elements.

Furthermore, apes have a big variation in the anatomy of their front and rear limb's end-effector. Primates like chimpanzees or gorillas show a quadrupedal walking behavior called knuckle walking. In this gait the rear feet are used normally and the sole establishes the ground contact but the finger tips of the front limbs are flexed. Only the outer part of the middle segment of their fingers has ground contact.

3.2.2 Mechanical Implementation

The technical implementation of the rear foot can be seen in Fig. 3.6(c). The multipoint contact foot consists of five rigid bodies, more precisely the base, the heel, the forefoot, and two toes. The angle of each connecting point is monitored by absolute angular encoders, so the shape of the foot is known at all times. Like the biological model, the core structure of the mechanical foot is rigid and covered by different materials. The outermost layer is represented by the sole, which adds traction and minor damping capabilities to the foot and provides mechanical protection to the sensitive inner parts as well. As indicated in Fig. 3.6(a) and Fig. 3.6(b), the foot is 195 mm long, which is inspired by the length of chimpanzee feet, as shown in Tab. 3.3. In addition, the foot has a width of 50 mm at the heel and 80 mm at the toes, and has a height of 80 mm without the force/torque sensor.

The weight of the foot is 350 g including its electronics. A flexibility is installed in the foot's pitch axis, indicated in Fig. 3.6(a) by the front and rear damper. This flexibility allows to absorb the occurring forces at the touchdown motion, when the foot hits the ground. If desired, this function can be deactivated mechanically. In addition, the toes can be actuated downwards to increase the traction between foot and ground. Due to space and weight limitations, the toe actuator is integrated in the thigh and connected to the toes via bowden cables. Active flexion of the toes of up to 75° are realized to increase grip or get hold while walking in inclines. An active extension is not possible; the movement in this direction is realized by

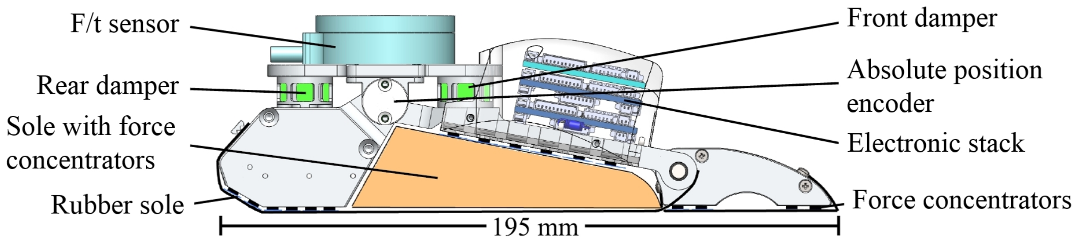

(a) CAD model of the foot structure with fully compressed damping structures. The IR-sensor and the bowden cables to actuate the toes are integrated inside the foot structure and not visible.

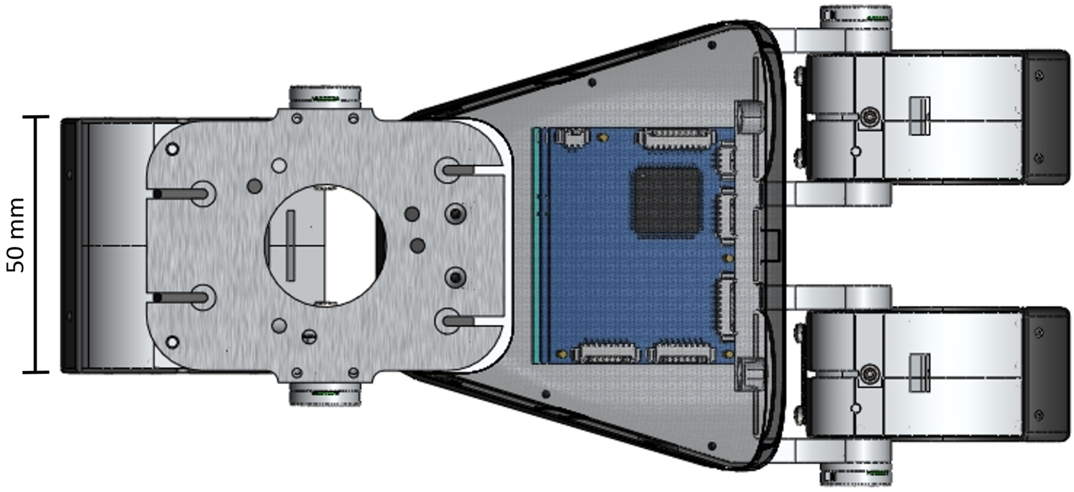

(b) Top view on the foot (CAD-rendering).

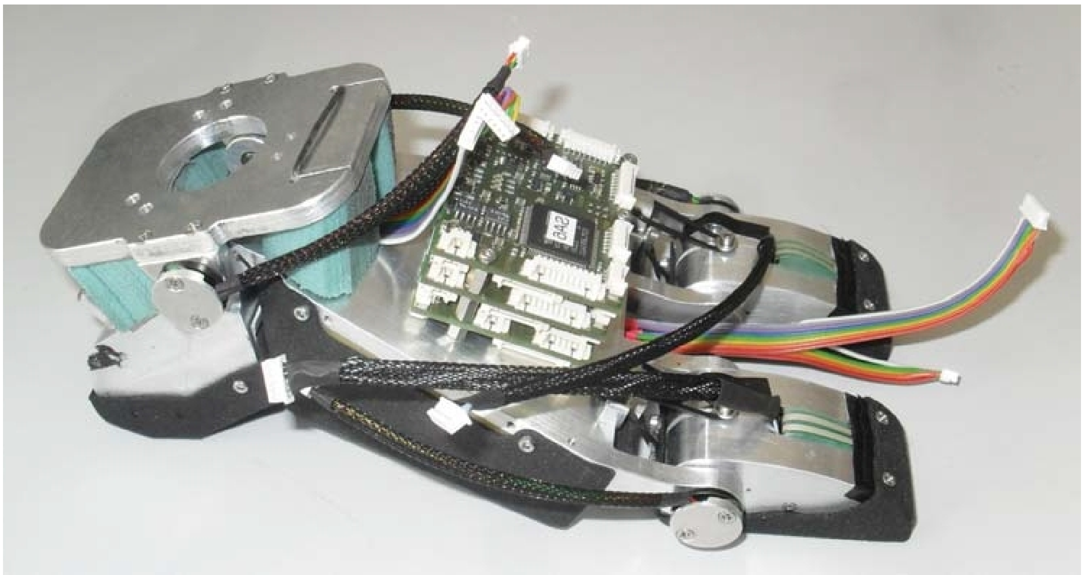

(c) Photograph of the designed and integrated foot structure including its PCB stack. The force/torque sensor, used as the mechanical interface to the ankle joint, is not displayed.

Figure 3.6: CAD model and implementation of Charlie's sensor foot.

installing flexible elements between toes and foot, which move the toes into their resting position, when no force is applied.

Front Limbs The front feet of Charlie differ from the rear feet in terms of complexity, sensory equipment, size, and weight. In Charlie, the front feet (see Fig. 3.7) are an abstracted and simplified version of ape-like hands. Inspired by the knuckle walking, see Fig. 3.7(a), the front foot is shaped like a hook, allowing a quadrupedal walking and is also suitable for climbing in particular environments.

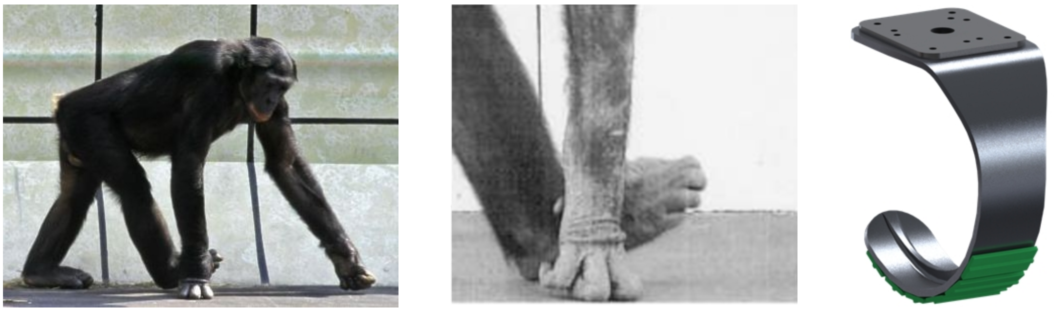

(a) Some primates show a special quadrupedal gait, referred to as knuckle walking. Source: http://uahost.uantwerpen.be.

(b) Knuckle walking as close up. Source: [DAC$^+$02]

(c) CAD drawing of the front foot with applied sensors.

Figure 3.7: Biological model and technical design of a lower leg structure for Charlie's the front feet.

3.2.3 Electronics and Sensors

By equipping robots with more sensors, the quantity, quality, and reliability of information can be increased. This is true for proprioceptive and for exteroceptive data. Consequently, the robot can use this quality of sensor data to improve its behavior while interacting with the world. A precise tactile perception of the environment in nature is realized by a high number of mechanoreceptors embedded in the skin. These receptors are able to respond to mechanical pressure. This way, a detailed surface description can be provided. A human foot sole features more than 100 of these mechanoreceptors [KI02]. However, due to the number, in a robotic system an abstraction of this principle is necessary.

Depending on the number of installed sensors, a direct wiring of these to the robot's main computer is not practical. Aside from the limited connectors on a computer, such a wiring can exceed the computational power of the main PC, can be complex, adds additional weight to the robot and is prone to error. A distributed approach appears to be useful, since the data can be preprocessed instantaneously locally and in parallel. As a result of the preprocessing, the information detail on a higher level of control is minimized, but in contrast to the lower level the situation awareness is high. By using numerous local controllers that work in parallel, the control, e.g., of single joints, can be executed with a much higher frequency. Due to the physical proximity of sensors and electronics, the probability of flipped bits or (in the analog case) altered sensor data on the basis of external interferences is minimized. Yet, the local preprocessing units have to be able to communicate with the higher levels.

To gain an increased perception of the environment, it is necessary to implement multiple sensors and suitable electronics into structures like a foot which is limited in space. Within the rear foot the following sensors are installed: a six-DoFs force/torque sensor, a pressure-sensing array with 49 elements, an acceleration sensor (three axes), a temperature sensor, and eight absolute encoder (one per toe, one per passive DoF).

An ATI mini45 six-DoF force/torque sensor [ATI16] is mounted on top of each foot (front and rear) and has a force sensing range of 580 N for the x- and y-axis and 1160 N for the z-axis with a resolution of 25 mN. The torque sensing range is at 20 N m for all three axes with a resolution of 5.3 mN m in x- and y-direction and 2.6 mN m for the z-axis. The sensor has a second purpose in serving as the only mechanical interface between the lower legs and the feet. Thus, all appearing forces and torques are going through this sensor and enable the robot to perceive all interaction forces between foot and ground. Because of this mechanical interface, the front and rear feet are easily interchangeable.

In order to increase the spatial resolution for tactile perception of the environment in a robotic foot, a pressure-sensing array consisting of 49 Force Sensing Resistors (FSRs) is installed in Charlie's rear foot. An FSR changes its resistance when a force is applied. Various principles like resistive sensors [KMM07], capacitive sensors [UC10], tactile sensors using fiber-optic sensor arrays [KK12], or mechanical methods [BBC+10] are described in literature and are able to perform the task of measuring the spatial distribution of forces applied to the foot. The selected sensor is on the basis of its size and weight well suited, but also because of structural and electrical requirements. It has a sensing area of 5.1 mm in diameter and a sensitivity of 20 $\frac{\mathrm{mN}}{\mathrm{cm}^2}$.

Fig. 3.8(b) shows the position of each FSR in the foot sole. During locomotion, the heel and the ball/toe area are the regions where the main load is applied (as above shown in Fig. 3.5). Thus, both parts are equipped with a higher sensor density (15 sensors on the heel, eight under each toe) than the foot arch, which houses twelve sensors. Additionally, six sensors are placed on the outside of the foot and serve as collision detectors. With this arrangement, a spatial resolution of 0.3 mm^2 to 4.5 mm^2 is achieved. The sensors are glued directly onto the respective structural components of the foot to prevent these from slipping. Due to their mechanical properties, the sensors have to be protected from shear forces. In addition, it is required to mount the sensors on a planar surface and to ensure that only the sensors become loaded and not the supporting or surrounding structure. Therefore, the sole is equipped with force concentrators (see Fig. 3.8(c)) to allow an ideal force transmission to the FSR. Without these force concentrators, some forces which were acting on the foot cannot be detected by the sensor array.

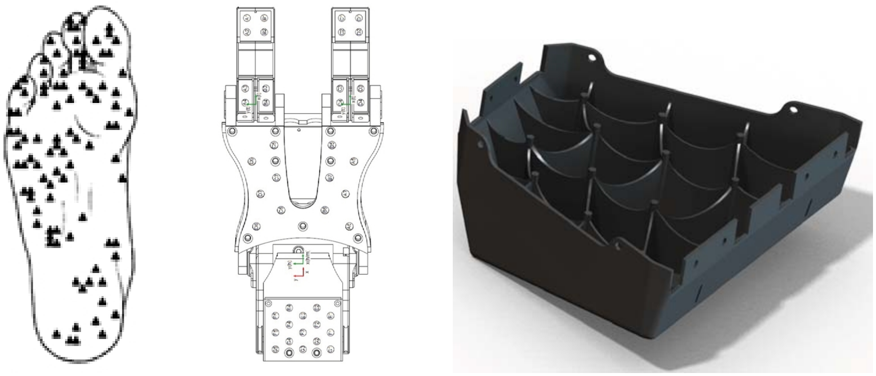

(a) Schematic drawing of the distribution of mechanoreceptors in the human foot (image adapted from [KI02]).

(b) Schematic drawing of the rear foot. Each circle indicates the position of a FSR sensor.

(c) Sole with integrated force concentrators for the FSR.

Figure 3.8: Charlie's rear foot with its customized sole.

The FSR array allows an insight of the spatial distribution of the applied forces to the foot, but their nominal value cannot be measured accurately. In contrast, the installed force/torque sensor measures the acting forces and torques with high accuracy, but does not allow a spatial resolution. Using both sensors the best respective functionality can be used and at the same time a redundancy regarding determination a ground contact is provided. The redundancy of sensor information is needed to evaluate the sensors and allows to exclude permanently incorrect sensor data from the evaluation process, to provide the overall system control with reliable data.

The heel features an optical distance sensor, which allows the robot to sense the distance between foot and ground. In a biological system such an information is nonexistent. However, a robotic system must not be a direct replica of its biological antetype, especially not when upgrades regarding the sensory equipments or the RoMs are possible. Using this information, the foot's velocity can be reduced prior to an early touchdown event. Furthermore, this sensor offers the opportunity to react to small holes or craters in the ground by triggering an establish-ground-contact behavior.

Further sensors can be found on the embodied foot electronics. As shown in Fig. 3.6(a), a stack of three PCBs is installed on top of the rear feet. Two PCBs are equipped with a STM32 microcontroller and are used to process the incoming sensor data. In addition, they feature two multiplexers, an amplifier, and an Analog-to-Digital Converter (ADC), enabling the stack to measure all 49 voltage differences coming from the FSRs. On the third PCB, a three-axis accelerometer is installed, allowing the measurement of the foot's acceleration. This sensor allows to determine if the feet begin to slip or have slipped while walking. The main use of the latter, however, is to reduce the complex cabling of the FSR sensor array and of the other sensors, by using the customized internal wiring on different layers in this PCB.

Another important purpose of the electronic stack is data preprocessing and communication to higher control levels. The generation and distribution of knowledge, e.g., the current condition of the foot, interaction forces, the coordinates of the local support polygon for each foot, or information about the surface allows the higher control levels like Charlie's Motion Control System (MCS) to save computational power by directly using this knowledge.

In Charlie the mechanical design of the front and rear feet differ, so that the installed sensory equipment and electronics differ as well. Seven single tape switch sensors are placed on the hook-shaped structure of the front feet (see Fig. 3.7(c)), allowing to determine the spatial position of the ground contact. The number is adequate to calculate the support polygon. Because of the arrangement of the sensors on the structure, a spatial resolution of about 2 cm regarding ground contact is obtained.

Due to the current shape of the front foot, additional DoFs (as introduced in Charlies rear legs) are not necessary and thus the lower leg and foot represent a design with lower weight and reduced complexity compared to the rear foot. However, the mechanical design of the lower leg is equal for all four limbs. If two additional DoFs for the front limbs are necessary, it is possible to use the ankle joint design of the rear feet for the front feet as well.

3.2.4 Validation

The validation of the MPCF will concentrate on results regarding the ground traction and the performance of the sensor array.

Ground Traction

One advantage of the designed multi-point contact foot is an increased traction compared to a single-point contact foot. To verify the functionality of Charlie's rear foot, an experiment is performed, comparing the static friction values of a spherically shaped foot of the robot SpaceClimber (c.f. Fig. 2.4(c) on page 18) to Charlie's foot shown in Fig. 3.6(c) on page 49. Both feet are attached one after the other to a vertical linear guidance system. A rollable plate is placed between the foot and the ground. The top of the rollable plate is firmly fixed with sandpaper and two experiments are performed, each with a different sand paper grain size (360 and 1500). The plate is pulled out horizontally at five different angles, 0°, 45°, 90°, 135° and 180°, where 0° comply to a movement towards the toes. A measurement unit is placed between the plate and the pulling handle to measure the force (i.e. the frictional force F_R) needed to pull the plate in the desired direction. Each measurement is repeated five times for each foot, on each sandpaper grain size, and in each direction.

The friction coefficient μ ($\mu = F_R/F_n$) is calculated for each direction. The higher the number, the better the grip between foot and ground. The results are shown in Fig. 3.9 in the polar diagram. It can be seen that the friction coefficient of Charlie's MPCF rear foot exceeds the one of the spherical shaped foot of SpaceClimber. This is true for all directions and on both grain sizes except for the finer grain size and a pulling direction of 90°, where the SPCF has a slightly higher friction coefficient. This effect is desired and can be explained with the mechanical design. Due to the arrangement of the individual parts in the foot, a passive adaptive behavior along the x-axis is allowed, but not on the y-axis. The heel and ball get tensed up against each other and therefore an increased force is necessary to provoke a slipping behavior of Charlie's foot.

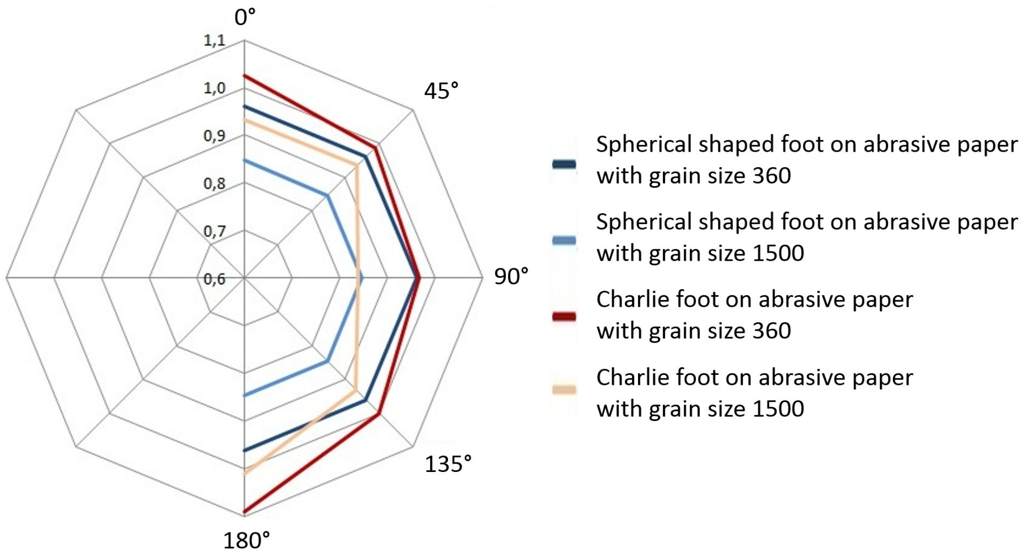

Figure 3.9: Average friction coefficient values of a spherically shaped foot and the foot for the Charlie robot.

The characteristic asymmetry of the friction values for Charlie's foot can also be seen in the plot. In general, while walking the load is mainly applied in the direction of 0°. It can be seen that the friction coefficient is higher if a force is applied on the front and rear than in lateral directions. This behavior of the foot is desired and can be explained with the foot's passive adaptive capabilities between heel and toe, which mainly work in these two directions.

FSR Sensor Array

In order to examine the output of the sensor array for its correctness, Charlie is placed with one rear foot on an industrial tactile pressure and force measurement plate designed by Tekscan[1]. The pressure mapping system consists of a sensor plate, data acquisition electronics with a reading frequency of about 100 Hz, and software for evaluation. Figure 3.10 shows simultaneously recorded screenshots of the graphical user interface used to visualize Charlie's sensor array data (Fig. 3.10(a)) and one from the Tekscan software (Fig. 3.10(b)). For Charlie's sensor array, blue means that no pressure is applied, green indicates a medium pressure, and red a high pressure. The same color coding can be seen in the Tekscan software, except that the color blue indicates a slight pressure. The white cross in Fig. 3.10(a) and the silvery square in Fig. 3.10(b) indicate the local CoM. Please note that due to a higher

---

[1] https://www.tekscan.com/products-solutions/systems/i-scan-system?tab=sensors accessed Feb. 2016

measurement range of each taxel of the Tekscan force plate, the colour coding is not comparable. Nevertheless, by comparing the recorded data and the resulting pictures, it can be clearly seen that a mapping of the pressure points as well as a local CoM calculation can be achieved in appropriate accuracy within the sensory foot.

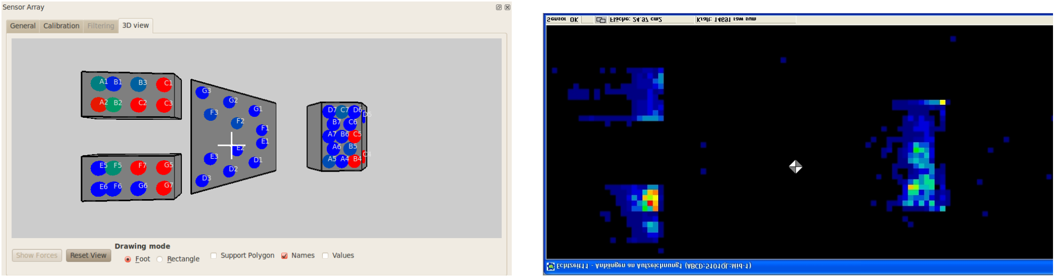

(a) Visualization of the incoming sensor array data in a quadrupedal pose.

(b) Visualization of applied forces on the Tekscan force plate.

Figure 3.10: Locally preprocessed sensor array data compared to externally measured data on a force plate.

3.3 Leg Design

This section describes the RoM in chimpanzees and humans. Afterwards, the mechanical design and actuation of Charlie's lower legs are described. The section is completed by depicting the mechanical implementation of the thighs.

The motion angles of chimpanzees during locomotion are analyzed in literature, e.g., by [PRR14] and [OLD+15], and are shown in Tab 3.4. By realizing these RoMs in the different joints in Charlie, the preconditions of the locomotor system are fulfilled to allow the robot a locomotion with both modes.

Table 3.4: Range of motion in chimpanzees while walking quadrupedal and bipedal.

Gait	Hip flexion in °	Hip adduction in °	Hip rotation in °	Knee flexion in °	Ankle flexion in °
Quadrupedal ([PRR14])	71	-	-	115	64
Bipedal ([OLD+15])	27 ± 4	16 ± 4	39 ± 2	78 ± 1	38 ± 5

However, these angles only describe the RoM required for locomotion. The possibility exists that a subsequent expansion of the robot's motion skills is limited, because the realized RoM of the joints was too focused on these two motion modes. Therefore, the maximum angles in humans, according to [Kap99a], are shown in the following. In humans, the maximum angles for the hip flexion ranges from −30° to 140°, whereas 140° indicates that the knee is close to the torso. The lateral motion is divided into abduction and adduction. With training, humans can reach a passive abduction of 180°, e.g., during a split. However, more common is a 90° angle. The hip's adduction is limited to 30°. The rotation ranges from −30° to 60°, whereas the 60° indicate a movement towards the second leg.

3.3.1 Lower Leg

The robot's lower leg is shown in Fig. 3.11. Its main structure is made of aluminium and includes on top an interface for the knee joint and one on the bottom for the ankle joint. The lowest segment is connected to the foot. Due to the design, this is an ideal location for measuring all interaction forces and torques induced onto the leg during locomotion. In the middle of the lower leg, one mounting for two motors on the rear and one for the control electronics in the front is integrated.

To realize an active roll and pitch foot movement, two motors are needed. Two Brushless Direct Current (BLDC) actuators are installed, each equipped with a reduction gear unit of 10:1, digital hall sensors, and incremental encoders. To stay within the limits of the limbs proportions (see Tab. 3.1), actuators and spindles are used and arranged in a parallel alignment. To convert the rotation motion of the actuator into a linear one, the actuators output shaft is connected to a lead screw and spindle nut mechanism. The lead inclination is 2 mm per turn. The motion is transmitted via two four-bar spatial linkages to the ankle joint. Both actuators are located close to the knee joint to reduce the legs moment of inertia (see Fig. 3.11).

For the control and sensor data acquisition, a customized FPGA-based electronic is used, with the ability to control two motors simultaneously. The hall sensors are used for motor commutation. The incremental encoders provide a relative position, thus the data of the absolute encoders installed in the ankle joint are needed to determine the initial pose of the foot. In addition, an inverse kinematic solution for the ankle joint is calculated directly in the FPGA.

Although only roll and pitch are actively driven, the ankle joint allows a third rotational DoF. A passive yaw motion is installed and can be mechanically enabled with minor effort, if desired. During the experiments for this thesis, this DoF is decommissioned. To allow an pose estimation of the ankle joint and thus the foot

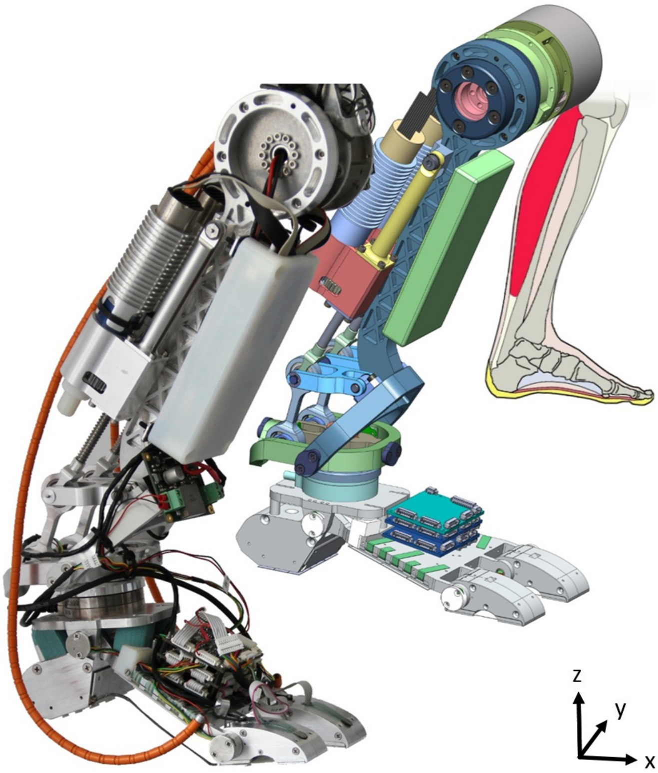

Figure 3.11: The installed lower rear leg including its inspiration model (in the back), the CAD sketch (middle) and in hardware (front). In addition, the orange bowden cable to actuate the toes is shown.

at the robot's start-up, all three axes are monitored by absolute angular encoders.

Actuated with this ankle joint design, the resulting RoM of the foot is shown in Fig. 3.12. Individual movements of 50° for roll, 130° for pitch, and 40° for yaw are realized. The angels required for locomotion, as shown in Tab. 3.4, are reached and even exceeded. A maximum angular velocity of 130 $\frac{\circ}{s}$ for the pitch and 190 $\frac{\circ}{s}$ for roll motion is achieved. Due to the ankle joint design the roll movement is faster, since the motors drive in different directions, whereas the pitch motion is accomplished if the actuators have the same direction of rotation.

3.3.2 Hip and Knee Actuators

Besides the ankle joint motors, the lower leg is equipped with an actuator on top, which serves simultaneously as interface between lower leg and thigh and as knee joint. The actuator is based on the BLDC motors developed within the Space-Climber project [HKBK09]. Each leg of Charlie is equipped with four of these actuators. Three are integrated in the hip and one is used as knee joint. The knee

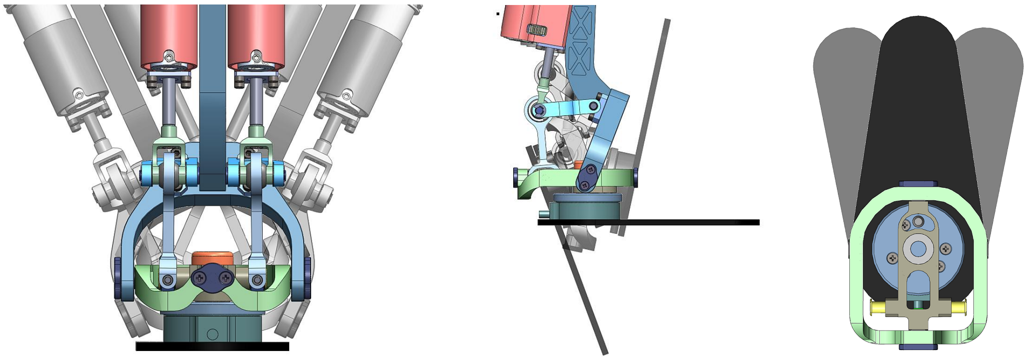
(a) Roll: ±25° (b) Pitch: 130° (c) Yaw: ±20°

Figure 3.12: Range of motion of the developed ankle joint.

joint actuator differs in size and is smaller, since the electronic stack is located in the robot's thigh. Otherwise, all of these actuators are identical.

As motor, ILM 50x8 BLDC modules from the manufacturer RoboDrive[2] are used, which come as rotor and stator with an outer diameter of 50 mm and without any housing. The motor has a rated power of 155 W, a rotation speed of 5500 rounds/min, a rated torque of 0.3 N m, and a peak torque of 0.9 N m. With a weight of 86 g the motor has a high torque density. Combined with a gear from Harmonic Drive, a compact and light-weight actuator is generated with a good torque-to-weight ratio. The motor-gear combination has a kind of self-inhibiting effect when a torque is applied to the output shaft, which is beneficial especially for walking robots.

The installed sensors and electronics allow an autonomous driving and control of the motor. Fig. 3.13 shows a sectional view of the BLDC motor. The electronic is stacked and has, like the motor and the gear, a hollow shaft allowing the cables to be routed inside each actuator. This offers the advantage that the cables are protected against external forces and possible mechanical damage. In addition, it allows the motor to rotate multiple turns (if the robot's morphology allows it) without the risk of cutting or tearing off the cable harness.

The electronics stack for Charlie's knee-joint is integrated into the thigh, to gain a smaller and more light-weight actuator. Since this stack is able to drive and control two motors, it is simultaneously responsible for the toe actuator.

The sensor feedback of each actuator includes its current speed, temperature, input Pulse-Width Modulation (PWM), supply voltage, power consumption, and

---

[2] http://www.tq-group.com/produkte/robodrive-standardmotoren/ accessed 02.2016

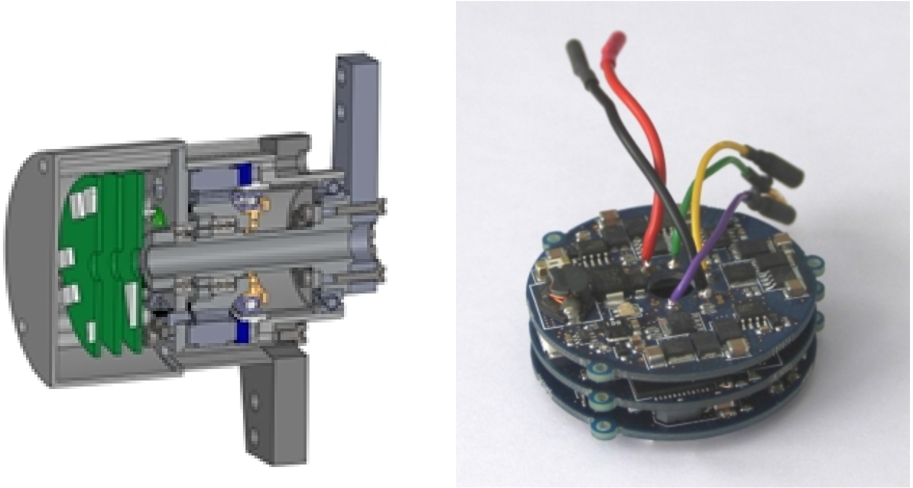
(a) Sectional view of the BLDC motor. (b) BLDC electronic stack

Figure 3.13: CAD design of an, in terms of control, autonomous actuator with an installed BLDC motor and Harmonic Drive gear (left hand side) and photograph of a compact motor control electronic (right hand side).

absolute angular position. A Spartan 6 FPGA is used in the electronics, allowing simultaneous control and communication with the main controller or other joints, due to the parallel architecture of the FPGA. One fully integrated, autonomous actuator used in Charlie's hip or shoulder joint has a diameter of 65 mm, a length of 87 mm and a weight of 420 g. The version installed in the knee joint is 18 mm smaller and weighs 360 g.

3.3.3 Thigh

To allow a technical realization of a rotary joint, like the hip or shoulder joint in nature, three of the above mentioned BLDC actuators (shown in Fig. 3.13(a)) are aligned in a serial manner. For each limb one of these triple joints is installed into Charlie and serves as hip or shoulder joint, respectively.

In a chain of three consecutive joints in which the rotation axes are aligned orthogonally to one another, six different arrangements are possible. Due to the requirement of allowing both, quadrupedal and bipedal locomotion, some joint orders become directly eliminated because of the occurrences of singularities or parallelisms of certain axes. In Charlie, the first joint is attached to the respective housing (front or rear body) and moves the leg to the front and rear. The second joint moves the leg to the left and right and with the third joint, a rotation of the foot can be realized.

It has to be noted that not all axes intersect at a pivot point.

The thigh itself is constructed of aluminium and allows the integration of electronics and an additional motor, which is used in the rear legs to actuate the toes via tendons (routed through the leg structure). Its design including a motor can be seen in Fig. 3.14. If the toe motor is not integrated, the electronic stack deals exclusively with the control of the knee actuator.

(a) Front view: thigh with electronic stack (CAD rendering).

(b) Rear view: photograph of the thigh with installed motor for toe actuation.

Figure 3.14: Design of the thigh installed in Charlie.

3.4 Active Artificial Spine

Introducing an active, artificial spine into a robotic system provides the potential to improve existing behaviors or gaits in terms of stability and energy efficiency. Furthermore, the possibility is given to realize new motion patterns with the robot. The following section first provides an overview of the design and function of spines in primates. Afterwards, the technical implementation for Charlie is described in detail and the section closes with a first analysis of the developed artificial spine.

3.4.1 Spines in Primates

The anatomy of a spinal column strongly depends on the occurring load cases, whereas the primary load case is the type of locomotion. Humans favor a bipedal locomotion and thus an S-shaped spine can be seen. The vertebral bodies are getting smaller from the pelvis to the head, since structural load introduced by the weight of the body parts becomes lesser [AAD02]. The S-shaped structure also protects the brain against shocks and vibrations occurring while walking or running. In chimpanzees, the primary gait is quadrupedal, therefore the appearance of the spine differs in form and size compared to a human spine. In this case, the basic structure of the spine is curved and the size of the vertebral bodies and intervertebral discs throughout the spine are almost identical, due to the different load cases (see Fig. 3.15).

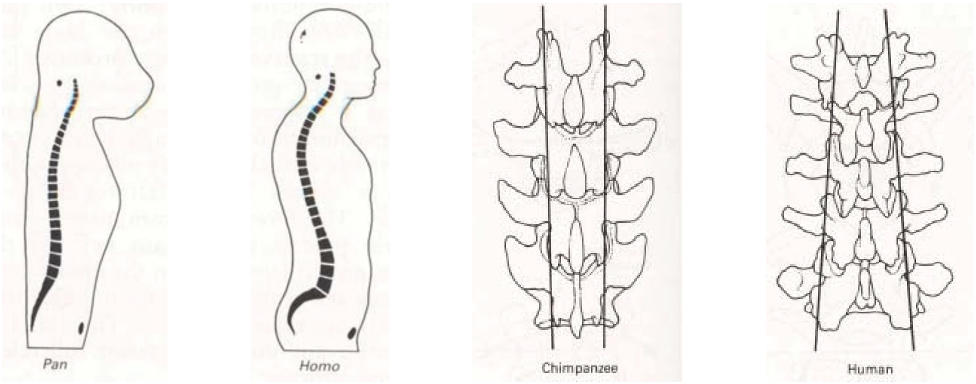

(a) Shape of spines in apes.

(b) Shape of spines in humans.

(c) The size of vertebrae in apes.

(d) The size of vertebrae in human.

Figure 3.15: Anatomy of a spine in apes and man (illustrations from [AAD02]).

Nature makes extensive use of these DoFs. In a hunting cheetah, the spine is periodically bending and stretching and thus supports the galloping gait of the animal. In humans, in a bipedal stance the spine can support manipulation tasks to such an extent that the legs can remain stationary. These two examples illustrate that the support of motion patterns highly depends on the favoured form of locomotion. The spine of a quadruped provides less flexibility, e.g., for manipulation capabilities, but provides an ideal support for locomotion.

A spine can usually be divided into three sections: the cervical, the thoracic, and the lumbar spine [Kap99b]. The thoracic and lumbar section are often merged and called thoracolumbar section. The RoM of the thoracolumbar spine section is displayed in Tab. 3.5, since it is the most interesting part for an technical abstraction and implementation in a robotic system.

Table 3.5: Range of motion of the thoracolumbar spine section in humans according to [Kap99b].

Degree of freedom	Range of motion in [°]
Left/right rotation (torsion)	−35 to 35
Backward / forward flexion	−35 to 105
Lateral flexion	−40 to 40

In preliminary studies, first experiments with an artificial spine were conducted. The robot LittleApe [KRS+09] was equipped with a passive spine consisting of a few pairs of vertebrae [KBG+10]. Based on this morphology, the concept for an active spine with a serial alignment can be seen in Fig. 3.16, where several artificial vertebrae can be connected. The result is a spine-like structure.

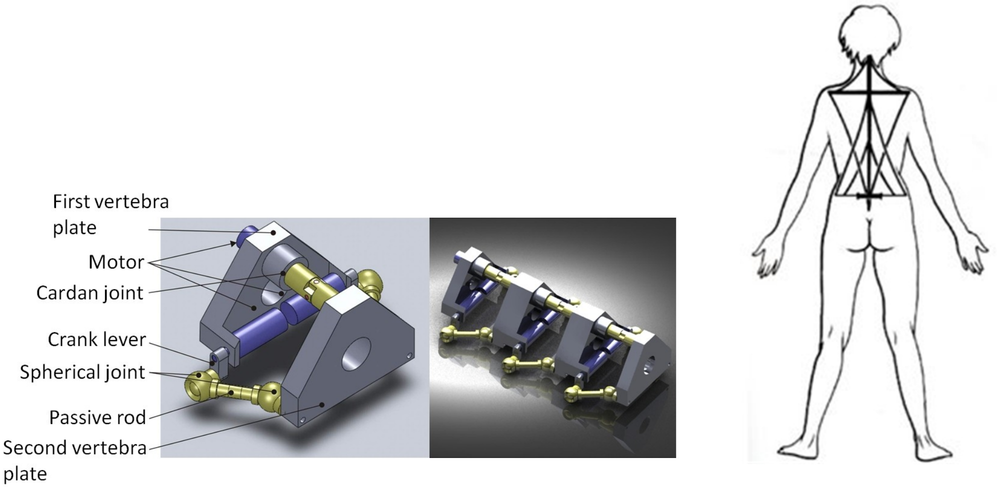

(a) CAD model of one artificial vertebra and the corresponding spine.

(b) Sketch of a human backbone. Source: [Kap99b].

Figure 3.16: Differences of the drive systems between the initially developed mechanical abstraction of a spine and the biological counterpart.

Although the design seems to be similar to a natural spine at first glance (shown in Fig. 3.16(b)), by looking into the overall mechanism, a major difference is revealed, regarding how a spinal column is stabilized and actuated in nature. By considering the spinal column as an independent functional unit, one disregards the complexity of this biomechanical system [Kap99b] (see Fig. 3.16(b)). It is connected to the skeletal structures nearby via muscles, ligaments, and tendons.

Providing a visual representation, Kapandji compares this system with a mast and rigging of a sailing boat [Kap99b]. The mast is in general bendable, but rigid in compression and stands for the spinal column. This mast is connected to numerous tension ropes (which are the muscles, ligaments and tendons) which apply (or even compensate) any bending moments generated by forces acting on the sail.

3.4.2 Technical Implementation

Anatomically seen the sail boat analogy is true up to a certain extent: the muscles are connected to bones, which are rigidly coupled to the spine. These, in technical terms called, lever arms are necessary to generate high bending moments out of the exerted forces.

Therefore, a serial design for the actuation of an artificial spine does not match with the spines seen in nature. An appropriately designed parallel kinematic mechanism on the other hand corresponds better to its natural counterpart. One drawback of parallel kinematics is that they have a more limited workspace compared to serial kinematics. But comparing the spine, e.g., to a leg or an arm, one can see that this is also true for a natural spine. The advantage of a parallel alignment is the higher stiffness and it can provide higher torque than a serial kinematics of comparable size and weight. When an external load is applied to this alignment, multiple actuators participate in generating a response, e.g., holding the position or generating torque, as it is true for the natural spine. By replacing the rigid body connecting the front and the rear legs, high forces and torques are to be expected to work on the artificial spine. Up to now, in robotics, these forces and torques have not been measured during locomotion. In Charlie, such a measurement is possible via integrated force sensors in the artificial spine. The recorded data is shown later on in section 5.5.2.6.

The design of Charlie's spine follows the principle of a Stewart platform [Ste65] and thus provides high stiffness with a possibility of light-weight design, which are excellent properties for the use as a body structure of a mobile robot. Charlie's front and rear body are connected via rods. The design of a 250 mm long rod is shown in Fig. 3.17(a). The thoracic and the lumbar sections of a natural spine are merged to one section (see Fig. 3.17(b)). In the middle of the spine a cable duct is installed, which is comparable to the natural spinal column, because of its main function of transmitting data between brain and body. The figure also shows the mechanical interfaces to implement the artificial spine into the robot. Each rod has an one DoF force sensor integrated and due to the rod arrangement, only compression and tension forces can occur. The rod is connected on top to one BLDC motor via a 20 mm lever and on the bottom with a hitch joint to the hip. In this technical realization, the lever arms are not applied to the spinal column like in nature, but they fulfill the same function. By comparing Fig. 3.16(b) with Fig. 3.17(b), the similarities between the spine in nature and the artificial one can be seen.

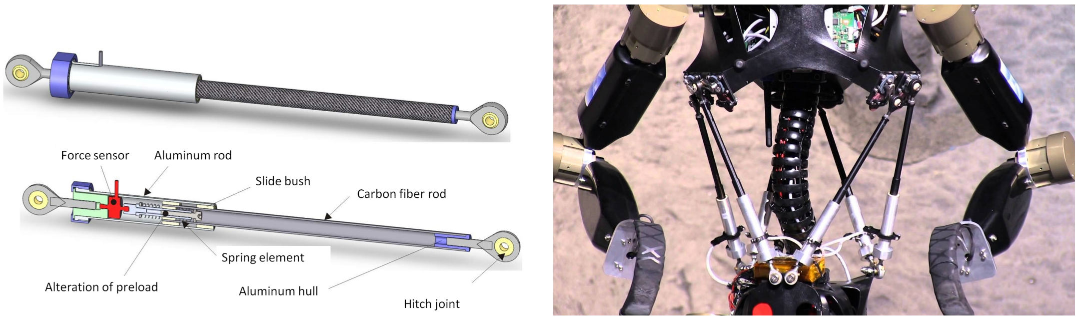

(a) Schematic drawing of a rod including damping and force sensor.

(b) Rods within the spine (close-up view).

Figure 3.17: Artificial spine in Charlie.

The spine actuators are equipped with a 246:1 reduction gear and are located in Charlie's upper body. To measure the motor position, absolute magnetic encoders are added off axis. The motor position is transmitted via an 1:1 gear wheel to the encoders. The diameter of the artificial spine is 305 mm at the front section and 190 mm at the rear section. The overall weight is 3.3 kg, which includes the motors, levers, rods, casing, and electronics.

3.4.3 Analysis of the Artificial Spine

For the analysis of the spine, the extended RoM of the spine is presented and experiments are shown to validate the functioning of the force/torque sensor.

The Spine's Range of Motion

The lever, connecting rod and motor, is 20 mm long and defines the workspace of the spine. By changing the lever length, the workspace of the spine changes as well. The RoM for each axis is shown in Fig. 3.18. The values in the diagram show the maximum values for each axis which cannot be reached simultaneously.

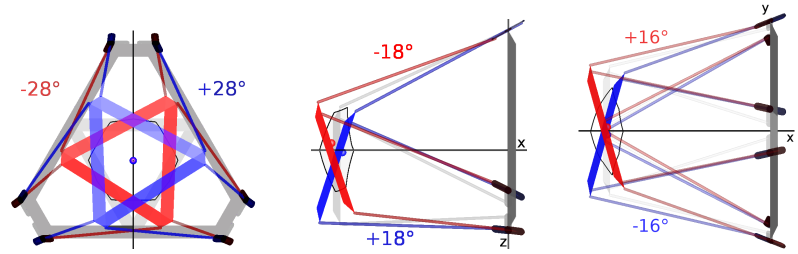

(a) Rotation on the x-axis in °.

(b) Rotation on the y-axis in °.

(c) Rotation on the z-axis in °.

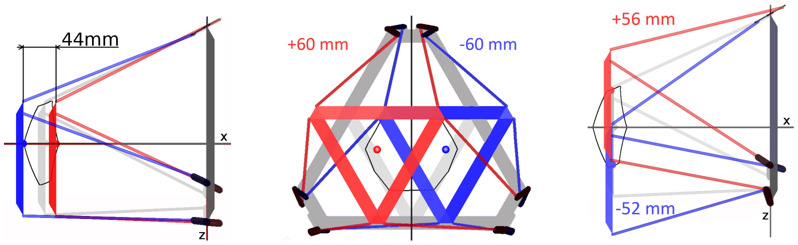

(d) Translation in x direction.

(e) Translation in y direction.

(f) Translation in z direction.

Figure 3.18: The range of motion of the spine structure. In diagrams (a), (b), and (c) two rotation axes are locked. In diagram (d), (e), and (f) two translations are locked [KBS+13b].

With Charlie's artificial spine, the maximum left/right rotation, i.e. the torsion, is from −28° to 28°, the forward / backward flexion is from −18° to 18°, and a maximum lateral movement from −16° to 16° is reached. The maximum translation on the x-axis is 44 mm, allowing the robot to vary its body length by stretching or shorten itself. On the y-axis, a lateral translation between front and rear body of together 120 mm is possible. On the z-axis, a shift of 108 mm between front and rear body can be realized. By increasing the lever lengths, the spine's RoM is increased as well.

As mentioned above, the individual values cannot be reached simultaneously. This becomes clearer when looking at the possible workspace shown in Fig. 3.19(a), where the possible movement of the rear body relative to the front body can be seen. The values within the figure are indicating the maximum position within the robot's body Coordinate Systems (CS), which has its origin in the rear plate of the front body. For example, a translation on the z-axis to its maximum (−246 mm from the CS origin) and a rotation on the same axis are mutually exclusive, since a rotation around this axis includes a modification of the translational position.

Applying the workspace of the artificial spine to the robot, the robot's overall

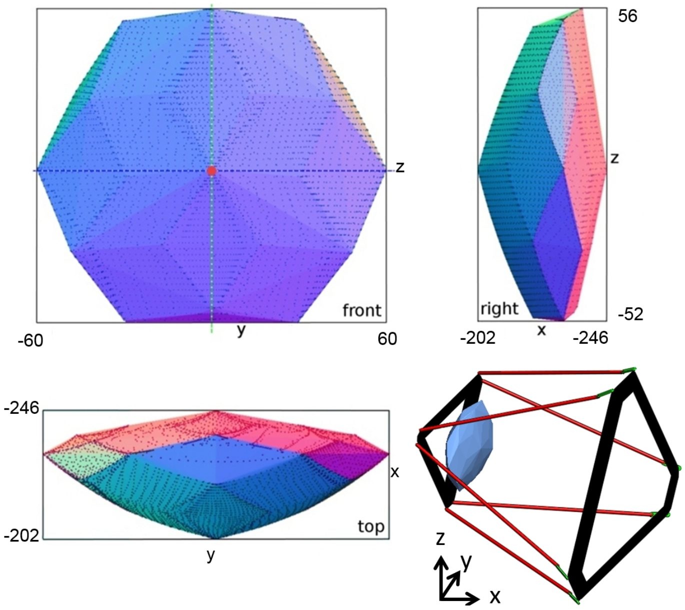

(a) Workspace of the hip section relative to the shoulder section in mm.

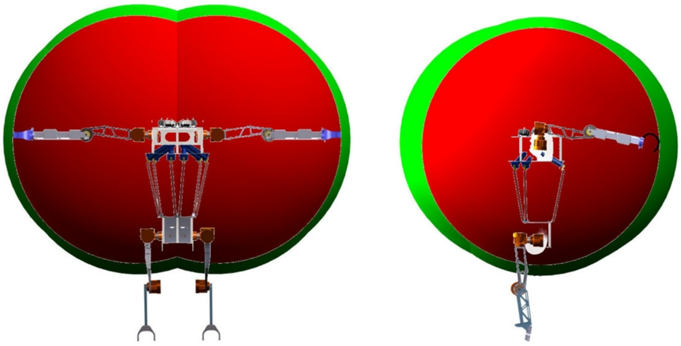

(b) The RoM of an end effector with and without spine actuation (front and lateral view).

Figure 3.19: The workspace of the spine and resulting RoM of an end effector with and without spine actuation [KSS+16].

workspace becomes increased as well. Taking the arms as an example, the extended RoM is pointed out in Fig. 3.19(b). The limbs workspace with an immobile, rigid spine is displayed in red. The green circle shows the combination of the limb's RoM extended by the extra RoM resulting from a movable artificial spine, which allows to shift the limbs workspace to the desired direction. By what percentage the workspace is increased depends highly on the position of the end effector and lies within 6 % to 16 %.

Validation of the Force/Torque Sensor

The signals of each force sensor integrated in the rods are connected to a control board located in the hip compartment of the robot. By combining the six single force sensors, the spine can be used as a six-axes force/torque sensor. To validate the functionality of this combined sensor are three experiments performed.

In the first experiment, pulling forces of 5 kg, 10 kg, and 15 kg are applied to the spine via weight plates and a wire rope hoist. Charlie is hovering over the ground in a quadrupedal posture. The pulling force is applied in all three directions, so one after the other each force pulls on the hip downwards, sidewards or to the back. The weight plates are applied to the spine via a wire. The data is shown in Tab. 3.6. As for the first experiment, all actuators are switched on to hold the position. It has to be noted that the weight plates actual weight differs from the advertised weight, thus the plates are lighter than specified. The difference depends on the individual weight plates and is not the same for each plate. For the 5 kg plate, the actual weight differs about 200 g, for the 10 kg plate about 350 g, and for the 15 kg plate the difference is 500 g.

Table 3.6: Pulling forces of 5 kg, 10 kg, and 15 kg are applied on the spine. The standard deviation in indicated in brackets.

Axis / Applied load	x-axis	y-axis	z-axis
4.8 kg	42.2 N (1.3)	45.9 N (2.4)	45.2 N (2.2)
9.7 kg	89.3 N (1.5)	91.5 N (2.4)	86.8 N (1.1)
14.5 kg	132.4 N (3.0)	132.3 N (2.4)	134.0 N (1.3)

As it can be seen in the table, the measures values are close to the expected ones of 47 N, 94 N, and 142 N, respectively. The differences between the three axes are probably because of minor differences in the lengths between the individual rods. The deviation can be explained with sensor accuracy as well as with the experimental setup, due to possible friction between wire and test rack.

The repeatability of the sensor data was tested in a second experiment and is shown in Fig. 3.20(a). The weight plates with the advertised weight of 15 kg are alternatingly applied and removed on the z-axis. In the figure, a measured load of about 135 N can be seen. Furthermore, a sensor reading can be observed on the x-axis. The deviation from the expected 142 N can be explained by the inaccuracy of the small and light-weight sensors and sensor noise, since six sensors are used to realize this virtual force/torque sensor. In addition, one can see an applied

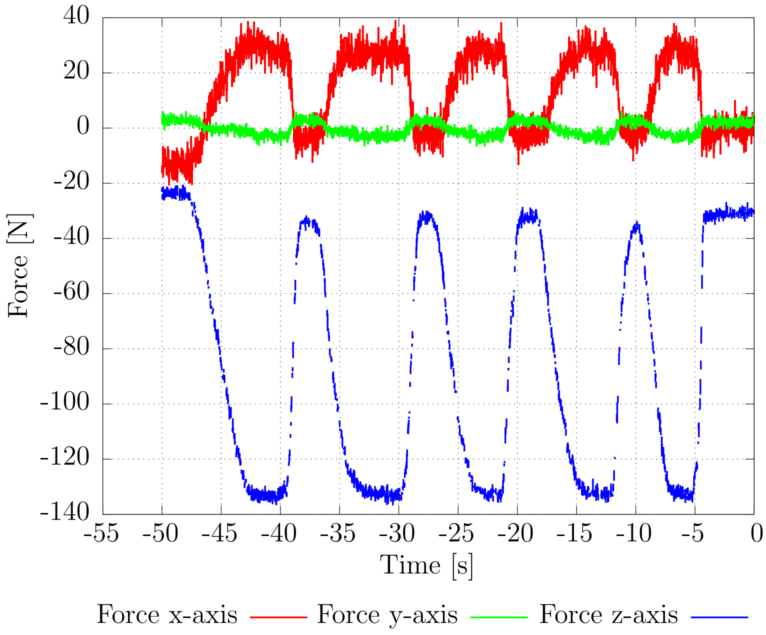

Figure 3.20: Usage of the force sensors in the rods as a six-axis force/torque sensor. 15kg are pulling alternating on the hip on the z-axis.

force on the x-axis as well. This is due the experimental setup, where it is difficult to introduce a dynamic force only on one axis. Nevertheless, the data indicates that with this virtual force/torque sensor a good repetition accuracy is achieved (standard deviation of about 1.6 N) as well as a fast adjustment to the applied forces.

3.5 Conclusion

The focus of this chapter lies on the natural counterpart of Charlie as well as on the design of the hominid robot with all its subsystems like actuators, multi-point contact feet, or the artificial spine. Because chimpanzees show a great variety of kinematic skills and motion behaviors, they were selected as a model for the multi-locomotion robot, enabling it to deal with different environments and to perform a diversity of tasks.

The dimensions of Charlie's limbs as well as its appearance are inspired by chimpanzees. The multi-point contact foot allows the integration of 60 sensors each. Overall, Charlie features more than 330 sensor inputs and has 36 DoFs. The power consumption of the entire control electronics is about 48 W. While standing on the ground in its quadrupedal posture (see Fig. 3.2(b)), only 3.4 W are additionally needed by the actuators to hold their position.

It is shown that the developed foot has a better friction coefficient compared to spherically shaped feet often used in robotic systems. With the lower leg design, a larger RoM of the feet is realized compared to a human foot. A roll and pitch motion is generated by two actuators, installed at the same location like the human calf, to reduce the moment of inertia.

The anatomy of a spinal columns seen in nature and their dependency of the respective load case are discussed in this chapter as well. In addition, the design of the artificial spine, which follows the principle of a Stewart platform, is presented in detail including the actuation and its sensory equipment. Due to the installed force sensors in the rods, the spine can be used as a six-axes force/torque sensor. The functionality of this virtual force/torque sensor is experimentally validated. Furthermore, it is shown that the spine increases the robot's RoM up to 16 %.

Chapter 4

Control

This chapter introduces a real-time control strategy to control a kinematically complex hominid robot, equipped with a variety of sensors. First, the hierarchical control concept is introduced, including a description of its different layers and the software modules within these layers. Second, the communication strategy between the lowest level, the reactive level, and the operator is described. The chapter closes with a description of the implementation and functioning of a local control loop as one part of the low level control, installed in the robot's rear legs.

This chapter is supported by the following peer-reviewed publications:

- D. Kuehn, F. Bernhard, A. Burchardt, M. Schilling, T. Stark, M. Zenzes, and F. Kirchner. *Distributed Computation in a Quadrupedal Robotic System.* In International Journal of Advanced Robotic Systems, 2014

- D. Kuehn, M. Schilling, T. Stark, M. Zenzes, and F. Kirchner. *System Design and Field Testing of the Hominid Robot Charlie* In Journal of Field Robotics, 2016

4.1 General Control Concept

In Charlie, a biologically inspired, hierarchically organized control is implemented. The robot control scheme is illustrated in Fig. 4.1 and shows the different layers.

The physical presence of the robot in the world allows an interaction with its environment (as indicated at the bottom of the figure). The interaction responses are perceived with the variety of employed sensors within the low-level control. This implies proprioceptive data (like telemetry data of an actuator) as well as exteroceptive data, e.g., occurring forces and torques. As shown on the left, the

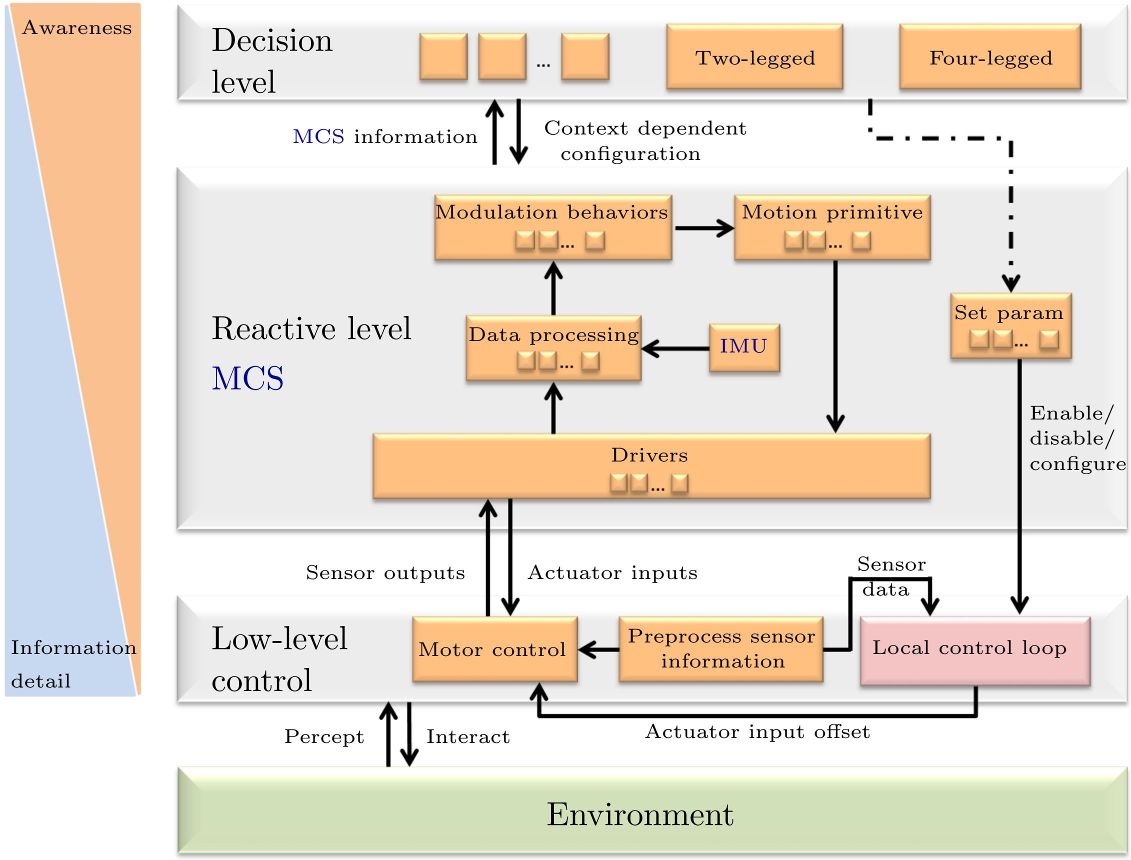

Figure 4.1: Scheme of the control approach implemented in Charlie.

higher the level of control, the less information detail is present. Yet, all preprocessed information is gathered at the higher levels. Therefore, the highest level has a situation awareness, which is not available at the lower level.

A coherent behavior is achieved through collaboration between single local nodes or subsystems; either control, actuator, or sensor processing nodes and combinations thereof are installed within the robot's structures, e.g., actuators, spine, and feet feature at least one control electronics of its own. Most of the perceived data is preprocessed at the lowest level and sent to the MCS. The communication structure is described in section 4.2. The distributed control allows each local controller to exercise fine granulated control over its assigned subsystem at high frequency. The low-level control is described in detail in section 4.3.

In Fig. 4.1, drivers represent the interface between different low-level control nodes and the MCS. Besides the sensors connected to the low-level control electronics, two IMUs, installed in Charlie's front and rear body, as well as the relay board are connected directly to the main processing unit. This indicates that some raw data processing takes place in the MCS as well, although in a limited manner compared to the low level control. The general behaviors are generated in Charlie's main processor and consist of different software modules. The generation of a stable locomotion bases on the biologically-inspired control approach proposed in [SK07]. This approach includes modulation behaviors as well as continuous rhythmic locomotion signals (or motion primitives). The modulation behaviors have an influence on the resulting position output of the actuators, i.e. postural and stability behaviors are responsible for keeping the robot statically stable and providing an interface to translate or rotate the body. These autonomous adjustments allow the robot to adapt its pose according to external influences (e.g. an inclination) without interrupting the walking pattern. To generate these reactive motions, the incoming sensor data is analyzed continuously. The MCS has to coordinate all of Charlie's 36 active DoFs to realize a fluid locomotion of the robot and the output is transmitted to the low-level control via the implemented drivers.

The local control loop in the feet is one example of such a controller. The MCS provides an interface to configure such local control loops as well as the required context information. A detailed description of the MCS including its software modules is given in section 4.4.

The control approach in [SK07] is extended with a local control loop [KBB$^+$14], depicted in Fig. 4.1 on the right hand side. In Charlie, due to the high number of sensors and the processing power in the ankle joint and feet, the desired foot trajectory can become adapted locally on the basis of external influences like varying surface characteristics, without commands from the main motion controller. As mentioned earlier, on the lower control level an awareness of the robot's current situation is not given. As shown later in the experiment section, at least modest context information is relevant for the local controller and is absolutely necessary, to improve the walking behavior. Thus the local controller features an interface for the MCS, enabling it to provide relevent context information to the local controller. The local controller is described in detail in section 4.5.

Although high-level control of a robotic system is an interesting research area, the presented work focusses on the electro-mechanical design of a hominid robot, the motion control system and the usage of local control loops and thus a deliberative level of control is not within the scope of this thesis. Imaging sensors like cameras or laser scanners are not yet installed in Charlie, thus an initial environmental model is not given, which would be part of the high level software. The highest level is therefore currently not represented by an autonomous decision level but by the operator. Still, interfaces from the decision level to the MCS are available and can be used later on to increase the robot's autonomy.

4.2 Communication

The generation of stable locomotion presupposes a robust data exchange between all single subsystems. To be able to distribute information, the installed heterogenous electronics require a standardized interface to be able to communicate with each other. Therefore, in Charlie a communication is implemented, where FPGA, microcontroller, and PC which makes use of the same protocol. The homogeneous point-to-point communication interconnects all installed single nodes. In the physical layer, each node operates with LVDS and the nodes are organized in logical daisy chains, i.e each leg is represented as one separate chain.

The MCU is the central node, to which all the daisy chains are connected. Similar to the RS422 standard, four wires allow a full-duplex data transmission. Electronically, a Node-level Data Link Communication (NDLCom) [ZKSS16] instance has two input and two output ports, comparable with the efferent and afferent signals in biological systems. One pair sends messages to and receives messages from nodes located upwards in the chain (afferent). The other one does the same for nodes situated downwards the respective node (efferent). Each node knows its own ID and the receiver ID, and is therefore able to distinguish, which port to use. The NDLCom instance is able to receive, transmit, and forward frames in parallel. At the PC level, a data link control protocol is implemented, which allows a connectionless data transmission. Therefore, each data packet carries its own individual address information.

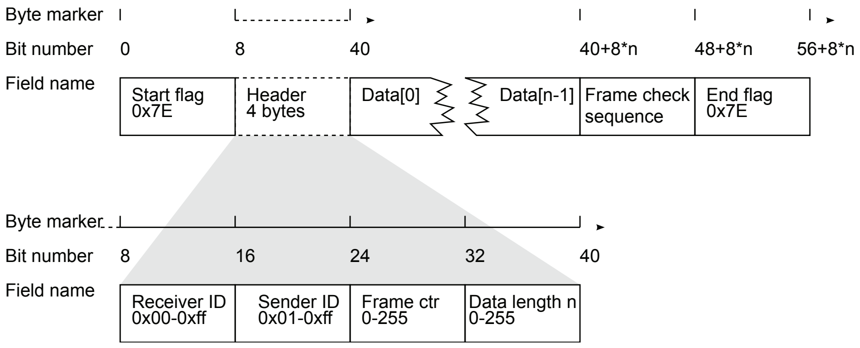

Figure 4.2: Schematic overview of the format of a NDLCom frame.

The resulting design of the NDLCom is depicted in Fig. 4.2. To minimize the transferred amount of data, a minimal NDLCom overhead is implemented. The overhead contains a start flag, the header, a check sum, and an end flag. The header has a size of four bytes and can be seen at the bottom of Fig. 4.2. Receiver ID, sender ID, and frame counter are one byte each. To allow frames with varying lengths, the length of the payload is given in the header as well. Using fixed frames would save one byte in the header, but would also mean that the length of the frame stays constant. For example, a fixed length of 50 bytes would always be sent, even if the payload has only a size of 10 bytes. Therefore, to reduce traffic, the length of the payload data is adapted dynamically.

Since single nodes are grouped to logical units and organized in a chain, each node forwards incoming frames which are not meant for the respective node. The selected forwarding mechanism is a *cut-through* method, where the node starts forwarding the frame even before the entire frame is received. As shown in Fig. 4.2(a), the destination address is within the first byte of the header. After receiving the header, the destination is known and the frame can be dispatched via the corresponding output port. Alternatively, it would be possible to use a method called *store and forward*, where the frame is stored until it is complete and is forwarded afterwards. However, this would result in a higher latency in communication.

In addition, information regarding the type of the payload data (e.g. actuator telemetry) as well as a time stamp are added, to allow the receiver the interpretation and processing of the data. Inside a node, different handlers are called, depending on the type of data. The time stamp, however, is used later on for a time-based data analysis.

4.2.1 Sensor Data Package Size

Table 4.1 shows the size of the telemetry data packages and the content send from each motor to the motion control system. For the motor nodes a distinction is made between the hip joints, the ankle joint nodes, and the spine, because of the differences in the installed sensors.

As mentioned above, for each packet 7 bytes have to be added, containing data like package header, CRC check sum or package identity (ID). It is most likely that start- and stop-flags appear also within the user data. Before sending, these bytes will be escaped. The occurrence of escape-bytes cannot be predicted and thus the packet length varies. Therefore, the values in the right column of the table indicate the minimal packet length. The telemetry data of each actuator includes actuator state, information about occurred errors, absolute position, motor speed, actual PWM, current consumption, input voltage, the temperature inside the motor housing, as well as debug data. In addition, the local spine controller combines the motor current to an overall spine current. For the ankle joint and spine, a motor temperature measurement is not included due to the spatial separation of actuator and PCB.

All installed sensors within the Charlie robot are shown in Tab. 4.2. The MCS is mostly provided with preprocessed sensor data, which includes merged data from certain notes, e.g., force/torque sensor information from the spine or the local support polygon of a rear foot. Since each node can be configured independently and the sending frequency of the data can be reduced if necessary, the right column shows the maximal possible frequency.

Table 4.1: Size of the data packages send from each motor node to the motion control system.

Node	Sensor	Number	Minimum length	Hz
Motor telemetry data		18	min. 32 byte	100
	State	1	2 byte	
	Error	1	1 byte	
	Warning	1	1 byte	
	Absolute position	1	2 byte	
	Encoder position	1	2 byte	
	Speed	1	4 byte	
	PWM	1	2 byte	
	Current	1	2 byte	
	Voltage	1	2 byte	
	Temperature	1	2 byte	
	Debug	1	12 byte	
Ankle Joints		4	min. 42 byte	100
	State	1	2 byte	
	Error	1	1 byte	
	Warning	1	1 byte	
	Pitch °	1	2 byte	
	Roll °	1	2 byte	
	Yaw °	1	2 byte	
	Motor position	2	4 byte	
	Motor speed	2	4 byte	
	Motor PWM	2	2 byte	
	Motor current	2	2 byte	
	Debug	1	8 byte	
Spine		1	min. 134 byte	100
	State	1	2 byte	
	Error	1	1 byte	
	Warning	1	1 byte	
	Absolute position	6	2 byte	
	Encoder position	6	2 byte	
	Motor speed	6	4 byte	
	Motor PWM	6	2 byte	
	Motor current	6	2 byte	
	Motor Debug	6	8 byte	
	Spine voltage	1	2 byte	
	Spine current	1	2 byte	
	Debug	1	6 byte	

Table 4.2: Implemented sensor nodes and their package size.

Node	Sensor	Number	Minimum payload	Hz
IMU		2	min. 56 byte	100
	Temperature	1	4 byte	
	Acceleration	3	4 byte	
	Turn rate	3	4 byte	
	Magnetometer	3	4 byte	
	Orientation	4	4 byte	
RelaisBoard		1	min. 20 byte	
	Voltage	1	4 byte	
	Channel status	8	2 byte	at request
Sensors spine		1	min. 32 byte	100
	Force/torque sensor	1	32 byte	
Sensors front feet		2	min. 64 byte	100
	6DoF force/torque sensor	2*1	32 byte	
Sensors rear feet				
	Sensor array	2*49	min. 204 byte	max. 100
	6DoF force/torque sensor	2*1	min. 32 byte	100
	Distance sensor	2*1	min. 5 byte	50
	Acceleration	2*2	min. 12 byte	100
	Absolute position	2*4	min. 17 byte	100
	Temperature	2*2	min. 3 byte	max. 2MHz

4.3 Low-Level Control

The foundation for a smooth, stable, and energy-efficient locomotion in robots is laid by the functionality, efficiency, and performance of its subsystems. In Charlie, the low-level controllers are implemented in every actuator controller, feet, and spine. For the actuator control, the electronics employ a FPGA, whereas the sensory data in the feet and spine is preprocessed by electronics featuring a micro-controller.

4.3.1 Actuator Control

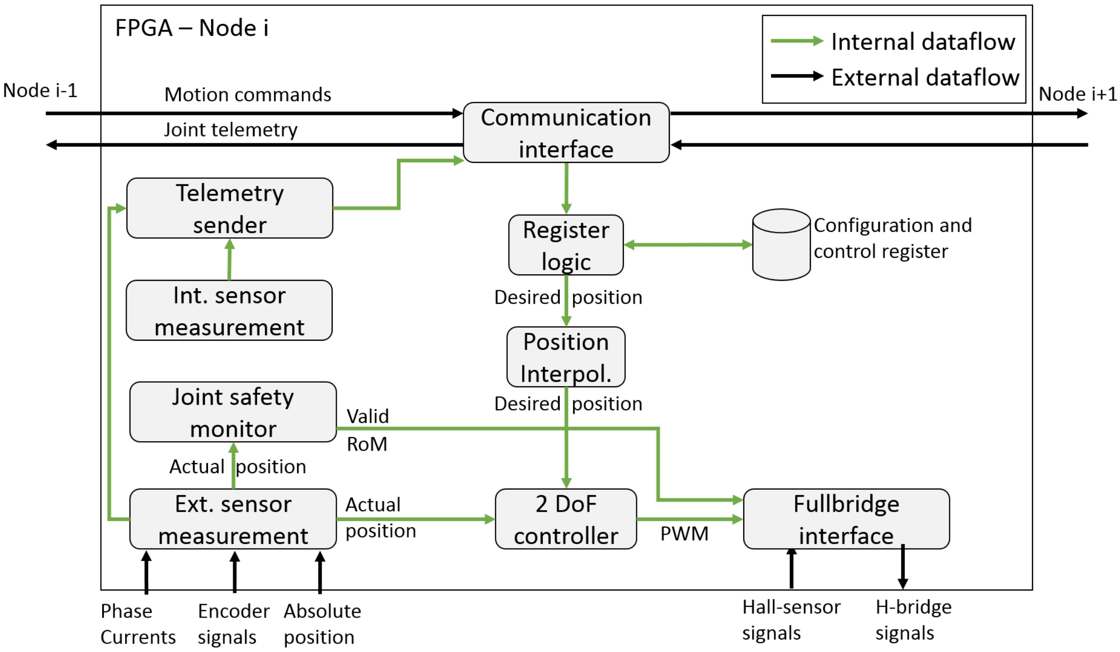

Figure 4.3: Schematic drawing of the FPGA joint control.

Figure 4.3 shows the control scheme for a single actuator. On top of the picture the communication interface can be seen, which handles incoming and outgoing data. Incoming data packets contain motion commands or configuration data. Apart from a few exceptions, most configuration data is stored in an Electrically Erasable Programmable Read-Only Memory (EEPROM). The motion commands are further processed by a position interpolation module. This module is responsible to generate a smooth motion through position interpolation and to reduce jitter of the control commands [JK13]. The filtered data is used by a two DoF controller, which generates the PWM output for motor commutation. Within this two DoF controller, a Proportional-Integral-Derivative (PID) controller is extended by two additional parameters, which help to reduce a possible overshoot, if the desired position is changed [JK13]. The fullbridge interface uses the PWM output, to generate the signals for the H-Bridge. The BLDC motor commutation, on which this implementation bases, is well summarized in [Bar13].

The actuator's initial position is measured by an absolute angular encoder and used to initialize an optical encoder. During operation the actuators' actual position and speed are calculated from the data of the optical encoder, due to a higher precision. The actuator control runs with a frequency of 1 kHz. A current, temperature, and voltage measurement as well as the actual time completes the actuator telemetry data packet, sent to the higher level with a frequency of 100 Hz. A software safety monitor can be set individually for each actuator. To prevent damages on the actuator or the robot, two limits are defined, a soft and a hard limit. During normal operation the motors are not exceeding the given individual soft limit, despite the desired position commands of the MCS. If, due to external influences, the hard limit is exceeded, e.g., by 5° or more the actuators are switched off.

For the ankle joint, spine, or head, a single control electronic is used to drive two (ankle joint) or six motors (spine and head). For each motor connected to the PCB, one copy of the above presented control module exists in the FPGA. Theses copies are running in parallel. Due to limited space on the FPGAs, modules like the communication interface are shared between the copies on one PCB and therefore exist only once. Even though two or more motors are participating in generating the particular joint motion, the control scheme is kept as consistent as possible. The MCS sends the desired angle for the ankle joints roll and pitch as well as the desired translation and rotation for the spine and head. The corresponding local control electronics have an additional inverse kinematics module implemented, enabling them to calculate the resulting motor positions locally.

4.3.2 Sensor Nodes

The potential space to apply electronics in the lower legs and feet of the rear legs is more limited compared to the lower arms in the front, since the front feet are not actuated and also equipped with less sensors. In contrast to the rear legs, the sensor processing electronics can be installed in the lower arms. For the rear legs, an alternative solution is needed. On top of each rear foot, a compact electronics stack with the dimensions of 40 mm by 50 mm and a height of 30 mm for sensor preprocessing is installed. The stack includes a board to allow multiplexed data acquisition (mdaq2) featuring an STM32 micro controller. The mdaq2 PCB tolerates input voltages between 5.3 V to 20 V, has a current consumption of 0.6 W and fulfills the spatial conditions as well as the demands of the resistive sensors installed in the sole (cf. chapter 3.2.3 on page 50).

Another mdaq2 PCB is used to process the force/torque sensors integrated in the spine. The data processing runs with a frequency of 100 Hz. Taking the foot as an example, the dataflow is shown as a schematic drawing in Fig. 4.4. The blackboard is used to store and share all data coming from different sensors. Like in the FPGA, a cut-through communication is implemented. The virtual spring implementation in the mdaq2 sends data not only to the motion controller but to the ankle joint controller as well. This message contains angle offsets, based on the torques applied on the feet.

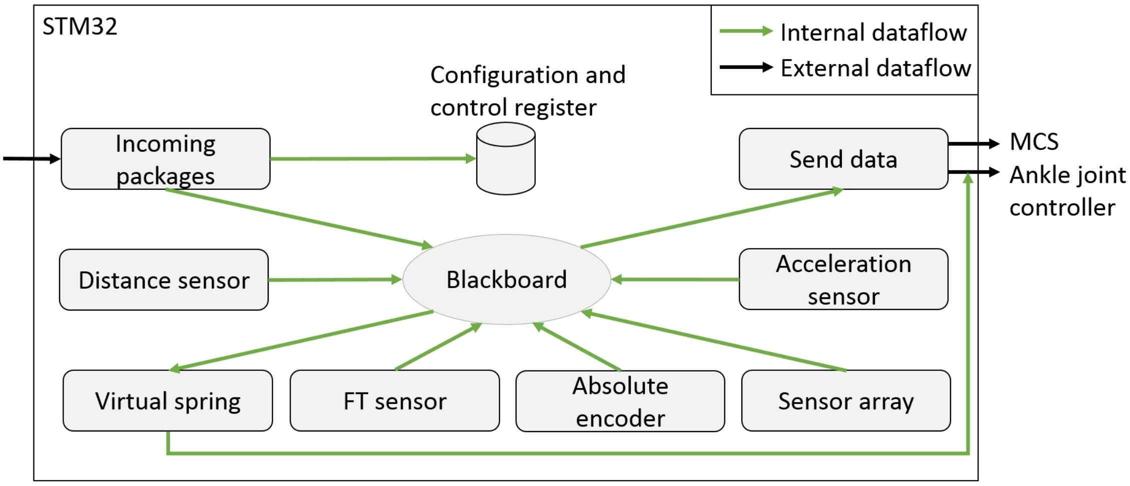

Figure 4.4: Schematic drawing of the dataflow in a sensory node.

4.4 Motion Control Software

The real-time control of a robot with 36 active DoFs in real-time is a demanding task. Charlie has no initial world model and no visual sensors to generate one, so its surrounding is unknown. This makes the real-time component even more essential, since for stability reasons the robot has to react within a limited time frame to occurring disturbances.

Hence, the MCS acts as a supervisory controller, collecting the data from all subsystems (see Fig. 4.1). Charlie's multi-threaded motion control software is executed on an Overo Gumstix board with a control frequency of 75 Hz. By sending the sensor data with a higher frequency to the MCS, it is ensured that in each control loop actual data is present. Based on the operators input, this central node is responsible not only to generate the motor output for a context-dependent coordinated motion, but also to communicate the output to the subsystems. Gait parameters like walking speed or direction are given to the robot from an operator. The trajectory of the resulting walking pattern in given in three-dimensional space, where an inverse kinematic solution is used to calculate the corresponding joint angles. To be able to use the commands context-independent, different CS are used in Charlie and introduced in section 4.4.1.

For walking, mainly the step height and step lengths, the frequency of one complete step cycle, and the offset between the legs can be adapted to change the rhythmic movement. Based on these parameters, the CPG module generates a rhythmic motion of the feet endpoints in a coordinated manner, to realize a walking behavior. A different gait can be realized by parameter adaption. The section 4.4.2 presents the realized walking pattern in detail.

However, different software modules have an influence on the subsystems and their trajectories (e.g. stability controller or the robot's posture), thus their outputs are merged via an add-merge, before an inverse kinematics solution is calculated to generate joint curves. Posture offsets can be set at any time, either from an operator or from the MCS itself. The inverse kinematics solver ignores unreachable configurations and reuses the last valid configuration.

Reflexes are by definition highly reactive and generate an immediate and well defined response to occurring disturbances, measured by the extensive sensory equipment. In contrast to reflexes, postural behaviors are suitable to control the robot's pose in slowly changing surrounding, e.g., while walking on an incline and are described in section 4.4.3.

4.4.1 Coordinate Systems

For locomotion control, different coordinate systems are defined and used in Charlie. The main one is called rest-CS. At start-up, the world-CS and Charlie's rest-CS lie on top of each other. While walking, the rest-position coordinate system moves with Charlie, whereas the world coordinate system is fixed on the initial point.Charlie's rest-CS is on the basis of the quadrupedal posture. The origin is located on the back plate of the shoulder housing and is oriented after a right-handed coordinate system, as it can be seen in Fig. 4.5. The x-axis (coloured in red) points in forward walking direction, the y-axis (green) to the left, and the z-axis (blue) up.

The rest coordinate system is fixed with respect to the gravity vector. It describes the pose of the body without any translations or rotations, introduced by modulation behaviors like the balance controller. The rest-CS is used to command the robot's walking direction. While walking upwards in a certain incline, the robot's body is rotated, but the rest-coordinate system does not. Thus, a commanded leg movement in x-direction in rest coordinates would result in a collision with the ground.

Therefore, an additional coordinate system, called body-CS, is used, e.g., to solve the inverse kinematics of the legs. The body-CS is defined by the axis along hip and shoulder and implemented relative to the rest-position coordinate system. Modulation behaviors add their offsets as well within the body-CS. Using only the body coordinate system would have the disadvantage that it changes with the robot's posture, e.g., in a bipedal stance, the x-axis of the body-coordinate system shows upwards and not in forward direction, like in the quadruped posture. Transformations between the different CSs are performed, to be able to use the same walking pattern generator for both postures.

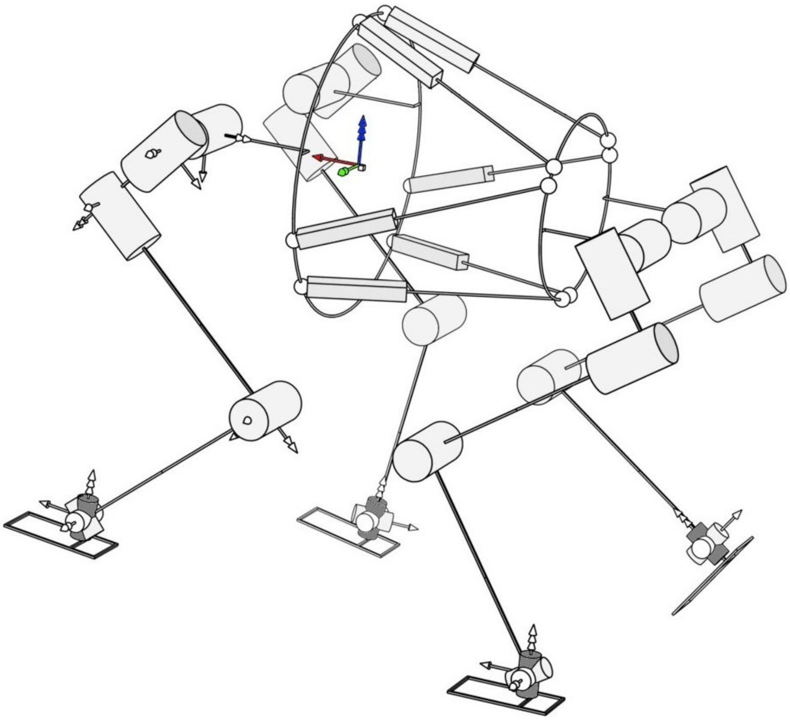

Figure 4.5: Position of the rest-position coordinate system in Charlie, indicated in colour: the x axis is shown in red, the y axis in green, and the z-axis in blue).

Charlie’s four limbs and the actuated spine can be moved independently in six DoFs. Besides the body, each leg has its own coordinate system. Within the MCS the limbs’ and body’s translations and orientations are described by three dimensional vectors and quaternions. Quaternions represent an orientation and rotation of an object in three dimensional space. Compared to Euler angles, a Gimbal lock cannot occur. Gimbal lock means the ”loss“ of one DoF and thus locking the respective system into two-dimensional space, which can happen if one axis rotates 90° resulting in an alignment of the remaining two axes. In Charlie, a Gimbal lock could happen if the robot’s posture is close to an upright position, due to a 90° rotation of the two IMUs mounted on Charlie.

4.4.2 Walking Pattern

In literature, the identification and classification of natural limb motion sequences for different gaits of quadrupeds is well documented [Hil65], [Hil67] and [MF68], especially for low speed locomotion. According to McGhee and Frank, only six gaits can be used, where at all times a maximum of one leg is in swing-phase and at least three feet have ground contact [MF68]. The possible leg sequences are shown in Fig. 4.6 and are called creeping gaits. Mc Ghee performed a mathematical analysis to show that only three of these footfall sequences produce a stable gait. Furthermore, among these stable leg sequences, one sequence exists which produces a gait “that maximizes static stability” [MF68], which is also the one observed during locomotion in animals. In Fig. 4.6 this creeping gait is shown in the bottom row in the middle (Crawl 1423).

4.4.2.1 Implemented Walking Pattern

The CPG behavior, a motion primitive (see 4.1), generates the rhythmic motion patterns for all legs. The output of this behavior is the desired positions of the feet in x, y, and z direction within the rest CS and is used as input for the kinematic module, where the output of modulation behaviors, e.g., the stability controller, serve as well as input.

Because of the maximized stability, the above mentioned statically stable gait (Crawl 1423) is implemented in Charlie. The generation of a walking pattern is implemented as a time-based state machine with different input parameters. As shown in Fig. 4.7, the two basic states are swing-phase and stance-phase; the leg is in the air in swing-phase and has ground contact in stance-phase.

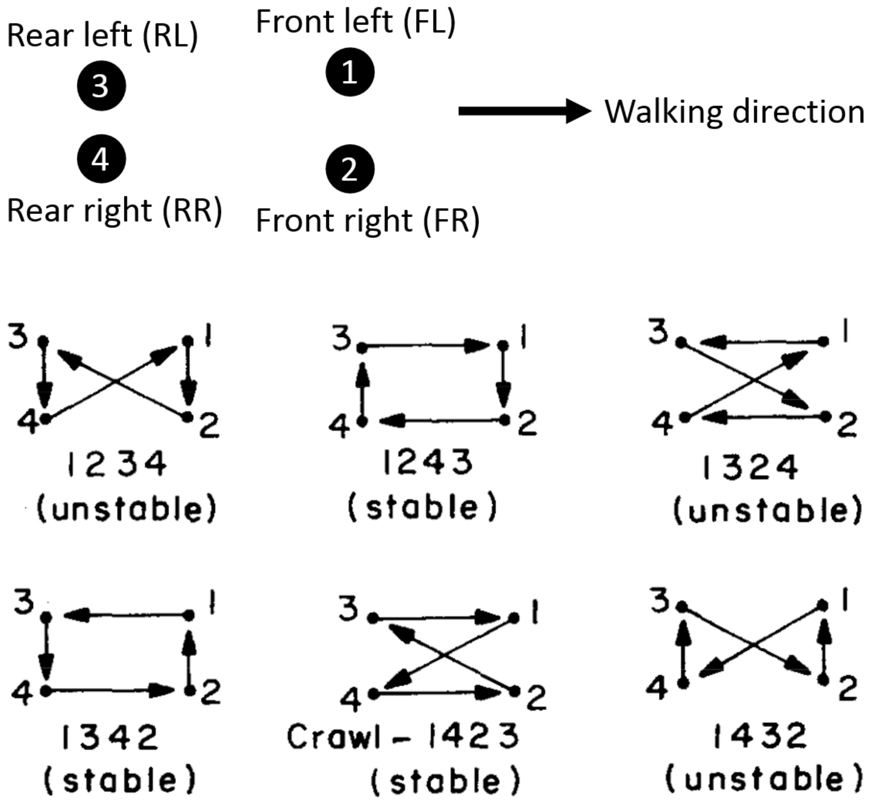

Figure 4.6: Possible creeping gaits in quadrupeds. The labeling of the feet and walking direction is shown on top, the six possible combinations of foot lifting and shifting is depicted at the bottom. Illustration adapted from [MF68].

In the swing-phase the foot is moved from the Posterior Extreme Position (PEP) to the Anterior Extreme Position (AEP). During the stance-phase the foot is moved parallel to the ground, whereas the swing-phase uses stitching Hermite splines [Wik16], to obtain a smooth trajectory of the feet in x, y, and z direction, as shown in Fig. 4.7. The transitions to and from the stance-phase are implemented accordingly.

The runtime of each phase is defined by an individual time, $T_{Leg\_i.Swing}$ and $T_{Leg\_i.Stance}$ respectively, whereas the condition $T_{Cycle} = T_{Leg\_i.Swing} + T_{Leg\_i.Stance}$ has to be met. In general, both phases (swing and stance) describe one step cycle for one leg. Besides the correct temporal offset for the starting point of each swing-phase, the time for one leg's swing-phase has to be $T_{Leg\_i.Swing} <= T_{cycle}/4$, to realize a crawl gait. If $T_{Leg\_i.Swing} < T_{cycle}/4$ is true for all legs, phases in the walking pattern can be seen where the robot has all four legs on the ground. The motion sequence shown in Fig. 4.8 is for $T_{Leg\_i.Swing} = T_{cycle}/4$. The stance-phase is indicated with red bars. The swing-phase is furthermore divided into a lift-phase $T_{Leg\_i.Lift}$ also

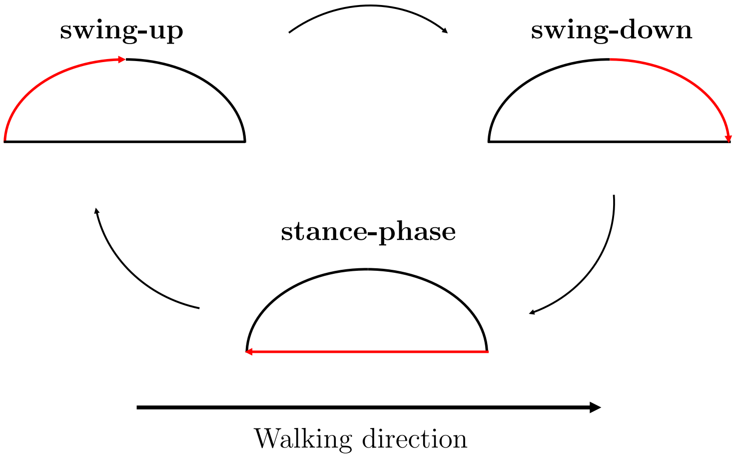

Figure 4.7: The three states per leg during one step while walking forward. The active phase is colored in red. During the stance-phase, the foot has ground contact. The swing-phase is divided into swing-up and swing-down.

called swing-up (green checkered in the figure) and shift-phase $T_{Leg\_i.Shift}$ also called swing-down (blue checkered) of the foot and ends with the foot's touchdown on the ground, resulting in $T_{Leg\_i.Swing} = T_{Leg\_i.Lift} + T_{Leg\_i.Shift}$.

In addition, the starting point of the leg's swing-phases have to be coordinated. The phase-offset parameter allows to determine the starting point of the leg's swing-phase. Figure 4.8 shows a phase-offset of 0 % for rear right (RR), 25 % for front right (FR), 50 % for rear left (RL) and 75 % for front left (FL). By changing the phase-offset, e.g., to 0 % for RR, 50 % for FR, 50 % for RL and 0 % for FL, a completely different gait is realized. The latter phase-offset results in a cross gait, where the front left leg and the rear right leg start their swing-phase simultaneously. After the touchdown of both legs, the front right leg and the rear left leg start their swing-phase.

In Charlie, to configure the walking pattern, the time for swing and stance can be set, as well as the overall cycle time, the phase-offset between the legs, stride length in x and y direction, and stride height in z direction. After the first experiments with the Charlie robot, initial walking parameters are determined, and set in the motion control system, e.g., a walking cycle time $T_{cycle} = 5s$ and a foot swing height during swing-phase of 100 mm. The initial phase-offset is 25 % of the overall cycle time for each leg's swing-phase. One gait cycle is completed when all four legs (in the quadrupedal posture) or both rear legs (in bipedal mode) have completed their individual swing- and stance-phases.

The gait progress counter starts at 0 with the lift-off motion of the rear right (RR)

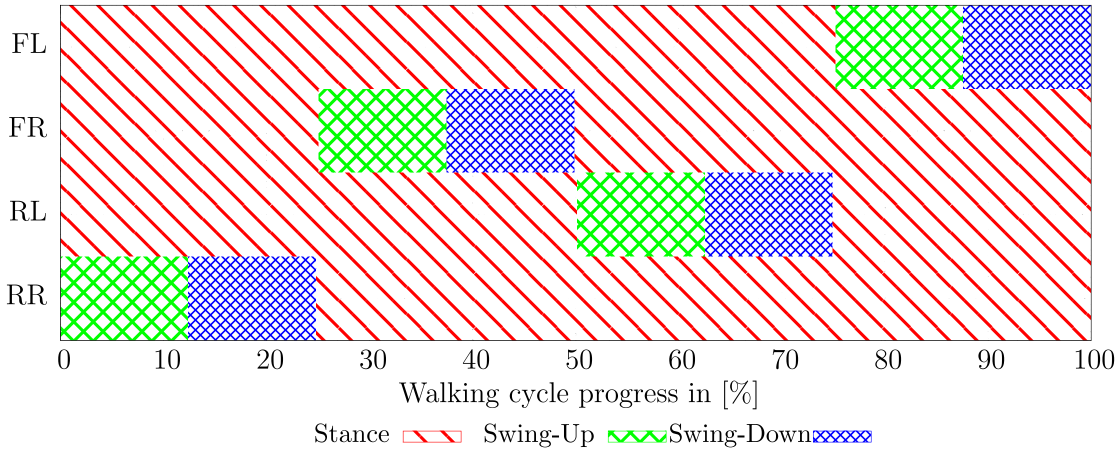

Figure 4.8: Limb motion sequence of the crawl gait in Charlie. The sequence starts with lifting the rear right leg (RR), the other legs follow accordingly one after another (FL stands for front left, FR for front right, and RL for rear left).

leg. It reaches its final value 1 after finishing the swing down phase of the front left (FL) leg and a new cycle starts. For data logging and evaluation purposes, each leg has its own progress counter starting with the motion of the swing-phase, allowing a phase-based alignment and comparison of sensor data coming from different legs. Changing the walking parameters during locomotion has no effect on the progress counter.

4.4.2.2 Walking with Spine Motion

In Charlie, the gait can be supported by the movement of the introduced actuated artificial spine. Its rotation and translation motions have an influence on the position and orientation of the front and rear feet and thus the trajectories of the limb's endpoints have to be adapted. The influence of the spine motion can be selected freely between 0 % and 100 % at any time of a walking motion. Setting the spine motion to 0 % entails that the spine actuators hold their position and the active spine acts as a rigid connection between front and rear body, letting only the leg joints participate in generating a forward or lateral motion (see Fig. 4.9(a) and Fig. 4.9(b)).

When set to 100 %, the spine covers as much of the distance, the legs have to travel, as possible, by its rotational and translational movements. This is only possible as long as the selected parameters, e.g., the step length and step height of the feet can be achieved only by moving the spine. To be more specific, by setting the desired step length to a very small value, e.g., to 20 mm per cycle, the leg joints hold their position and a forward motion including the lift-off and touchdown of a foot is realized only through the movement of the spine. The maximum step length the spine can cover by itself is highly specific and depends on the predefined rotation and translation offsets (as to be seen in the illustration of the spine workspace in Fig. 3.19(a)), as well as on the robot's footprint.

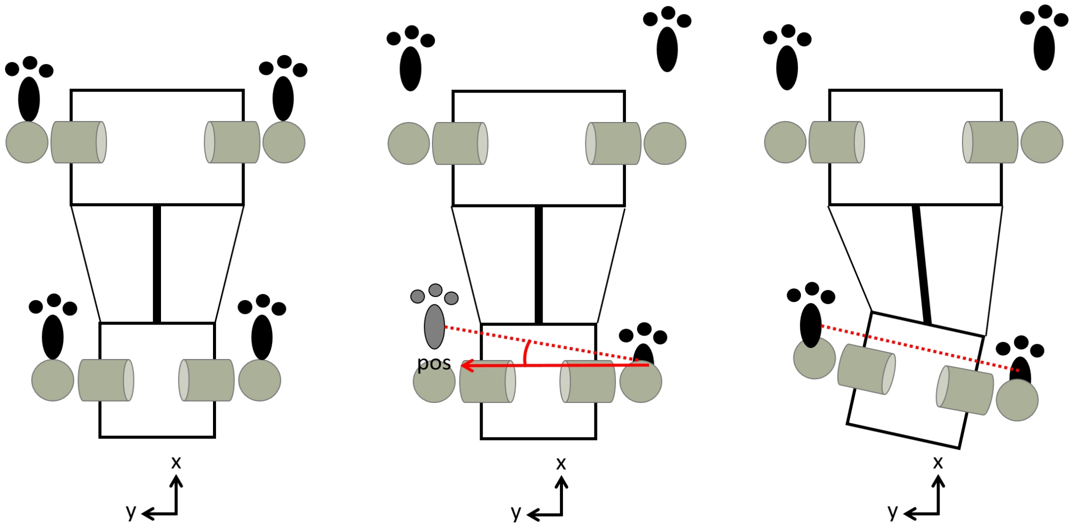

(a) The spine can act as a rigid body.

(b) Actual and desired position of the RL leg (*pos* and the greyed out foot, respectively).

(c) Movement of the hip with respect to the shoulder to reach the desired foot position.

Figure 4.9: Schematic drawing of the spine motion while walking.

A calculation the supporting spine motion is continuous and depends on which foot is supported next. When during a step the RL is supported, the actual coordinates of the RL and RR are used. Using the position of the RR leg as origin, one can determine an angle on the y-axis from the actual and the desired position, indicated with *pos* and the greyed out rear left foot, respectively, in Fig. 4.9(b). This angle is used to calculate the desired angle of the rear body's y-axis with respect to the front body's y-axis, as shown in Fig. 4.9(c).

4.4.3 Posture Control

A robotic system is statically stable as long as its projected CoM lies within its support polygon. The individual masses of all body parts in Charlie are known as well as the robot's pose. Hence, the MCS can calculate Charlie's CoM.

The robot's overall support polygon is calculated within the MCS as well. Due to the local computational power, each rear foot calculates its convex hull and provides the coordinates of its local support polygon. For the robot's support polygon calculation, a maximum of 16 instead of 49 contact points from each sensor array are used. Due to the shape of the foot and the sensor placement, no more than 16 points can be relevant to describe the local convex hull. In contrast, the dimension and shape of the front feet allow a direct use of the coordinates from the inverse kinematic solution.

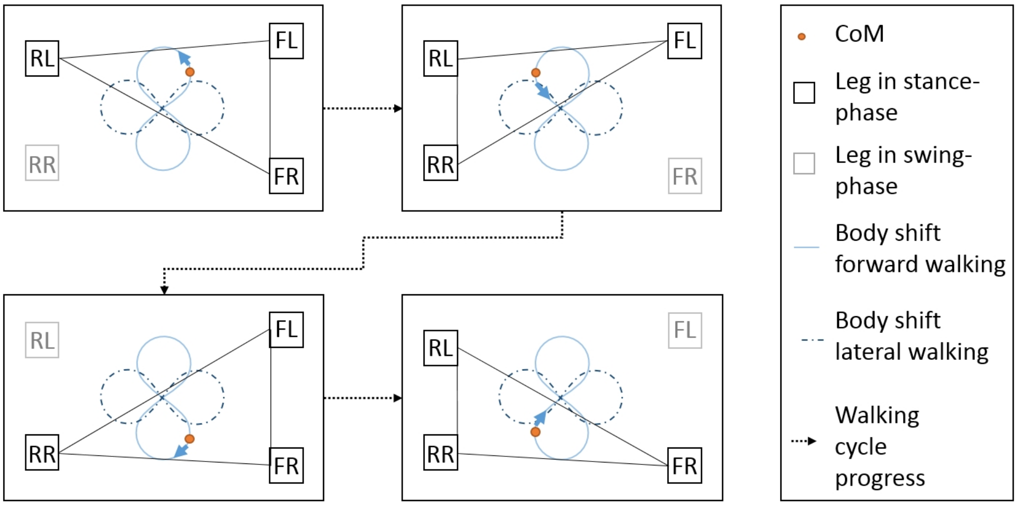

(a) Schematic drawing of body translations and resulting CoM shift during forward walking.

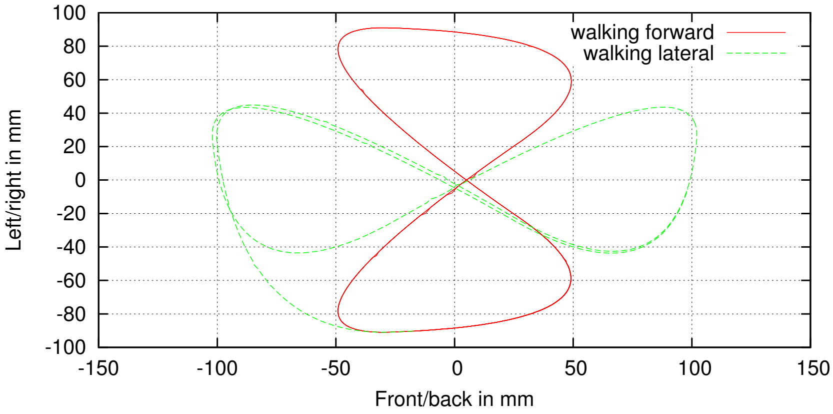

(b) Adaption of the CoM trajectory from walking forward ("8"-shaped trajectory in red) to lateral walking ("∞"-shaped trajectory in green). The transition can be seen in the lower left [KBB+14].

Figure 4.10: Localization of Charlie's CoM while walking.

For the described support polygon calculation the robot's posture (quadrupedal or bipedal) makes no difference. Because of the MPCF, during the stance-phase sufficient coordinates are available to allow a support polygon calculation.

As simplification, it is assumed that the CoM has a fixed position in the robot's body frame. It was observed that the projection of the robot's CoM on a completely leveled floor lies close to the edge of the support polygon during the lifting and shifting motion of one leg. While walking, to keep the CoM inside the support polygon with a certain distance to the edges, a shifting of the torso is necessary. In Charlie's MCS, this is a modulation behavior (see Fig. 4.1). The generation of a smooth motion trajectory for the main body is realized by implementing a similar method as proposed in [PMS07]. For each leg, four control points are located diagonally to the respective leg and define the targets of the trajectory. The trajectory consists of stitched Hermite splines. Before a leg starts its swing-phase, the goal position of the CoM trajectory is changed to the control point diagonal to this leg and thus the main body is moved accordingly, as shown in Fig. 4.10(a).

This shifting results in a CoM trajectory in the form of an eight-shaped curve. Due to the stitched Hermite splines, while walking a smooth transition to another CoM trajectory can be realized, if, for example, the execution of another walking pattern with a different footfall pattern is desired. The resulting trajectory of the CoM for a transition from forward to lateral walking is shown in Fig. 4.10(b). In the stability control, the Hermite spline starting point is constantly reset to the current position, thus it is possible to change the goal position at any point in time. However, changes in the walking pattern apply only after completing the step cycle.

As shown in Fig. 4.11 through the example of climbing up a slope, without a stability controller the projected CoM comes close the edge of the support polygon. By keeping a close distance between CoM and Center of Support Polygon (CoSP), the stability controller shifts the body to the front and thus maintains the robot's stability.

The projection of the robot's CoM to the ground changes during walking constantly. While walking longitudinal in different inclines, the stability controller adapts the robot's posture by shifting the body along the robot's x-axis. This means that for uphill walking the body is leaned forward, whereas for downhill walking the body is shifted backwards.

4.4.4 Robot Stability

In Charlie's robot control software (see Fig. 4.1), modulation behaviors are responsible to control the robot's stability. A simplified overview of the stability controller is

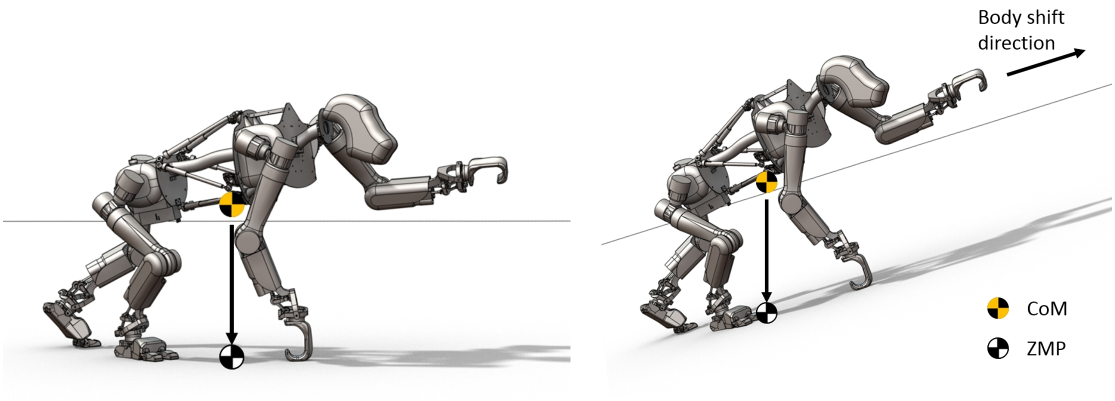

(a) Standing on level ground.

(b) Standing in an incline.

Figure 4.11: Localization of the CoM and its projection to ground while standing, along the gravity vector to obtain the ZMP [KSS+16].

depicted in Fig. 4.12(a). The walking pattern is known and consequently the current and next support polygon with their centers (CoSP) can be estimated. To increase the robot's stability while walking, the concept behind the ZMP is integrated into the stability controller. The actual velocity of the robot is measured by the IMUs.

The controller aims to adjust the CoM position by shifting the body longitudinal (in x direction) or lateral (in y direction). The estimated CoSP position, the actual ZMP and the velocity of the CoSP ($\dot{CoSP}$) serves as input for the stability controller. The difference between estimated CoSP position and ZMP is used as error for Proportional-Integral (PI) controllers $\chi\alpha$ and $\int$ to compensate disturbances.

By taking the IMU orientation data into account, Charlie is able to adapt itself autonomously while walking in inclines. Like the walking pattern generation, the stability controller is an independent process in the control software. It is always active, even if the robot stands still. All experiments in a quadrupedal pose shown in the next sections are performed using this stability control.

After performing the first bipedal walking experiments, the stability controller was enhanced to minimize the error between desired and actual CoM. Figure 4.12(b) shows the second controller as a schematic overview. The desired position and acceleration of the CoSP ($CoSP$ and $\ddot{CoSP}$) as well as the estimated gravitational acceleration $\vec{g}$ serves as input for the inverted pendulum model, to obtain the desired CoM ($\hat{CoM}$) position at a certain time. The error between desired and actual CoM is multiplied with an error gain $\chi\alpha$. In addition, $\chi\beta$ and $\chi\gamma$ describe error gains as

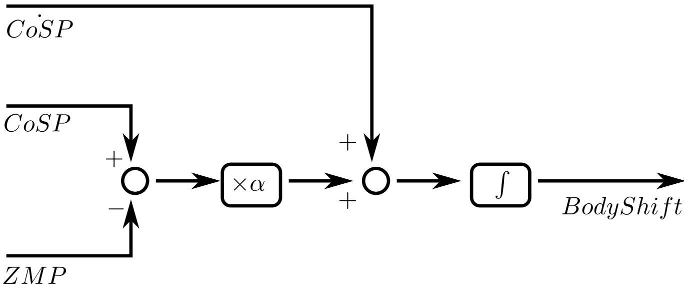

(a) Schematic overview of the quadrupedal stability controller.

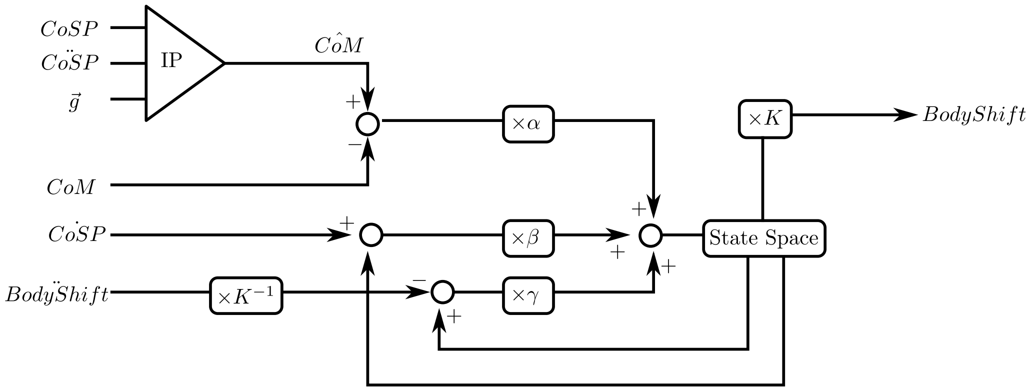

(b) Schematic overview of the bipedal stability controller. IP: Inverted Pendulum model.

Figure 4.12: Stability controller as schematic overview [KSS+16].

well.

An acceleration of the body shift ($\ddot{BodyShift}$) is determined within the rest-CS, whereas a CoM acceleration is determined in the body-CS. It has to be noted that shifting the body a certain distance does not necessarily mean that the robot's CoM is shifted over the entire length as well, because the legs introduce a certain weight as well. In $\chi K^{-}1$, the $\ddot{BodyShift}$ is multiplied with the inverted factor to enable a computation with the predicted acceleration of the CoM. The *State Space* controller contains the desired CoM position as well as the CoM's predicted speed and acceleration. It aims to minimize the error between desired and current CoM position and velocity. In χK, the CoM position is multiplied with a factor K to gain the desired body shift. The experiments in a bipedal pose are performed with this controller.

4.5 Local Controller

In a typical distributed control architecture, e.g., as shown in [EQBC96], each module in the lower control level has an individual, self-contained task to fulfill. Compared to behaviors of higher levels, they face the big disadvantage of no context awareness, thus the control issues are limited to monotonous tasks like processing sensor data or position control of an actuator, and each node transmits its data constantly to the main processing unit. When necessary, the overall control software calculates appropriate counter reactions to disturbances and sends new motion commands to the lower control levels.

In Charlie, the local control loop emulates a spring-mass-damper system by processing measured torques. Similar mechanisms have been implemented for impedance control [DWAS11]. The response time between impact and foot motion is still higher compared to a real damper system, because the torques have to be measured first and are then converted into a motion signal. Yet, this emulation has the advantage that the spring characteristics can be adapted or switched off, depending on the varying demands of the terrain or walking mode, which is not possible with a physical spring-damper system, or, if it is, only with a considerable amount of additional weight.

The local control loop is implemented in both lower legs of the rear limbs (see Fig. 4.13) and adapts the roll and pitch angles of the ankle joint to maximize the foot's ground contact, which also maximizes the robot's traction and in turn reduces slip during movement. This way, an enhanced traction as well as an increased system stability are to be expected. In addition, a reaction can be achieved with less latency and communication bandwidth, as well as less computational power is needed on the main computer.

Fig. 4.13 shows all nodes involved to realize the local control loop. The ground interaction forces are measured by a force/torque sensor (#1), installed between ankle joint and foot. To increase the context knowledge, an abstraction of the principle of the efference copy is applied. Using prior knowledge, the sensor values to be expected can either be stored in or sent to the lowest level. In the current implementation, the expected sensor data are implemented as thresholds and the position offset calculation depends on the current walking phase of the respective leg (#2). Due to the computational power installed in the foot, in future the expected sensor outcome can be processed and compared to the actual sensor information. As long as the torques do not exceed a certain threshold, the foot drives to the position

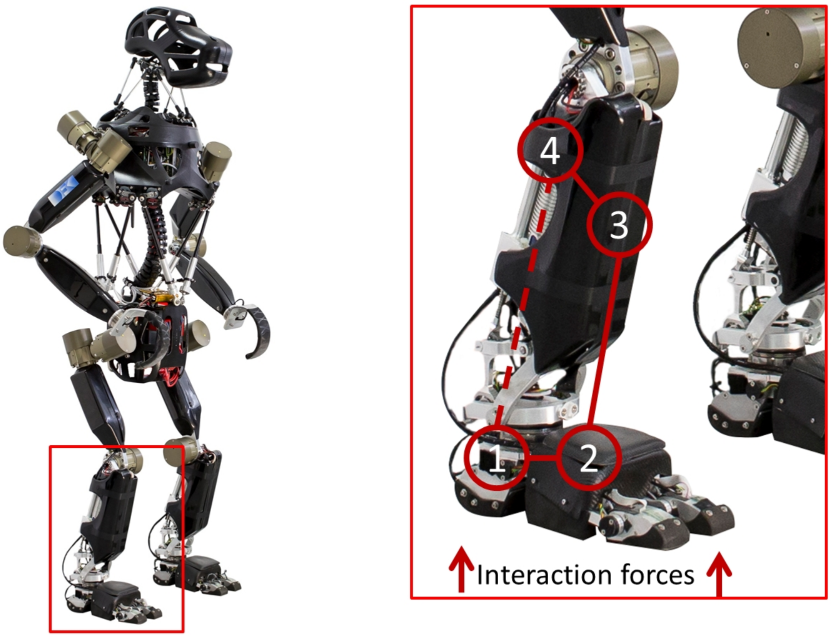

Figure 4.13: Components involved realizing the local control loop implemented in Charlie: 1) force/torque sensor, 2) local sensor PCB, 3) ankle joint control electronics and 4) ankle joint actuators. The lower leg is able to react on the sensor input preprocessed by the sensor foot without a high-level interference [KSS+16].

the MCS commands. The thresholds implemented are empirically deduced.

In addition to the usage of prior knowledge, the local control loop implementation allows periodic updates from the higher levels. If a robot model is implemented within the MCS or a higher control level, the expected sensor values could be adjusted more fine-grained. After exceeding a threshold, an angular offset for the ankle joint is calculated and send to the ankle joint node (#3), which generates a foot movement accordingly to reduce the torques (#4). This implementation can be seen as closed control loop, since a foot movement impacts the measured forces and torques directly.

In the following experiment section it is shown that the benefit of the local controller strongly depends on Charlie's context, e.g., its pose, the environment and the desired walking mode. To increase the control possibilities of a local controller, basic context information should be provided, to allow an adaption of the control to the particular context. One possible way to provide context information to the lower level is an abstraction of the principle of efference copy.

The efference copy was proposed in 1866 by von Helmholtz as an extension of his thesis on sensory-motor coordination. However, his idea did not gain acceptance until years later von Holst and Mittelstaedt concluded that their findings in experiments with flies could not have been observed without the principle of the efference copy [vHM50], [vH54].

The term efference describes a signal from the central nervous system to the motor system. Afference signals are referred to as signals from the sensory system to the central nervous system. The copy of an efference signal serves as input to a forward model. Its output delivers the predicted sensor feedback as a consequence of the given motor command. Hence, the efference copy allows a constant monitoring of the sensor data discrepancy between the actual and nominal value during motion. In humans, the effect also explains why one cannot tickle themselves. Due to the internal forward models, the brain is able to predict the effect of the action of the hand and thus the perception is shielded from self-induced effects.

The MCS provides updates of the current context of the robot for the local control loop, like selected gait, gait progress, inclines, etc. In addition, as shown earlier in the robot control chart (see Fig. 4.1), the MCS can configure the local controller in real-time. The virtual spring characteristics to be altered include I, k and D (the moment of inertia, the damping constant and the spring constant, respectively) and also the effective motion, a clockwise and counterclockwise direction of rotation. Furthermore, the maximum angular displacement $\Delta\phi$ and the threshold, when to react on the measured external torque M_{ext}, are modifiable.

The local control loop is performed with a frequency of 75 Hz. The spring stiffness is adapted with respect to the current walking cycle progress, as it is provided by the higher level control. During the respective rear legs stance-phase, the spring constant D is increased from 0.1 mNm/deg to 400 mNm/deg from a soft and adaptive to a hard, position holding behavior. By changing into another phase, the spring constant is adapted accordingly and decreased from 400 mNm/deg to 0.1 mNm/deg during the swing-up phase. For the swing-down phase it is kept constant at 0.1 mNm/deg. The moment of inertia I is $0.1\,\mathrm{kg\,m^2}$, for all phases. These values are based on empirical experiments.

Because of this gait progress dependent behavior, the ankle joint can adapt the pose of the foot to the ground after touchdown as well as carry the robot's weight during the stance-phase. The desired angular offsets have to remain within a predefined corridor, to maintain a stable walking pattern. This implementation does not exclude the sensor data transfer to the MCU. If a deflection of the incoming sensor signal is relevant for the MCS, the motion controller will react accordingly.

4.6 Validation

To validate the function of the local controller, the robot is walking on place with the crawl walking pattern. The forward motion and thus the walking speed is zero. Initially, two data sets are recorded on a laboratory floor, one with deactivated local controller (base line) and one in which the controller is active.

Setup In the first part of the experiment, an obstacle is placed underneath one rear foot during the leg's swing-up motion and the data is recorded with deactivated local controller. In the second part the controller is activated.

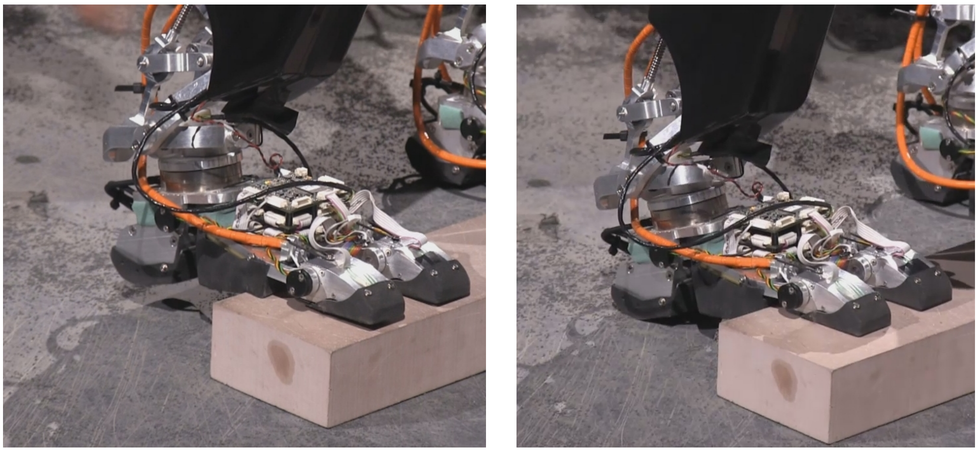

(a) The local control loop is deactivated, no adaption is taking place. The heel is hovering in the air.

(b) By using the local control loop, the heel is able to establish ground contact.

Figure 4.14: Walking on the spot with an obstacle under the rear right foot to demonstrate the effect of the local control loop.

After swing down, the front part of the foot establishes contact with the obstacle (see Fig. 4.14, the obstacle is placed under the rear right foot). Repeatable experiments with this obstacle and deactivated local control loops cannot be shown. The obstacle has a height of 5 cm, which is high enough to decrease Charlie's stability and provoke an unstable behavior. The robot tends to tipple lateral, when the foot hits the obstacle and leg becomes more and more extended in its swing-down phase. Because of this, an early touch-down behavior is activated, stopping the legs swing-down motion in z-direction (i.e. downwards), when the foot establishes a contact with the obstacle. To allow data comparison, this behavior is active for the both experiments. For this experiment, the footfall sequence is front left, rear right, front

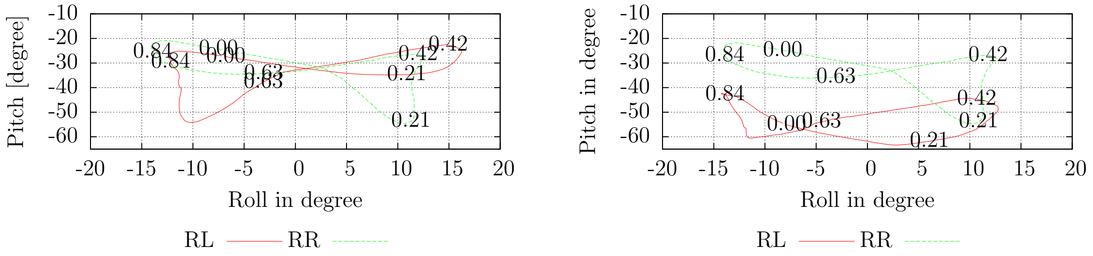

(a) Roll and pitch show a mirror symmetric behaviour for the right and left foot.

(b) An obstacle is placed under the rear left foot. The rear left ankle has a constantly decreased pitch, the movement of the right ankle is not influenced.

Figure 4.15: Measured roll and pitch angle in the ankle joint of both rear legs while Charlie is walking on the spot. The numbers in the plot annotate the robot's walking cycle progress. Due to the order of leg movements, the rear left leg and the rear front leg have a phase-offset of 50 %, resulting in a mirror symmetry.

right, and rear left. To demonstrate the effect of the local controller on a single obstacle, thresholds to limit the maximum deflection between the actual and desired position are extended from 20° to 30° in this experiment.

Observations The foot's non-adaptive behavior when stepping on an obstacle is shown in Fig. 4.14(a). The foot stands rigid on the obstacle and the heel is hovering in the air.

If the local control loop is activated, a deviation of the desired pitch angle can be seen, resulting in maximizing the contact between foot sole and ground (see Fig. 4.14(b)). By decreasing the pitch angle, the ankle adapts itself actively and establishes additional ground contact with the heel. The forefoot is not affected by this motion and remains in contact with the ground.

The curves in Fig. 4.15(a) show the ankle joint angles while walking on place with active local controller. In Fig. 4.15(b) the roll and pitch angles are shown while stepping with the rear left foot on the above mentioned obstacle. The numbers in the plot indicate the robot's walking cycle progress, ranging from zero to one, whereas 0.0 (or 0 %) indicate the start of the front left legs swing-phase and 1.0 (or 100 %) is equal to end of the rear left legs stance-phase and thus of the walking cycle. For walking without stepping on an obstacle (depicted in Fig. 4.15(a)), the desired trajectories of the MCS for roll and pitch are fulfilled and the feet are kept parallel to the ground.

The differences of the ankle joints pitch angle can be seen as soon as the rear left foot establishes contact to the obstacle. Based on the perceived torque applied to the individual legs, the local control loop sets an offset to the desired pitch angles. The basic shape of the trajectory is recognizable, since the offset, the local controller is adding to the motion command, is limited. A maximum deflection of about 30° for the left foot (e.g. at 21 %) can be seen, compared to Fig. 4.15(a). As described in Sec. 4.5, to the end of the stance-phase, the spring within the local control loop is getting stiffer and thus the deflection between actual position and desired position is getting smaller. For this crawl gait with the footfall sequence front left, rear right, front right, and rear left, the rear left legs stance-phase ends at 75 % of the overall walking cycle. The deviation is in this case around 5°. It is observed that the deflection is not zero, which is due to the obstacle size. The obstacle is large enough to prevent the foot driving to the desired position of the MCS. Due to the shape of the obstacle, the roll trajectory remains unchanged and is equal to the one shown in the setup without obstacle.

Conclusion With a deactivated local control loop, the foot does not adapt to the ground. When one part of the foot steps on a rigid obstacle, the remaining foot hovers in the air. A positive aspect of these first experiments is that the mechanical design of the rear foot is able to withstand point loads as well as the motor and gear dimensioning within the ankle joint are sufficient to withstand the applied load.

When the local control loop is active, the resulting motion maximizes the contact between the foot sole and the ground. This behavior increases the traction between foot and ground. The local controller has no effect on the forefoot, which remains in contact with the ground at all times.

4.7 Conclusion

In this chapter the control approach including the walking pattern implemented on Charlie is described. In addition to the main processor, the robot is equipped with additional computational power in the actuators and structures like the feet or spine, to deal with the large amount of data necessary for a precise perception of the environment. This allows a reduced cabling effort, which results in a system less prone to error and a reduced weight, less connectors and calculation load on the main CPU, as well as a parallel data processing. For data transmission from the different, heterogeneous nodes in Charlie to the main controller as well as for inter-node communication, one protocol is used. The protocol allows dynamic packet sizes depending on the payload to transmit and thus reduces the traffic compared to fixed packet sizes.

Charlie's software architecture bases on the approach shown in [SK07] and follows a biologically inspired, hierarchical approach. The walking pattern generation bases on the principle of CPGs. In addition to the walking pattern, the stability controller as well as Charlie's coordinate systems are described in detail. The architecture is expanded by a local control loop in the lower leg structure. This loop is only possible due to the high sensor density and the local data preprocessing capabilities. The local data preprocessing has a further advantage: since subsystems like foot or spine communicate their knowledge and not raw data, the overall data traffic can be reduced.

The function of the local control is experimentally evaluated in a first experiment. It can be stated that the local control loop allows a form closure between foot and ground, which increases the robot's support polygon as well as the traction. In addition, the mechanical design of the lower leg and foot including the torques of the selected actuators are able to withstand the applied force.

Chapter 5

Quadrupedal Walking Experiments

This chapter deals with the experimental evaluation of the robot Charlie and its quadrupedal motion mode. In the beginning, the different experimental setups are described. The robot's evaluation comprises the suitability of (a) the robot's design and its hardware to deal with different environments and (b), the impact of the local control loop on the system state like power consumption stability as well as occurring forces and torques acting on feet and spine. After walking in flat terrain, the experiments are expanded to various inclines. The chapter closes with a conclusion of the quadrupedal walking experiments.

This chapter is supported by the following peer-reviewed journal publications:

- D. Kuehn, F. Bernhard, A. Burchardt, M. Schilling, T. Stark, M. Zenzes, and F. Kirchner. *Distributed Computation in a Quadrupedal Robotic System.* In International Journal of Advanced Robotic Systems, 2014

- D. Kuehn, M. Schilling, T. Stark, M. Zenzes, and F. Kirchner. *System Design and Field Testing of the Hominid Robot Charlie* In Journal of Field Robotics, 2016

5.1 Experimental Environment

To allow a comprehensive, scientific evaluation of the developed robot Charlie, the system is tested in different environments. Figure 5.1 shows the DFKI RIC outdoor test track for mobile robots from above. Charlie is tested on solid grounds, indoor or on a garden path, as well as on loose soil like a gravel field.

Figure 5.1: DFKI RIC robot outdoor test track.

The sodded outdoor slope has different inclinations at very frequent intervals, thus consistent and reliable data for several steps in a certain incline cannot be recorded. For that reason a wooden indoor ramp with a dimension of 3 m x 6 m is used. The slope is infinitely variable between 0° to 45°. Besides the mentioned grounds, Charlie's walking behavior was tested indoor in a laboratory on linoleum floor, also referred to as *terrain lab*. In summary, the experiments are performed on:

- *Terrain lab*: laboratory, linoleum floor
- *Terrain garden*: garden path, consisting of sand and pebbles
- *Terrain grass*: grass
- *Terrain gravel*: gravel, with varying dimensions from 1.5 cm x 1.5 cm x 2.5 cm to 3 cm x 3.5 cm x 4.5 cm
- *Terrain ramp*: wooden slope with inclinations ranging from $-20°$ to $20°$, varied in 5° steps.

5.2 Experimental Setup

The mechatronic design of the presented hominid robot Charlie allows its locomotion in various terrains, the demonstration of different motion modes, and the introduction of local control loops. The experiments presented in the following investigate the functionality of the robot's overall design, the installed structures as well as the software approach. Besides the expected benefits, possible weak points of the presented approaches are discussed and solutions are presented, to remedy potential deficiencies.

Although Charlie is carrying its own energy supply (rechargeable batteries), for all experiments it is connected to an external power supply. This ensures a constant supply voltage of 48 V. It has to be mentioned that, even though they are not used, the rechargeable batteries are integrated in the robot at all times, to retain the systems weight. To minimize potential packet loss of the robot's telemetry data, which would result in incomplete logging data, the available WiFi capabilities on Charlie are not used. Instead, the robot's telemetry data is transferred via an

Table 5.1: Overview Selected Quadrupedal Experiments (1/2).

Experiment Series	Experiments	Motive and Expected Results
Static system evaluation (electrical properties)	Power consumption	Initial data set of power consumption with and without loaded joints.
System evaluation (electrical properties) while walking on a planar and rigid surface (*terrain lab*)	Walking with different setups: A) No spine motion, no local control B) Active spine motion, no local control C) No spine motion, active local control D) Spine motion and local control active	Initial data recording to be able to compare the robot's system state in different setups while walking in a controlled environment. It is expected that current spikes are reduced, when the local controller is active, due to the compliant behavior of the foot. Due to the terrain properties, the robot's stability should be equal in all four setups.
	Repetition of A) to D) with a different walking speed	System analyses with varying walking speeds to determine the effects of the walking speed to the system state and be able to generate statements which are equally applicable and not speed dependent. It is expected that the walking speed has an influence on the robot's current consumption, however, the existing differences between the setups will remain.

Ethernet cable. During all experiments special attention is paid to ensure that the cabling (power and data uplink) is not affecting the robot's behavior.

To analyze and evaluate the effects of an active local control loop on the robot's behavior, Charlie is tested with and without active local control loop. The same is true for measuring the impact of the utilization of the artificial spine. Combined with the local control loop, the four resulting combinations or "setups" are:

- *Setup* $\overline{L}$ $\overline{S}$: Walking with an inactive local control loop ($\overline{L}$) and an inactive spine motion ($\overline{S}$) as base line experiment
- *Setup* $\overline{L}$ S: Walking with an inactive local control loop ($\overline{L}$) and with an active spine motion (S)

Table 5.2: Overview Selected Quadrupedal Experiments (2/2).

Experiment Series	Experiments	Motive and Expected Results
Walking on varying surfaces	Walking with different setups	Walking on an outdoor footpath, lawn, and in a gravel field with different setups will allow to make a ground independent statement regarding system state while walking with and without the local controller. It is expected that the local control will increase the system state due to its reactive behavior.
	Walking with varying speed	Like for the experiments on *terrain lab*, these experiments are performed to allow a more general statement regarding the robot's system state in different setups which are not dependent on the robot's walking speed.
Walking in varying inclinations ranging from $-20°$ to $20°$ using different setups	Longitudinal walking, slope inclination adapted in $5°$ steps	This experiments will show the robot's system state in longitudinal inclinations. In addition, the influence of the artificial spine on the leg-joint can be analyzed. It is expected that walking with active local control requires again less energy than walking without local control and the robot's CoM is more stable.

- *Setup* $L\ \overline{S}$: Walking with an active local control loop (L) and with an inactive spine motion ($\overline{S}$)
- *Setup* $L\ S$: Walking with an active local control loop (L) and with an active spine motion (S)

To analyze the effects of the walking speed, the following three different speeds are defined:

- *Speed setting medium*: Walking speed 60 $\frac{\mathrm{mm}}{\mathrm{s}}$
- *Speed setting fast*: Walking speed 90 $\frac{\mathrm{mm}}{\mathrm{s}}$
- *Speed setting ramp*: Walking speed 30 $\frac{\mathrm{mm}}{\mathrm{s}}$

The performed walking experiments with Charlie are a combination of the different grounds, setups and walking speeds. Because of the similarity in the results between *terrain lab*, *terrain garden* and *terrain grass*, the evaluation in this thesis omits *terrain garden* and *terrain grass* and focus on *terrain lab*: laboratory floor and *terrain gravel*: the gravel field. In the following, data is shown where each individual setup is tested on these two terrains, e.g., *terrain lab* with *setup* $\overline{L}\ \overline{S}$, *setup* $\overline{L}\ S$, *setup* $L\ \overline{S}$, and *setup* $L\ S$, resulting in eight different data sets.

These eight combinations are conducted with two different speeds, *speed setting medium* and *speed setting fast*. Each experiment is repeated at least three times. A run is considered as complete if the robot has performed at least 10 full walking cycles. One walking cycle is complete, if all four legs (or two legs, in the bipedal case later on) are moved.

Terrain ramp is characterized by a 6 m long, infinitely variable slope. Experiments are performed in inclinations ranging from −20° to 20°, varied in 5° steps. Starting at an inclination of 15° a slight slipping while walking with *speed setting medium* was observed. The steeper the slope, the more slipping can be seen, if Charlie's walking parameter set is not adapted. To keep the experiments as comparable as possible, the third walking speed (*speed setting ramp*) has been defined, which is the slowest of the presented walking speeds and allows the robot to walk the 20° slope up and down without slipping.

All experiments are performed with the presented crawl gait, as shown in Fig. 4.8 on page 87. As mentioned earlier, the walking pattern implementation provides that the feet are lifted 100 mm during their swing-phase. The cycle time is set to 5 s.

5.3 Data Evaluation

For plotting, the data of each step cycle in one run is synchronized on the basis of the step cycle progress of the walking behavior and unified into one single curve by calculating the mean value. Each curve includes also the standard deviation of the entire recording, indicated with the same but lighter color drawn in the plot.

Using the cycle progress of the walking behavior allows to synchronize the leg's telemetry data of the individual steps in two different ways. The default synchronization uses the global walking cycle progress (wcp) of the walking pattern, thus the curves show a chronological sequence of the legs and their different phases like: RR swing-phase, RR stance-phase, FR swing-phase, FR stance-phase, and so on.

For the second synchronization approach, the touchdown event of each leg is used to phase-align the telemetry of the four legs. This means that the data does not show a chronological sequence of the four legs in motion. Instead, the curves in the plot show the touchdown event in the beginning, followed by the stance-phase, and ends with the swing-phase for each leg. This allows a better presentation of similar events, which occur in each leg, e.g., the curves of the forces acting on the individual legs at touchdown are thus put on top of each other.

The respective data is always shown within the rest coordinate system, where Charlie's x-axis points forward, the y-axis to the left, and the z-axis upwards (see section 4.4.1 on page 82). If the actual current consumption or acting forces are shown, on top of each figure the respective legs swing-phase is indicated, whereas $\|$ marks the end of the swing-phase of one leg and the beginning of the following.

5.4 Power Consumption

The actuators' current consumption measured by the motor electronics excludes the consumption of the PCB itself and refers exclusively to the current the actuators require to drive or to hold a position. Therefore, table 5.3 lists the current consumption of the PCBs separately. In later experiments the motor current is shown, which means that the overall current consumption of Charlie's electronics must be added. For the data shown in the table the robot is fixed load free and the current consumption is measured by a multimeter as well as an external power supply unit. The voltage is set to 48 V.

The term "initial configuration" means that the robot's main CPU, the relay board, its IMUs, power converter boards, as well as the ethernet switch and WiFi module are electrically supplied and the motion control software is running. Due to the same electro-mechanical design between left and right front legs as well as left and right rear legs, the data for the robot's right hand side is omitted.

For the load free case one can observe that there is no measurable difference between activated and deactivated actuators. The differences in the current consumption between front and rear legs are due to the additional sensors and PCBs installed in the rear legs. The complete operational robot consumes 48 W in a quadrupedal pose if it is load free. While standing on the ground, the consumption is increased by 3.4 W.

Table 5.3: Detailed listing of the subsystems current consumption.

No.	Configuration	Overall consumption	
		in mA	in W
(1)	Initial configuration	230	11
(2)	like (1) with active spine electronics including voltage transformer board, MDAQ2, 6*1DoF force/torque sensor, absolute encoder, actuators are not active	350	16.8
(3)	like (1) with FL leg electronics switched on, actuators not active	330	15.9
(4)	like (1) with RL leg electronics switched on, actuators not active	400	19.2
(5)	like (1) with all leg and spine electronics switched on, no actuator active	900	43.2
(6)	like (5) with all actuators active	910	43.7
(7)	like (6) walking pose, load free	1000	48
(8)	like (7) standing on ground, actuators are supporting the robot's weight	1070	51.4

5.5 Description and Evaluation of Experiments on Flat Ground

In this section, the effect of the local controller is shown and its influence on the system's stability is evaluated, as well as the impact of different terrains on the system state. In addition, subsequent analysis shows the different effects of the four setups to the robot's stability and power consumption. The section closes with a conclusion of the experiments on flat ground.

5.5.1 Analyzes of the Local Control Loop

The objective of this experiment is to record a data set while walking on *terrain lab* with *speed setting medium* and *setup* $\overline{L}\ \overline{S}$. To analyze the effect of the local control loop to the current consumption of the robot's joints and its stability, in a second experiment the robot is walking as well with *setup* $L\ \overline{S}$.

Presumption It is expected that the robot's stability is unaffected by the activation of the local control, since the flat and obstacle-free terrain poses no challenges. For the current consumption, a reduction of the peak values is expected, if the local controller is active. This is due to the assumed reduction of tensions between the legs.

Observations In Fig. 5.2, the roll and pitch angels for the rear left foot on laboratory floor for *setup* $\overline{L}\ \overline{S}$ with *speed setting medium* are shown. The figure shows the recorded data for the same experiment but with *setup* $L\ \overline{S}$ as well. A more detailed figure including the error between desired and actual roll and pitch angle of the ankle joint is shown in the appendix (see Fig. 1 on page 202). While walking with *setup* $\overline{L}\ \overline{S}$, the desired roll and pitch angle hardly differ from the measured angle. At the beginning of the swing-phase (between $wcp = 50\,\%$ and $wcp = 75\,\%$ of the walking cycle progress), the ankle joint is driven in a way that the toes move closer to the robot's tibia (negative pitch value) to increase the distance between foot and ground. In preparation of the foot's touchdown, the ankle joint is driven in the opposite direction.

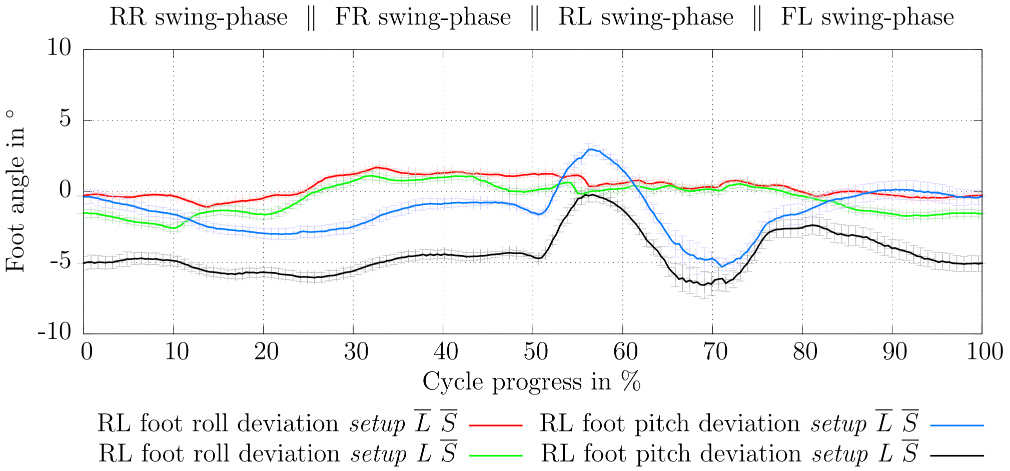

Figure 5.2: Comparison of the measured angles in the ankle joint for *setup* $\overline{L}\ \overline{S}$ (without local control) and *setup* $L\ \overline{S}$ (with local control), while walking on laboratory floor with *speed setting medium*.

However, if the local control loop is active, the expected deviation between measured and requested roll and pitch is recognizable over the entire step cycle. Therefore, the roll and pitch position deviation between $wcp = 0\,\%$ and $wcp = 50\,\%$ as well as between $wcp = 80\,\%$ and $wcp = 100\,\%$ is more distinct compared to *setup* $\overline{L}\ \overline{S}$. Since the local control loop applies only a limited offset of ± 20° while walking to the given position, the requested trajectory of the MCS is basically met. The rear left foot is in the swing-phase between $wcp = 50\,\%$ and $wcp = 75\,\%$ of the walking cycle progress. The process of the local control loop, from a soft and adaptive behavior to a more rigid one, can be seen in the data between *wcp* = 95 % to *wcp* = 50 %. The pitch deviation is getting smaller the closer the leg comes to the end of the stance-phase.

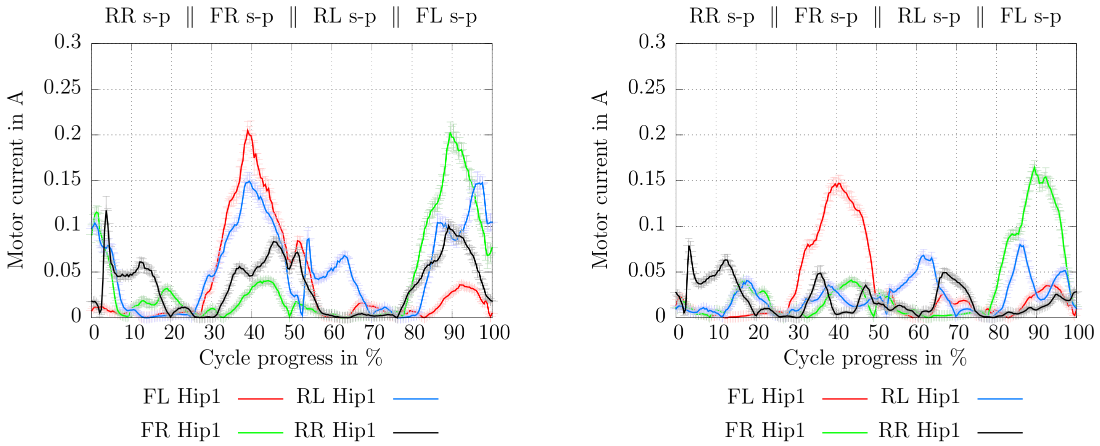

(a) Current consumption of hip joint 1 while walking with *setup* $\overline{L}$ $\overline{S}$.

(b) Current consumption of hip joint 1 while walking with *setup* L $\overline{S}$.

Figure 5.3: Current consumption of hip joint 1 while walking on *terrain lab* with *speed setting medium* and two different setups.

Fig 5.3 shows the current consumption of the first hip joint for all four legs. The current consumption of hip joint 2 and hip joint 3 is similar in both setups and therefore not shown. In Fig. 5.4 the current consumption for the robot's knee joints are displayed. On top of each figure, the respective leg's swing-phase is shown.

Current peaks of the front legs can be seen in both figures at *wcp* = 40 % and *wcp* = 90 %, which is the time where the respective other front leg is in its swing-phase. Yet, the peaks in the setup with active local control loop are reduced by *wcp* = 25 % for the first joint. In general, the power consumption of the hip joint 1 of the rear legs is reduced as well. It can be seen that during the swing-phase of the respective legs the power consumption is always at about 50 mA, yet the consumption of the rear joints during the swing motion is higher than for the front legs. This can be explained by the higher weight of the rear legs.

Compared to the hip joints, the knee joints power consumption is higher during walking. In contrast to the first hip joint, where the front legs have a higher current peak than the rear legs, the knee joints show a more balanced picture. In Fig. 5.4(b), all knee joints have their peak during the swing-phase. The magnitude of the peaks, however, does not differ much between *setup* $\overline{L}$ $\overline{S}$ and *setup* L $\overline{S}$. For the rear legs, it can be seen that between *wcp* = 5 % to *wcp* = 10 % the left and between *wcp* = 55 %

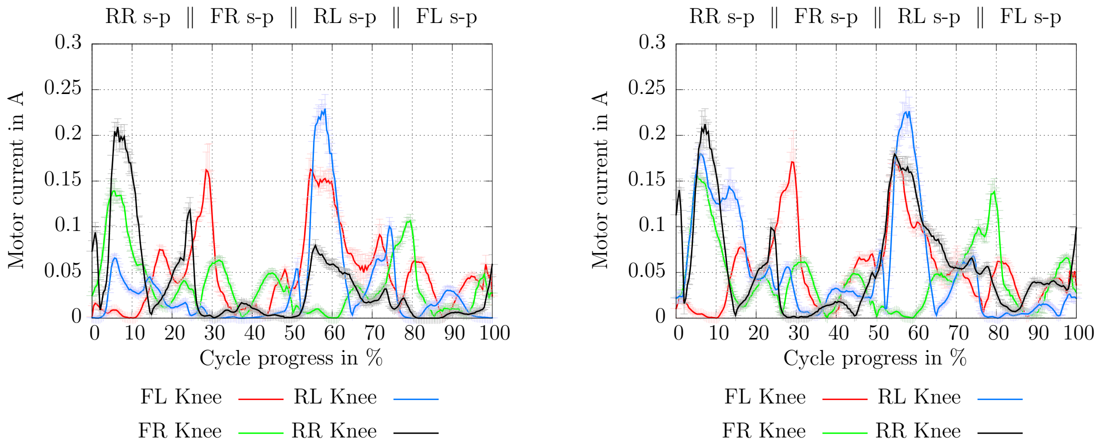

(a) Current consumption of the knee joint while walking with inactive local control (*setup* $\overline{L}\ \overline{S}$).

(b) Current consumption of the knee joint while walking with active local control (*setup* $L\ \overline{S}$).

Figure 5.4: Comparison of the current consumption for the four knee joints while walking on *terrain lab* with *speed setting medium* and two different setups.

to $wcp = 60\,\%$ of the walking cycle the right knees have a higher power consumption of about 50 mA in *setup* $L\ \overline{S}$ compared to *setup* $\overline{L}\ \overline{S}$.

Conclusion These experiments are performed to analyze the influence of the local control loop to the walking behavior of the robot. For the current consumption, a reduction of current peaks in the first hip joint is observed in the setup with activated local control loop (*setup* $L\ \overline{S}$). This is most likely due the minimized torques acting on the legs, whereby a possible tension between the legs is reduced. However, due to the not demanding environment, an improvement or deterioration of the robot's stability could not be observed (see appendix Fig. 2 on page 203).

5.5.2 Different Terrain Substrates

The following experiments are performed to analyze Charlie's system state while walking on different terrain substrates. To analyze the effect of the different setups, each setup is tested on *terrain lab* and *terrain gravel*. To determine, if the walking speed influences the results of the setups, different speeds are tested as well.

5.5.2.1 Experimental Setup

In this experiment, data is shown while walking with *speed setting medium* and *speed setting fast* on *terrain lab* and *terrain gravel* (see Fig. 5.5). The four combinations are performed with each setup.

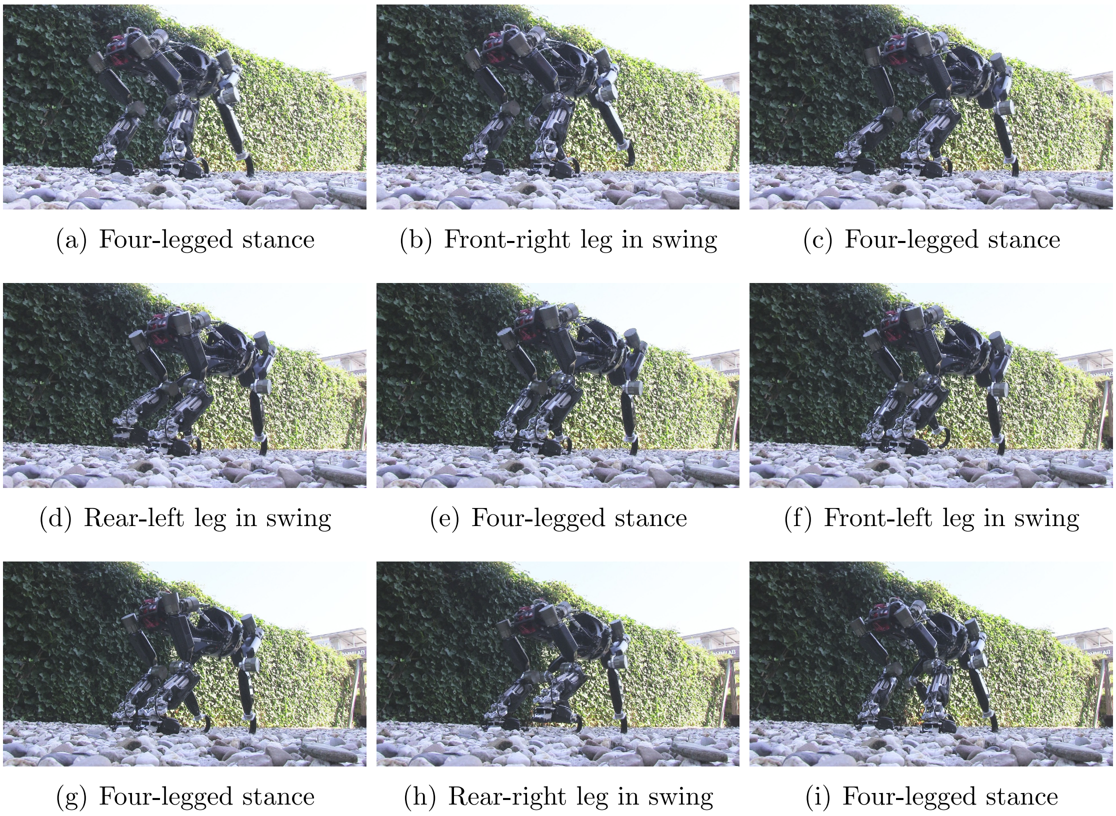
(a) Four-legged stance (b) Front-right leg in swing (c) Four-legged stance

(d) Rear-left leg in swing (e) Four-legged stance (f) Front-left leg in swing

(g) Four-legged stance (h) Rear-right leg in swing (i) Four-legged stance

Figure 5.5: Walking sequence of Charlie crossing a gravel field [KSS+16].

This section is divided into three parts. First, the effects of each setup with respect to the individual joints current consumption are investigated. The data shows the power consumption of each actuator, measured by its control electronics. The power consumption of 48 W needed by Charlie's installed electronics (see Table 3.2) is not included. The data shows only the additionally required current to generate the robot's forward motion. Second, the robot's stability is investigated. Third, the occurring forces and torques at the end-effectors and in the spine are analyzed.

5.5.2.2 Power Consumption

Presumption It is expected that the power consumption increases the more unstructured the terrain is. This can be explained by the additional movements necessary to stabilize the robot.

The different setups will also have an influence on the overall power consumption. While walking on rigid terrain, like *terrain lab*, it is expected that setups with deactivated local control loop cause a higher current consumption compared to setups with activated local control loop, since the local controllers try to minimize occurring torques and a possible tension between the robots legs will be reduced.

Walking on a more unstructured and, in particular, deformable surface like a *terrain gravel*, the active local control loop will increase the current consumption of the rear legs due to the additional foot movement. In contrast, in the setups with deactivated local control loop increased longitudinal and lateral body shifts are to be expected, which also have an influence on the overall power consumption. One can argue for an increased current consumption for both cases on *terrain gravel*. However, it is to be expected that in setups with activated local control loop less current is needed compared to setups with deactivated local controller, since an increased traction of the feet is gained with active local controller, which results in a more stable behavior and requires less adjustments of the body position. Therefore, lower body accelerations are measured by the IMU, which means that the projected CoM is close to the desired CoSP and the respective countermovements are likely to be minor.

Compared to *speed setting medium*, *speed setting fast* requires that the robot walks with longer steps in order to travel a greater distance per second. Walking with *speed setting medium*, smaller steps are made and thus each leg has to perform more swing-phases and stance-phases to cover the same distance compared to a walking with *speed setting fast*. During the swing-phase, the leg's mass is accelerated in order to move from the PEP to the AEP. PEP describes the position of leg, where, due to the walking cycle, the foot is close to its lift off. The AEP is the starting position for the legs stance-phase. While walking with smaller steps, more swing-phases are needed but walking with larger steps require a higher acceleration (for forward walking in hip joint 1 and the knee joint) and thus should result in a higher current consumption. In addition, a higher walking speed results in a faster CoM shifting for the creep gait and thus again higher accelerations in the hip joint 2 and hip joint 3.

Despite the expected higher overall power consumption, *speed setting fast* is expected to have a higher energy efficiency, due to the greater distance covered. Smaller accelerations are affecting the robot's CoM while walking with *speed setting medium*, thus a higher stability of the system is expected.

Evaluation To allow a clear overview of the results, the data is divided into four figures. In Fig. 5.6 and Fig. 5.7, the data of the experiments with *speed setting medium* are shown and in Fig. 5.8 and Fig. 5.9 the data for walking with *speed setting fast* are presented.

Figure 5.6 shows the robot's current consumption while walking on *terrain lab* with *speed setting medium* and all four setups. In the figure, the right rear leg's (indicated in black in the plot) swing-phase starts at $wcp = 0\,\%$ of the walking cycle progress. The walking cycle for this leg starts with the lift up motion, therefore the leg will be load free. A drop in the current consumption at about $wcp = 2\,\%$ can be seen, followed by an increased power consumption due to leg's acceleration in the swing-phase. During the stance-phase, which starts at $wcp = 25\,\%$, a slower movement speed of the joints is needed and thus the power consumption is reduced again. At about $wcp = 75\,\%$ again an increased current consumption in the RR leg can be seen. This is because the FL leg starts its swing-phase and the CoM is shifted to the RR leg; this shift is performed to increase the stability (the distance of the CoM is increased to the edges of the support polygon) and to reduce the load on the FL leg.

Like for the RR leg, in the data for the FR leg (indicated in green in the plot), before starting the swing-phase at $wcp = 25\,\%$ the power consumption is reduced, which indicates that the leg is load free. Also at about $wcp = 75\,\%$ the CoM is already shifted to the robot's right side and the FL leg is load free. Thus an increased current consumption in the FR leg can be noticed. This pattern can be observed also for the RL leg (indicated in blue) and the FL leg (indicated in red).

In general, a difference in power consumption of the front and rear legs has two possible reasons. First, the rear legs have a significantly higher weight compared to the front legs. Second, the rear legs are equipped with more active DoFs. In setups without active spine support the data still show a low power consumption of the six spine actuators. This is because the spine is not a rigid coupling between front and rear body. Since external forces are acting on the spine, the actuators have to produce a certain torque to maintain the desired position.

The unevenness of *terrain gravel* is not compensated, e.g., by extending a leg while detecting an early touchdown. Because of this, if individual legs step on a small obstacle, they will be loaded with an increased share of the robot's weight during their stance-phase, which results in a less homogeneous power consumption between the individual steps. In the data this is reflected in greater deviations, indicated by lightly drawn errorbars in the respective colour.

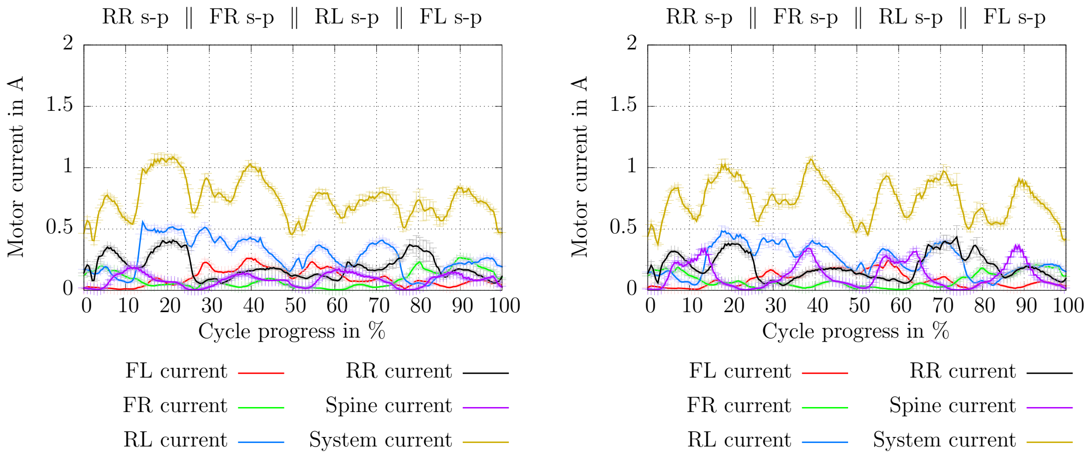

(a) Local control loop and spine both inactive (*setup* $\overline{L}\ \overline{S}$).

(b) Local control loop inactive and spine active (*setup* $\overline{L}\ S$).

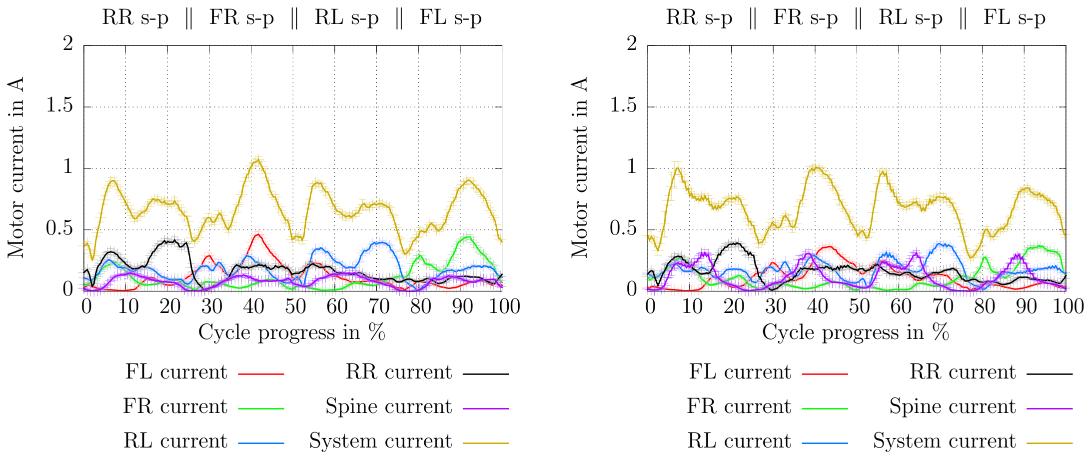

(c) Local control loop active and spine inactive (*setup* $L\ \overline{S}$).

(d) Local control loop and spine both active (*setup* $L\ S$).

Figure 5.6: Measured current of the legs and spine while walking on *terrain lab* with *speed setting medium* and varying setups; s-p stands for swing-phase.

In *setup* $\overline{L}\ \overline{S}$ (shown in Fig. 5.6(a)) the higher current consumption of the rear legs compared to the front legs can be seen. This is true nearly for the complete step cycle. The data for *setup* $\overline{L}\ S$ is presented in Fig. 5.6(b). As it can be seen, the current consumption of the spine (indicated in brown) increases in the respective peaks. Like in *setup* $\overline{L}\ \overline{S}$, the overall consumption stays above the 0.5 A mark.

Comparing *setup* $\overline{L}\ \overline{S}$ with *setup* $L\ \overline{S}$ (depicted in Fig. 5.6(c)), in *setup* $L\ \overline{S}$ a reduction of the rear leg's current consumption can be observed, as well as a more homogenous distribution of the current consumption between the legs. Furthermore,

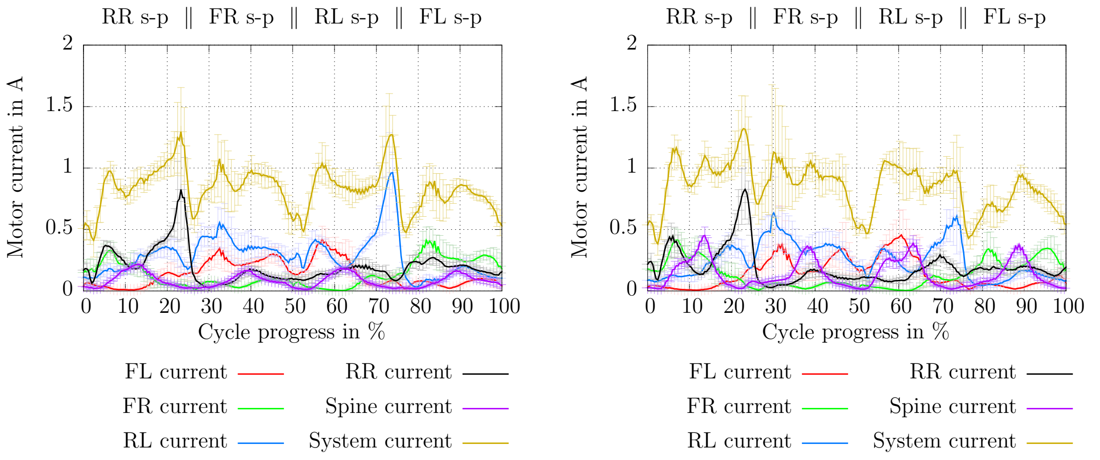

(a) Local control loop and spine both inactive (*setup* $\overline{L}$ $\overline{S}$).

(b) Local control loop inactive and spine active (*setup* $\overline{L}$ S).

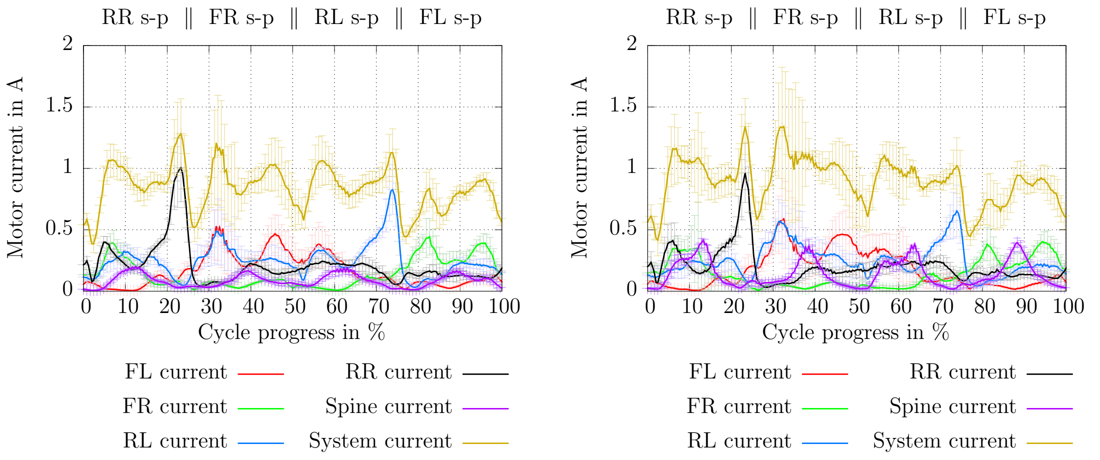

(c) Local control loop active and spine inactive (*setup* L $\overline{S}$).

(d) Local control loop and spine both active (*setup* L S).

Figure 5.7: Measured current of the legs and spine while walking on *terrain gravel* with *speed setting medium* and varying setups. s-p stands for swing-phase.

the overall power consumption is reduced if the local control loop is active and lies temporarily under the 0.5 A mark. The curves for *setup* L S are shown in Fig. 5.6(d). In addition, in this setup a reduction of the current consumption is noticed compared to *setup* $\overline{L}$ S. The homogeneous distribution can also be seen in this setup.

Fig. 5.7 shows the leg wise current consumption while walking on *terrain gravel* with *speed setting medium* for varying setups. Compared to walking on level ground (as shown in Fig. 5.6), the overall power consumption is significantly higher in all four corresponding setups, due to the uneven and deformable surface of the gravel field. Nearly no deviation of the current or acting forces between several steps is recognized while walking on *terrain lab*, whereas on *terrain gravel* large discrepancies between each single step exist. This is indicated by a higher standard deviation. Furthermore, it is observed that a higher load occurs on the rear legs before their respective swing-phase, which is due to the MPCF. This can be seen in all four setups, although to different extent. The slightly increased power consumption of the spine indicates an increase of the occurring load, due to a reduction of the systems stability.

Comparing the setups with active local control loop with the one(s), where the local control loop is deactivated, it can be seen that the overall current consumption as well as the existing peaks do not differ much. Although a lower power consumption while walking on a rigid surface in setups with active local control loop compared to *setup* $\overline{L}\ \overline{S}$ *and* $\overline{L}\ S$ could be determined, this effect cannot be seen on compliant and deformable ground. Nevertheless, it can be noted that despite the additional movement of the rear feet, an increase in the overall power consumption cannot be discovered.

Table 5.4: Power consumption while walking on *terrain lab* and *terrain gravel* with *speed setting medium* and varying setups. The value is the mean value of one complete step cycle. The value specified in brackets is the standard deviation.

Setup/ Terrain	*Setup* $\overline{L}\ \overline{S}$ in W	*Setup* $\overline{L}\ S$ in W	*Setup* $L\ \overline{S}$ in W	*Setup* $L\ S$ in W
Terrain lab	35.5 (± 1.5)	35.5 (± 1.5)	31.7 (± 1.0)	32.1 (± 1.5)
Terrain gravel	40.0 (± 6.2)	41.2 (± 7.5)	40.0 (± 6.2)	44.0 (± 8.5)

Energy efficiency	in $[\frac{\mathrm{W}}{\mathrm{m}}]$	in $[\frac{\mathrm{W}}{\mathrm{m}}]$	in $[\frac{\mathrm{W}}{\mathrm{m}}]$	in $[\frac{\mathrm{W}}{\mathrm{m}}]$
Terrain lab	118.3	118.3	105.7	107.3
Terrain gravel	133.3	137.3	133.3	146.7

Table 5.4 shows the average power consumption while walking on *terrain lab* and *terrain gravel* with *speed setting medium* in varying setups. The value specified in braces is the standard deviation. It can be seen for both walking speeds that if the local control loop is deactivated, the overall current consumption is slightly increased. This can be explained by a reduced tension between the legs, if the local control loop is active. However, the standard deviation is slightly increased in setups with active local control loop, because the ankle joints produce a different movement pattern in each step. In the lower section, the energy efficiency is specified as required Watt per meter. The lower the value the more energy efficient is the

walking. The distance covered for this speed setting is 30 cm per step cycle.

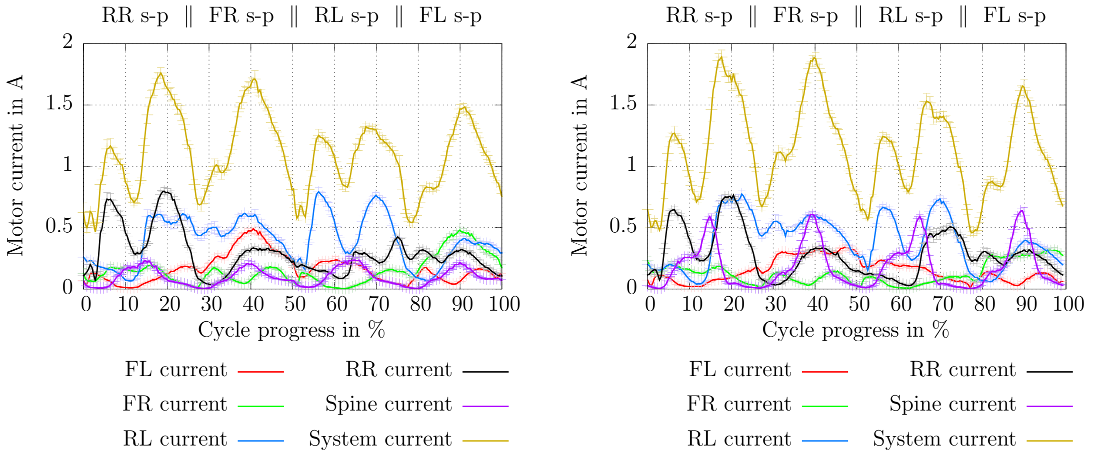

(a) Local control loop and spine both inactive (*setup* $\overline{L}$ $\overline{S}$).

(b) Local control loop inactive and spine active (*setup* $\overline{L}$ S).

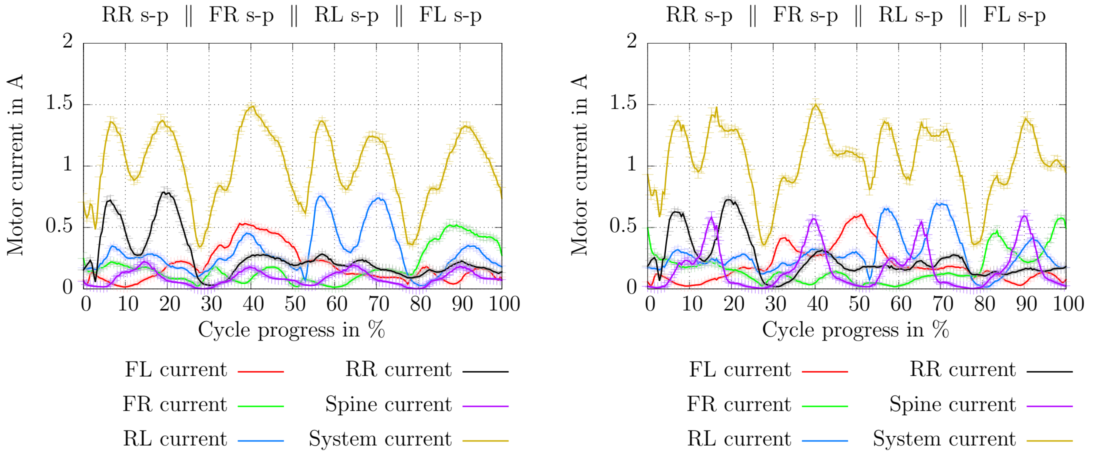

(c) Local control loop active and spine inactive (*setup* L $\overline{S}$).

(d) Local control loop and spine both active (*setup* L S).

Figure 5.8: Measured current of the legs and spine while walking on *terrain lab* with *speed setting fast* and varying setups. s-p stands for swing-phase.

Speed Setting 2 Fig. 5.8 shows the leg wise current consumption while walking on *terrain lab* with *speed setting fast* for varying setups. This experiment series shows similar results as the experiments while walking on level ground with *speed setting medium* (as shown in Fig. 5.6). By comparing *setup* $\overline{L}$ $\overline{S}$ *and* $\overline{L}$ S with *setup* L $\overline{S}$ *and* L S (the latter two being displayed in Fig. 5.8(c) and Fig. 5.8(d), respectively), a reduction of the overall power consumption can be seen in both setups with activated local control loop.

The local maxima do not exceed the 1.5 A mark, if the local control loop is active. As in the experiment with *speed setting medium* on *terrain lab*, a more homogeneous distribution of the power usage between the front and rear legs can be noticed.

In this speed setting, the acceleration of all legs is increased during the swing-phase. Due to this, the acceleration and deceleration phases of the rear legs can be seen more clearly in the data, e.g., for the RR leg between $wcp = 2\,\%$ to $wcp = 5\,\%$ and $wcp = 12\,\%$ to $wcp = 20\,\%$. These phases cannot be seen for the front legs, due to the lower weight compared to the rear legs.

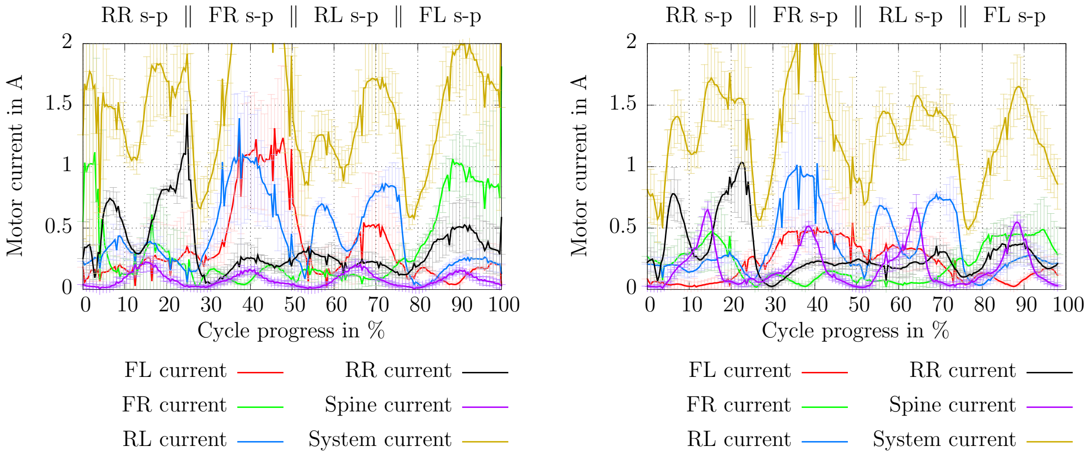

(a) *Terrain gravel* with *speed setting fast* and local control loop active and spine inactive (*setup* $L\ \overline{S}$).

(b) *Terrain gravel* with *speed setting fast* and local control loop and spine both active (*setup* $L\ S$).

Figure 5.9: Measured current of the legs and spine while walking on gravel. For *terrain gravel* and *speed setting fast* with *setup* $\overline{L}\ \overline{S}$ as well as with *setup* $\overline{L}\ S$, due to the systems decreased stability on this surface, no reliable could be recorded. s-p stands for swing-phase.

Fig. 5.9 shows the leg wise current consumption while walking on *terrain gravel* with *speed setting fast* for *setup* $L\ \overline{S}$ and *setup* $L\ S$. In both setups with deactivated local control loop (*setup* $\overline{L}\ \overline{S}$ and *setup* $\overline{L}\ S$), no reliable data could be recorded, since the robot tends to tip over laterally after a few steps and requires user intervention to maintain stability. Due to the compromised data, these runs are not shown in the figure.

As for the walking with *speed setting medium* on this deformable surface, one can see that there is a high deviation in the current consumption between the single steps. Fundamentally, the homogeneous load distribution can be seen also in this experiment. The standard deviation in this experiment is between 0.3 A to 0.8 A (see also tab. 5.5), whereas it is between 0.1 A to 0.2 A in the comparable experiment on *terrain lab*.

Table 5.5: Power consumption while walking on *terrain lab* and *terrain gravel* with *speed setting fast* and varying setups. The value is the mean value of one complete step cycle. The value specified in brackets is the standard deviation.

Setup/ Terrain	*Setup* $\overline{L}$ $\overline{S}$ in W	*Setup* $\overline{L}$ *S* in W	*Setup L* $\overline{S}$ in W	*Setup L S* in W
Terrain lab	52.8 (± 2.0)	55.2 (± 2.0)	47.5 (± 1.5)	49.5 (± 2)
Terrain gravel	n.a.	n.a.	77.0 (± 36.0)	60.0 (± 12.0)

Energy efficiency	in $[\frac{\mathrm{W}}{\mathrm{m}}]$	in $[\frac{\mathrm{W}}{\mathrm{m}}]$	in $[\frac{\mathrm{W}}{\mathrm{m}}]$	in $[\frac{\mathrm{W}}{\mathrm{m}}]$
Terrain lab	117.3	122.7	105.6	110
Terrain gravel	n.a.	n.a.	171.1	133.3

Table 5.5 shows the average power consumption while walking on *terrain lab* and *terrain gravel* with *speed setting fast* and varying setups. A deformable ground entails an increased standard deviation, since no step is like the one before. This effect is even more distinct when walking with *speed setting fast*. A reduction of the overall power consumption for setups with active local control loop, as shown for *terrain lab*, cannot be seen for *terrain gravel*. Compared to the walking with *speed setting medium* on even ground, the current consumption is with this walking speed 14 % higher (see table 5.4). However, as one can see in the lower part of the tables, Charlie's energy efficiency is nearly equal for both walking speeds. A distinction and thus a preference of one walking speed cannot be made.

However, more important than the positive influence on the power consumption for *terrain lab* is the fact that the robot is only able to pass through the gravel field in a stable manner with activated local control loop. Due to the necessity of external support during these experiments for *setup* $\overline{L}$ $\overline{S}$ and *setup* $\overline{L}$ *S*, the log data is compromised and therefore not shown. Nevertheless, in both setups with active local control loop, Charlie was repeatedly able to cross the gravel field. Yet, for this walking speed the overall current consumption and standard deviation is significantly increased, in this terrain.

Conclusion It is shown that for walking on a flat and rigid surface, the active local controller decreases the robot's overall power consumption. A decrease of about 10 % in power consumption is measured from the setup where the spine and local control loop are both inactive (*setup* $\overline{L}\ \overline{S}$) to walking with active local control loop (*setup* $L\ \overline{S}$). This holds for both tested walking speeds.

For walking on a flexible and deformable environment, the robot's power consumption is equal between *setup* $\overline{L}\ \overline{S}$ and *setup* $L\ \overline{S}$ for *speed setting medium*. The absence of reliable data for *terrain gravel* and the setups with deactivated local control loop does not mean that the robot is generally not capable of overcoming a gravel field with *speed setting fast*. It is to be expected that by changing Charlie's walking parameters and adjusting its stability controller, the robot will be able to pass through the field in a stable manner. Thus one can argue that an inadequate pattern was chosen to perform the experiments. On the other hand, it can be stated that the robot is able to traverse the gravel field with an active local control loop, even though the pattern may be not ideal. Therefore, it can be stated that the local control loop helps to improve the robot's stability and softens the necessity of the existence of an ideal walking parameter set to generate a stable walking, even if the local control loop is detached from the main controller supervision.

The robot's overall current consumption increases with speed. However, by taking the energy efficiency in account, in Charlie the needed current per meter is nearly equal for both walking speeds.

5.5.2.3 Stability in Unstructured Environment

Presumption Subsequent to the presentation of the robot's current consumption, the objective of the following analysis is an evaluation of the effect of the local controller on the robot's stability. It is expected that an active local controller has no influence on the stability while walking on a flat and even surface, because only low torques are expected to occur. If, however, the terrain becomes more unstructured, the local controller contributes to the robot's stability. This is due to the expected form closure between the feet and the ground and the increased traction.

Setup The setup is equal to the one in the previously described experiment.

Evaluation To determine, whether or not the local controller improves the balance of the robot, the trajectories of Charlie's CoM are analyzed. While walking on rigid surfaces, the robot's stability is not at risk. The trajectories between the setup with deactivated local control loop (*setup* $\overline{L}\ \overline{S}$) and with active controller (*setup* $L\ \overline{S}$) are too similar to allow a distinction between both setups and are therefore only shown in the appendix (Fig. 2 on page 203).

A difference can be seen while walking in unstructured environment like on the gravel field. Fig. 5.10 shows the CoM trajectories for both setups while walking on *terrain gravel*. The color of the curve indicates the progress of the overall walking cycle and changes from green (start of the walking cycle) to blue (end of the walking cycle). The curve itself shows the average CoM-shifting in x- and y-direction while walking forward with *speed setting medium*. Since multiple steps are performed, gray bars are added to the data line to point out the deviation from the mean value in x and y direction over the distinct runs.

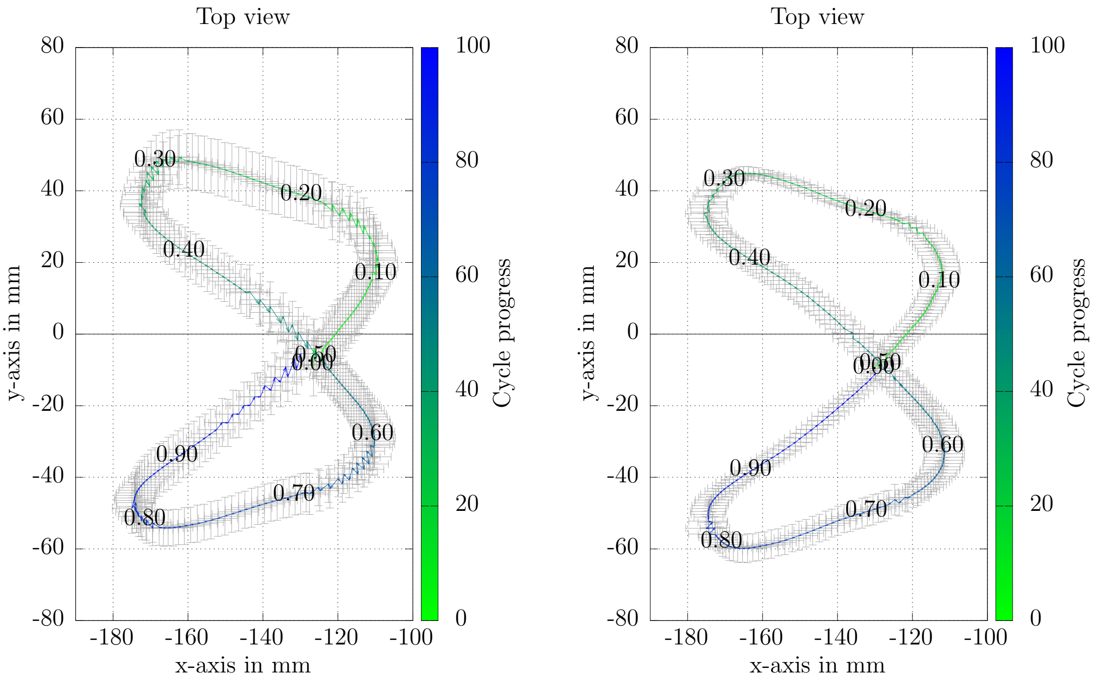

(a) Local control loop and spine both inactive (*setup* $\overline{L}$ $\overline{S}$).

(b) Local control loop active and spine inactive (*setup* L $\overline{S}$).

Figure 5.10: CoM movement while walking on *terrain gravel* with *speed setting medium* and different setups.

For *setup* $\overline{L}$ $\overline{S}$, indicated in Fig. 5.10(a), the trajectory deviation is considerably higher compared to *setup* L $\overline{S}$, shown in Fig. 5.10(b). This is true for the complete walking cycle, but most visible at the maximum lateral shifting between $wcp = 15\,\%$ to $wcp = 30\,\%$ and $wcp = 65\,\%$ to $wcp = 80\,\%$ of the cycle progress. In addition, it can be seen that the CoM is shifted 1 cm on the y-axis to the right. Due to the quality of the IMU's sensor reading as well as the flexible ground, a minor tilted position cannot be ruled out. Charlie's stability controller relies on the orientation the IMU provides and adapts the position of the limbs accordingly.

Conclusion In summary, it can be said that in a less challenging environment the activation of the local controller has no influence on the robot's balance. The CoM trajectories are nearly similar for the different setups while walking on *terrain lab*. For *terrain gravel*, however, an improvement can be shown. The individual steps show only a small deviation of the CoM compared to its desired trajectory, if the local controller is activated. Furthermore, as already stated in the analysis of the power consumption, the local controller increases the stability in a way that enables the robot to deal with an unstructured environment, even though the walking pattern may not be ideal. In experiments with the highest walking speed and deactivated local controller, Charlie is not able to traverse the gravel field with the selected gait. When, however, the controller is active, a stable motion while walking on gravel or generally more compliant soil can be seen.

5.5.2.4 Forces Acting on the Feet

Presumption In the following, the forces acting on the feet are analyzed while walking with different setups. On the z-axis, the interaction force between foot and ground is measured. The investigation is made to determine the effect of the local control loop on mechanical forces, acting on the robot's limbs. In addition, this analysis allows revealing potential tensions between the legs.

As described, the local controller reacts to torques occurring on the feet. By reducing the torque, a reduction of tensions possibly present between the legs is expected, which can have an influence on the measured forces as well. In addition, a reduction of possible force peaks in the rear legs is expected, due to the compliant behavior of the rear feet.

Setup The setup is equal to the one in the previously described experiment.

Evaluation The recorded data shows no difference between the left and right limbs, thus the forces applied on the feet are exemplary presented for the left front (Fig. 5.11) and left rear leg (Fig. 5.12). Because of this, the data recorded from the robot's right limbs are omitted. In addition, the data of traversing the gravel field (*terrain gravel*) is similar to the one recorded on *terrain lab*. This is true for all four setups. The data is therefore presented in the appendix, in

Fig. 4 on page 205 for the front left foot and in Fig. 5 on page 206 for the rear left foot.

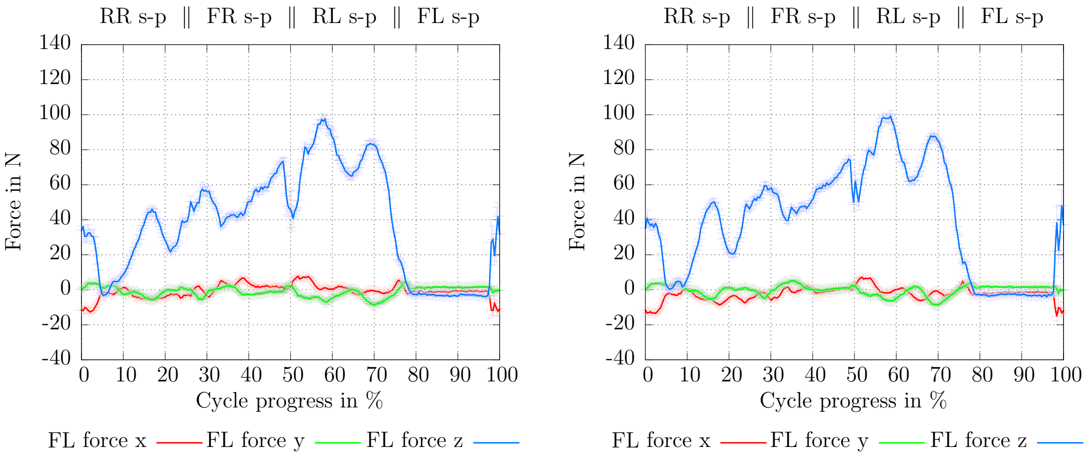

(a) Local control loop and spine both inactive (*setup* $\overline{L}$ $\overline{S}$).

(b) Local control loop inactive and spine active (*setup* $\overline{L}$ S).

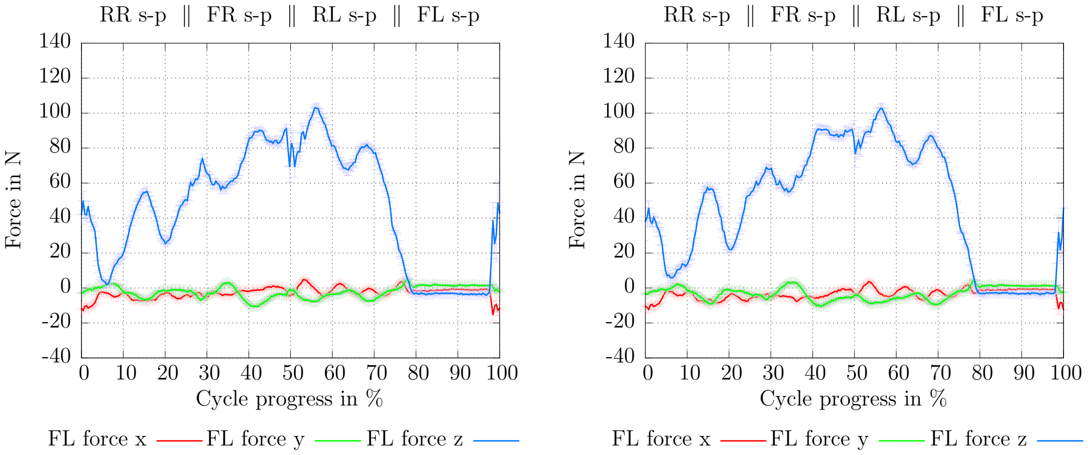

(c) Local control loop active and spine inactive (*setup* L $\overline{S}$).

(d) Local control loop and spine both active (*setup* L S).

Figure 5.11: Measured forces of the front left leg while walking on *terrain lab* in different setups with *speed setting medium*.

The curves in Fig. 5.11 indicate that the lift-up motion of the rear leg, which is diagonally located of the respective front leg, influences the front leg's ground contact. The momentum introduced by the lift-up motion of the rear right leg can be seen at $wcp = 6\,\%$ and causes a brief, but measurable force reduction at the front left leg. This can be seen in all four setups, but it is more distinct in setups with deactivated local control loop (*setup* $\overline{L}$ $\overline{S}$ *and* $\overline{L}$ S). The applied force of the left front leg increases, when the rear leg's acceleration remains constant during the swing-phase. For the setups with activated local control, the measured force tends to the expected nominal force of 72 N (per leg in a tripod stance, without dynamic influences). In *setup* $\overline{L}\ \overline{S}$ *and* $\overline{L}\ S$, a larger deviation to the expected force is measured.

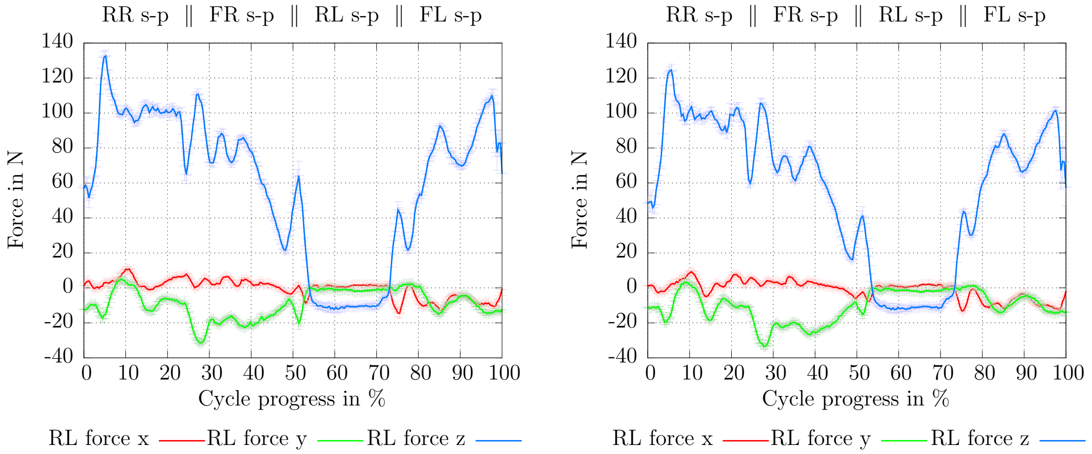

(a) Local control loop and spine both inactive (*setup* $\overline{L}\ \overline{S}$).

(b) Local control loop inactive and spine active (*setup* $\overline{L}\ S$).

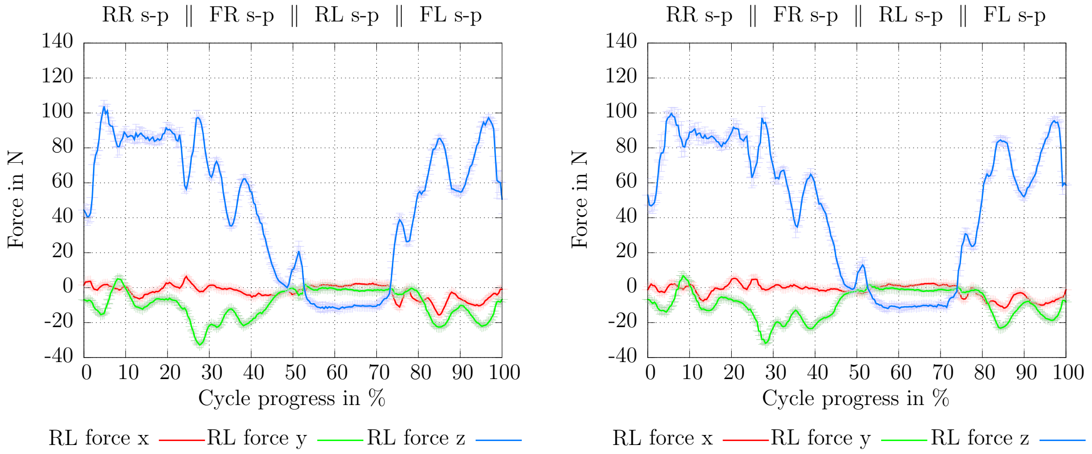

(c) Local control loop active and spine inactive (*setup* $L\ \overline{S}$).

(d) Local control loop and spine both active (*setup* $L\ S$).

Figure 5.12: Measured forces of the rear left leg while walking on *terrain lab* in different setups with *speed setting medium*.

The right rear leg introduces a second momentum, starting at $wcp = 15\,\%$ with its swing-down movement, where the leg's motion speed is reduced. The effect is equal in all four setups.

At $wcp = 50\,\%$, a decrease occurs due to similar effects resulting from the lateral CoM shifting. The reduction can be observed in each of the four figures, but is more distinct with deactivated local control loop. In these two setups the reduction is between 25 N to 35 N, whereas in *setup* $L\ \overline{S}$ *and* $L\ S$ a reduction of 10 N to 20 N is measured. Hence, the compliant behavior of the foot increases the traction generated by the front feet. The applied load on the front left leg is at its maximum when the left rear leg is in its swing-phase. The swing-phase of the front left leg starts at $wcp = 75\,\%$ of the walking cycle. Therefore, forces tend to zero between $wcp = 77\,\%$ to $wcp = 98\,\%$.

Fig. 5.12 shows the force measurements of the rear left foot while walking on *terrain lab* with *speed setting medium* in different setups. Forces acting in x-direction and y-direction are increased in comparison to the ones at the front foot, due to the differences in size and traction between both feet. In the setups with deactivated local control loop, a maximum force of around 130 N is observed between $wcp = 0\,\%$ to $wcp = 10\,\%$ (see Fig. 5.12(a) and Fig. 5.12(b)). In setups with activated local controller, the maximum load is reduced by about 25 % to 100 N. In addition, for the lateral CoM shift at $wcp = 50\,\%$ of the step cycle, it can be seen that the absolute force is smaller as well and does not exceed 20 N, which entails a more smooth translation into the leg's swing-phase. The maximum force applied to the front legs, on the other hand, is neither reduced nor increased by the usage of the local control loop (see 5.11). Between $wcp = 54\,\%$ to $wcp = 73\,\%$ the leg is in its swing-phase. During this time, the force in z-direction is negative, due to the weight of the rear foot.

Conclusion As expected, the introduced forces acting in x- and y-direction are larger compared to the ones at the front feet, due to the size of the rear foot. The forces acting on the front feet while walking on all three axes are similar for all four setups. For the rear legs this is only true for the x- and y-axis. On the z-axis, the maximum load is reduced by about 25 % in setups with activated local controller, due to the compliant behavior of the feet.

5.5.2.5 Measured Torques at the Feet

In the following, the occurring torques at the feet are analyzed while walking with different setups over *terrain lab*.

Presumption For *setup* $\overline{L}\ \overline{S}$ *and* $\overline{L}\ S$, it is expected that the measured torques at the front legs are significantly smaller compared to the ones in the rear legs, due to the size of the MPCF. Because of the function of the local controller, it is assumed that the torques in the rear legs are reduced significantly, as soon as the local controller is activated. However, a change of the applied torque on the front feet is not expected.

Setup The setup is equal to the one in the previously described experiment.

Evaluation The recorded data shows no difference between the left and right limbs, thus the torques acting on the feet are exemplary presented for the left front (Fig. 5.13) and left rear leg (Fig. 5.14). Because of this, the data recorded from the robot's right limbs are omitted. In addition, the data of traversing the gravel field (*terrain gravel*) is similar to the one recorded on *terrain lab*. This is true for all four setups. The data is therefore presented in the appendix, in Fig. 6 on page 207 for the front left foot and in Fig. 7 on page 208 for the rear left foot.

Fig. 5.13 shows the measured torques at the front left foot while walking on *terrain lab* for all four setups. It can be seen that the torque remains constant for the front legs, despite the activation of the local control loop in the rear legs. The distribution of the measured torque is nearly equal and always below 5 N m in all four setups.

Fig. 5.14 shows the measured torques at the rear left foot while walking on *terrain lab* for all four setups. In setups with deactivated local control loop (*setup* $\overline{L}\ \overline{S}$ *and* $\overline{L}\ S$), the peak of the absolute torque is at 12 N m. In comparison, in *setup* $L\ \overline{S}$ *and* $L\ S$ the peak torque is below 5 N m. These peaks occur at the end of the acceleration phase of the remaining three limbs.

If the local control loop is activated, the amplitudes of the measured longitudinal and lateral torques in the rear legs are reduced by more than 50 %. Similar to the front legs, these torques do not exceed the 5 N m mark, not even the absolute torque. The gradient of the curve at $wcp = 75\,\%$ is due to the touchdown event of the rear left leg. After establishing ground contact, the local controller starts to reduce the occurring torque. A significant difference between *setup* $L\ \overline{S}$ without and *setup* $L\ S$ with spine movement cannot be determined. This is already the case for the occurring forces, as shown earlier.

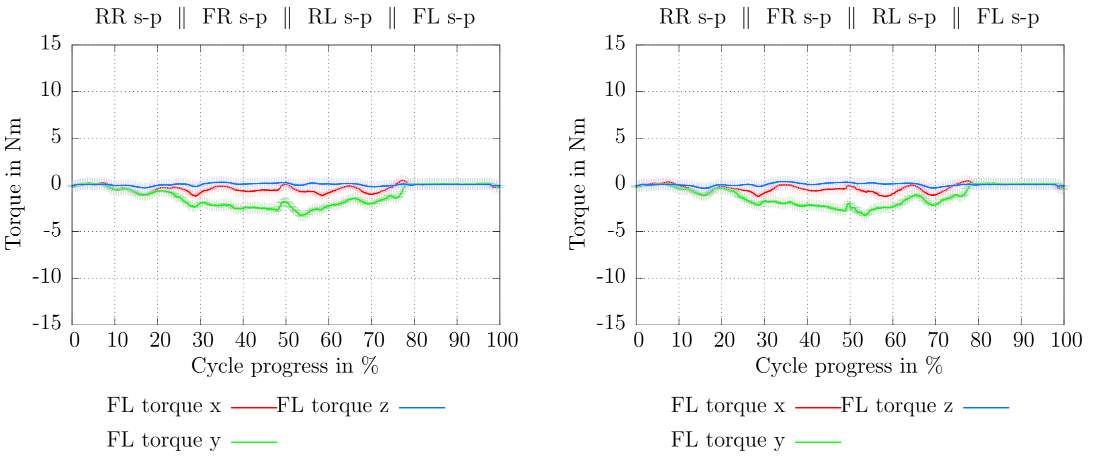

(a) Local control loop and spine both inactive (*setup* $\overline{L}$ $\overline{S}$).

(b) Local control loop inactive and spine active (*setup* $\overline{L}$ S).

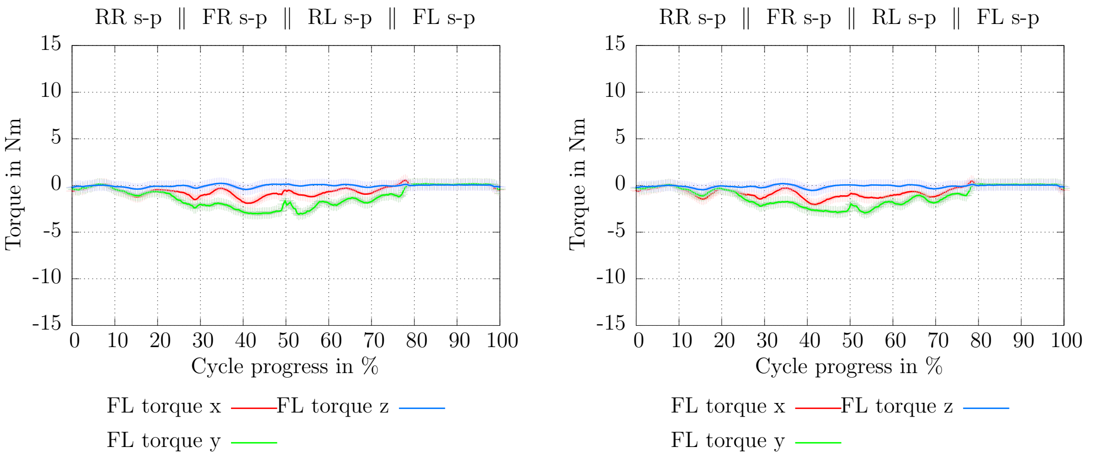

(c) Local control loop active and spine inactive (*setup* L $\overline{S}$).

(d) Local control loop and spine both active (*setup* L S).

Figure 5.13: Measured torques of the front left leg while walking on *terrain lab* in different setups with *speed setting medium*.

Conclusion The data shows that the torques occurring on the front legs remain constant in all four setups. In this case, an activation of the local control loop in the rear legs has no influence on the front legs. For the rear legs, however, the expected reduction of the occurring torques was confirmed. The torques at the rear legs are more than 50 % reduced in setups with activated controller (*setup* L $\overline{S}$ *and* L S) compared to setups with deactivated controller. In *setup* L $\overline{S}$ *and* L S, the measured torques on the rear legs are below 5 N m and therefore as low as the ones measured on the front legs.

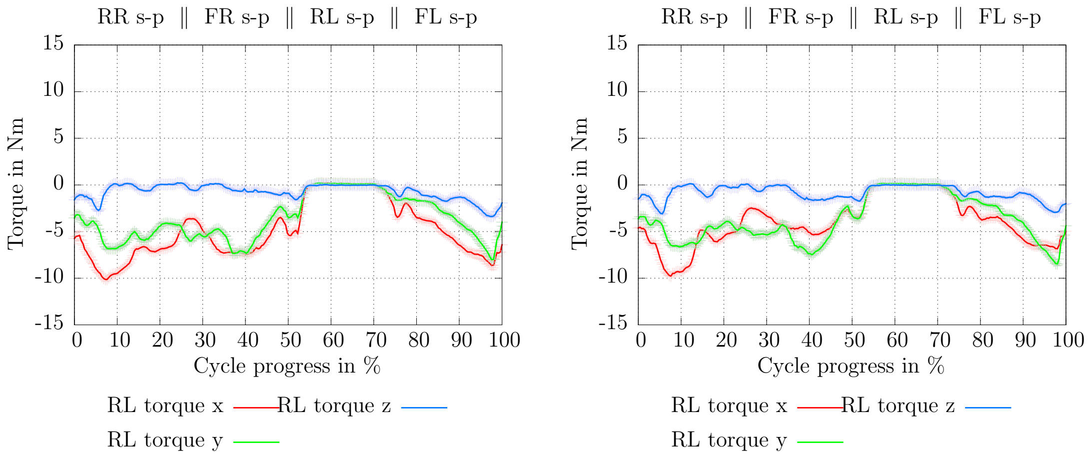

(a) Local control loop and spine both inactive (*setup* $\overline{L}$ $\overline{S}$).

(b) Local control loop inactive and spine active (*setup* $\overline{L}$ S).

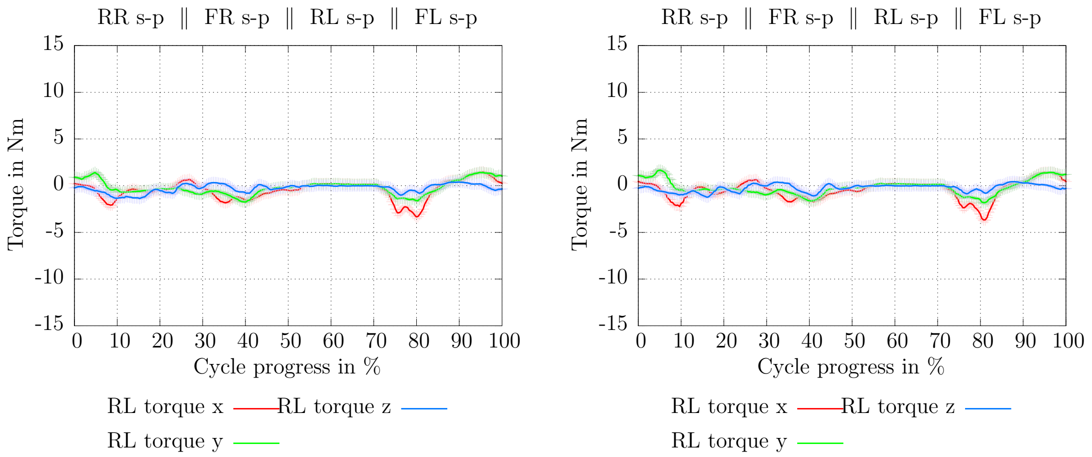

(c) Local control loop active and spine inactive (*setup* L $\overline{S}$).

(d) Local control loop and spine both active (*setup* L S).

Figure 5.14: Measured torques of the rear left leg while walking on *terrain lab* in different setups with *speed setting medium*.

5.5.2.6 Forces Acting on the Spine

Presumption As mentioned above, most robots have a rigid body with attached legs. Charlie's artificial spine consists of six rods, which interlink the front and rear body. In each rod, an one DoF force sensor is integrated. All six sensors can be combined into a virtual six DoF force/torque sensor, which is able to measure the forces and torques between hip and shoulder. In the following, the acting forces are shown for the different setups. As shown earlier for the legs, it is expected that in setups with activated local controller the forces are reduced compared to *setup* $\overline{L}$ $\overline{S}$

and $\overline{L}\ S$, due to the compliant foot behavior.

Setup The setup is equal to the one in the previously described experiment.

Evaluation The columns in Tab. 5.6 list the mean value of forces acting on the spines x-, y-, and z-axis while walking on *terrain lab*. The upper part of the table shows the data for the different setups with *speed setting medium* and the lower part the data for walking with *speed setting fast*. The standard deviation is given in parentheses. For *speed setting medium*, the force applied on the x-axis increases minimally of about 2 N in setups with active local control loop and remains constant on the y-axis. A significant change can be seen on the z-axis, where the applied force is reduced by about 17 N (or 60 %). Walking with a higher speed amplifies the effect even more. Here, the changes on x- and y- axis are marginal, however, for the z-axis a reduction of about 20 N is measured.

Table 5.6: Measured spine forces while walking on *terrain lab* (mean values of one complete step cycle). The standard deviation is indicated in brackets [KSS+16].

Speed setting medium Setup	x-axis in N	y-axis in N	z-axis in N
Setup $\overline{L}\ \overline{S}$	3.7 (± 2.8)	7.7 (± 2.9)	−28.6 (± 3.1)
Setup $\overline{L}\ S$	2.9 (± 2.7)	8.1 (± 2.7)	−29.3 (± 3.0)
Setup $L\ \overline{S}$	5.7 (± 2.6)	9.0 (± 2.8)	−11.3 (± 2.6)
Setup $L\ S$	6.1 (± 2.9)	7.6 (± 3.1)	−10.0 (± 3.1)
Speed setting fast Setup			
Setup $\overline{L}\ \overline{S}$	4.3 (± 3.2)	7.5 (± 3.3)	−26.5 (± 3.3)
Setup $\overline{L}\ S$	6.4 (± 3.0)	9.4 (± 3.1)	−24.6 (± 2.9)
Setup $L\ \overline{S}$	7.2 (± 3.2)	9.2 (± 3.2)	−6.8 (± 2.9)
Setup $L\ S$	6.6 (± 3.2)	8.6 (± 3.4)	−5.1 (± 2.8)

Conclusion The presented data indicates that the local controller has not only an effect on the legs, but also on the entire body. The forces acting on the robot's x-axis and y-axis remain nearly constant in all four setups. On the z-axis, however, a more significant change is observed. In setups with activated local controller, the applied force is reduced by around 60 %. This result is even more amplified when walking with a higher speed.

5.5.2.7 Measured Torques in the Spine

Presumption Since this is the first time, to the best knowledge of the author, that occurring torques between front and rear body can be measured, no comparative data is available. Therefore, with *setup* $\overline{L}\ \overline{S}$ an impression regarding the present torque is gained, which allows a comparison with all other setups later on. The local controller is only implemented in the feet, yet it affects the overall robot, as already shown. For the perceived torques in the spine it is expected that in setups with activated local controller distortions, which may be present between front and rear body, are reduced.

Setup The setup is equal to the one in the previously described experiment.

Evaluation Table 5.7 shows the measured torques for the x-, y,- and z-axis while walking on *terrain lab* with different speeds and with different setups. Comparing *setup* $\overline{L}\ \overline{S}$ *and* $\overline{L}\ S$ with *setup* $L\ \overline{S}$ *and* $L\ S$ in the experiments with *speed setting medium*, it can be seen that the occurring torques are decreased by 15 N to 17 N. As for the measured force in the spine on the z-axis in Tab. 5.6, the data shows the same effect on the z-axis for the torque (yaw): the occurring moment is nearly reduced to zero in setups with activated local control loop. A torque on the x-axis suggests torsion between front and rear body. A positive value indicates that the spine lifts up the left side of the robot.

Only the torque on the y-axis (pitch) remains, yet with a reversed sign. A positive value on the y-axis indicates that the height of the rear legs is not ideal and therefore a torque is introduced to the spine. The reversed sign on this axis in setups with activated local control can be explained by the compliant feet.

This effect is even more noticeable while walking with *speed setting fast*. The torque on the z-axis again tends to zero. The torque on the x-axis, however, now is increased in negative direction, meaning that the front body is pulling on the rear body. This can be explained by the more dynamic leg movement and the non-compliant behavior of the front legs.

Conclusion The torque reducing local controller implemented in the feet has a measurable result on the spine as well. The data shows that for both tested walking speeds in setups with activated local controller (*setup* $L\ \overline{S}$ *and* $L\ S$) about 90 % less torque can be measured on the spine z-axis compared to setups with deactivated controller (*setup* $\overline{L}\ \overline{S}$ *and* $\overline{L}\ S$). In addition, the spine force/torque sensor allows to

Table 5.7: Measured spine torque values (mean values of one complete step cycle). The standard deviation is indicated in brackets [KSS+16].

Speed setting medium Setup	x-axis in Nm	y-axis in Nm	z-axis in Nm
Setup $\overline{L}$ $\overline{S}$	14.5 (± 3.3)	8.8 (± 2.7)	−20.9 (± 2.9)
Setup $\overline{L}$ S	16.9 (± 3.4)	7.9 (± 2.7)	−17.7 (± 2.9)
Setup L $\overline{S}$	−2.4 (± 2.9)	−10.8 (± 2.7)	1.6 (± 2.7)
Setup L S	−1.8 (± 3.4)	−8.1 (± 3.3)	1.0 (± 3.0)
Speed setting fast Setup			
Setup $\overline{L}$ $\overline{S}$	12.4 (± 3.5)	8.3 (± 3.5)	−20.4 (± 3.4)
Setup $\overline{L}$ S	9.3 (± 3.4)	5.9 (± 3.3)	−20.0 (± 3.2)
Setup L $\overline{S}$	−8.1 (± 3.3)	−12.4 (± 3.0)	0.7 (± 3.0)
Setup L S	−7.0 (± 3.2)	−10.3 (± 3.1)	1.0 (± 3.0)

determine possible tensions between the front and rear body. In this case, these can mainly be seen on the pitch axis.

5.5.3 Conclusion Ground Experiments

This section summarizes the results obtained on flat surfaces. It can be stated that the robot is designed such that it is able to withstand a wide range of experiments without failure. Using the data the FSR sensors (implemented in the sole of the rear feet) provide, the different kinds of terrain can be distinguished without the need of imaging modalities (see Appendix, Fig. 3 on page 204). The installed actuators (including the sensors and control electronics) in the limbs, their RoM and operating speed enable the robot to deal with different environments.

It is shown that the local controller has a positive influence on the current consumption when walking in flat and rigid terrain. Different walking speeds are tested with the four setups. A decrease of about 10 % for the current consumption is measured, when walking with *setup* L $\overline{S}$ compared to *setup* $\overline{L}$ $\overline{S}$ with the respective matching walking speed. While walking in a deformable environment, however, this effect of the local controller cannot be seen.

For the robot's stability, on rigid surfaces no difference in the data between activated and deactivated local controller is observed. In more challenging environment, like a gravel field, a lower standard deviation was recorded and thus the optimal and predicted CoM trajectory is met more precisely. Furthermore, it can be stated that the robot is able to traverse unstructured environment, which it could not cover in a stable manner with deactivated local control. By changing the robot's walking parameters including the stability controller, it would as well be able to overcome the selected terrain. Yet, it shows that an active local control loop enables the robot to cover unstructured environment even though the walking pattern may be not ideal.

Due to the local controller, the torques acting on the rear feet are decreased by more than 50 %. The maximum peak forces, perceived on the rear feet, are reduced by about 25 %. In addition, it is shown that the compliant behavior of the foot increases the traction of the front feet.

The experimental data indicates that in Charlie the local controller can be useful. For further validation the local control loop is tested in different inclinations, which will be described in the following section.

5.6 Description and Evaluation of Experiments on Inclines

In the following, walking experiments with the hominid robot Charlie in various inclines are described. Due to the previously shown similarity between *setup* $\overline{L}\ \overline{S}$ *and* $\overline{L}\ S$ (both with deactivated local control loop) as well as between *setup* $L\ \overline{S}$ *and* $L\ S$ (both with activated local control loop) and for the sake of clarity and readability, the analysis regarding current consumption and stability focusses on the comparison between *setup* $\overline{L}\ S$ and *setup* $L\ S$, with one exception. For the following experiment, *setup* $\overline{L}\ \overline{S}$ is also analyzed since it is the baseline experiment.

5.6.1 The Active Spine and its Influence on the Limb Joints

Presumption During the forward walking behavior, the movement of the spine actively supports the swing motion of the limbs from PEP to AEP. The first hip joint and the knee joint are affected most. Thus it is to be expected that the maximum speed of the joints, which are mainly used to generate the forward motion, is reduced in the swing-phase compared to walking without active spine motion.

Setup For these experiments, an infinitely variable, indoor ramp with a wooden surface is used, as described earlier (cf. Section 5.1). The incline is increased in 5°

steps and ranges from −20° to 20°. A positive degree indicates an uphill walking of the robot and a negative degree stands for downhill walking. Figure 5.15 shows Charlie walking uphill in an incline of 20°.

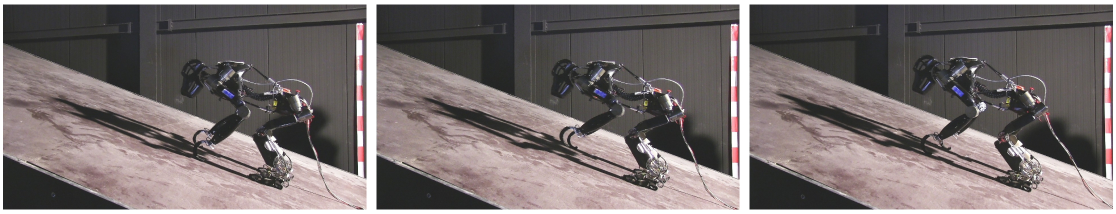
(a) Four-legged stance (b) Front-left leg in swing (c) Four-legged stance

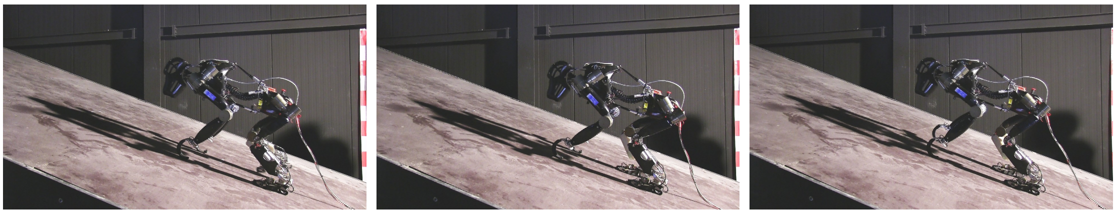
(d) Rear-right leg in swing (e) Four-legged stance (f) Front-right leg in swing

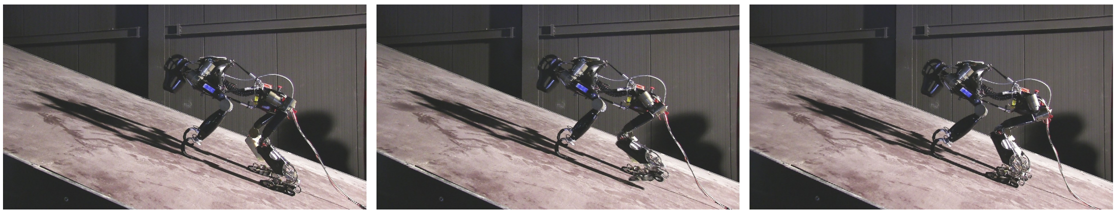
(g) Four-legged stance (h) Rear-left leg in swing (i) Four-legged stance

Figure 5.15: One step cycle of walking uphill on a 20° slope [KSS+16].

The data shown in the following figures and tables are the mean values over three runs covering a distance of at least two meters (14 complete step cycles). To gain a stable walking pattern with minimal slip, the *speed setting ramp* was used in all inclines, which means that the forward motion is $30\,\frac{\mathrm{mm}}{\mathrm{s}}$ with a total cycle time of 5 s. To obtain authentic and undistorted results, a safety harness or alike is not used during the experiments. However, in Fig. 5.15 cables can be seen, which supply power and the data uplink. While performing the experiments, no parameter aside from the respective inclination and the selection of the desired setup has been modified by the operator.

In the introduction of this experiment series it is stated that the focus lies on *setup* $\overline{L}\ S$ and *setup* $L\ S$. Since these are both setups with spine motion, for this analysis *setup* $\overline{L}\ \overline{S}$ is considered as well.

Evaluation Fig. 5.16 shows the measured maximum joint velocity of the right rear hip joint 1 and the knee while walking various inclines. The red line marks *setup* $\overline{L}\ \overline{S}$, where spine and local control loop are deactivated. The results for *setup* $\overline{L}\ S$ are shown in green and *setup* $L\ S$ is colored in blue.

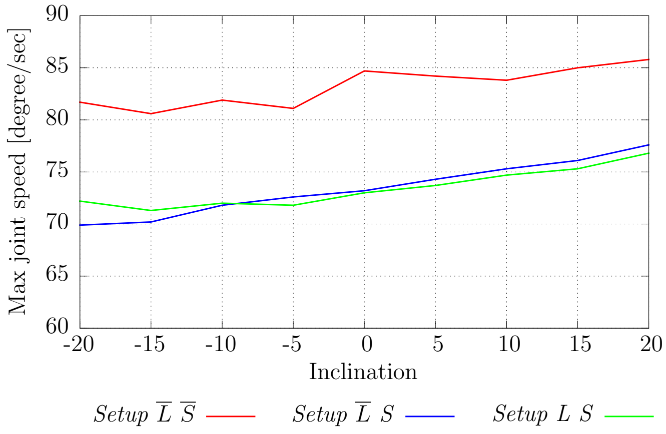

(a) RR hip joint 1

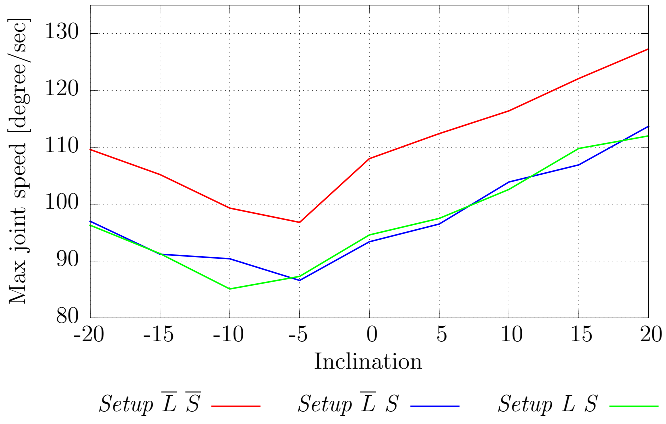

(b) RR knee joint

Figure 5.16: Maximum joint speeds in the rear right leg in different inclinations.

It can be seen that in setups with active spine motion the maximum joint velocity is constantly reduced compared to *setup* $\overline{L}\ \overline{S}$. This is true for all inclines. The joint speed changes in different inclines due to the posture adaption of the stability controller. For both joints a reduction between $10\,\frac{\circ}{\mathrm{s}}$ to $15\,\frac{\circ}{\mathrm{s}}$ is recorded, which corresponds to a decrease of up to 14 %. The overall power consumption, however, remains nearly constant for all setups. The spine motors need additional power for driving, however, energy is saved by the legs due to lower accelerations.

Conclusion As expected, while walking the spine motion helps to reduce the maximum joint speed requirements to generate a forward motion. A reduction of the maximum speed has several electro-mechanical advantages. Lower accelerations entail less mechanical stress to the motor and the gear, as well as a lower power requirement on the three motor phases. Both have a positive effect on reliability and lifetime of the actuator including its local electronics. For walking, this can result in an increase of walking speed of the robot, since the same cycle time allows larger steps.

5.6.2 Power Consumption

In the following, the power consumption of the robot while walking in different inclines is investigated. The analysis focusses on the behavior of the local control loop for uphill and downhill walking. The data presented is recorded with *setup* $\overline{L}$ S and *setup* L S.

Presumption It is expected that the energy consumption increases with increased inclines. As for the walking in flat terrain, it is expected that the overall power consumption in both experiments, uphill and downhill walking, is decreased in *setup* L S compared to *setup* $\overline{L}$ S. The load applied to the legs should be better distributed in the setups with active local control loop. While walking uphill, the rear legs are expected to show a higher power consumption compared to an incline of 0° and for downhill walking the front legs will have to carry more load than the rear legs.

Setup The setup is equal to the previously described experiment.

Evaluation As mentioned earlier, the power consumption shown in the following figures and tables refers to the measured motor currents. The energy needed by the control electronics is not included (see Tab. 3.2).

Table 5.8 shows in the first row the average power needed for walking uphill with *speed setting ramp* and *setup* $\overline{L}$ S. The average current consumption with activated local control loop is shown in the second row. In *setup* $\overline{L}$ S it can be seen that from $wcp = 5\,\%$ to $wcp = 15°$ the overall current consumption slightly increases by about 5 W the steeper the inclination is; this is about 12.6 % of the robot's motor power consumption or 5.1 % of the robot's overall power consumption. At 20°, the needed power is minimally reduced. For *setup* L S on the other hand, the overall current consumption is mainly constant in all inclines. It is further observed that the robot's power consumption while walking uphill with *setup* $L\ S$ is lower compared to *setup* $\overline{L}\ S$.

Table 5.8: Average current consumption while walking uphill with *setup* $\overline{L}\ S$ and *setup* $L\ S$ in different inclinations. The standard deviation is indicated in brackets. The values are rounded to the nearest half.

Angle Setup	0°	5°	10°	15°	20°
Setup $\overline{L}\ S$	34.5 W (± 2.0)	35.5 W (± 2.5)	37.0 W (± 2.5)	40.0 W (± 4.0)	38.5 W (± 4.5)
Setup $L\ S$	36.0 W (± 2.0)	34.5 W (± 2.0)	34.5 W (± 2.0)	35.0 W (± 3.0)	35.0 W (± 3.0)

Figure 5.17 provides a more detailed view on the data and visualizes the average consumption of the limbs and the spine during a walking cycle for both setups. The data recorded with *setup* $\overline{L}\ S$ is displayed on the left hand side and the data for *setup* $L\ S$ on the right hand side. Starting in the first row with the recorded data while walking in an incline of 0°, in each row the incline is increased by 5°. The average motor current is shown for each leg (FL in red, FR in green, RL in blue, and RR in black) as well as for the spine (in magenta). The overall current consumption of the robotic system is displayed in the yellow curve.

By comparing *setup* $\overline{L}\ S$ with *setup* $L\ S$, it can be seen that the overall current consumption is decreased in *setup* $L\ S$ in all inclines. In addition, the current peaks in *setup* $L\ S$ are reduced as well. A diagonal load shifting can be observed while walking uphill with *setup* $\overline{L}\ S$. The load on the rear left leg is increased if the front right leg is in its swing-phase ($wcp = 25\,\%$ to $wcp = 50\,\%$ of the cycle progress). The load on the rear right leg, however, is increased if the front left leg is in its swing-phase ($wcp = 75\,\%$ to $wcp = 100\,\%$). The front legs power consumption is generally lower than the one of the rear legs, due to the uphill walking.

In *setup* $L\ S$ the load is distributed more homogeneously between the legs, which mean that the maximum motor current of the rear legs is decreased in setups with local control loop, but the current consumption of the front legs is increased. In addition, the individual curves show a smaller deviation from the mean value, which indicates a more repeatable and thus more stable gait.

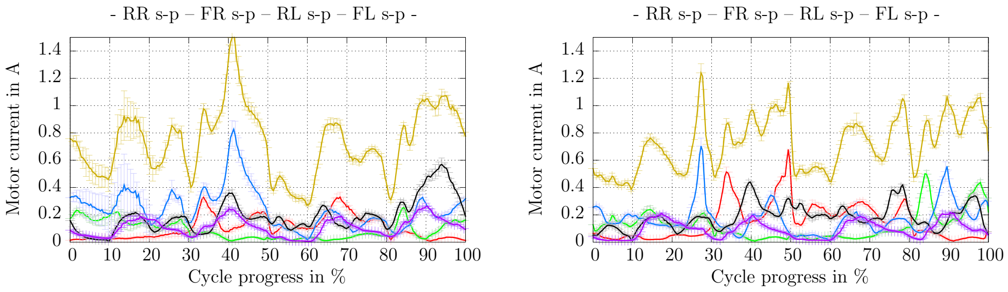

(a) Incline of 5° with *setup* $\overline{L}$ *S*.

(b) Incline of 5° with *setup L S*.

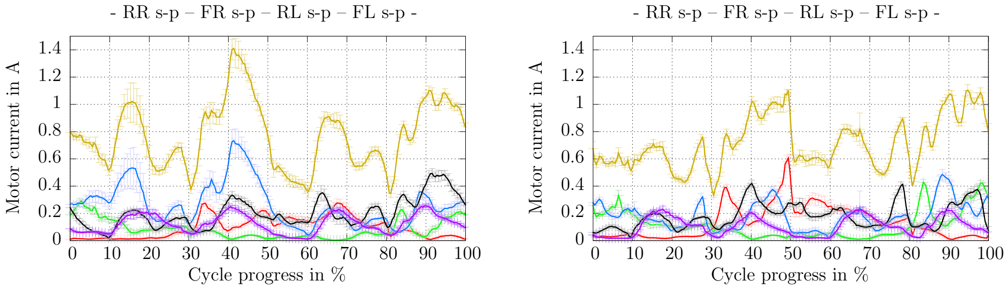

(c) Incline of 10° with *setup* $\overline{L}$ *S*.

(d) Incline of 10° with *setup L S*.

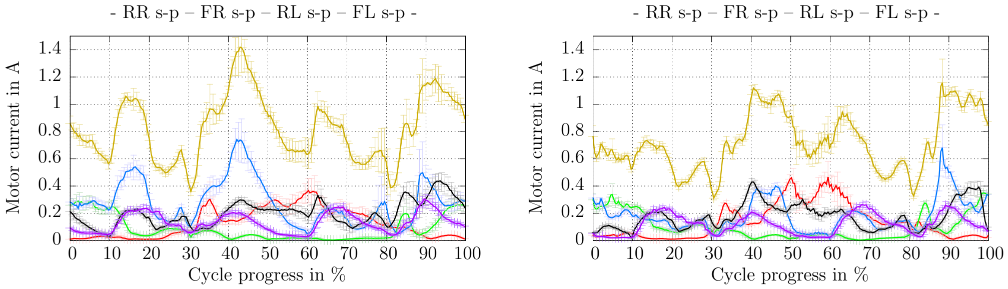

(e) Incline of 15° with *setup* $\overline{L}$ *S*.

(f) Incline of 15° with *setup L S*.

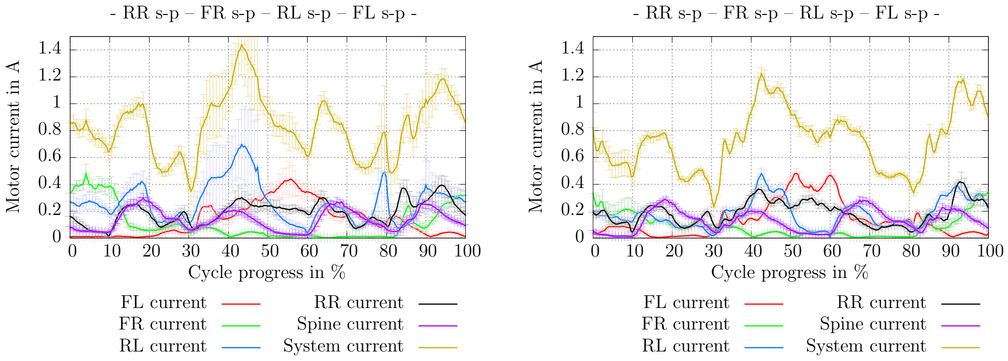

(g) Incline of 20° with *setup* $\overline{L}$ *S*.

(h) Incline of 20° with *setup L S*.

Figure 5.17: Motor currents while walking on *terrain ramp* with *speed setting ramp* in different setups and inclines.

The data shows an unexpected drawback of the local control loop in the downhill walking scenario. Table 5.9 shows the average power consumption for all runs with negative inclination for *setup* $\overline{L}\ S$ in the first row and the current consumption for *setup* $L\ S$ in the second row. In the first row it can be seen that the average power consumption is increased minimally, the steeper the incline is. Starting with a consumption of 35 W in −5°, it increases by 3 W for −20°. With active local control loop, the power consumption increases even more. In the −5° case the average is 37.5 W and goes up to 50 W while walking in the −20° scenario.

Table 5.9: Average current consumption while walking uphill with *setup* $\overline{L}\ S$ and *setup* $L\ S$ in different inclinations. The standard deviation is indicated in brackets. The values are rounded to the nearest half.

Angle / Setup	0°	−5°	−10°	−15°	−20°
Setup $\overline{L}\ S$	34.5 W ± 2.0	35.0 W ± 1.5	35.5 W ± 2.0	36.5 W ± 2.5	38.0 W ± 2.5
Setup $L\ S$	36.0 W ± 2.0	37.5 W ± 2.0	42.0 W ± 2.0	47.0 W ± 3.0	50.0 W ± 3.5

Fig. 5.18 gives a more detailed view on the robot's power consumption, *setup* $\overline{L}\ S$ is shown on the left hand side and *setup* $L\ S$ on the right hand side, both setups range from −5° to −20°. In the setup without active local control loop, the front legs have to carry a higher load and thus have a higher current consumption than the rear legs. This can be seen in all negative inclines, but the steeper the incline the more the front legs can be distinguished from the rear legs. If one of the front legs is in its swing-phase, the other front leg's load is increased, which is expected due to the downhill walking.

In the setup with active local control loop it can be seen that the overall current consumption is increased compared to *setup* $\overline{L}\ S$. Yet, the load is also applied to the rear legs, reducing the front legs current consumption, e.g., between $wcp = 65\,\%$ to $wcp = 75\,\%$ in 5.18(h) compared to 5.18(g). But the occurring load peaks, e.g., at $wcp = 35\,\%$ for the front left leg or $wcp = 85\,\%$ for the front right leg, are higher while walking in *setup* $L\ S$.

Conclusion In order to ensure comparability, the initially chosen parameter sets for the walking pattern or local control loop are not changed during the scenarios and are the same used for flat surfaces as well as in unstructured terrain. The robot is able to walk up- and downhill in a stable manner in both setups. It is demonstrated that the overall current consumption can be reduced if the local controller is activated while walking uphill. An average current consumption of 35 W is needed, regardless of the inclination.

However, it can be stated that this configuration is not as beneficial for walking downhill as it is for uphill walking. An average consumption between 35 W and 38 W is measured, when the local controller is deactivated. By activating the controller, the overall power consumption increases by up to 15 W walking downhill a $-20°$ inclination.

In an unstructured environment, the local controller increases the robot's stability. During up- and downhill walking, a more stable behavior could make up for a higher current consumption. Therefore, the following section deals with the robot's stability in inclines.

5.6.3 Stability in Inclines

After analyzing the robot's power consumption, the stability of the robot in inclines is evaluated, whether the stability is sufficiently increased (like in unstructured environment) justifying an increased energy consumption while walking downhill with *setup L S*.

Presumption It is assumed that the steeper the slope, the more the deviation of the trajectory of the CoM and ZMP increases. Nevertheless, it is anticipated that in *setup L S*, similar to the walking in an unstructured environment, the deflection is smaller compared to *setup* $\overline{L}$ *S*. It is presumed that this outcome can be seen only for uphill walking. As the previous experiments showed, the robot's power consumption for downhill walking is increased in all legs, which indicates either an increased torque applied to the actuators or increased limb and body movements.

Setup The setup is equal to the previously described experiment.

Evaluation The following figures show the robot's average ZMP shifting during one step as top view. This way, the ZMP movement and its deviation (visualized by gray bars) from the mean value can be seen on the x-axis and y-axis. The progress of the walking cycle is indicated by the changing color from green to blue. For a better overview, additional numbers are attached to the respective curve.

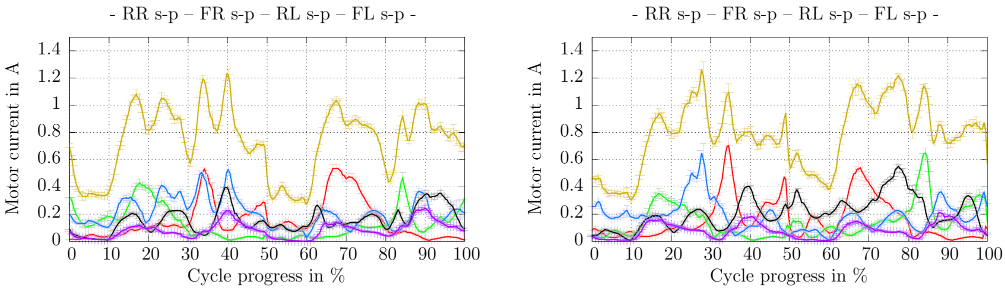

(a) Incline of −5° with *setup* $\overline{L}$ *S*. (b) Incline of −5° with *setup* *L* *S*.

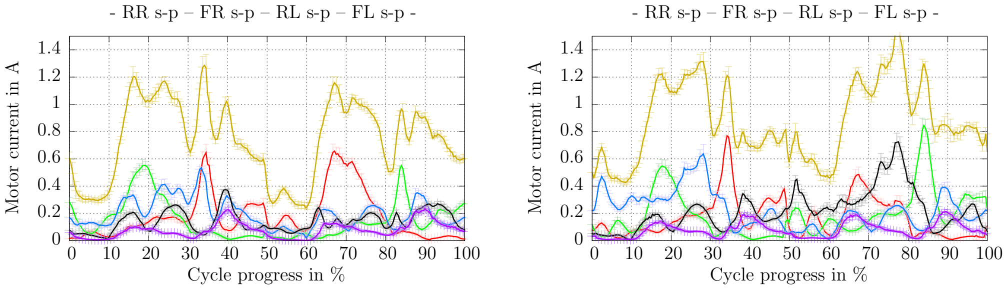

(c) Incline of −10° with *setup* $\overline{L}$ *S*. (d) Incline of −10° with *setup* *L* *S*.

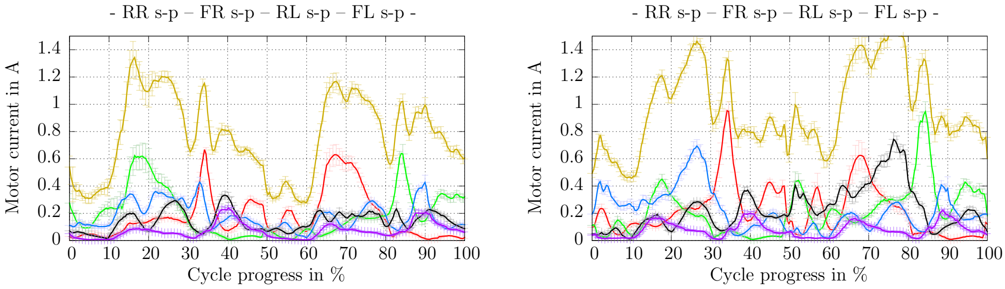

(e) Incline of −15° with *setup* $\overline{L}$ *S*. (f) Incline of −15° with *setup* *L* *S*.

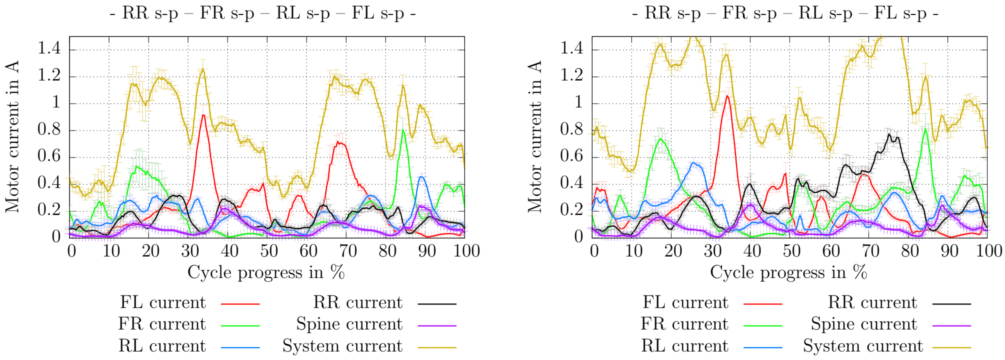

(g) Incline of −20° with *setup* $\overline{L}$ *S*. (h) Incline of −20° with *setup* *L* *S*.

Figure 5.18: Motor currents while walking on *terrain ramp* with *speed setting ramp* in different setups and inclines.

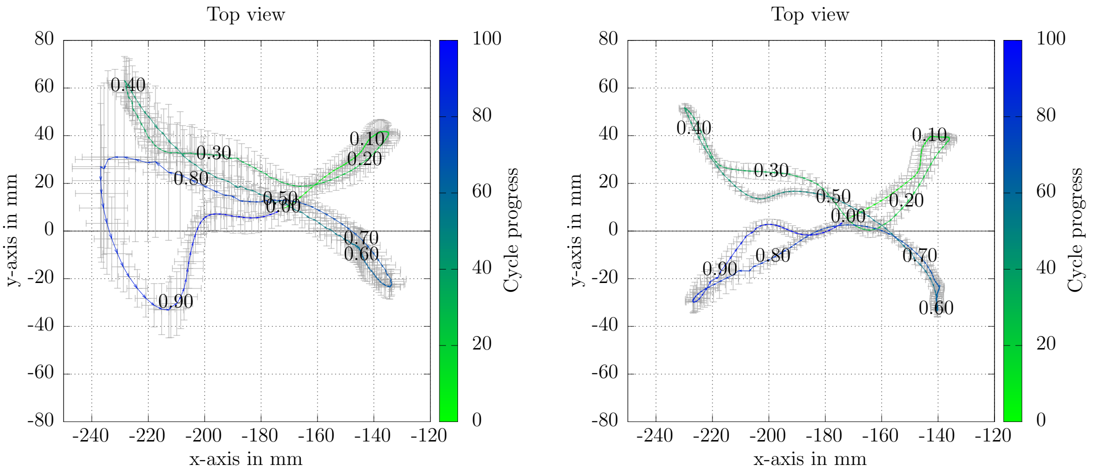

(a) Local control loop inactive and spine active (*setup* $\overline{L}$ S).

(b) local control loop and spine both active (*setup* L S).

Figure 5.19: Shifting the zero moment point while walking uphill a slope of 20° with different setups and *speed setting ramp*.

By comparing the movement of the ZMP in an incline of 20° from *setup* $\overline{L}$ S, as shown in Fig. 5.19(a) with the one from *setup* L S (displayed in Fig. 5.19(b)), it can be seen that the deviation in the setup with active local control loop is much less compared to *setup* $\overline{L}$ S. This is the result of the reduction of occurring torques in the beginning of the stance-phase. In addition, a better form closure between sole and ground is achieved with active local control loop, which leads to an increased traction.

This is similar to the earlier presented result regarding the ZMP motion in the gravel field, where the local control loop also produced a motion with less deviation, resulting in a more reliable walking. A smaller deviation in *setup* L S compared to *setup* $\overline{L}$ S can be seen in all experiments, where the robot is walking uphill.

While walking downhill with *setup* $\overline{L}$ S, the deviation of the ZMP is much smaller than for uphill walking. Still, *setup* L S shows an improvement for all inclines up to $-10°$.

However, in slopes with an incline of $-15°$ or $-20°$, the mean deviation is equal or even larger than the one from *setup* $\overline{L}$ S. Fig. 5.20(a) shows the data for *setup* $\overline{L}$ S in an incline of $-20°$ and Fig. 5.20(a) the one of *setup* L S.

Conclusion In positive inclines as well as in slopes with inclines of up to $-10°$ the robot's CoM moves in a more consistent manner with only a few outliers when the local control loop is active. The shown ZMP trajectories are more erratic compared

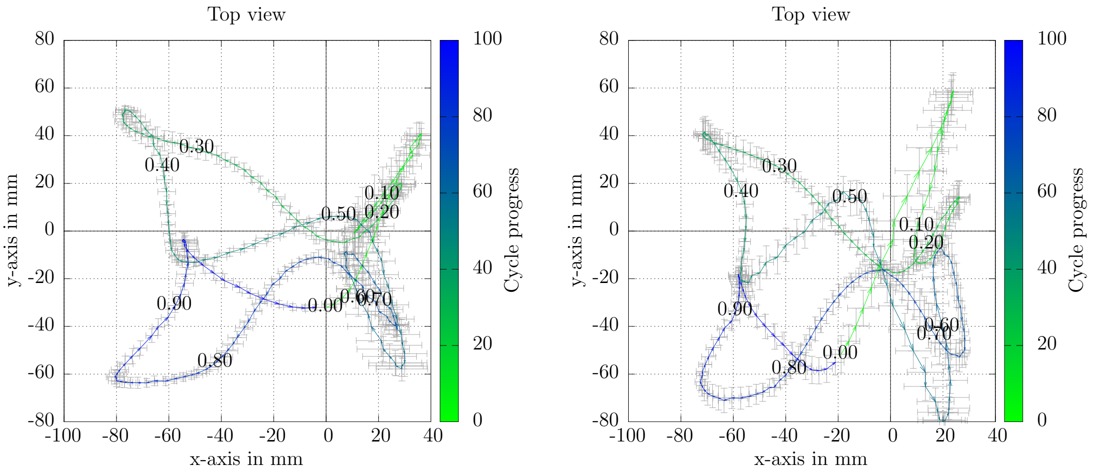

(a) Local control loop inactive and spine active (*setup* $\overline{L}$ S).

(b) Local control loop and spine both active (*setup* L S).

Figure 5.20: Shifting the zero moment point while walking downhill a slope with −20° with different setups and *speed setting ramp*.

to CoM trajectories, because of occurring short-term accelerations during walking and autonomous posture changes, but allow a clearer presentation of the differences between *setup* $\overline{L}$ S and *setup* L S. Yet, also for the ZMP trajectories, a smaller deviation is observed in all uphill walking scenarios as well as in downhill walking up to −10°. Lower outliers indicate a more stable behavior of the robot.

For this experiment, the central question is whether the stability is sufficiently increased to justify the increased energy consumption. Unfortunately, for inclines of more than −10°, a larger deviation is observed in the ZMP trajectory. It can be stated that the robot's increased energy consumption does not result in a more stable downhill walking. One possible solution to remedy the situation is a context-based adaption of the local control loop, which is shown in the following section.

5.6.4 Context-Based Adaption

As seen earlier, with increased inclines the local control loop is more and more inefficient while walking downhill. To remedy this drawback, an increased context-based adaption for uphill- and downhill walking of the local control loop is needed, to merge the best aspects of each setup into Charlie's control system. Currently, the low level controller has only limited context awareness regarding the step cycle progress. Additional information has to be either provided by higher levels or higher levels have to adjust the behavior of the local controller directly.

As depicted in 4.1 in chapter 4 on page 72, an interface between MCS and the local controller is implemented to allow an external parameter configuration. For the following experiment, the implementation of Charlie's control software has been extended in such a way that the MCS provides the local controller with high-level data like the robot's roll and pitch values. The local controller uses this data to modify its own behavior: a desired position offset of the feet is sent to the ankle joint while walking on a level surface or uphill. When the body pitch is below -5°, the local controller remains active but stops sending position offsets to the ankle joint.

Presumption After providing the local controller with the robot's orientation data, it is expected to see two different behaviors in the ankle joint while walking in inclines. In addition, it is to be expected that neither the robot's turning motion on an incline nor the mode switching of the local controller results in an unstable behavior of the robot.

Setup In this experiment, Charlie is walking uphill a slope with an incline of 10°, performs a 180° turn on top and starts walking downhill. The walking pattern is not stopped at any time of the experiment. Due to missing imaging systems and the absence of autonomy regarding self-localization and decision making, the operator has to decide when to start and stop the turning motion. The operator's involvement, however, is limited to this one action.

Evaluation In Fig. 5.21, the adaption of the local control loop behavior by the MCS is shown in an exemplary manner on the rear right foot. In contrast to the data shown before, in which average values per walking cycle progress are presented so far, the data in this figure is depicted over the total experiment runtime. The measured and desired pitch angles of the right rear leg are shown in green and blue, respectively, and the robot's pitch angle, measured by the installed IMU, is indicated in red.

The turning motion starts at $t = -130\,\mathrm{s}$, when the robot reaches the top of the ramp, and is terminated after a 180° turn at $t = -20\,\mathrm{s}$. During the uphill walking, the local control loop remains active. This decision is made based on the given context, consisting of the robot's walking mode and the incline measured by the IMU. The movement of the ankle joint, as in the former experiments, is based on the progress of the walking cycle for each leg. With the turning motion, the context

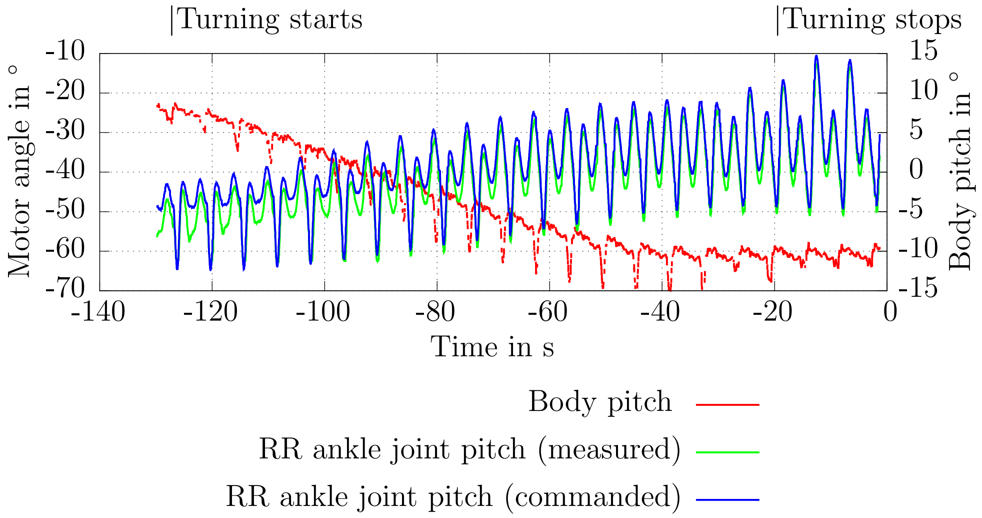

Figure 5.21: Walking up and down a slope with 10° and active local control loop. In the beginning (while walking uphill) a deviation of the foot's pitch of up to 20° is allowed, however, with the turning motion the context changes (from uphill motion to downhill motion) and thus does the behavior of the local control loop.

starts to change and so does the behavior of the local control loop, as it can be seen in the figure starting at $t = -83\,\mathrm{s}$. The pitch angle is constantly decreased and as soon as it is below $-5°$, the local control loop configuration is autonomously changed from *setup* $L\ S$ to *setup* $\overline{L}\ S$ and a deviation from the desired trajectory is no longer allowed. However, in the data a small deviation of about 2° can be seen. This is mainly because of two factors, mechanical play and the control error within the position controller.

Conclusion In this experiment it is shown that it is generally possible to modify the behavior of the local controller online and based on the given context. While walking uphill, the robot takes benefit of the local controller. As soon as the body pitch is decreased to $-5°$ or below, the robot changes the configuration from *setup* $L\ \overline{S}$ to *setup* $\overline{L}\ \overline{S}$, or from *setup* $L\ S$ to *setup* $\overline{L}\ S$. In addition, it can be stated that the turning motion on the incline (resulting in an oscillating body pitch) and the simultaneous executed mode switches of the local controller show no negative effects on the robot's stability.

In a next step, this approach can be extended by the behavior library implementation introduced in [DBBK15]. In Dettmann et. al's approach, a multi-legged robot learns from the experiences it makes during the interaction with the environment, measures its performance and creates a knowledge base. This knowledge base links the robot's locomotion behaviors to the evaluated performance for the known contexts. Then, a case-based reasoner is used to select the most suitable motion control parameters for the desired action based on the given context.

5.7 Conclusion of Four-Legged Walking Experiments

In the following, the gained results and impressions during the experiments with the Charlie are summarized and the benefits and deficits are pointed out. At first, it can be stated that the robot's morphology as well as its mechatronic design allows to carry out a large number of experiments in different tested terrains and inclines. Experiments are performed within the laboratory on a flat surface, on the slope with an adjustable inclination of $-20°$ to $20°$, and outside in different substrates, e.g., a gravel field. With these experiments, the functionality, e.g., of the local control loop is analyzed in different environments.

It can be stated that the local control loop not only reduces the overall power consumption of the legs but has also an effect on the forces and torques acting on the robot's body. Even more important is the fact that the local control loop improves the robot's stability and allows the system to traverse certain terrains, which it could not cover in a stable manner with deactivated local controller. This means, that at least for the Charlie robot, the local controller softens the necessity to use an ideal walking parameter set based on the given context to gain stable locomotion.

While walking in inclines, however, an initial drawback using the local control loop is shown for downhill walking. The robot is stable while walking downhill, but activating the local controller results in an increased overall power consumption, whereas the stability remains the same. This initial drawback could be dissolved by increasing the context-based adaption abilities of the local controller.

Chapter 6

Control- and Pattern Reusability

A defining feature of a multi-locomotion robot is its ability to move forward with different motion patterns, allowing an extension of possible fields of application. In addition, such a robotic system like Charlie could also be used for another scientific problem. The nature of the development of bipedalism is still an unsolved question and with, e.g., thermoregulatory advantages [Whe91], a decreased availability of resources [IY96], the cost of walking [SRP07] [PRS09], various theories exists trying to explain this evolutionary process. Due to the selected quadrupedal and bipedal motion mode, Charlie offers the possibility to evaluate, if control mechanisms and motion patterns from quadrupeds can be used for bipedal locomotion.

This chapter presents the evaluation of the experiments performed with the robot Charlie in bipedal motion mode. First, the posture transition from a quadrupedal stance to the bipedal posture is shown. Second, the first parameter transfer from crawl gait to bipedal gait is described. In the first experiments, the robot is externally supported to determine optimal walking parameters like walking speed or stability controller offsets. In a next step, experiments of unsupported bipedal walking are performed. The recorded data allows a comparison of the motor trajectories used for quadrupedal and bipedal walking. These trajectories can be compared with each other since both walking gaits are performed with one robot without the need of mechanical modification. The chapter concludes with the experimental evaluation of transferring the local controller used for quadrupedal locomotion to bipedal locomotion.

This chapter is supported by one peer-reviewed publication:

- D. Kuehn, M. Schilling, T. Stark, M. Zenzes, and F. Kirchner. *System Design and Field Testing of the Hominid Robot Charlie* In Journal of Field Robotics, 2016

6.1 Posture Transition

To realize context-based, adaptive locomotion, the robot Charlie has to change its posture in order to be able to perform quadrupedal or bipedal locomotion. In contrast to walking, the posture transition is not an uniform, rhythmic motion. Two behaviors are needed, to make the posture change complete. The stand-up behavior is needed for a transition from a quadrupedal to a bipedal pose. The bi-to-quadrupedal behavior is responsible for the opposite, the transition from a hominid stance to the quadrupedal pose. The stand-up and bi-to-quadrupedal behaviors are defined motion sequences, whose primary requirement has to be met: the termination of the walking process. The image sequence in Fig. 6.1 shows the transition from the quadrupedal posture into an upright pose. During the transition, the robot is stable at all times, since the CoM stays inside the support polygon spanned by Charlie's MPCF.

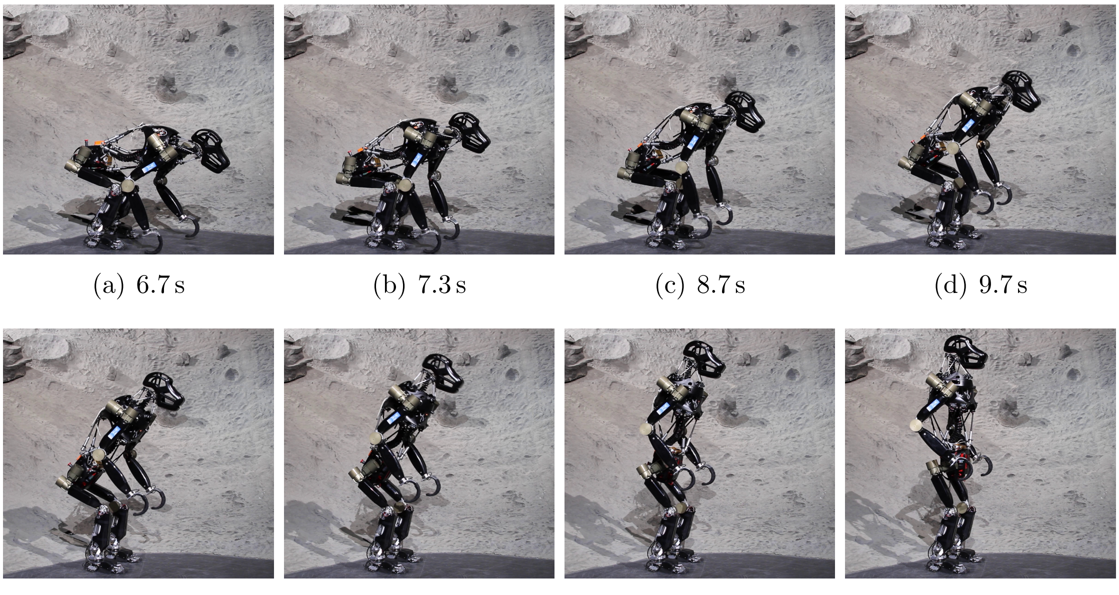
(a) 6.7 s (b) 7.3 s (c) 8.7 s (d) 9.7 s

(e) 10.5 s (f) 11.1 s (g) 11.9 s (h) 12.7 s

Figure 6.1: Charlie's transition from a quadrupedal into a bipedal posture [KSS+16].

The complete motion sequence takes about 15 s and can be divided into different phases. In the first phase of the stand-up motion, the position of the rear legs is adapted according to the desired footprint for bipedal walking. The rear legs are lifted one after the other and moved closer together on the y-axis compared to the quadrupedal walking posture, in order to avoid a straddle stance in the final bipedal pose. The narrower the stance, the less motion of the CoM is necessary to stay inside the support polygon before one leg is lifted later on while walking. In the second step, the front legs have to be freed from supporting the body weight. To achieve this, Charlie's CoM is shifted backwards until the projection of the CoM on the ground lies within a convex hull, which is formed only by the MPCF. To shift the CoM, the limbs as well as the spine are actively involved (shown in Fig. 6.1(b)). After the shifting phase, the rear legs are maintaining the robot's stability and the front legs are completely load free, see Fig. 6.1(c). In the final phase, the upper body rises until an upright position is reached, see Fig. 6.1(h). This motion, again, is supported by the leg joints and the spine.

While standing in the final upright posture, the power consumption of all joints to hold the position is 2.4 W (50 mA at 48 V). In comparison, standing in the quadrupedal posture requires about 3.4 W. This is due to the robot's pose, where the angular position of the joints in the rear legs is favourable for the occurring torque on the joints and also less joints are loaded.

Basically, the transition from a bipedal stance into a quadrupedal posture works the other way around. First, the robot bends the knees of its rear legs and rotates the spine, until the stretched right front arm establishes ground contact. The spine is driving to its zero position, while the second front arm establishes ground contact as well. Afterwards, the CoM is shifted to the CoSP of all four legs. The last step is performed by the rear legs, which are lifted and shifted back to the starting position for quadrupedal walking on the y-axis.

Once a transition to either a bipedal or quadrupedal posture is completed, the respective walking pattern can be started. During the transition, the internal CSs are adapted as well, except for the body-CS. Thus the context has no influence on the walking pattern generator. Parameters like forward direction, lateral motions, foot swing height or step length are posture independent and stay on the same axes within their used CS. This implementation simplifies the control of the robot for both, a human or a future deliberative control layer. In addition, it is also beneficial for experimental evaluations, as shown in the following.

Figure 6.2 presents the sum of the measured forces in the rear feet in the robot's body coordinate system, where the x-axis points in forward direction, y to the left and z upwards. As mentioned in the control section, the body-CS x-axis is defined by the axis along hip and shoulder. In the beginning, the robot's weight is distributed to all four legs. In the further course, the robot's CoM is shifted between its rear feet and the force in z-direction increases.

At about 8 s, the robot's CoM is between its rear feet and the front feet are load

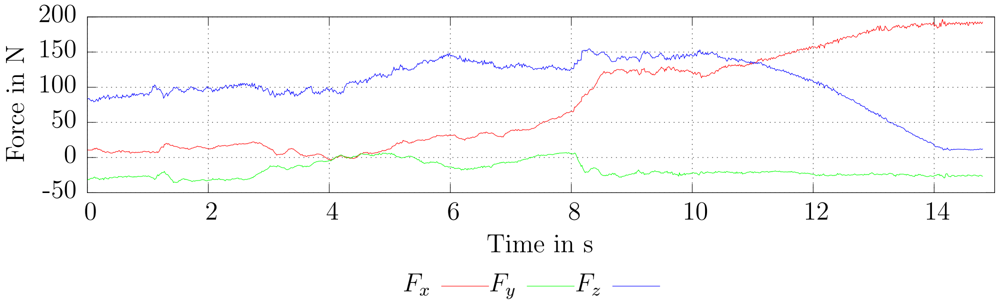

Figure 6.2: Sum of the measured force within the body-CS of both rear feet during the transition from a quadrupedal to a bipedal posture.

free. During the transition, the body rotates about 85° around the y-axis and so does the body-CS. This affects the body-CS in a way that the x-axis points now upwards and the z-axis now points into negative x-direction of the rest-CS. This can be seen at 11 s. At the end of the stand up motion, the measured force in x Fx is close to the expected force of 211 N (due to the robot's weight of about 21.5 kg). Since the body is rotated around 85°, a force in z Fz is measured as well and has to be added to Fx, to get the overall force $Fabs$. The force measured on the y-axis can be explained with tensions which build up between the legs during the stand-up motion.

6.2 From Quadrupedal to Bipedal Walking

Once the robot stands upright, it is possible to experiment with the bipedal walking pattern. Since one aim is an investigation if (and if so how much of) the walking pattern, activation pattern (in form of trajectories) or control functions (partially or in general, like the local control loop) of the four-legged walking can be transferred to a two-legged walking, the four-legged motion pattern including its cycle time is reused as a starting point for bipedal walking. The walking pattern generator is the same as for four-legged walking, since parameters like foot swing height or step length are commanded within the rest CS and therefore still on the z- or x-axis, respectively, of the transformed body coordinate system. This is particularly relevant to avoid a switching between otherwise context-dependent control software regarding behaviors or motion templates.

In the first test runs it has been observed that an external support is needed to keep the robot stable. This is true for all three walking states, the start-up phase of the walking, the walking with the desired speed and also for the slow down phase. However, reusing the quadrupedal parameter set seems to be a promising approach, since from a subjective point of view, the robot needed only little support while walking with the desired speed.

In general, locomotion with multiple legs is significantly more stable compared to bipedal locomotion, since multi-legged robots are able to span a larger support polygon. In literature, different approaches have been explored to improve the stability of humanoid robots by interacting with the environment, like finding hold on railings [HHK+04], or by using additional tools like trekking sticks [KC14], or canes [KAS+13a], resulting in a tripod stance and thus generating a larger support polygon. In addition, alternative methods are studied in which the arms of the robot are used to compensate for the moments of inertia of the feet [KKK+03]. In contrast to these robots, preliminary studies, which are not described in this thesis, indicated that Charlie's front legs have not enough weight for this purpose.

However, Charlie's stiff claw on the front legs can act as hand and allows a human to support the robot externally. Therefore, in contrast to the above mentioned examples, for the following experiment an approach is chosen, which requires no modification of the robot's hardware, to maintain the robot's body weight and its weight distribution.

Objective The objectives of this experiment are (i) to determine the required external support while walking, (ii) to investigate, if the robot's movement speed relates to the needed support and (iii) to analyze, if the stability is increased when the desired trajectories are executed faster. The experiment is motivated by the subjective opinion is that during the first walking trials only little support was necessary to realize a stable motion.

Experimental Setup During bipedal walking, the front legs are motionless and hold their commanded position as it can be seen in Fig. 6.1(h). Since in Charlie each limb features a six DoF force/torque sensor, the necessary human support to stabilize the robot can be measured at all times. For this stabilisation, the robot has to stretch the arm to the side (see Fig. 6.3). When one leg is in its swing phase, the support polygon is as small as the dimension of one rear foot.

For a static bipedal walking (no forward motion), the CoM-trajectory is shaped like an line for each step. This is in contrast to the quadrupedal CoM-trajectory which is shaped like an "8", as shown above. Critical phases concerning stability are the outermost points of the CoM-trajectory, in which the CoM's direction of motion is inverted. By moving the CoM in direction of the other foot, an acceleration occurs, which moves the robot's ZMP in the opposite direction and provides a possibility that the ZMP exceeds the border of the support polygon, resulting in a robot which tends to tip over. The stability controller in Charlie's MCS is optimized for quadrupedal walking. For bipedal walking, the output of this controller is reduced to 30 % to obtain less shifting along the y-axis. This reduction is specified on the basis of preliminary tests with this setup.

In this experiment series, the walking cycle time starts at 5 s and is reduced in each run. This results in experiments with a walking cycle time of 5 s, 4.7 s, 4.3 s, 4 s, 3.7 s, and so forth. The last experiment in this series is performed with a cycle time of 1.3 s. For each cycle time, the experiment is repeated three times with at least ten complete steps per run. One step cycle includes the lift-off, shifting, touchdown, and stance phase for both legs. The overall walking distance on the other hand is kept constant and is set to 100 $\frac{\text{mm}}{\text{s}}$. This means that when the cycle time is reduced, the step length decreases as well.

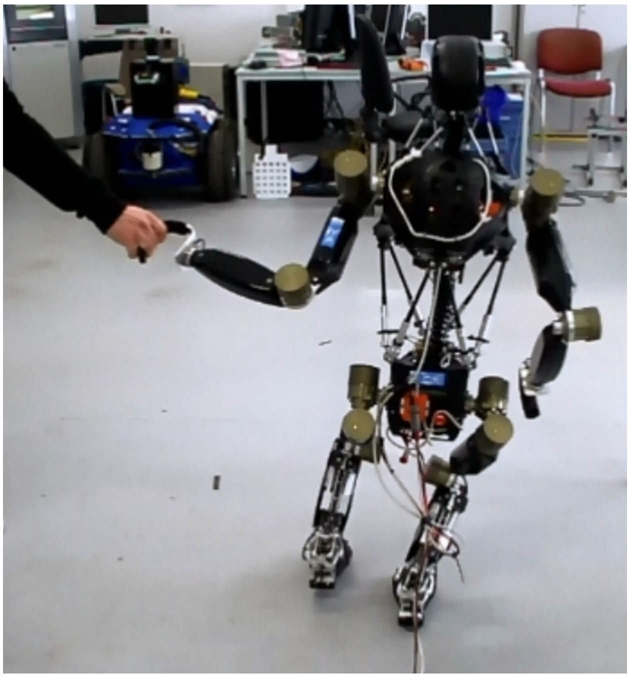

Figure 6.3: Charlie is externally supported on its front left arm while walking on two legs.

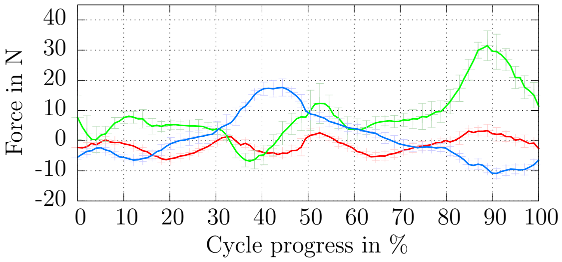

(a) Measured forces at a gait cycle of 5 s.

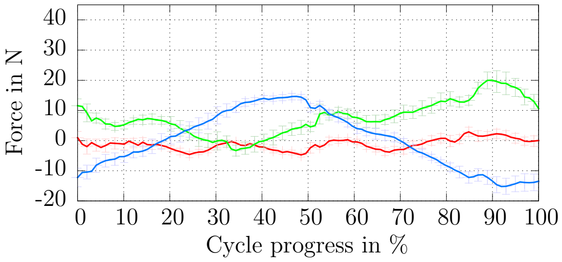

(b) Measured forces at a gait cycle of 4 s.

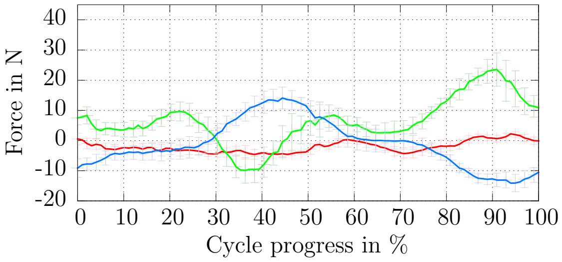

(c) Measured forces at a gait cycle of 3 s.

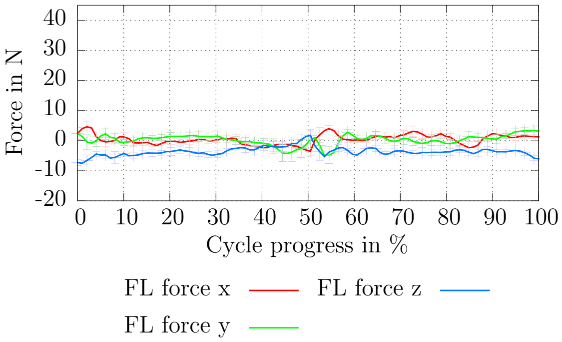

(d) Measured forces at a gait cycle of 2 s.

Figure 6.4: Measured force data of the front left arm while walking bipedal with support.

Evaluation The data in Fig. 6.4 show the measured forces of the left arm while walking one complete step cycle; in other words, the support needed for walking. The figure shows only results gained from the experiments where the walking cycle time (*wct*) is an integer number. The remaining plots are presented in the appendix of the thesis (see Fig. 8 on page 209 and Fig. 9 on page 210). To allow a better comparability between the different cycle times, the cycle time is shown as percentage of the overall gait progress. The absolute temporal component is not shown within the plot, but indicated below each figure.

During walking, two phases can be identified (one for each leg's swing-phase), where the robot requires external support, as the blue line indicates in Fig. 6.4. This is between $wcp = 25\,\%$ and $wcp = 50\,\%$ for the left leg and between $wcp = 75\,\%$ and $wcp = 0\,\%$ for the right leg. Between $wcp = 0\,\%$ to $wcp = 25\,\%$ and between $wcp = 50\,\%$ to $wcp = 75\,\%$, the ZMP is shifted laterally. In these phases, both feet are on the ground.

While walking with a cycle time of 5 s (see Fig. 6.4(a)), it can be seen that during the first leg swing motion an external support of less than 20 N is required to stabilize the robot, including shear forces. During the swing motion of the right leg, shear forces on the y-axis are introduced to the force/torque sensor, resulting in an absolute force of 30 N. The z-axis, however, measures a support of only 10 N.

The faster the walking is, the less support is needed. In Fig. 6.4(b), it can be seen that the needed support is reduced to an absolute force of 15 N during the swing motion of the left leg and 25 N for during the right leg's swing phase. Walking with a cycle time of 2 s, shown in see Fig. 6.4(d), a distinct amplitude cannot be seen in the data.

Conclusion In this experiment series, the designed time to complete one step cycle is reduced in each run. The walking speed, however, is kept constant at $100\,\frac{\mathrm{mm}}{\mathrm{s}}$. Walking with a cycle time of $wct = 5\,\mathrm{s}$ result in a step length of about 500 mm, whereas a $wct = 2\,\mathrm{s}$ result in a step length of about 200 mm per cycle. A reduction of the cycle time results in faster limb movement, yet with smaller steps per cycle. Walking with $wct = 5\,\mathrm{s}$ required two steps to cover a distance of 100 cm, whereas with a cycle time of $wct = 2\,\mathrm{s}$ five steps are necessary. Due to acceleration and speed limitations in Charlie's actuators, the speed can be increased only up to a certain limit, thereafter the actuators cannot follow their given motion trajectory. This is the case for a cycle time of $wct = 1.3\,\mathrm{s}$.

It can clearly be seen that the faster the robot performs its motion, the less support is required (see Fig. 6.4(d)). In fact, the data indicate that for Charlie an ideal cycle time for bipedal walking is at about 1.6 s. This results in a step length of about 160 mm per cycle.

The output of the stability controller is reduced to decrease a shifting on the y-axis. When the controller output remains equal to the one used for the quadrupedal walking experiments, a force can be measured also while walking with a cycle time of $wct = 2.0\,\mathrm{s}$ or below (not shown in this section).

6.3 Bipedal Walking

In Charlie, a ZMP based control approach is implemented, as it is used in many humanoid robots. The mass of the individual structures as well as their positions are used and considered as one single point. In the previously performed experiment, it is found that Charlie is generally able to walk with a stable bipedal walking pattern with a gait cycle time of about 1.6 s. By increasing the cycle time to gain a slower and more static pattern, which can be compared with Charlie's four-legged locomotion pattern, the robot requires external stabilizing assistance. In literature, the bipedal and quadrupedal locomotion in chimpanzees is analyzed in detail and a comparison of the rear limbs joint angles can often be seen, e.g., in [SRP07], [PRR14], or [OLD+15].

Objective The following experiment is performed to determine, if a similar walking pattern or at least a similar actuator activation pattern can be used for bi- and quadrupedal walking.

Experimental Setup To generate an appropriate walking pattern, the robot's morphology has to be taken into account. Charlie's morphology differs from the one of humans and humanoid robots, therefore the walking patterns of humans, which are very well documented in literature, are only partially suitable. The bipedal walking in chimpanzees was analyzed by Sockol [SRP07]. In addition, he compared the walking mechanics between chimpanzees and humans and showed the differences, e.g., in the posture between both (see Fig. 6.5). Therefore, Charlie's body height during the bipedal stance is reduced by 10 cm, which results in a bent-hip - bent-knee posture while walking (shown in the center image in Fig. 6.5). It is to expect that this posture requires more energy in the first hip joint and knee joint compared to a posture with stretched knees, but leads to a more stable walking gait in Charlie, because of a lower CoM.

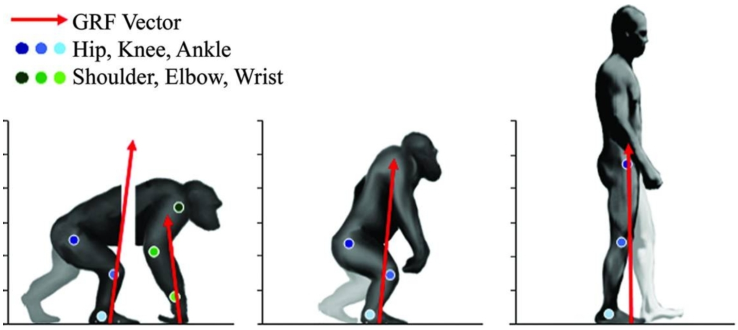

Figure 6.5: Comparison of walking postures in chimpanzees and humans (source: [SRP07]). GRF: ground reaction force.

In [PRR14], Pontzer stated that Chimpanzees tended to use shorter and faster strides when walking bipedal compared to the quadrupedal gait. To allow a comparison between the quadrupedal and supported bipedal gait, parameter set *speed setting ramp* with a walking speed of 30 $\frac{\mathrm{mm}}{\mathrm{s}}$ is chosen, which results in a stride length of 150 mm per cycle. In comparison, the stride length for unsupported bipedal walking is 160 mm per cycle and thus only marginally different.

However, to minimize dynamic influences on the robot, the lift-off motion of the feet is set to 40 mm, which reduces occurring moments of inertia from the legs' lifting motion. The remaining parameters are equal to the one used while walking in a quadrupedal posture and the data is recorded on laboratory floor without active local control loop and without active spine motion (*setup* $\overline{L}\ \overline{S}$). In addition, for supported bipedal walking the output of the stability controller is equal to the one used for quadrupedal walking.

For unsupported bipedal walking, the following parameters have to be adapted, to realize an interference-free walking: the cycle time is set to 1.6 s and the step length is set to 100 mm, which results in a stride length of 160 mm per cycle. In addition, like in the previous experiment, the output of the balance controller for a lateral motion is reduced to 30 % and for the robot's body, no pitch and roll motions are allowed, to obtain less shifting along the y-axis. The desired ZMP is shifted 30 mm in walking direction, to lean the robot's body and its CoM to the front of the feet.

To gain reproducible data of the walking experiments, the data is recorded while walking indoor on linoleum floor. The image sequence in Fig. 6.6 shows the bipedal walking. In this figure, the bent-hip - bent-knee posture can be seen.

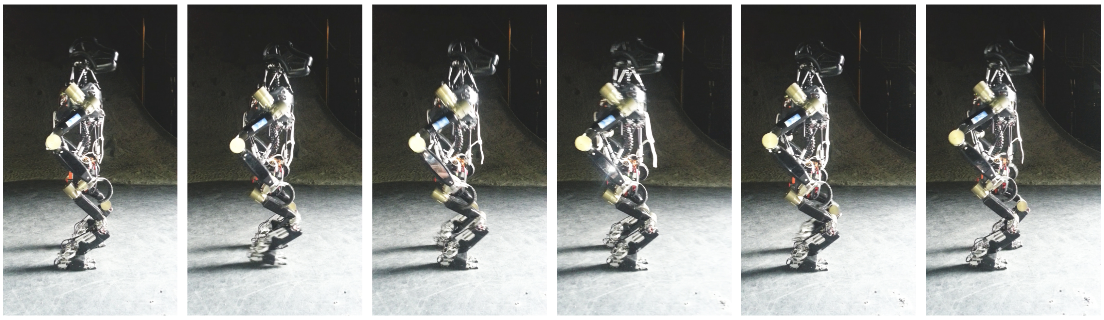

(a) Double limb stance (b) Swing phase right leg (c) Touch down right leg (d) CoM shift (e) Swing phase left leg (f) Touch down left leg

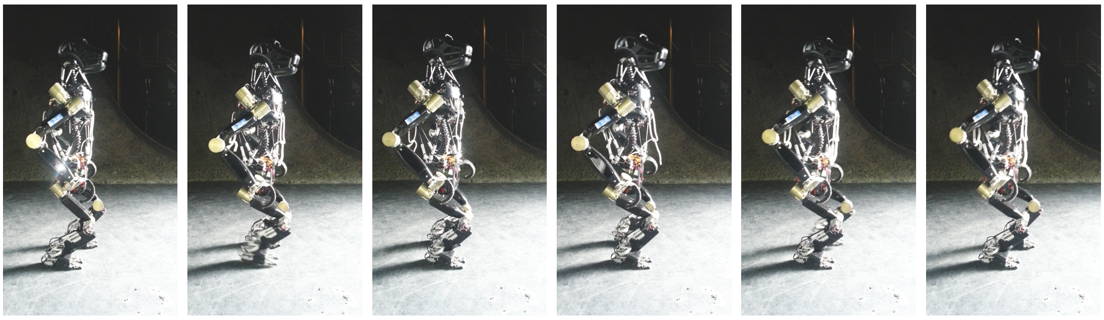

(g) CoM shift (h) Swing phase right leg (i) Touch down right leg (j) CoM shift (k) Swing phase left leg (l) Touch down left leg

Figure 6.6: Image sequence of Charlie walking bipedal.

Evaluation Figure 6.7 depicts the measured joint angles of both motion modes for the rear left leg. The joint angles while walking with the externally supported bipedal gait are visualized with a green line and the results from the faster bipedal gait without assistance are shown in blue. Due to the similarities between left and right leg, the data for the right leg is omitted at this point, but shown in the appendix (Fig. 10 on page 211).

The robot's CoM is shifted from the left side to the right vice visa between $wcp = 10\,\%$ and $wcp = 20\,\%$ of the walking cycle progress as well as between $wcp = 60\,\%$ and $wcp = 70\,\%$, respectively. During these two phases, both rear legs have ground contact.

The data shows that the joint trajectories are not identical, but a similarity in shape can be seen. This is especially true for the quadrupedal walking compared to the bipedal walking with external support. For the first hip joint, an angle offset of about 100° can be seen in Fig. 6.7(a), which is due to the different posture between both motion modes. The amplitude range does not differ significantly between quadrupedal and assisted bipedal walking, but for bipedal walking without

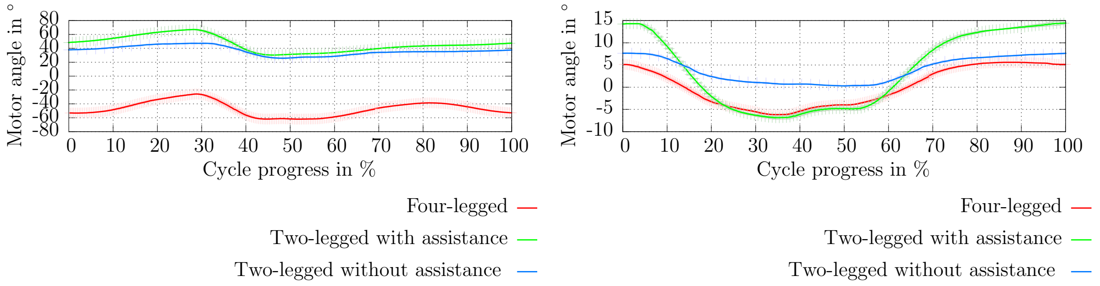

(a) Rear left hip joint 1 (b) Rear left hip joint 2

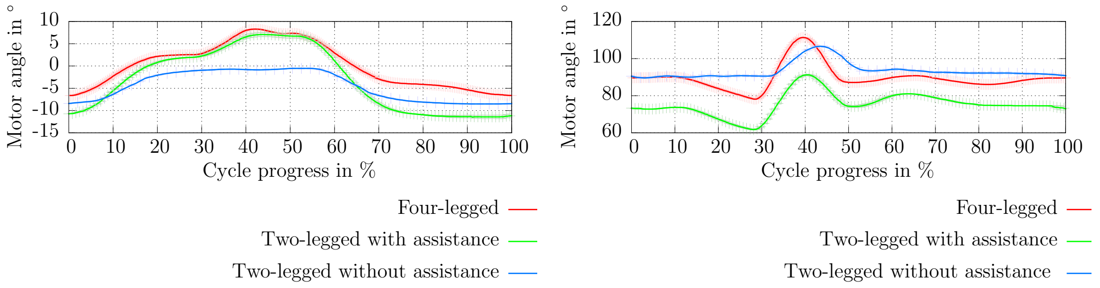

(c) Rear left hip joint 3 (d) Rear left hip knee joint

Figure 6.7: Comparison of the rear left leg's joint angles while walking quadrupedal and bipedal.

assistance, due to the reduced gait cycle time.

The amplitude of hip joint 2, shown in Fig. 6.7(b), differs around 10° between quadrupedal and assisted bipedal walking. A difference of around 5° between both walking patterns can also be observed in hip joint 3 in Fig. 6.7(c). Both joints are mainly responsible to allow lateral movements of the robot, which includes a lateral shifting of the CoM. In bipedal walking, the support polygon is limited to the rear feet and thus considerably smaller compared to the one obtained with the quadrupedal gait, where at least three legs form the support polygon. Therefore, for bipedal walking without assistance, the lateral body shift is reduced to obtain a certain distance between the ZMP and the edges of the support polygon. This can be seen in the amplitude for hip joint 2 and hip joint 3 in the corresponding figures.

The data of the knee joint, displayed in Fig. 6.7(d), again show a slightly shifted RoM. Like for hip joint 1, this is due to the pose of the robot. The differences in both bipedal trajectories can be explained with the adjusted parameter to allow Charlie to walk unsupported.

Conclusion It is shown that in Charlie a stable bipedal locomotion is realized with a bent-hip bent-knee walking. However, while walking especially with the unsupported bipedal gait, due to the dynamics of the movement speed the applied load on the rear feet is very high, which in a long term has detrimental effects on the actuator temperature and bearings in the ankle joint.

In Charlie, the joint angles of the two different gaits (quadrupedal and supported bipedal locomotion) display similar shaped trajectories in all four leg joints, as it could be expected due to the similarities of the respective parameter sets. More interesting is that this is also true for the unassisted bipedal walking trajectories, albeit in a weakened form. It can be seen, that minor adaption is needed to get from one gait to the other. To the best of my knowledge, this is the first time that trajectories of different kinds of locomotion are compared in one robotic system in a real-world application without taking changes in the morphology into account and the electromechanical design of the robot allows therefore the execution of further studies in this field.

A mechanical play within the structure of the rear leg is noticeable in the bipedal pose. When projecting Charlie's CoM on the ground while standing on one leg in a bipedal posture and a minor lateral force is applied, a CoM movement of about $\pm 29\,\mathrm{mm}$ in lateral direction can be measured. This also explains why an external assistance is required while walking with a slower motion. The heel structure, e.g., has a width of $50\,\mathrm{mm}$ (see Fig. 3.6 on page 49) and due to the mechanical play it is likely that the robot's CoM exceeds the edges of the support polygon, when one leg is in its swing-phase. For the faster walking, dynamic effects remedy the situation.

6.4 Local Controller for Bipedal Posture

An active compliance is implemented within the ankle joints in form of a local control loop (see section 4.5 on page 93). With this controller active, the ankle adapts itself actively by increasing or decreasing its roll and pitch angles, depending on the locally perceived torque. The controller can be compared to a monosynaptic reflex, the stronger the stimulus, the stronger the response. This means that the larger the measured value, the greater the roll-pitch motion.

Objective It is to investigate, if the implemented local control structure, which turned out to be useful for quadrupedal walking in unstructured environment, can contribute to the bipedal motion mode as well, either directly or in a modified form.

Therefore, the local controller is at first tested in a static case, where the robot stands motionless on a laboratory floor in a bipedal posture.

The parameters within the controller are optimized for the quadrupedal motion mode, where the acting torques are divided to three or four legs and are not perceived on only one or two limbs, as it is the case for bipedal walking. It is to determine if for the bipedal pose a different parameter set for the local control loop is required.

Presumption As shown in the quadrupedal experiments, the ankle joints are softened at the beginning of the touchdown phase and become more rigid, the more the walking cycle proceeds. It is expected that for bipedal walking this behavior is not feasible. The foot and ankle joint have to be rigid and not flexible at the beginning of the touchdown phase, otherwise the robot will not be stable at all and tipple over in walking direction. With the inverted functioning, the local controller is used in a different mode, and with the expected torques acting on the MPCF, an overshoot of the foot's roll and pitch angle is possible.

Setup As expected, in the first experiment-run with activated local controller it is immediately evident that the unmodified controller is not able to maintain a bipedal walking. The gait-states (swing- and stance-phase) can be applied to the legs and the local controller, even though the legs remain stationary. As soon as a torque is applied to the foot which is in the stance-phase, the pitch angle is decreased and the robot tumbles over.

On the basis of this observation, the local controller and its functionality are expanded by introducing an inverted operation mode. In the inverted mode, the foot is not adapting to the ground, but is moved according to the locally perceived torque. The actual pose is known to the MCS, therefore it is able to realize a context-based change of the local controller during runtime.

To determine, if a new parameter set for the local controller is needed as well as to investigate, how the local controller affects the robot's stability, the following experiment is performed. The robot is in a still stance on two legs with laterally extended arms. Alternating, on each hand a maximum force of about 13 N to 14 N is applied in direction of the robot's y-axis. When pressed with a force greater than 15 N, the robot tends to tip over laterally in the first of the following setups. The rear legs ground reaction forces are measured in four setups:

(i) Global stability control and local control are turned off

(ii) Global stability control is switched on and local control remains off

(iii) Global stability control is turned off and the local controller is active
(iv) Global stability control and local control are both active

Evaluation Since the first experiment with activated local controller did not result in a stable behavior, the evaluation focusses on the inverted function of the local controller. A force of 13 N to 14 N is applied to Charlie's left hand (in direction of the robot's y axis). Due to the manual application of lateral forces and the resulting reaction movements of Charlie, the application of a perfectly constant force was not possible. The rear legs ground reaction forces are measured in four setups (see Fig. 6.8). Initially, the force measured is approximately 105 N for each rear leg. A lower value indicates that the left leg of the robot is going to be levered and begins to lose ground contact. The higher the value, the more force is introduced onto the ground, which results in an uniform stance and also improves the traction between the foot and the ground.

It can be seen that in the first setup (i), in which both controllers are turned off, the contact between the foot and the ground is at its minimum compared to the other three setups (see Fig. 6.8). In the second setup, the global stability control of the robot is switched on, this means the higher control level tries to keep the system stable by using the appearing and measured acceleration by the IMU. In this case, an improvement of about 15 N can be measured. When the local control is enabled and the global stability control switched off, an improvement compared to the first setup of about 12 N can be seen. This value is kept in the same range, if both controllers are activated at the same time.

Conclusion The function of the local controller may be beneficial for the quadrupedal pose, but using it in the bipedal posture results in the robot tipping over nearly immediately. Therefore, Charlie's MCS was changed such that it can reconfigure the functioning of the local controller according to the given context. By inverting the local controller, the robot shows a stable behavior.

In the feet, the lowest force is measured when Charlie's stability controller and the local controller are deactivated. By activating either the local controller or the stability controller a higher force between foot and ground is measurable, which results in an improvement between 32 % to 36 %, respectively. Interestingly, the local controller produces a ground reaction force, which is nearly as high as the one achieved by the global stability control. When both controllers are active, an improvement of about 28 % can be seen compared to the initial setup, where the

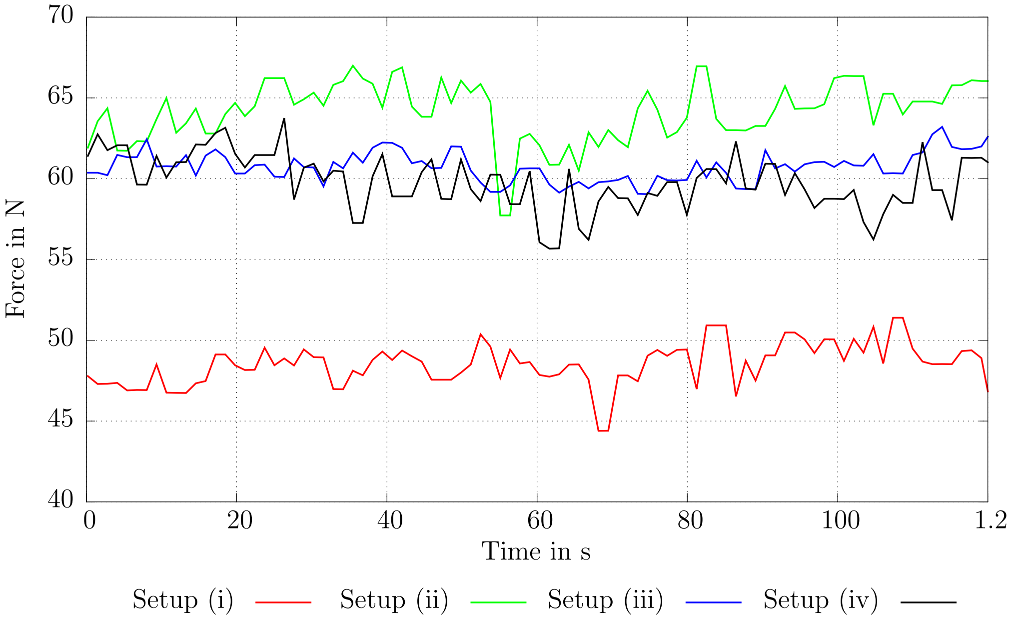

Figure 6.8: Measured force in z direction on the rear left leg while applying a lateral force of 15 N to the left front arm.

stability and local controller are deactivated.

However, when both controllers are active they seem to affect one another and the applied force to the ground is slightly reduced compared to the setups in which only one controller is active. In a next step, this controller is used during bipedal locomotion to analyze its influence in a dynamic case.

6.5 Two-Legged Walking with Active Local Control Loop

In a static case, where the robot is standing still, the local controller increases the measured ground reaction force between foot and ground. In addition to the static case, to allow a general statement regarding the transferability of this local controller, it has to be analyzed while walking, too.

Objective The following experiment is performed to examine, if the inverted local controller can be used for bipedal locomotion as well.

Presumption It is expected that for bipedal walking a limitation of the ankle joint's maximum deviation from the commanded angle will be necessary. Otherwise, due to the dynamic gait with the expected high moments during unsupported walking, the roll-pitch adaption can destabilize the robot. In addition, it is assumed that the local controller is more beneficial while walking with a slower speed, due to the reduced dynamics acting on the feet and force/torque sensor. However, this gait cannot be tested without external support. Therefore, it cannot be determined, if the human support or the local controller is responsible for potential improvements.

Setup The experimental setup is equal to the one described earlier in section 6.3. In addition, the local controller is activated and the function inverted. The acting moments on the rear feet are increased compared to the quadrupedal posture, due to halving the number of legs participating in locomotion. In preliminary performed empirical studies the internal parameters of the local controller were redefined, including the threshold of the stiffness of the compliant behavior. The larger the threshold the smaller the movement of the foot. These initial runs showed that a reduction of the maximum allowed deflection from the desired angle from 20° to max. 4° is useful. A deviation, e.g., of the pitch angle of up to 20° has a destabilizing effect to the robot.

Evaluation The changes in the threshold are necessary to allow the robot to walk. Besides, the changes affect the intensity of how the foot is reacting to the occurring torques as well. The larger the allowed deflection, the less is the robot able to walk without support. Even a small deflection of 4° results in a behavior, where the robot is out of balance after some time, therefore no reliable data could be recorded.

Conclusion For the local controller no internal parameter set is found, to increase the stability of the robot's bipedal walking behavior. A limitation of the maximum allowed deflection from the desired angle is necessary as well, to allow the locomotion. However, the closer the limits are to zero, the more stable is the walking.

It is assumed that for a less dynamic gait, as shown with the supported bipedal walking, the local controller can contribute to the stability of the bipedal walking. However, as long as human support is needed, the source of potential improvements cannot be determined.

6.6 Conclusion of Two-Legged Walking Experiments

It can be stated that the morphology and the mechatronic design of Charlie enables the robot to adopt two fundamentally different postures. In Charlie, a posture transition behavior is implemented, allowing the robot to change from a quadrupedal to bipedal pose and vice versa. Once in the bipedal pose, the quadrupedal walking pattern is used as a starting point to determine a parameter set which allows Charlie to demonstrate bipedal locomotion. Experiments are performed with two bipedal walking patterns, the first one results in a slower movement of the limbs, where it is necessary to support Charlie externally and the second one in a more dynamic walking, in which no external support is needed.

A mechanical play within the structure of the rear leg is noticeable in the bipedal pose, resulting in a possible, yet undesired, lateral CoM movement. Projecting the robot's CoM on the ground while Charlie stands in a bipedal pose on one leg and applying a minor lateral force, the movement of about ±29 mm in lateral direction can be measured. This is why the start-up of the bipedal gait results in an unstable system. Using a Finite Element Method (FEM) simulation, the mechanical play can be seen in the rear foot's ankle joint (±5.9 mm), an elastic deformation of ±19 mm can be seen in the leg structure and ±4 mm results of rotational play within the hip actuators.

In forward direction, the measured play is less than in lateral direction (about ±15 mm). The pitch axis of the ankle joint allows a movement of ±9.8 mm of the projected CoM. The spindle drive is determined as main source of error. Due to the shape of the thigh and the lower leg, the elastic deformation is only ±1.2 mm. Like for the y-direction, the mechanical play of the hip actuators is about ±4 mm.

Charlie's heel and mid-foot structure have a width of 50 mm and 80 mm, respectively, and therefore it is likely that the robot's CoM exceeds the edges of the support polygon, while the system is standing on one leg. This explains the required external assistance while walking with a lower motion. The walking becomes stable when walking with a faster motion and reduced lateral shifting of the robot's body. However, this play can not be easily resolved but would result in changing the mechanical design of the leg structure.

Nevertheless, it can be stated that Charlie's locomotor system basically enables the robot to walk quadrupedal as well as with a rudimentary bipedal gait. This presents the possibility to investigate the transferability of motion patterns and control schemes from one gait to another in further studies. Yet, it has to be mentioned that Charlie is modeled after chimpanzees and therefore its morphology differs from systems which are categorized as humanoid robots and so does the bipedal walking gait.

Based on performed experiments and presented results, in Charlie's walking patterns distinctive characteristics in the individual joint movement trajectories are identified, which are similar for both, the quadrupedal and bipedal locomotion mode. The parameter set chosen for the quadrupedal gait, which has an effect on the characteristics of the joint trajectories of this gait, may not be the optimum and should be subjected to further investigations. In a further experiment, the local controller function is adapted based on the bipedal context. Unfortunately it has to be stated that the local controller does not improve the bipedal walking in the same manner as the quadrupedal walking. In a static case, the feet ground reaction forces are measured, while applying a lateral force. It is shown that the applied force to the ground with activated local controller is nearly as high as the one achieved by Charlie's internal stability controller, but also that the local controller affects the stability controller.

Chapter 7

Conclusion and Outlook

This chapter summarizes the results of this thesis and presents the lessons learned during the performed experiments. The thesis closes with an overview of possible future tasks including an outlook regarding improvements in the system design and control.

7.1 Thesis Summary

The aim of this thesis is the development, control, and evaluation of a mobile, hominid multi-locomotion robot, designed to be highly mobile and able to walk in different postures. Currently, most mobile and light-weight robots focus on one motion mode. But the capability of using different motion modes and therefore comprising a high mobility has substantial benefits for a robotic system, e.g., allowing it to operate in disaster response or security scenarios. In unstructured environment, the quadrupedal posture allows a stable locomotion, whereas the bipedal motion mode can be more beneficial when it is important to create a visual overview of the situation or for locomotion in man-made environments.

In the beginning of this thesis a research regarding biological models is shown, because of the desired multi-locomotion ability, which was a design requirement for the intended robot. Chimpanzees are chosen as model, since these multi-talented animals are known to be capable of walking with different gaits like quadrupedal, bipedal, or on three legs and regularly show climbing as well as manipulation abilities. Therefore, their morphology is an ideal base for the design of a multi-locomotion robot. The morphology of the developed robot Charlie, the number and placement of its DoFs, and the limbs' RoM are determined considering the one observable in chimpanzees. In addition, the specifically newly designed subsystems, i.e., the sensor foot or the active artificial spine, are biologically inspired as well.

Altogether, the final hominid robot Charlie comprises 36 active and six passive DoFs. The weight of the fully equipped robot including its rechargeable lithium polymer batteries (44.4 V with 2.4 A h) is at 21.5 kg. In a load free case, the robot's power consumption for all installed control and sensor electronics is about 48 W. Additional 3.4 W are required for the quadrupedal pose or 2.4 W for the bipedal posture, to hold the respective position while standing on the ground.

Charlie's motion control software is running with a frequency of 75 Hz on a single core CPU with 800 MHz. The software architecture is based on a biologically inspired, reactive approach. The architecture is expanded by a local control loop, which is implemented in the lower leg structure. This local controller is only made possible due to the high sensor density and the local data preprocessing capabilities within the individual structures.

On the basis of experiences gained in former work with the LittleApe robot [KRS+09] [KBG+10], subsystems like feet and spine are specified and developed. Charlie's highly integrated, multi-point contact rear foot features 60 sensors, including a pressure-sensing array consisting of 49 sensors to allow a spatial resolution of the applied force and a tactile perception of the environment. In addition, it is shown that the developed rear foot has a better friction coefficient compared to spherical shaped feet, which are commonly used in multi-legged robotic systems.

The spine design is a hexapod structure with a single force sensor in each connecting rod. By using the RoM of the artificial spine, the workspace of the limbs is increased between 6 % to 16 %, depending on the position of the limbs. These two subsystems as well as the robot's actuators feature local control electronics, allowing data reading and processing directly on the lowest control level. In addition, subsystems like foot or spine communicate preprocessed sensor data, i.e., information and not raw data, which reduces the overall data traffic in the robot. The support polygon of the foot, for example, has due to its shape and sensor placement a theoretical maximum of 16 points to describe the local convex hull. This means that the data traffic for this sensor-array (49 sensors in total) is reduced to 33 % in the worst case and to 6 % in the best case scenario.

For walking on rigid terrain with no incline, it is shown that the local controller has a positive influence on the current consumption. Different walking speeds are tested, which revealed that for each speed a medium decrease of the current consumption about 10 % is reached, when the local controller is active compared to a deactivated local controller. While walking in flexible and deformable terrain, however, an energy saving effect of the local controller cannot be seen. Nevertheless, for the optimal and predicted CoM trajectory a lower standard deviation is recorded, which means that the predicted CoM trajectory is met more precisely. Furthermore, it can be stated that the robot is able to traverse unstructured environment, which it can only cover in a stable manner with activated local controller. While other, optimized gaits might also allow the robot to cope with the terrain, it still can be shown that the local control loop enables the robot to cope with terrain even when walking with a sub-optimal quadrupedal gait. Yet, it shows that an active local control loop enables the robot to cover unstructured environment even though the walking pattern may be not ideal.

Charlie is able to walk in a stable manner in inclines ranging from $-20°$ to $20°$. In positive inclines as well as in slopes with inclines up to $-10°$, the robot's CoM moves in a more consistent manner when the local controller is activated. As for flat terrain, the recorded data indicates that the overall current consumption can be reduced with an activated local controller. In positive inclines, an average power consumption of 35 W for walking is needed. However, for downhill walking the local controller is not as beneficial as it proofed to be for uphill walking and increased the robot's power consumption.

In order to remedy this situation, the local controller and Charlie's motion controller are extended. Charlie now modifies the behavior of the local controller online based on the given context, e.g., the incline. It is experimentally shown that in Charlie's control software a context-based adaption takes place and the currently ideal behavior of the local controller is selected while walking in inclines.

A defining feature of a multi-locomotion robot is the ability to demonstrate different motion patterns. A statically stable transition between Charlie's quadrupedal pose and its bipedal posture is implemented. Once in bipedal pose, Charlie presents the possibility to investigate a transferability of motion patterns and control schemes from one gait to another.

For bipedal walking, experiments are performed to determine an ideal walking speed, which allows Charlie to walk without external assistance. It can be seen that the faster the robot's limb movements are, the less support is needed.

Due to Charlie's morphology, the posture for bipedal walking as well as the motion pattern are realized with a bent hip and knee joint. By comparing the joint trajectories of the quadrupedal walking pattern with the one from bipedal walking, similarities between the respective trajectories can be seen, albeit in a weakened form. Yet, the existence of a parameter set, which can improve the quadrupedal gait, is likely and should be subjected to further investigations, e.g., by applying evolutionary algorithms. A modified parameter set entails an effect on the characteristics of the joint trajectories of the crawl gait, which can strengthen or weaken the similarities of both patterns. Nevertheless, to the best of the author's knowledge, this is the first time that trajectories of these two motion patterns are compared on one real-world robotic system (thus not in simulation) without changing the robot's morphology in-between.

Mechanical play of about ±29 mm within the structure of the rear leg can be seen in the bipedal pose. Charlie's heel has a width of 50 mm. Therefore it is likely that the robot's CoM exceeds the edges of the support while walking at the point, when one leg is in its swing-phase and the support polygon dimensions are equal or smaller than the size of one MPCF, which establishes the ground contact. Due to this, external assistance while walking with a lower motion is required. The walking becomes more stable when walking faster, since before the robot can tip the respective leg's swing-phase has ended and ground contact is established.

Besides the walking pattern, the transferability of the local controller from the quadrupedal to the bipedal posture is investigated. The function of the local controller has to be inverted compared to the quadrupedal case, otherwise the robot would not be able to stand stable. For the static case, in terms of increasing the ground reaction forces, the local controller produces a result as good as the one achieved by the global stability controller. During first walking experiments it is noticed that in Charlie for bipedal walking the local controller is rather obstructive.

As a final statement it can be said that the robot's morphology is designed accordingly to meet the multi-locomotion requirement and the defining features of both motion modes were considered in its design. This increases its mechatronic complexity compared to e.g. robots with a single motion mode, yet it is shown that such a robot is controllable. In addition to the robot's hardware, the chosen sensor density is as well suitable for both locomotion modes. To deal with the expected variety of data, a local data preprocessing is implemented within the structures, to limit data traffic throughout the robot. Furthermore, the robustness of the system was analyzed. During this thesis, more than 250 experiments with Charlie were performed, without the observation of severe damage on or within the structures, electronics, or sensors. This shows that the robot is able to withstand a wide range of experiments without failure. Charlie's mechatronic design (including the design of the actuators and selected sensors and control electronics), the RoM and operating speed of the limbs allow the robot to deal with different environments. It was shown that the robot Charlie presents the possibility to investigate the transferability of motion patterns and control schemes from one gait to another and therefore provides the foundation to conducting further in-depth studies without the need of manually changing the robot's morphology in-between.

7.2 Future Work

Charlie, with its electro-mechanical design, its highly integrated subsystems, and the embedded sensory equipment, is predestined to intensify further scientific work on and with the robot. The possibilities for research are numerous: Charlie's perception capabilities have not yet been exploited and could contribute, e.g., to the eSLAM [SJK13] approach and enhance the generation of maps by information of perceived ground properties; by adding imaging systems to the robot's head, research in the area of navigation and planning can be conducted. The possibility to change from a quadrupedal stance into a bipedal posture would increase the robot's field of view and provides additional advantages, e.g., to look over obstacles of a certain height to minimize blind spots in the map. Charlies multi functionality could be increased further by adding more dynamic quadrupedal gaits to the robot's repertoire, e.g., a cross gait to be able to cover greater distances in a shorter time or climbing stairs to increase the robot's range of action in man-made environments. By replacing the hook, which serves as a front foot, with an artificial actuated hand, the limbs RoM combined with the RoM of the active spine would result in an interesting research topic regarding dual-arm manipulation.

Even though the robot Charlie allowed conducting all different kinds of experiments, due to the intensive work, possible improvements of the robot's hardware are identified. To reduce the overall play, reworking the ankle joint and the thigh structure appears most promising. After the transition from the quadrupedal posture to the bipedal stance, during the first steps of the bipedal gait Charlie has to be stabilized. By reducing the mechanical play, an improvement of the bipedal gait is expected. This would allow conducting experiments with a slower, statically stable bipedal gait. The local control loop implemented in the ankle joint of the rear feet could be investigated further during this locomotion. In addition, the local controller can be implemented and analyzed within other subsystems, like the artificial spine.

Due to the multitude of installed sensors within the robot, the implementation and study of a force-based robot control is possible. The torques that are applied by the rear legs to the body can be perceived within the spine and due to its motion capabilities, the flow of forces can be supported and transferred to the front legs, to gain a fast and energy-efficient walking pattern.

Adding new behavior sets to the robot's reactive controller could result in faster reaction to terrain irregularities. By adapting the concept of the behavior library [DBBK15] on Charlie, the information gathered about the substrate allows a higher control level to choose a suitable locomotion behavior depending on the given context.

A final personal note: I am looking forward to continue my work with Charlie, since this robot offers so many possibilities. I am gladly take part in implementing its mechanical improvements, increasing its sensory abilities as well as realizing the proposed extensions of Charlie's control software in the near future.

Part II

Appendix

List of Figures

List of Tables

Bibliography

[AAD02] A. Aiello, L. Aiello, and C. Dean. *An Introduction to Human Evolutionary Anatomy.* Elsevier Academic Press, London, 2002.

[ADH05] J. Albiez, R. Dillmann, and T. Hinckel. Reactive foot-control for quadruped walking. In *3rd International Symposium on Adaptive Motion in Animals and Machines*, 2005.

[AE93] T. L. Allinger and J. R. Engsberg. A method to determine the range of motion of the ankle joint complex, in vivo. *Journal of Biomechanics*, 26(1):69 – 76, 1993.

[Alb07] J. Albiez. *Verhaltensnetzwerke zur adaptiven Steuerung biologisch motivierter Laufmaschinen.* PhD thesis, Universität Fridericiana zu Karlsruhe (TH), Fakulittät fütr Informatik., 2007.

[ARH88] R.C. Arkin, E. Riseman, and A. Hanson. Aura: An architecture for vision-based robot navigation. *Proceedings of the 1987 DARPA Image Understanding Workshop, Los Angeles, CA*, pages 417–431, 1988.

[Ark98] R.C. Arkin. *Behavior-based Robotics.* MIT Press, 1998.

[ASHF09] T. Aoyama, K. Sekiyama, Y. Hasegawa, and T. Fukuda. Experimental verification of 3d bipedal walking based on passive dynamic autonomous control. In *Intelligent Robots and Systems, 2009. IROS 2009. IEEE/RSJ International Conference on*, pages 1308 –1313, oct. 2009.

[ATI16] Ranges and resolution of the ati mini45 six axis force torque sensor. http://www.ati-ia.com/products/ft/ft_models.aspx?id=Mini45, 2016.

[Atl16] Atlas robot. http://www.boston dynamics.com/img/Atlas-p2_nt.jpg, 2016.

[Bar13] S. Bartsch. *Development, Control, and Empirical Evaluation of the Six-Legged Robot SpaceClimber Designed for Extraterrestrial Crater Exploration*. PhD thesis, University of Bremen, 2013.

[Bar14] S. Bartsch. Development, control, and empirical evaluation of the six-legged robot spaceclimber designed for extraterrestrial crater exploration. *KI - Kuenstliche Intelligenz, German Journal on Artificial Intelligence–Organ des Fachbereiches "Kuenstliche Intelligenz" der Gesellschaft fuer Informatik e.V. (KI)*, 2014.

[BBC+10] S. Bartsch, T. Birnschein, F. Cordes, D. Kuehn, P. Kampmann, J. Hilljegerdes, S. Planthaber, M. Roemmermann, and F. Kirchner. Spaceclimber: Developement of a six-legged climbing robot for space exploration. In *Proceedings of the International Symposium on Robotics (ISR-2010)*. VDE Verlag GmbH, 2010.

[BBR+12] S. Bartsch, T. Birnschein, M. Roemmermann, J. Hilljegerdes, D. Kuehn, and F. Kirchner. Development of the six-legged walking and climbing robot spaceclimber. *Journal of Field Robotics*, Volume 29, Issue 3, Special Issue on Space Robotics(Part 1):506–532, 6 2012.

[BD216] Bigdog - the most advanced rough-terrain robot on earth. http://www.bostondynamics.com/robot_bigdog.html, 2016.

[Bic88] D. B. Bickler. Articulated suspension system, 1988.

[BK06] S. Bartsch and F. Kirchner. Robust control of a humanoid robot using bio-inspired approach based on central pattern generators, reflexes and proprioceptive feedback. In *IEEE International Conference on Robotics and Biomimetics (ROBIO 2006)*, 2006.

[Bou69] G.H. Bourne. *The chimpanzee. Anatomy, behaviour, and diseases of chimpanzees*. Karger Basel, New York, 1969.

[Bro11] T. G. Brown. The intrinsic factors in the act of progression in the mammal. *Proceedings of the Royal Society of London*, Series B,(84):308 – 319, 1911.

[Bro14] T. G. Brown. On the nature of the fundamental activity of the nervous centres; together with an analysis of the conditioning of rhythmic activity in progression, and a theory of the evolution of function in the nervous system. *Journal of Physiology*, (48):18 – 46, 1914. London.

[Bro86] R.A. Brooks. A robust layered control system for a mobile robot. *Robotics and Automation, IEEE Journal of*, 2(1):14–23, Mar 1986.

[Bro91] R. A Brooks. How to build complete creatures rather than isolated cognitive simulators. *Architectures for intelligence*, pages 225–239, 1991.

[BVSA10] H.J. Bidgoly, A. Vafaei, A. Sadeghi, and M.N. Ahmadabadi. Learning approach to study effect of flexible spine on running behavior of a quadruped robot. *Proceeding of International Conference on Climbing and Walking Robots 2010, CLAWAR*, 2010.

[Che16] Cheetah robot. http://www.bostondynamics.com/robot_cheetah.html, 2016.

[CNSJ+94] B. Calancie, B. Needham-Shropshire, P. Jacobs, K. Willer, G. Zych, and B.A. Green. Involuntary stepping after chronic spinal cord injury: Evidence for a central rhythm generator for locomotion in man. *Brain*, 117(5):1143–1159, 1994.

[COB+14] F. Cordes, C. Oekermann, A. Babu, D. Kuehn, T. Stark, and F. Kirchner. An active suspension system for a planetary rover. In *In Proceedings of the International Symposium on Artificial Intelligence, Robotics and Automation in Space (i-SAIRAS 2014)*, 2014.

[Cro96] R. H. Crompton. Inertial properties of primates: New techniques for laboratory and field studies of locomotion. In *American Journal of Physical Anthropology 99, 547-570*, 1996.

[DAC+02] K. DAoût, P. Aerts, D. De Clercq, K. De Meester, and L. Van Elsacke. Segment and joint angles of hind limb during bipedal and quadrupedal walking of the bonobo (pan paniscus). *AMERICAN JOURNAL OF PHYSICAL ANTHROPOLOGY*, 2002.

[DBBK15] A. Dettmann, A. Born, S. Bartsch, and F. Kirchner. Experience-based adaptation of locomotion behaviors for kinematically complex robots in unstructured terrain. In *In Proceedings of IEEE/RSJ International Conference on Intelligent Robots and Systems (IROS 2015)*, 2015.

[DeS09] J. M. DeSilva. Functional morphology of the ankle and the likelihood of climbing in early hominins. *Proceedings of the National Academy of Sciences*, 106(16):6567–6572, 2009.

[DO03] S. Dalley and J. P. Oleson. Sennacherib, archimedes, and the water screw: The context of invention in the ancient world. *Technology and Culture 44, no. 1*, 2003.

[DWAS11] A. Dietrich, T. Wimbock, and A. Albu-Schaffer. Dynamic whole-body mobile manipulation with a torque controlled humanoid robot via impedance control laws. In *Intelligent Robots and Systems (IROS), 2011 IEEE/RSJ International Conference on*, pages 3199–3206. IEEE, 2011.

[EH08] G. Endo and S. Hirose. Study on roller-walker-adaptation of characteristics of the propulsion by a leg trajectory. *IEEE/RSJ International Conference on Intelligent Robots and Systems (IROS)*, 2008.

[EH12] G. Endo and S. Hirose. Study on roller-walker - improvement of locomotive efficiency of quadruped robots by passive wheels. *Advanced Robotics*, 26(8 - 9):969 – 988, 2012.

[EM35] H. Elftman and J. Manter. The evolution of the human foot, with especial reference to the joints. *Journal of Anatomy*, 70(Pt 1):56, 1935.

[EMM$^+$08] G. Endo, J. Morimoto, T. Matsubara, J. Nakanishi, and G. Cheng. Learning cpg-based biped locomotion with a policy gradient method: Application to a humanoid robot. *The International Journal of Robotics Research*, 27(2):213 – 228, February 2008.

[EQBC96] K. S. Espenschied, R. D. Quinn, R. D. Beer, and H. J. Chiel. Biologically based distributed control and local reflexes improve rough terrain locomotion in a hexapod robot. *Robotics and Autonomous Systems*, 18:59 – 64, 1996.

[Fer95] C. Ferrell. Global behavior via cooperative local control. *Automonous Robots*, 2(2):105 – 125, 1995.

[FGHR80] H. Forssberg, S. Grillner, J. Halbertsma, and S. Rossignol. The locomotion of the low spinal cat. ii. interlimb coordination. *Acta Physiologica Scandinavica*, 108(3):283–295, 1980.

[FKB$^+$12] K. Fondahl, D. Kuehn, F. Beinersdorf, F. Bernhard, F. Grimminger, M. Schilling, T. Stark, and F. Kirchner. An adaptive sensor foot for a bipedal and quadrupedal robot. In *Proceedings of IEEE International Conference on Biomedical Robotics and Biomechatronics*, 2012.

[FKK$^+$14] M. Fallon, S. Kuindersma, S. Karumanchi, M. Antone, T. Schneider, H. Dai, C. P. D'Arpino, R. Deits, M. DiCicco, D. Fourie, T. Koolen, P. Marion, M. Posa, A. Valenzuela, K. Yu, J. Shah, K. Iagnemma, R. Tedrake, and S. Teller. An architecture for online affordance-based perception and whole-body planning. Technical report, MIT CSAIL, 2014.

[FKSH07] T. Fukuda, S. Kojima, K. Sekiyama, and Y. Hasegawa. Design method of brachiation controller based on virtual holonomic constraint. In *Proceedings of the IEEE/RSJ International Conference on Intelligent Robots and Systems (IROS)*, pages 450 –455, 2007.

[GD09] P. Giguere and G. Dudek. Clustering sensor data for autonomous terrain identification using time-dependency. *Autonomous Robots*, 26(2-3):171–186, 2009.

[GFASH09] P.Robuffo Giordano, M. Fuchs, A. Albu-Schaffer, and G. Hirzinger. On the kinematic modeling and control of a mobile platform equipped with steering wheels and movable legs. In *Robotics and Automation, 2009. ICRA '09. IEEE International Conference on*, pages 4080–4087, May 2009.

[GSVI13] S. Gay, J. Santos-Victor, and A. Ijspeert. Learning robot gait stability using neural networks as sensory feedback function for central pattern generators. In *Intelligent Robots and Systems (IROS), 2013 IEEE/RSJ International Conference on*, pages 194–201, Nov 2013.

[hBDC] http://www.technischesmuseum.at/res/00/00/40/88/0000408853 Big-Display-Crop.jpg.

[HBM+15] P. Hebert, M. Bajracharya, J. Ma, N. Hudson, A. Aydemir, J. Reid, C. Bergh, J. Borders, M. Frost, M. Hagman, J. Leichty, P. Backes, B. Kennedy, P. Karplus, B. Satzinger, K. Byl, K. Shankar, and J. Burdick. Mobile manipulation and mobility as manipulation - design and algorithms of robosimian. *Journal of Field Robotics*, 32(2):255–274, 2015.

[hcdsrd] http://www.designboom.com/wp-content/uploads/2015/02/boston-dynamics-spot-robot designboom01.jpg.

[hcfD] http://www.therobotics challenge.org/sites/default/ files/TeamKAIST_DRCHubo2_main.png.

[HDB14] D. Helmick, B. Douillard, and M. Bajracharya. Small body surface mobility with a limbed robot. In *IEEE/RSJ International Conference on Intelligent Robots and Systems (IROS)*, 2014.

[Hev08] M. Heverly. A wheel-on-limb rover for lunar operation. *9th International Symposium on Artificial Intelligence, Robotics and Automation for Space*, 2008.

[HGB+12] M. Hutter, C. Gehring, M. Bloesch, M. A. Hoepflinger, C. D. Remy, and R. Siegwart. Starleth: A compliant quadrupedal robot for fast, efficient, and versatile locomotion. In *Climbing and Walking Robots (CLAWAR)*, 2012.

[HHC07] S. Hyon, J.G. Hale, and G. Cheng. Full-body compliant human: Balancing in the presence of unknown external forces. *Robotics, IEEE Transactions on Humanoid Interaction*, 23(5):884–898, Oct 2007.

[HHK+04] K. Harada, H. Hirukawa, F. Kanehiro, K. Fujiwara, K. Kaneko, S. Kajita, and M. Nakamura. Dynamical balance of a humanoid robot grasping an environment. In *Proceedingsof the IEEE/RSJ International Conference on Intelligent Robots and Systems*, volume 2, pages 1167–1173 vol.2, Sept 2004.

[Hil65] M. Hildebrand. Symmetrical gaits of horses. *Science*, 150(3697):701–708, 1965.

[Hil67] M. Hildebrand. Symmetrical gaits of primates. In *American Journal of Physical Anthropology, 26: 119-130*, 1967.

[HK06] O. Holland and R. Knight. The anthropomimetic principle. In *Proceedings of the AISB06 Symposium on Biologically Inspired Robotics*, 2006.

[HKBK09] J. Hilljegerdes, P. Kampmann, S. Bosse, and F. Kirchner. Development of an intelligent joint actuator prototype for climbing and walking robots. In *International Conference on Climbing and Walking Robots and the Support Technologies for Mobile Machines (CLAWAR)*, 2009.

[HLWI07] M.K. Habib, Guang Lei Liu, K. Watanabe, and K. Izumi. Bipedal locomotion control via cpgs with coupled nonlinear oscillators. In *Mechatronics, ICM2007 4th IEEE International Conference on*, pages 1–6, May 2007.

[HMFMQ10] M. Heverly, J. Matthews, M. Frost, and Ch. Mc-Quin. Development of the tri-athlete lunar vehicle prototype. *Proceedings of the 40th Aerospace Mechanisms Symposium*, May 2010.

[HRH$^+$10] M.A. Hoepflinger, C.D. Remy, M. Hutter, L. Spinello, and R. Siegwart. Haptic terrain classification for legged robots. In *Robotics and Automation (ICRA), 2010 IEEE International Conference on*, pages 2828–2833, May 2010.

[hrj] http://www.robotshop.com/blog/en/files/asimo-robot 1.jpg.

[HSK05] J. Hilljegerdes, D. Spenneberg, and F. Kirchner. The construction of the four legged prototype robot ARAMIES. In *Proceedings of the 8th International Conference on Climbing and Walking Robots (CLAWAR 2005)*, pages 335–342, London, UK, September 2005.

[htt] http://www.expo21xx.com/cipmedia/18224/10.jpg.

[HUEC11] E.W. Hawkes, J. Ulmen, N. Esparza, and M.R. Cutkosky. Scaling walls: Applying dry adhesives to the real world. In *Intelligent Robots* *and Systems (IROS), 2011 IEEE/RSJ International Conference on*, pages 5100–5106. IEEE, 2011.

[HYT97] S. Hirose, K. Yoneda, and H. Tsukagoshi. Titan vii: Quadruped walking and manipulating robot on a steep slope. In *Proceedings of the 1997 IEEE International Conference on Robotics and Automation, Albuquerque, New Mexico*, 1997.

[Ijs08] A. J. Ijspeert. Central pattern generators for locomotion control in animals and robots: A review. *Neural Networks*, 21(4):642 – 653, 2008. Robotics and Neuroscience.

[IY96] L. A. Isbell and T. P. Young. The evolution of bipedalism in hominids and reduced group size in chimpanzees: alternative responses to decreasing resource availability. *Journal of Human Evolution*, 30(5):389 – 397, 1996.

[JK13] L. Y. Ji and F. Kirchner. Reducing intersample ripple of actuator in multirate environment by a joint space interpolator. In *The 6th IFAC Symposium on Mechatronic Systems. IFAC Symposium on Mechatronic Systems (Mechatronics-2013), 6th, April 10-12, Hangzhou, China*, 4 2013.

[JWK10] M. Jantsch, S. Wittmeier, and A. Knoll. Distributed control for an anthropomimetic robot. In *Intelligent Robots and Systems (IROS), 2010 IEEE/RSJ International Conference on*, pages 5466–5471, 2010.

[KAC$^+$01] B. Kennedy, H. Agazarian, Y. Cheng, M. Garrett, G. Hickey, T. Huntsberger, L. Magnone, C. Mahoney, A. Meyer, and J. Knight. Lemur: Legged excursion mechanical utility rover. *Autonomous Robots*, 2001.

[Kap99a] I. A. Kapandji. *Funktionelle Anatomie der Gelenke - Schmematisierte und kommentierte Zeichnungen zur menschlichen Biomechanik Band 1 - untere Extremität*. Hippokrates Verlag, Stuttgart, 3 edition, 1999.

[Kap99b] I. A. Kapandji. *Funktionelle Anatomie der Gelenke - Schmematisierte und kommentierte Zeichnungen zur menschlichen Biomechanik Band III: Wirbelsäule*. Hippokrates Verlag, Stuttgart, 3 edition, 1999.

[KAS+13a] T. Kobayashi, T. Aoyama, M. Sobajima, K. Sekiyama, and T. Fukuda. Bipedal walking by humanoid robot with cane; preventive usage of cane based on impulse force. In *Micro-NanoMechatronics and Human Science (MHS), 2013 International Symposium on*, pages 1–6, Nov 2013.

[KAS+13b] T. Kobayashi, T. Aoyama, M. Sobajima, K. Sekiyama, and T. Fukuda. Locomotion selection strategy for multi-locomotion robot based on stability and efficiency. In *Intelligent Robots and Systems (IROS), 2013 IEEE/RSJ International Conference on*, pages 2616–2621, Nov 2013.

[KBB+12] D. Kuehn, F. Beinersdorf, F. Bernhard, K. Fondahl, M. Schilling, M. Simnofske, T. Stark, and F. Kirchner. Active spine and feet with increased sensing capabilities for walking robots. In *International Symposium on Artificial Intelligence, Robotics and Automation in Space (iSAIRAS-12)*, 2012. September 4-6, Turin, Italy.

[KBB+14] D. Kuehn, F. Bernhard, A. Burchardt, M. Schilling, T. Stark, M. Zenzes, and F. Kirchner. Distributed computation in a quadrupedal robotic system. *International Journal of Advanced Robotic Systems*, 11, 2014.

[KBG+10] D. Kuehn, F. Bernhard, F. Grimminger, S. Simon, and F. Kirchner. Development of passive spine and actuated rear foot for an ape-like robot. In *International Conference on Climbing and Walking Robots and the Support technologies for Mobile Machines (CLAWAR-10)*, 2010.

[KBS+13a] M. Khoramshahi, H. J. Bidgoly, S. Shafiee, A. Asaei, A. J. Ijspeert, and M. N. Ahmadabadi. Piecewise linear spine for speed-energy efficiency trade-off in quadruped robots. *Robotics And Autonomous Systems*, 61(12):1350–1359, 2013.

[KBS+13b] D. Kuehn, F. Beinersdorf, M. Simnofske, F. Bernhard, and F. Kirchner. Towards an active spine for mobile robots. In *3rd IFToMM International Symposium on Robotics and Mechatronics. International Symposium on Robotics and Mechatronics (ISRM-2013), October 2-4, Singapur, Singapore.* o.A., 10 2013.

[KC14] O. Khatib and S. Y. Chung. Suprapeds: Humanoid contact-supported locomotion for 3d unstructured environments. In *IEEE International Conference on Robotics and Automation (ICRA)*, pages 1–6, Nov 2014.

[KDBA11] M.H.H. Kani, M. Derafshian, H.J. Bidgoly, and M.N. Ahmadabadi. Effect of flexible spine on stability of a passive quadruped robot: Experimental results. In *Robotics and Biomimetics (ROBIO), 2011 IEEE International Conference on*, pages 2793–2798, Dec 2011.

[KI02] P. M. Kennedy and J. T. Inglis. Distribution and behaviour of glabrous cutaneous receptors in the human foot sole. *The Journal of Physiology*, 538(Pt 3):995 – 1002, 2002.

[KK12] P. Kampmann and F. Kirchner. Towards a fine-manipulation system with tactile feedback for deep-sea environments. *Robotics and Autonomous Systems*, 2012. To appear.

[KKK$^+$03] S. Kajita, F. Kanehiro, K. Kaneko, K. Fujiwara, K. Harada, K. Yokoi, and H. Hirukawa. Resolved momentum control: humanoid motion planning based on the linear and angular momentum. In *Intelligent Robots and Systems, 2003. (IROS 2003). Proceedings. 2003 IEEE/RSJ International Conference on*, volume 2, pages 1644–1650 vol.2, Oct 2003.

[KMM07] A. Kalamdani, C. Messom, and Siegel M. Robots with sensitive feet. *IEEE Instrumentation & Measurement Magazine*, 10:46–53, 2007.

[KRS$^+$09] D. Kuehn, M. Römmermann, N. Sauthoff, F. Grimminger, and F. Kirchner. Concept evaluation of a new biologically inspired robot littleape. In *IEEE/RSJ International Conference on Intelligent Robots and Systems (IROS-09)*, 2009.

[KSG$^+$09] D. Kuehn, N. Sauthoff, F. Grimminger, M. Römmermann, and F. Kirchner. Towards a biologically inspired ape-like robot. In *International Conference on Climbing and Walking Robots and the Support technologies for Mobile Machines (CLAWAR-09)*, 2009.

[KSL02] F. Kirchner, D. Spenneberg, and R. Linnemann. A biologically inspired approach towards robust real world locomotion in an 8-legged robot. In *J. Ayers, J. Davis, and A. Rudolph (Eds.), Neurotechnology for Biomimetic Robots. MIT-Press, MA, USA*, 2002.

[KSS+16] D. Kuehn, M. Schilling, T. Stark, M. Zenzes, and F. Kirchner. System design and field testing of the hominid robot charlie. *Journal of Field Robotics*, 07 2016.

[KST+08] S. Kim, M. Spenko, S. Trujillo, B. Heyneman, D. Santos, and M. R. Cutkosky. Smooth vertical surface climbing with directional adhesion. In *IEEE Transactions on Robotics, Vol. 24*, 2008.

[KST+13] M. Khoramshahi, A. Sprowitz, A. Tuleu, M. N. Ahmadabadi, and A. Ijspeert. Benefits of an Active Spine Supported Bounding Locomotion With a Small Compliant Quadruped Robot. In *Proceedings of 2013 IEEE International Conference on Robotics and Automation*, 2013.

[KWK+15] T. Kamioka, T. Watabe, M. Kanazawa, H. Kaneko, and T. Yoshiike. Dynamic gait transition between bipedal and quadrupedal locomotion. In *International Conference on Intelligent Robots and Systems (IROS)*, 2015.

[LWF14] Z. Li, Z. Wu, and Y. Fu. Active/passive walking strategy for a biped robot using cpg with sensory interaction. In *Mechatronics and Automation (ICMA), 2014 IEEE International Conference on*, pages 873–878, Aug 2014.

[LWT09] D. Liu, L. Wang, and K. C. Tan, editors. *Design and Control of Intelligent Robotic Systems (Studies in Computational Intelligence).* Springer-Verlag Berlin Heidelberg, 2009.

[LZH+14] J. Luo, Y. Zhang, K. Hauser, H.A. Park, M. Paldhe, C.S.G. Lee, M. Grey, M. Stilman, J. H. Oh, J. Lee, I. Kim, and P. Oh. Robust ladder-climbing with a humanoid robot with application to the darpa robotics challenge. In *Robotics and Automation (ICRA), 2014 IEEE International Conference on*, pages 2792–2798, May 2014.

[MBK13] M. Manz, S. Bartsch, and F. Kirchner. Mantis - a robot with advanced locomotion and manipulation abilities. In *In Proceedings of* *the 12th Symposium on Advanced Space Technologies in Robotics and Automation, (ASTRA-2013)*, 2013.

[MF68] R.B. McGhee and A.A. Frank. On the stability properties of quadruped creeping gaits. *Mathematical Biosciences*, 3:331–351, 1968.

[MIT] MIT. http://www.ai.mit.edu.

[MIT12] A. Makovsky, P. Ilott, and J. Taylor. Mars science laboratory telecommunications system design. *DESCANSO Design and Performance Summary Series*, 2012.

[MMN+05] T. Matsubara, Jun Morimoto, J. Nakanishi, M. Sato, and K. Doya. Learning cpg-based biped locomotion with a policy gradient method. In *Humanoid Robots, 2005 5th IEEE-RAS International Conference on*, pages 208–213, Dec 2005.

[MNS+07] I. Mizuuchi, Y. Nakanishi, Y. Sodeyama, Y. Namiki, T. Nishino, N. Muramatsu, J. Urata, K. Hongo, T. Yoshikai, and M. Inaba. An advanced musculoskeletal humanoid kojiro. In *Proceedings of the IEEE-RAS International Conference on Humanoid Robots (Humanoids 2007)*, 2007.

[MSM+11] M. P. Murphy, A. Saunders, C. Moreira, A. A. Rizzi, and M. Raibert. The littledog robot. *The International Journal of Robotics Research*, 30(2):145–149, 2011.

[MTY+02] I. Mizuuchi, R. Tajima, T. Yoshikai, D. Sato, K. Nagashima, M. Inaba, Y. Kuniyoshi, and H. Inoue. The design and control of the flexible spine of a fully tendon-driven humanoid kenta. In *Intelligent Robots and Systems, 2002. IEEE/RSJ International Conference on*, volume 3, pages 2527 – 2532 vol.3, 2002.

[MWH+15] C. Mastalli, A. Winkler, I. Havoutis, D. G. Caldwell, and C. Semini. On-line and on-board planning and perception for quadrupedal locomotion. In *2015 IEEE International Conference on Technologies for Practical Robot Applications (TEPRA)*. IEEE, May 2015.

[Nag03] F. Nagashima. A motion learning method using cpg/np. In *Proceedings of the 2nd international symposium on adaptive motion of animals and machines*, 2003.

[NHBC14] J. Nassour, P. Henaff, F. Benouezdou, and G. Cheng. Multi-layered multi-pattern cpg for adaptive locomotion of humanoid robots. *Biological cybernetics*, 2014.

[NTNM11] D. Nakhaeinia, S. H. Tang, S. B. Mohd Noor, and O. Motlagh. A review of control architectures for autonomous navigation of mobile robots. *International Journal of the Physical Sciences*, pages 169–174, January 2011.

[OLD$^+$15] M. C. O'Neill, L.-F. Lee, B. Demes, N. E. Thompson, S. G. Larson, J. T. Stern Jr, and B. R. Umberger. Three-dimensional kinematics of the pelvis and hind limbs in chimpanzee (pan troglodytes) and human bipedal walking. *Journal of Human Evolution*, 2015.

[Or10] J. Or. A hybrid cpg-zmp control system for stable walking of a simulated flexible spine humanoid robot. *Neuronal Networks*, 23(23):452–460, 2010.

[Or13] J. Or. Humanoids grow a spine: The effect of lateral spinal motion on the mechanical energy efficiency. *Robotics Automation Magazine, IEEE*, 20(2):71–81, 2013.

[OSJ$^+$13] C. Ordonez, J. Shill, A. Johnson, J. Clark, and E. Collins. Terrain identification for rhex-type robots. *Proc. SPIE*, 8741:87410Q–87410Q–12, 2013.

[PB07] J. D. Pruetz and P. Bertolani. Savanna chimpanzees, pan troglodytes verus, hunt with tools. *Current Biology*, 17(5):412–417, 2007.

[PC05] F. Pfeiffer and H. Cruse. *Autonomes Laufen.* Springer Verlag, 2005.

[PMS07] D. Pongas, M. Mistry, and S. Schaal. A robust quadruped walking gait for traversing rough terrain. In *Robotics and Automation, 2007 IEEE International Conference on*, pages 1474–1479. IEEE, 2007.

[PRR14] H. Pontzer, D. A. Raichlen, and P. S. Rodman. Bipedal and quadrupedal locomotion in chimpanzees. *Journal of Human Evolution*, 2014.

[PRS09] H. Pontzer, D. A. Raichlen, and M. D. Sockol. The metabolic cost of walking in humans, chimpanzees, and early hominins. *Journal of Human Evolution*, 56(1):43 – 54, 2009.

[Rai86] M. H. Raibert. *Legged robots that balance.* Massachusetts Institute of Technology, Cambridge, MA, USA, 1986.

[RBN+08] M. Raibert, K. Blankespoor, G. Nelson, R. Playter, and the BigDog Team. Bigdog, the rough-terrain quadruped robot. In *Proceedings of the 17th World Congress The International Federation of Automatic Control Seoul, Korea, July 6-11, 2008*, 2008.

[RCK14] T. M. Roehr, F. Cordes, and F. Kirchner. Reconfigurable integrated multirobot exploration system (rimres): Heterogeneous modular reconfigurable robots for space exploration. *Journal of Field Robotics*, Special Issue on Space Robotics, Part 2:3–34, 2014.

[RI06] L. Righetti and A.J. Ijspeert. Programmable central pattern generators: an application to biped locomotion control. In *Proceedings IEEE International Conference on Robotics and Automation, ICRA*, pages 1585–1590, May 2006.

[RN04] S. J. Russell and P. Norvig. *KÃ¼nstliche Intelligenz. Ein moderner Ansatz.* Pearson Studium, 2., Ã¼berarb. a. edition, 2004.

[SBK+13] A. Sprowitz, E. Badri, M. Khoramshahi, A. Tuleu, and A. J. Ijspeert. Use Your Spine! Effect of Active Spine Movements on Horizontal Impulse and Cost of Transport in a Bounding, Quadruped Robot. In *Proceedings of DW*, 2013.

[She06] C. S. Sherrington. *The integrative action of the nervous system.* Cambridge University Press, 1906.

[SHK+08] D. Santos, B. Heyneman, S. Kim, N. Esparza, and M. R. Cutkosky. Gecko-inspired climbing behaviors on vertical and overhanging surfaces. In *Proceedings of the IEEE International Conference on Robotics and Automation (ICRA)*, 2008.

[SHK+15] A. Stentz, H. Herman, A. Kelly, E. Meyhofer, G. C. Haynes, D. Stager, B. Zajac, J. A. Bagnell, J. Brindza, C. Dellin, et al. Chimp, the cmu highly intelligent mobile platform. *Journal of Field Robotics*, 32(2):209–228, 2015.

[SJK13] J. Schwendner, S. Joyeux, and F. Kirchner. Using embodied data for localisation and mapping. *Journal of Field Robotics*, o.A.:—, 11 2013.

[SK00] D. Spenneberg and F. Kirchner. Omnidirectional walking in an eight legged robot. In *International Symposium on Robotics and Automation (ISRA)*, 2000.

[SK07] D. Spenneberg and F. Kirchner. *The Bio-Inspired SCORPION Robot: Design, Control & Lessons Learned*, chapter Climbing & Walking Robots, Towards New Applications, pages 197–218. I-Tech Education and Publishing, Wien, Austria, 10 2007. ISBN: 978-3-902613-16-5.

[SLBB14] B. Satzinger, C. Lau, M. Byl, and K. Byl. Experimental results for dexterous quadruped locomotion planning with robosimian. In *Proc. International Symposium on Experimental Robotics (ISER)*, 2014.

[SMK04] D. Spenneberg, K. McCullough, and F. Kirchner. Stability of walking in a multilegged robot suffering leg loss. In *Proceedings of ICRA04.*, volume 3, page 2159, 2004.

[SN02] J. Shan and F. Nagashima. Neural locomotion controller design and implementation for humanoid robot hoap-1. In *20th annual conference of the robotics society of Japan*, 2002.

[SN05] T. Sugihara and Y. Nakamura. A fast online gait planning with boundary condition relaxation for humanoid robots. In *Robotics and Automation, 2005. ICRA 2005. Proceedings of the 2005 IEEE International Conference on*, pages 305–310, April 2005.

[Spe16] ASIMO Specs. http://asimo.honda.com/asimo-specs/, 2016.

[SRP07] M.D. Sockol, D.A. Raichlen, and H. Pontzer. Chimpanzee locomotor energetics and the origin of human bipedalism. *Proceedings of the National Academy of Sciences*, 104(30):12265, 2007.

[SSK$^+$08] H. Sawada, K. Sekiyama, M. Kojo, T. Aoyama, Y. Hasegawa, and T. Fukuda. Locomotion stabilization with transition between biped and quadruped walk based on recognition of slope. In *International Symposium on Micro-NanoMechatronics and Human Science (MHS)*, pages 424 –429, nov. 2008.

[Ste65] D. Stewart. A platform with six degrees of freedom. *Proceedings of the institution of mechanical engineers*, 180(1):371–386, 1965.

[STG+11] C. Semini, N.G. Tsagarakis, E. Guglielmino, M. Focchi, F. Cannella, and D.G. Caldwell. Design of hyq–a hydraulically and electrically actuated quadruped robot. *Proceedings of the Institution of Mechanical Engineers, Part I: Journal of Systems and Control Engineering*, 225(6):831–849, 2011.

[SWA+02] Y. Sakagami, R. Watanabe, C. Aoyama, S. Matsunaga, N. Higaki, and K. Fujimura. The intelligent ASIMO: System overview and integration. In *IEEE/RSJ International Conference on Intelligent Robots and Systems*, volume 3, pages 2478 – 2483, 2002.

[TC06] S.K.S. Thorpe and R. H. Crompton. Orangutan positional behavior and the nature of arboreal locomotion in hominoidea. *American Journal of Physical Anthropology*, 2006.

[TLTK90] A. Takanishi, H. Lim, M. Tsuda, and I. Kato. Realization of dynamic biped walking stabilized by trunk motion on a sagittally uneven surface. In *IEEE International Workshop on Intelligent Robots and Systems: 'Towards a New Frontier of Applications'*, pages 323–330 vol.1, Jul 1990.

[TNMY05] M. Takahashi, T. Narukawa, K. Miyakawa, and K. Yoshida. Combined control of cpg and torso attitude control for biped locomotion. In *IEEE/RSJ International Conference on Intelligent Robots and Systems (IROS)*, pages 4051–4056, Aug 2005.

[UC10] J. Ulmen and M. Cutkosky. A robust, low-cost and low-noise artificial skin for human-friendly robots. In *Proceedings of the IEEE International Conference on Robotics and Automation (ICRA)*, 2010.

[VB04] M. Vukobratovic and B. Borovac. Zero-moment point - thirty five years of its life. *I. J. Humanoid Robotics*, 1(1):157–173, 2004.

[vH54] E. von Holst. Relations between the central nervous system and the peripheral organs. *The British Journal of Animal Behaviour*, 2(3):89 – 94, 1954.

[vHM50] E. von Holst and H. Mittelstaedt. Das reafferenzprinzip - wechselwirkungen zwischen zentralnervensystem und peripherie. *Die Naturwissenschaften*, 20:464 – 476, 1950.

[Vol14] R. Volpe. 2014 Robotics Activities at JPL. In *International Symposium on Artificial Intelligence, Robotics and Automation in Space (i-SAIRAS)*, 2014.

[Wal50] W. Walter. An electro-mechanical animal 1. *dialectica*, 4(3):206–213, 1950.

[WC04] W.J. Wang and R.H. Crompton. Analysis of the human and ape foot during bipedal standing with implications for the evolution of the foot. *Journal of Biomechanics*, 37(12):1831 – 1836, 2004.

[Whe91] P.E. Wheeler. The thermoregulatory advantages of hominid bipedalism in open equatorial environments: the contribution of increased convective heat loss and cutaneous evaporative cooling. *Journal of Human Evolution*, 21(2):107 – 115, 1991.

[Wik16] Wikipedia. https://en.wikipedia.org/wiki/cubic_hermite_spline, 04.2016.

[WMB$^+$10] D. Wooden, M. Malchano, K. Blankespoor, A. Howardy, A.A. Rizzi, and M. Raibert. Autonomous navigation for bigdog. In *Robotics and Automation (ICRA), 2010 IEEE International Conference on*, pages 4736–4741, 2010.

[YTK93] J.-I. Yamaguchi, A. Takanishi, and I. Kato. Development of a biped walking robot compensating for three-axis moment by trunk motion. In *Intelligent Robots and Systems '93, IROS '93. Proceedings of the 1993 IEEE/RSJ International Conference on*, volume 1, pages 561–566 vol.1, Jul 1993.

[ZKSS16] M. Zenzes, P. Kampmann, T. Stark, and M. Schilling. Ndlcom: Simple protocol for heterogeneous embedded communication networks. In

Proceedings of the Embedded World Exhibition & Conference. Embedded world Exhibition & Conference, located at Embedded World 2016, February 23-25, Nuernberg, Germany. o.A., 2016.

[ZYLG13] X. Zhang, H. Yu, B. Liu, and X. Gu. A bio-inspired quadruped robot with a global compliant spine. In *IEEE International Conference on Robotics and Biomimetics (ROBIO)*, pages 1312–1316, Dec 2013.

Additional Experimental Data

Quadrupedal Experiments

Only when the foot has to cover a large distance as occurs during the movement in swing-phase, due to the latency between command and motor movement, an error can be observed between 50 % and 75 % of the cycle progress.

Stability in Flat Terrain

Figure 2 shows the Zero Moment Point (ZMP) in a top view for the walking on flat terrain with and without local control. The color of the curve indicates the progress of the overall walking cycle and changes from green (start of the walking cycle) to blue (end of the walking cycle). The curve itself shows the average ZMP-shifting in x- and y-direction while walking forward with *speed setting medium*. Since multiple steps are performed, gray bars are added to the data line to point out the deviation from the mean value in x and y direction.

The swing-phase of the rear right leg and rear left leg is between 0 % to 25 % and 50 % to 75 % of the walking cycle, respectively. The data shows that the ZMP movement with activated local controller is equal to *setup* $\overline{L}$ $\overline{S}$, due to the less challenging terrain.

Distinction of Different Soils

The following Fig. 3 shows the values of the sensor array integrated while walking on different soils. It can be seen that a distinction of different soils is possible.

Forces on the Front Left Foot while Walking in a Gravel Field

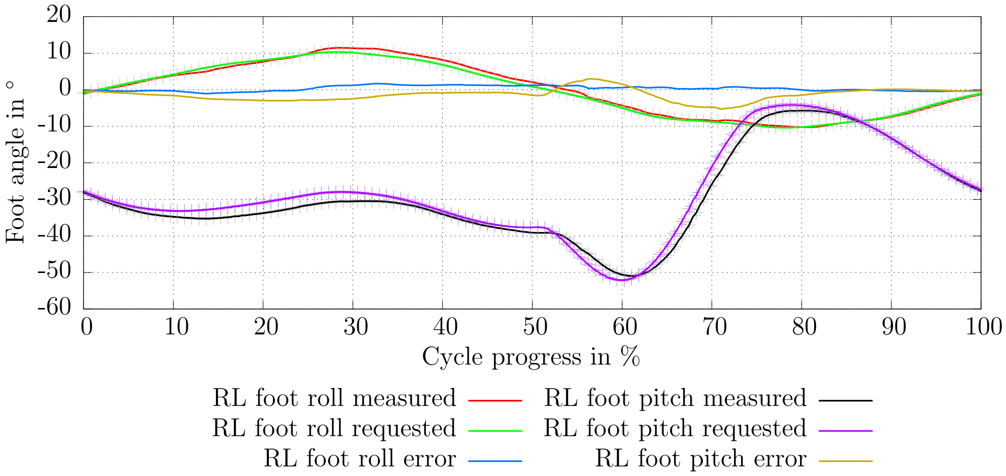

(a) Laboratory floor, walking with *speed setting medium* and *setup* $\overline{L}$ $\overline{S}$.

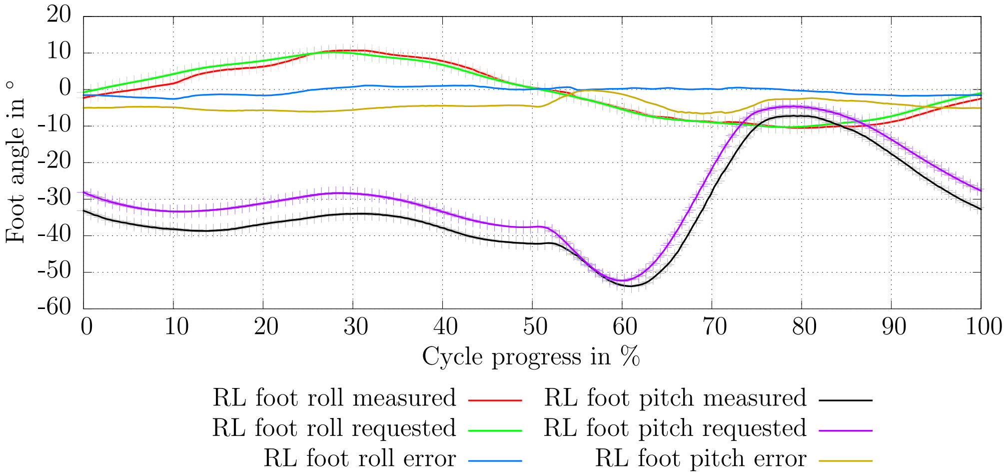

(b) Laboratory floor, walking with *speed setting medium* and *setup* L $\overline{S}$.

Figure 1: Measured angles in the ankle joint in *setup* $\overline{L}$ $\overline{S}$ (without local control) and *setup* L $\overline{S}$ (with local control) [KSS+16].

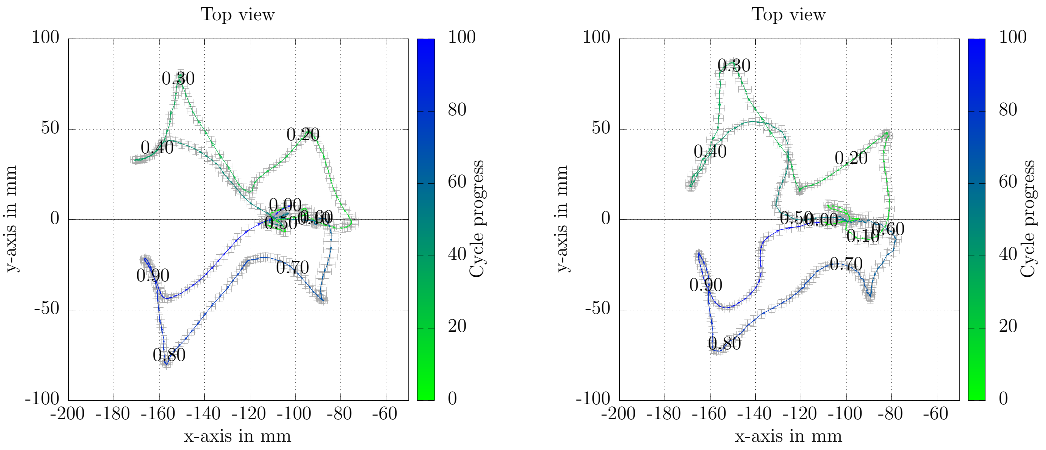

(a) *Terrain lab*: Laboratory floor with *speed setting medium* and *setup* $\overline{L}\ \overline{S}$ (without local control).

(b) *Terrain lab*: Laboratory floor with *speed setting medium* and *setup* $L\ \overline{S}$ (with local control).

Figure 2: Walking on flat terrain with and without active local controller in the rear feet. It can be observed that with an active local control loop smaller deviations of the ZMP occur as well as the ZMP follows a more smooth path.

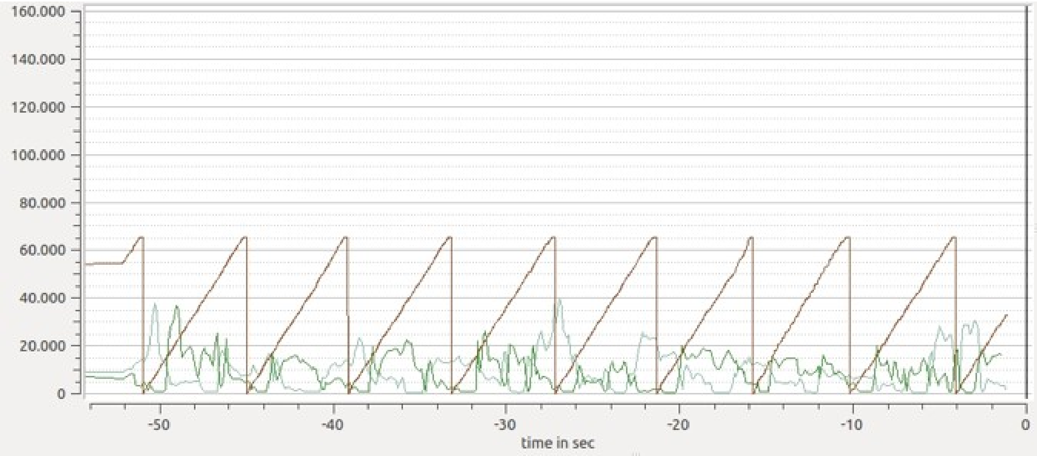

(a) Walking on *terrain garden*.

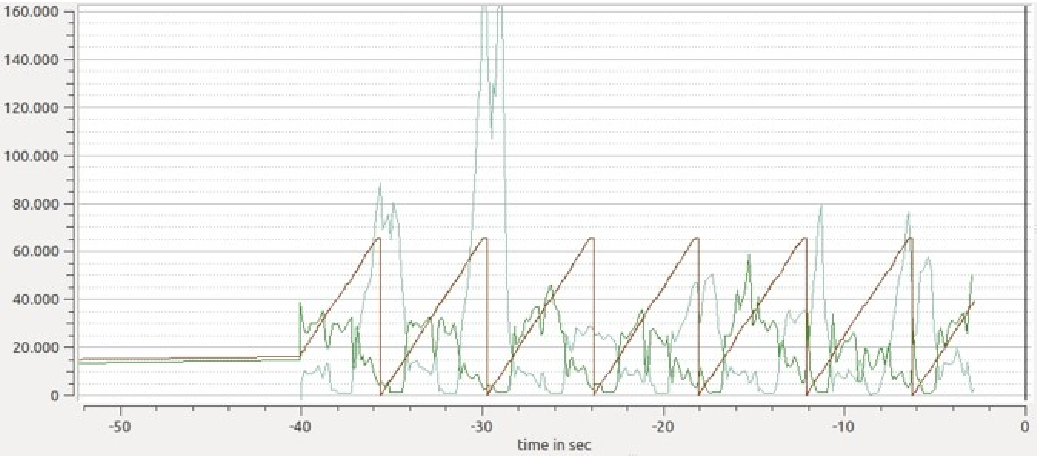

(b) Walking on *terrain grass*.

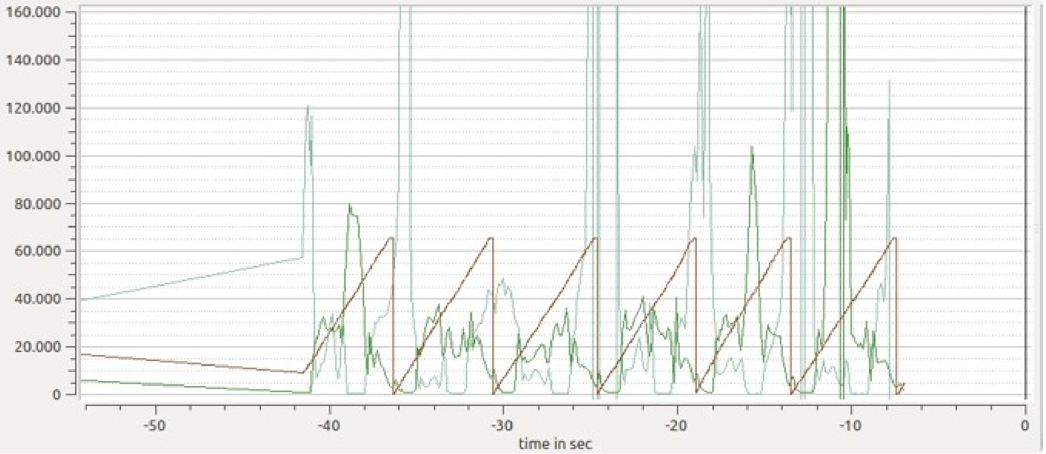

(c) Walking on *terrain gravel*.

Figure 3: Sensor array raw data while walking on different soils are indicated in green. In brown, the overall walking cycle progress is shown.

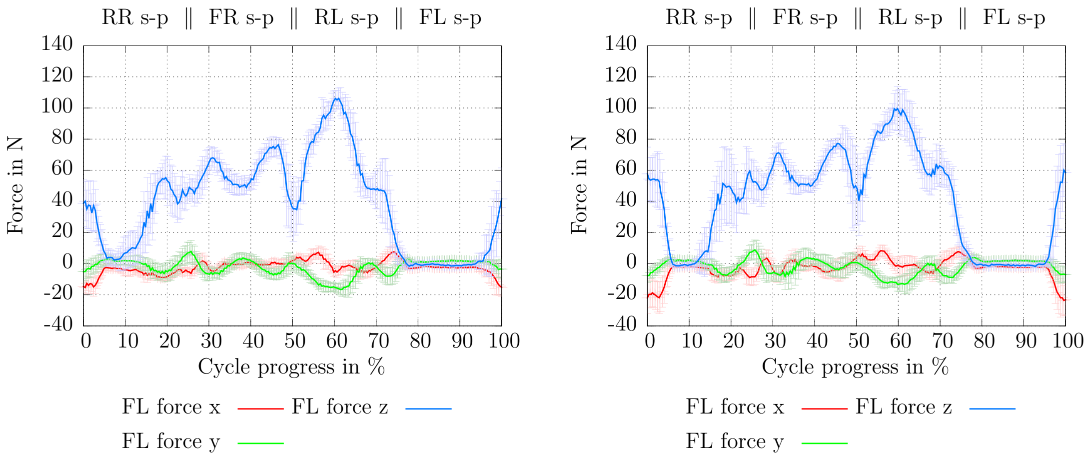

(a) *Terrain gravel*: gravel field, local control loop and spine both inactive (*setup* $\overline{L}$ $\overline{S}$).

(b) *Terrain gravel*: gravel field, local control loop inactive and spine active (*setup* $\overline{L}$ S).

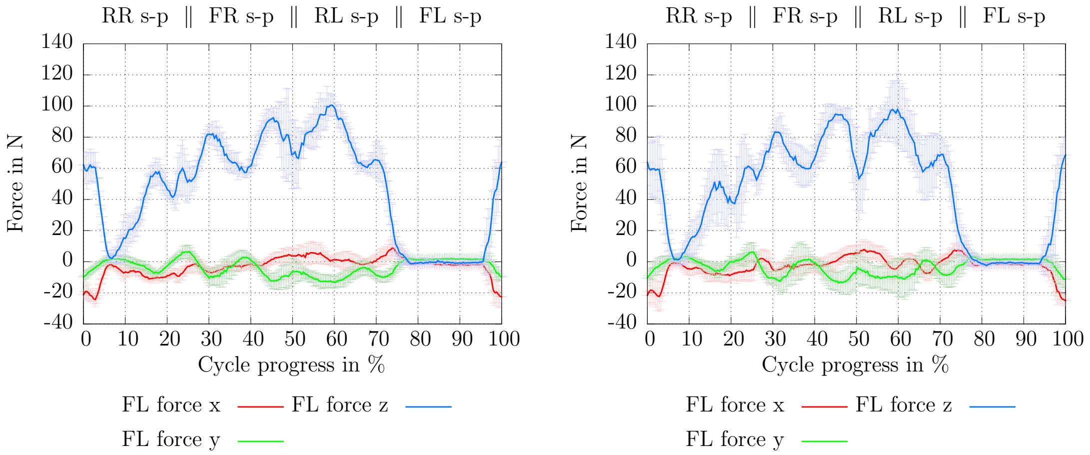

(c) *Terrain gravel*: gravel field, local control loop active and spine inactive (*setup* L $\overline{S}$).

(d) *Terrain gravel*: gravel field, local control loop and spine both active (*setup* L S).

Figure 4: Measured forces acting on the front left leg in different setups with *speed setting medium*.

Forces on the Rear Left Foot while Walking in a Gravel Field

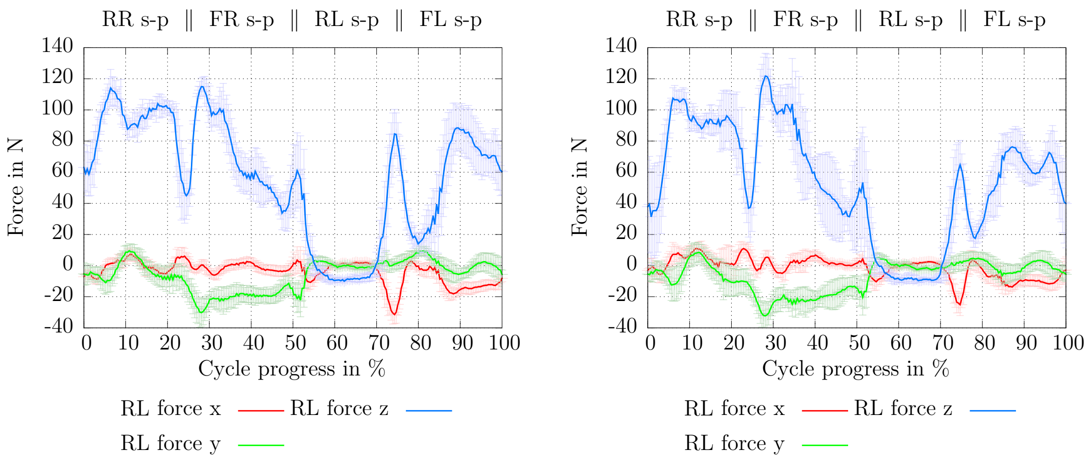

(a) *Terrain gravel*: gravel field, local control loop and spine both inactive (*setup* $\overline{L}$ $\overline{S}$).

(b) *Terrain gravel*: gravel field, local control loop inactive and spine active (*setup* $\overline{L}$ S).

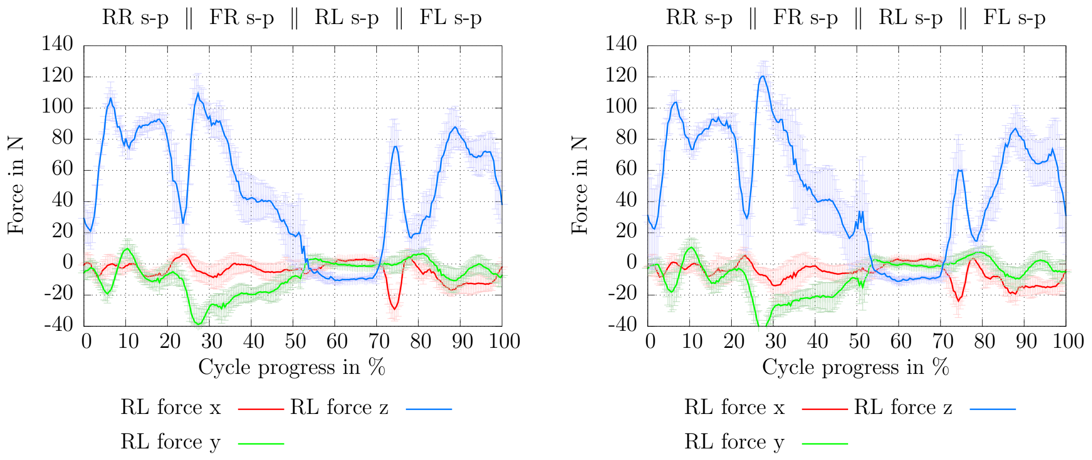

(c) *Terrain gravel*: gravel field, local control loop active and spine inactive (*setup* L $\overline{S}$).

(d) *Terrain gravel*: gravel field, local control loop and spine both active (*setup* L S).

Figure 5: Measured forces acting on the rear left leg in different setups with *speed setting medium*.

Torque on the Front Left Foot while Walking in a Gravel Field

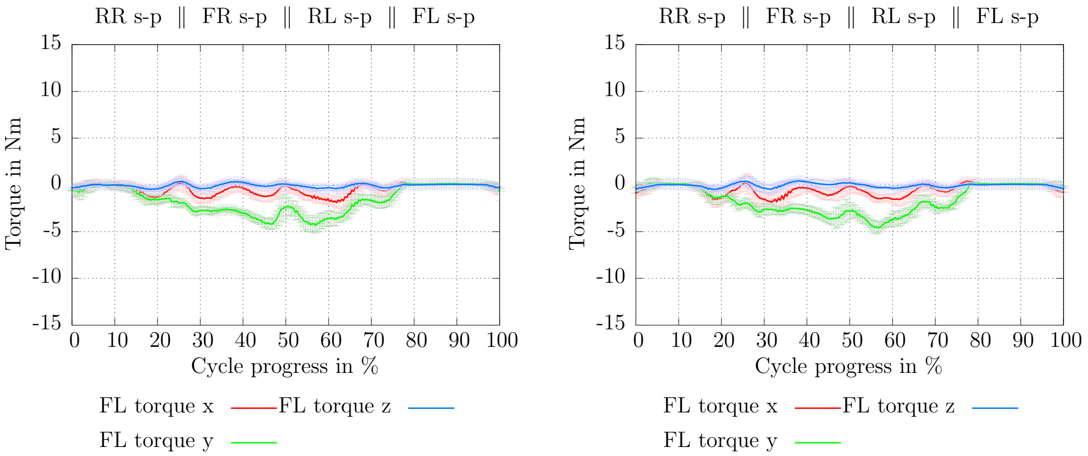

(a) *Terrain gravel*: gravel field, local control loop and spine both inactive (*setup* $\overline{L}$ $\overline{S}$).

(b) *Terrain gravel*: gravel field, local control loop inactive and spine active (*setup* $\overline{L}$ S).

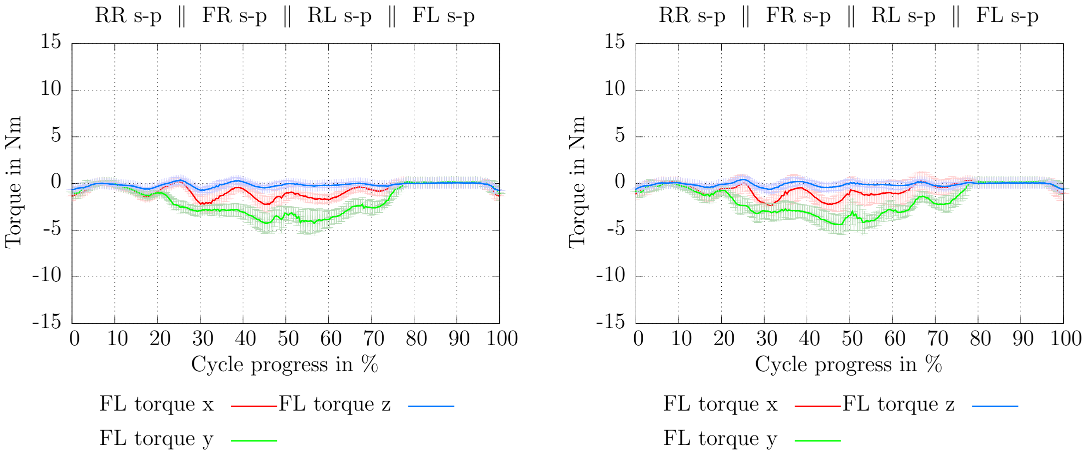

(c) *Terrain gravel*: gravel field, local control loop active and spine inactive (*setup* L $\overline{S}$).

(d) *Terrain gravel*: gravel field, local control loop and spine both active (*setup* L S).

Figure 6: Measured torque acting on the front left leg in different setups with *speed setting medium*.

Torque on the Rear Left Foot while Walking in a Gravel Field

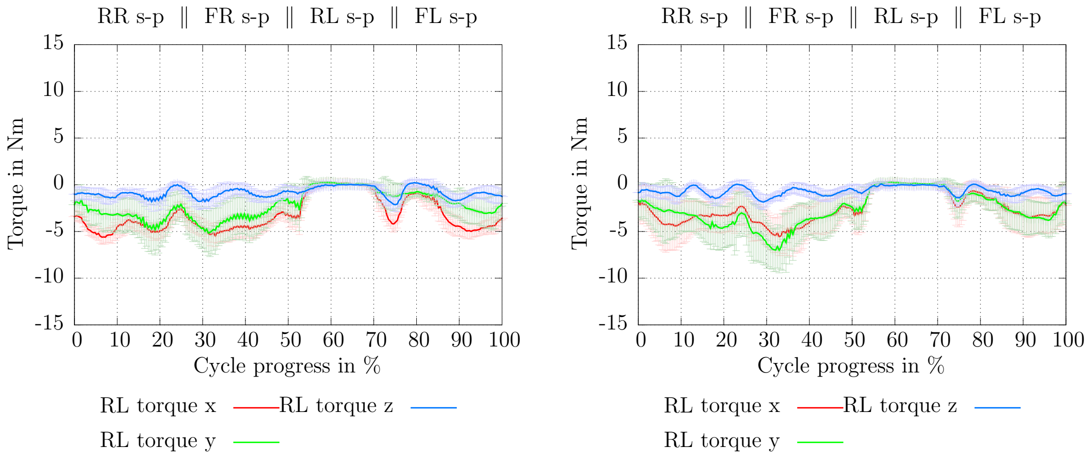

(a) *Terrain gravel*: gravel field, local control loop and spine both inactive (*setup* $\overline{L}\ \overline{S}$).

(b) *Terrain gravel*: gravel field, local control loop inactive and spine active (*setup* $\overline{L}\ S$).

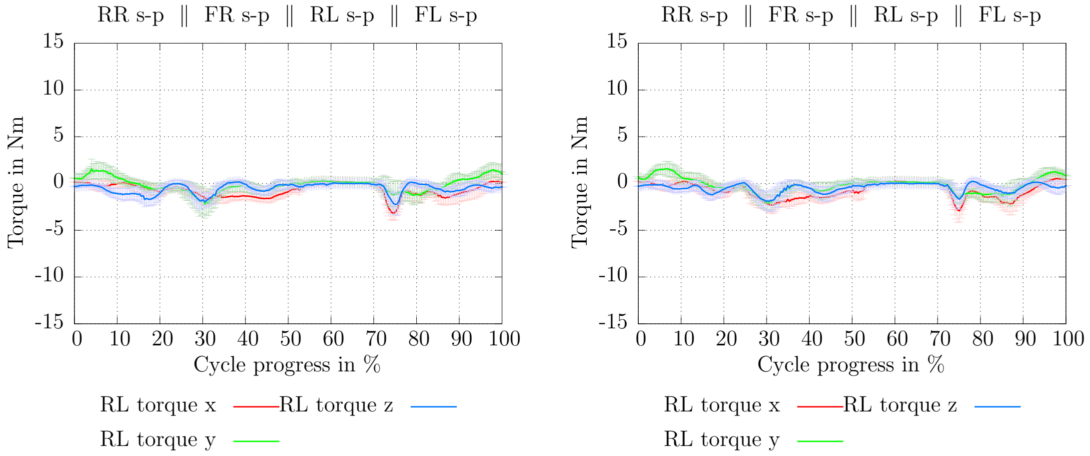

(c) *Terrain gravel*: gravel field, local control loop active and spine inactive (*setup* $L\ \overline{S}$).

(d) *Terrain gravel*: gravel field, local control loop and spine both active (*setup* $L\ S$).

Figure 7: Measured torque acting on the rear left leg in different setups with *speed setting medium*.

Bipedal Experiments

Towards Bipedal Walking

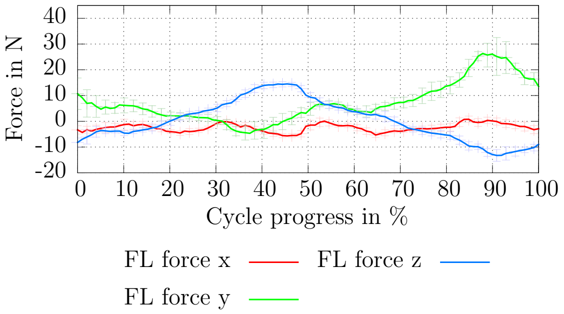

(a) Measured forces at a gait cycle of 4.6 s.

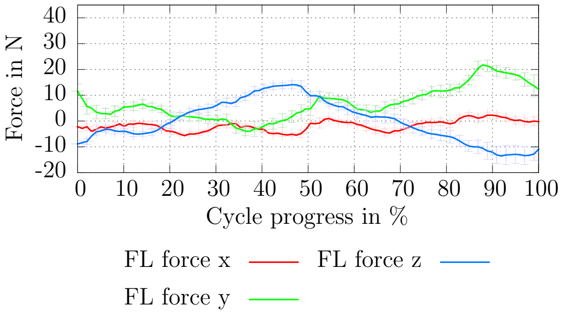

(b) Measured forces at a gait cycle of 4.3 s.

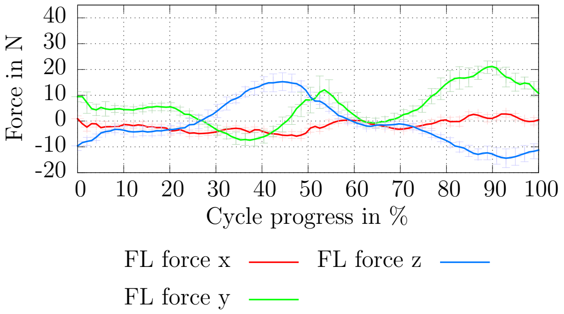

(c) Measured forces at a gait cycle of 3.6 s.

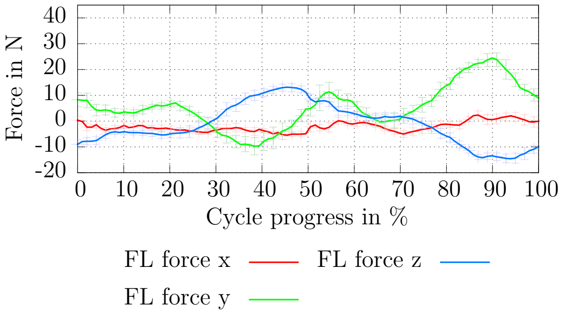

(d) Measured forces at a gait cycle of 3.3 s

Figure 8: Measured absolute forces data of the front left arm while walking bipedal with support with cycle times between 4.6s and 3.3s.

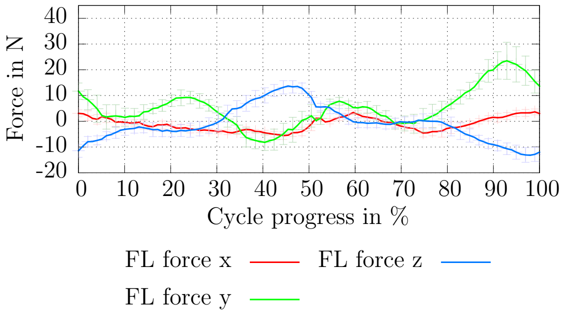

(a) Measured forces at a gait cycle of 2.6 s.

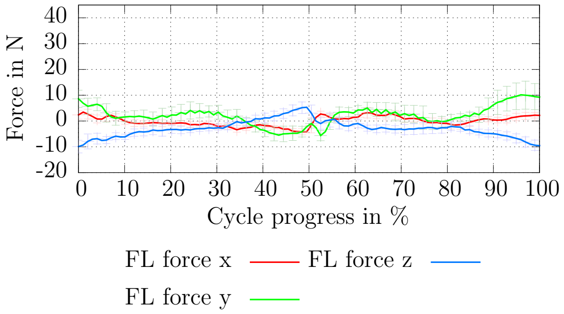

(b) Measured forces at a gait cycle of 2.3 s.

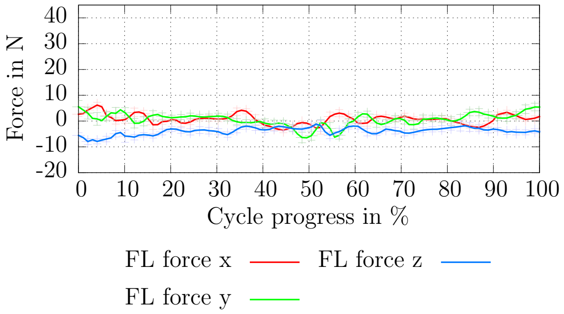

(c) Measured forces at a gait cycle of 1.6 s.

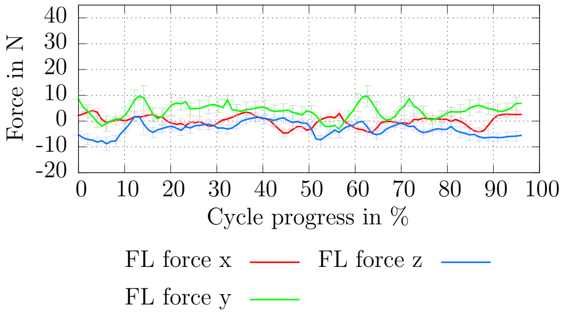

(d) Measured forces at a gait cycle of 1.3 s.

Figure 9: Measured absolute forces data of the front left arm while walking bipedal with support with cycle times between 2.6s and 1.3s.

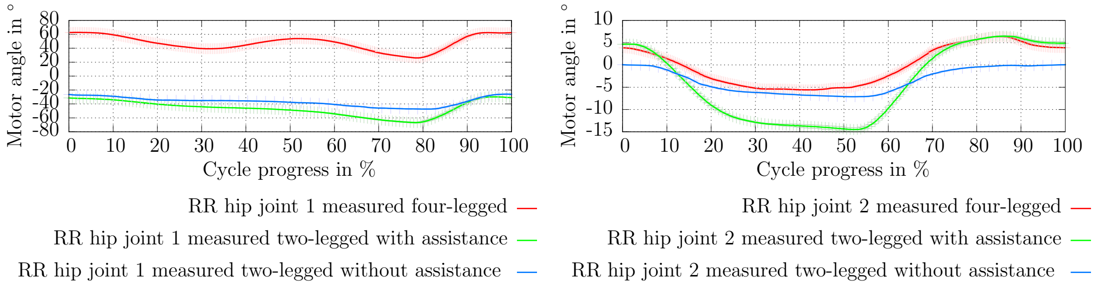

(a) Rear right hip joint 1 (b) Rear right hip joint 2

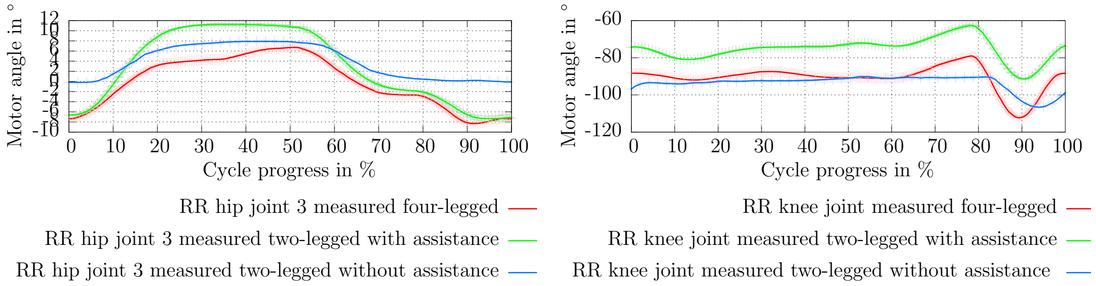

(c) Rear right hip joint 3 (d) Rear right hip knee joint

Figure 10: Angle plots of the rear right leg while walking quadrupedal and bipedal.